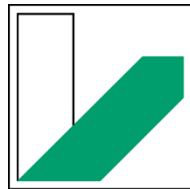


Investigations on the amorphous state and high-resolution patterns prepared by scanning probe lithography

Dissertation

zur Erlangung des akademischen Grades
eines Doktors der Naturwissenschaften (Dr. rer. nat.)
im Promotionsprogramm „Polymer Science“
der Bayreuther Graduiertenschule für Mathematik und Naturwissenschaften



**UNIVERSITÄT
BAYREUTH**

vorgelegt von

Felix Krohn

Geboren in Leipzig

Bayreuth, 2021

Der experimentelle Teil der Arbeit wurde in der Zeit von Juni 2015 bis Dezember 2019 am Lehrstuhl Makromolekulare Chemie I der Universität Bayreuth unter der Betreuung von Herrn Prof. Dr. Hans-Werner Schmidt angefertigt.

Vollständiger Abdruck der von der Bayreuther Graduiertenschule für Mathematik und Naturwissenschaften (BayNAT) der Universität Bayreuth genehmigten Dissertation zur Erlangung des akademischen Grades eines Doktors der Naturwissenschaften (Dr. rer. Nat.).

| | |
|---------------------------------------|------------|
| Dissertation eingereicht am: | 10.08.2020 |
| Zulassung durch das Leistungsgremium: | 23.09.2020 |
| Wissenschaftliches Kolloquium: | 19.03.2021 |

Amtierender Direktor: Prof. Dr. Markus Lippitz

Prüfungsausschuss:

Prof. Dr. Hans-Werner Schmidt (Gutachter)

Prof. Dr. Jürgen Senker (Gutachter)

Prof. Dr. Georg Papastavrou (Vorsitz)

Prof. Dr. Ernst Rößler

„Et is wie et is.

Et kütt wie et kütt.

Et hätt noch emmer joot jejange!“

§1-3 Kölsches Jrundjesetz

Table of Contents

| | |
|---|------|
| Abbreviations..... | I |
| Symbols..... | V |
| Short summary | VII |
| Kurzzusammenfassung..... | X |
| List of Publications..... | XIII |
| 1. Introduction..... | 1 |
| 1.1. The History of Glasses | 1 |
| 1.2. General Theory of Glasses | 2 |
| 1.3. Organic glasses - applications and properties..... | 9 |
| 1.4. Micro- and Nanolithography | 24 |
| 1.5. References..... | 34 |
| 2. Objective of the Thesis | 55 |
| 3. Synopsis | 59 |
| 3.1. Overview of the thesis..... | 59 |
| 3.2. Organic Glasses of High Glass Transition Temperatures Due To Substitution with Nitrile Groups | 61 |
| 3.3. Main and secondary relaxations of non-polymeric high- T_g glass formers as revealed by dielectric spectroscopy | 63 |
| 3.4. Dynamics of a completely miscible binary non-polymeric organic glass-forming system..... | 65 |
| 3.5. Poly(olefin sulfone)s as new resist materials for thermal scanning probe lithography. | 68 |
| 4. Publications and manuscripts..... | 71 |
| 4.1. Individual contributions to joint publications | 71 |
| 4.2. Organic Glasses of High Glass Transition Temperatures Due To Substitution with Nitrile Groups | 75 |
| 4.3. Main and secondary relaxation of non-polymeric high- T_g glass formers as revealed by dielectric spectroscopy | 99 |
| 4.4. Reorientational Dynamics of highly asymmetric binary non-polymeric mixtures – a dielectric spectroscopy study | 135 |
| 4.5. Poly(olefin sulfone)s as new resist materials for thermal scanning probe lithography | 175 |
| 5. Danksagung | 203 |

Abbreviations

| | |
|---------|--|
| 2,7-DCS | 2,7-dicyano-9,9'-Spirobi[9H]fluorene |
| 2-CS | 2-cyano-9,9'-Spirobi[9H]fluorene |
| 2D | two-dimensional |
| 2-PC | 3,3',4,4'-benzophenone tetracarboxylic dianhydride |
| 2-PS | 2-phenyl-9,9'-Spirobi[9H]fluorene |
| 3D | three dimensional |
| AFM | atomic force microscopy |
| ALD | atomic layer depositon |
| BTEAC | benzyltriethyl ammonium chloride |
| CD | compact disc |
| DC | direct current |
| DH 379 | spirobichroman compound |
| DHIQ | decahydroisoquinoline |
| DLS | depolarized light scattering |
| DMA | dynamic mechanical analysis |
| DOP | dioctyl phosphate |
| DS | dielectric spectroscopy |
| DSC | dynamic scanning calorimetry |
| DUV | deep-UV |
| e-beam | electron beam |
| EBL | e-beam lithography |
| ESI | electronic supplementary information |

ABBREVIATIONS

| | |
|----------------|--|
| EUV | extreme ultra-violet |
| EW | excess wing |
| FD | felodipine |
| FT | Fourier transform |
| FTIR | Fourier transform infrared spectroscopy |
| FTS | frequency time superposition |
| HSQ | hydrogen silsesquioxane |
| IC | integrated circuit |
| JG | Johari-Goldstein |
| <i>m</i> | meta |
| <i>m</i> -CPS | 2-(meta-cyanophenyl)-9,9'-Spirobi[9H]fluorene |
| MCV | maximum crystal growth velocity |
| M_p | melting point |
| <i>m</i> -TCP | meta-tricresyl phosphate |
| <i>m</i> -TPTS | 2-(meta-tert-butylphenyl)-2'-tert-butyl-9,9'-Spirobi[9H]fluorene |
| NIL | nano-imprint lithography |
| NMR | nuclear magnetic resonance |
| <i>o</i> | ortho |
| <i>o</i> -CPS | 2-(ortho-cyanophenyl)-9,9'-Spirobi[9H]fluorene |
| OFET | organic field-effect transistor |
| OKE | optical Kerr effect |
| OLED | organic light emitting diode |
| <i>p</i> | para |
| PAG | photo-acid generator |
| PCHS | poly(cyclohexyl sulfone) |

| | |
|----------------|--|
| <i>p</i> -CPS | 2-(para-cyanophenyl)-9,9'-Spirobi[9H]fluorene |
| PDMS | poly(dimethyl siloxane) |
| PMMA | poly(methyl methacrylate) |
| PMPS | poly(2-methylpentyl sulfone) |
| PPA | poly(phthal aldehyde) |
| PS | polystyrene |
| PVD | physical vapor deposition |
| SBC | spirobichroman |
| SEC | size-exclusion chromatography |
| SEM | scanning electron microscope |
| SIS | sequential infiltration synthesis |
| SPL | scanning probe lithography |
| STA | scanning thermal analysis |
| STM | scanning tunneling microscope |
| TAAC | tetraamylammonium chloride |
| TBAC | tetrabutylammonium chloride |
| TBAN | tetrabutylammonium nitrate |
| TBAPC | tetrabutylammonium perchlorate |
| Tbit | tera bit |
| TCPS | 2-tert-butyl-2'-(3-cyano-9,9'-Spirobi[9H]fluorene) |
| T _g | glass transition temperature |
| TGA | thermo-gravimetical analysis |
| T _m | melting point |
| Tol | toluene |
| TPP | tripropyl phosphate |

ABBREVIATIONS

| | |
|-------|------------------------------------|
| t-SPL | thermal scanning probe lithography |
| TTP | tritoyl phosphate |
| UV | ultra-violet |
| VFT | Vogel-Fulcher-Tamann |
| wt% | weight percent |
| x-PS | crosslinked polystyrene |

Symbols

| | |
|---------------------------------|--|
| \AA | Angström |
| α | volume expansion coefficient |
| α | power-law exponent |
| β_K (also β_{KWW}) | Kohlrausch stretching parameter |
| c | concentration |
| C_p | specific heat capacity at constant pressure |
| E | energy |
| E' | mechanical storage modulus |
| E'' | mechanical loss modulus |
| E_A | activation energy |
| ϵ' | dielectric storage |
| ϵ'' | dielectric loss |
| ϵ^* | complex dielectric permittivity |
| ϵ_∞ | high-frequency permittivity |
| $\Delta\epsilon$ | dielectric relaxation strength |
| $F(0)$ | steady state flow at low temperatures |
| G | Gibbs Free Energy |
| $g_\beta(E)$ | width of energy distribution of the β -process |
| H | enthalpy |
| η | viscosity |
| k_B | Boltzmann constant |
| λ | wavelength |
| M | molar mass |

SYMBOLS

| | |
|-------------------|---|
| NA | numerical aperture |
| ν | frequency |
| \bar{v} | specific volume |
| p | pressure |
| R | universal gas constant |
| R | resolution |
| S | entropy |
| $\Delta S_{tr,m}$ | entropy of phase transition between T_g and T_m |
| T | temperature |
| $T_{-50\ wt\%}$ | temperature of 50 % weight loss |
| T_K | Kautzmann temperature |
| $T_{g,1}$ | T_g of the matrix |
| $T_{g,2}$ | T_g of the additive |
| τ | relaxation time |
| τ_D | Debye relaxation time |
| $\Phi(\tau)$ | step-response function |
| V | volume |
| V_f | free volume |
| φ | fluidity |
| χ | dielectric susceptibility |
| ω | angular frequency |
| ω_p | peak frequency |

Short summary

This thesis focuses on the synthesis, fundamental characterization, and partly the application of *amorphous low molecular weight materials and polymers*.

Non-polymeric glass formers, so-called *molecular glasses*, have gained increasing attention in the last decades. Their application ranges from thin-film processing for micro-manufacturing over organic electronics to pharmaceuticals. However, there is still a lack of understanding concerning fundamental properties of this material class. In particular, detailed investigations on the influence of presence and substitution position of dipolar substituents on T_g , glass-forming ability, and the dynamics of such glasses are missing. Furthermore, specific features in the behavior of asymmetric binary mixtures have recently been discovered. Further investigations of these specific features require tailor-made synthesis of novel molecular glasses to form stable mixtures with low molecular weight additives. While molecular glasses are used in many applications including lithography, they fail to offer specific requirements for resist materials in thermal scanning probe lithography. Thus, the use of polymers for this technique is inevitable. So far only one polymer has been established as resist material, therefore the development of further possible resist materials is of high interest.

In this context, the introduction gives an overview about general properties of glass-forming materials, such as glass transition and relaxation behavior. The focus is on (non-polymeric) organic glasses and an overview of design principles yielding stable, high- T_g molecular glasses is presented. The focus then shifts to dynamics as observed in organic glasses and a literature overview is presented dealing with main and secondary relaxation phenomena as observed in organic glasses. As specific features are observed in dynamics of binary mixtures of such glass formers, literature studies addressing these phenomena are presented in more detail and current debates about this topic are discussed. The last part of the introduction gives an overview of the evolution of micro- and nano-lithography, briefly presenting the principles of UV-lithography and focusing on alternative lithographic techniques. State-of-the-art in thermal scanning probe lithography is presented including strategies to improve pattern transfer as well as recent developments of applications going beyond classical lithography for microelectronics.

In total, this cumulative thesis consists of four additional chapters, two of which were published as two peer-reviewed full papers. The other two chapters are presented in a manuscript form and intended for submission as full papers shortly. An overview of these topics is presented along with a summary of the major results in the synopsis.

The *first chapter* focuses on the influence of dipole containing nitrile groups and their respective substitution position on T_g and glass-forming ability of molecular glasses based on 9,9'-spirobi[9H]fluorene. The introduction of such highly interacting substituents raises T_g as a function of molar mass by a much higher extent than other substituents previously published in literature. The findings of this topic provide new insight in thermal properties of molecular glasses and may be beneficial for the application of molecular glasses in several fields of research and application.

The *second chapter* features selected compounds studied in the *first chapter* and focuses on the influence of dipole containing nitrile groups on dielectric relaxation phenomena of these compounds. A clear difference is observed between nitrile groups that have a fixed orientation with respect to the stiff core and others that can change their orientation. The relaxation spectra are compared to those of other well-investigated glass formers. For compounds with a fixed nitrile group, a secondary process with features that have not been reported before is observed.

In the *third chapter* a new asymmetric, binary system of non-polymeric glass formers with a high T_g -contrast of more than 200 K showing neither demixing nor crystallization over the entire temperature and concentration range is developed. Using dielectric spectroscopy, dynamic scanning calorimetry, and dynamic mechanical analysis, a conclusive picture of the dynamics of the investigated system is shown. The relaxation of the high- T_g component shows a plasticizer-effect upon mixing with moderate broadening of the process. The dynamics of the additive at low respective concentrations show a broad distribution of relaxation times and an Arrhenius-like evolution with temperature resembling that of materials in confined space. The obtained results support the interpretation that the concentration-dependent T_g of the α_2 -process shows a maximum at intermediate additive concentrations, a currently highly debated issue.

The *fourth chapter* focuses on poly(olefin sulfone)s as new resist materials for thermal scanning probe lithography. These polymers feature a low ceiling temperature and are therefore ideal candidates for this technique. In this context, high-resolution lithography with a resolution down to 10 nm is demonstrated. The obtained patterns are stable towards acidic conditions and thus offer new possibilities for the application of this technique. Sequential infiltration synthesis is used to obtain an etch-resistant hard-mask usable for a subsequent pattern transfer.

Kurzzusammenfassung

Die vorliegende Arbeit befasst sich mit der Synthese, der grundlegenden Charakterisierung und teilweise der Anwendung *amorpher niedermolekularen Materialien und Polymeren*.

Nicht-polymere Glasbildner, sogenannte *molekulare Gläser*, haben in den vergangenen Jahrzehnten eine verstärkte Aufmerksamkeit erfahren. Ihre Anwendungen reichen von Dünnschicht-Prozessierung für Mikrofabrikation über organische Halbleiter bis hin zu pharmazeutischen Formulierungen. Dennoch herrscht immer noch Unklarheit bezüglich einiger fundamentaler Eigenschaften solcher Gläser. Insbesondere gibt es keine detaillierten Untersuchungen über den Einfluss der Präsenz dipolarer Substituenten sowie ihrer Position auf die Glasübergangstemperatur, die Stabilität der amorphen Phase sowie die Dynamik in solchen Verbindungen. Des Weiteren wurden in asymmetrischen, binären Systemen Besonderheiten in der Dynamik der beteiligten Verbindungen entdeckt. Die weitere Untersuchung dieser Phänomene setzt eine maßgeschneiderte Synthese neuer organischer Gläser voraus, die in der Lage sind, stabile Mischungen mit niedermolekularen Additiven zu bilden. Während organische Gläser in vielen Feldern, wie zum Beispiel der Lithographie, angewendet werden, so erfüllen sie dennoch nicht alle speziellen Anforderungen um als Resist-Material für die thermische Rastersonden-Lithographie eingesetzt zu werden. Hier ist die Anwendung von Polymeren notwendig. Da bisher nur ein Polymer alle benötigten Eigenschaften in sich vereint, ist die Untersuchung weiterer möglicher Materialien wünschenswert.

In diesem Zusammenhang gibt die Einleitung einen Überblick über die allgemeinen Eigenschaften glasbildender Materialien, wie zum Beispiel die Glasübergangstemperatur oder das Relaxationsverhalten. Der Fokus wird auf (nicht-polymere) organische Glasbildner gelegt und es wird ein Überblick über die Designprinzipien für stabile Hoch- T_g Glasbildner aufgezeigt. Im weiteren Verlauf ist ein Überblick über die aktuelle Literatur bezüglich primärer und sekundärer Relaxationsphänomene in organischen Glasbildnern gegeben. Aufgrund der Besonderheiten, die in der Dynamik binärer, asymmetrischer Glasbildner entdeckt wurden, sind Studien über diesen Sachverhalt im Detail dargestellt und diskutiert. Der letzte Teil der Einleitung gibt einen Überblick über die Entwicklung der Mikro- und Nano-Lithographie, beschreibt kurz das Prinzip der UV-Lithographie und konzentriert sich dann auf alternative

Lithographie-Techniken. Der aktuelle Stand der Technik bezüglich thermischer Rastersonden-Lithographie ist zusammen mit Strategien für den Übertrag der Strukturen in das Substrat sowie neuen Ansätzen der Anwendung, die über die klassische Lithographie hinausgehen, aufgezeigt.

Diese kumulative Arbeit besteht aus vier weiteren Kapiteln, von denen bereits zwei in „peer-reviewed“ Zeitschriften als „Full Papers“ veröffentlicht worden sind, während die anderen zwei als Manuskripte, welche demnächst eingereicht werden sollen, beiliegen. Ein Überblick über die dort behandelten Themen findet sich zusammen mit einer kurzen Präsentation der wichtigsten Ergebnisse in der Synopsis.

Das *erste Kapitel* befasst sich mit dem Einfluss dipolarer Nitrilgruppen und der Position ihrer Substitution auf die Glasübergangstemperatur und die Stabilität der amorphen Phase einiger *9,9'-spirobi[9H]fluorene*. Das Einführen solch stark wechselwirkender Substituenten erhöht den T_g im Bezug auf die molare Masse um ein Vielfaches stärker als andere Substituenten, die bisher in der Literatur untersucht wurden. Die Resultate dieses Kapitels liefern neue Einblicke in die thermischen Eigenschaften von molekularen Gläsern und können dadurch einen wichtigen Beitrag zur Anwendung dieser Verbindungen leisten.

Im *zweiten Kapitel* werden ausgewählte Verbindungen aus dem ersten Kapitel mittels dielektrischer Spektroskopie charakterisiert und so der Einfluss der dipolaren Nitrilgruppe und ihrer Position auf die Relaxationsphänomene untersucht. Es konnte ein klarer Unterschied zwischen Verbindungen, bei denen die Nitrilgruppe fest mit dem Kern verbunden ist und solchen, bei denen die Nitrilgruppe relativ zum Kern rotieren kann, gefunden werden. Die erhaltenen Relaxationsspektren werden mit denen von bekannten Verbindungen aus der Literatur verglichen. Für solche Verbindungen, bei denen die Nitrilgruppe fest mit dem Kern verbunden ist, wurde ein neuartiger Sekundärprozess festgestellt.

Im dritten Kapitel wird ein neues binäres, asymmetrisches System aus zwei nicht-polymeren organischen Glasbildnern mit einem hohen T_g -Kontrast von über 200 K entwickelt, welches weder Entmischung noch Kristallisation über den gesamten untersuchten Konzentrations- und Temperaturbereich zeigt. Mittels dielektrischer Spektroskopie, dynamischer Differenzkalorimetrie und dynamisch-mechanischer Analyse konnte ein schlüssiges Bild vom Verhalten des untersuchten Systems gezeichnet werden. Die Relaxation des Hoch- T_g -Glasbildners zeigt

bei Mischen mit dem Additiv einen Weichmachereffekt mit moderater Spektrenverbreiterung. Die Dynamik des Additivs hingegen zeigt bei niedrigen Konzentrationen eine breite Verteilung der Relaxationszeiten sowie ein Arrhenius-Verhalten der Temperaturabhängigkeit. Diese Eigenschaften ähneln Beobachtungen von Verbindungen, die in kleinen Poren eingebracht sind. Die in diesem Kapitel gewonnenen Ergebnisse unterstützen die Interpretation, dass bei mittleren Konzentrationen ein Maximum im konzentrationsabhängigen Verlauf vom T_g des α_2 -Prozesses vorliegt. Dieser Sachverhalt ist in der Literatur derzeit heftig umstritten.

Im vierten Kapitel werden Polyolefinsulfone als neue Resist-Materialien für die thermische Rastersonden-Lithographie untersucht. Diese Polymere zeigen eine niedrige Ceiling-Temperatur und sind daher vielversprechende Kandidaten für diese Anwendung. Hochaufgelöst geschriebene Strukturmuster mit 10 nm Strukturgröße werden gezeigt. Die so erhaltenen Strukturen sind auch im sauren Milieu stabil und eröffnen dadurch weitere Anwendungsmöglichkeiten für diese Technik. Sequentielle Infiltrations-Synthese wurde durchgeführt, um ätzresistente Hartmasken herzustellen, die einen anschließenden Strukturübertrag in das Substrat ermöglichen.

List of Publications

The following publications and manuscripts are presented within the thesis:

- [1] F. Krohn, C. Neuber, E. A. Rössler, and H.-W. Schmidt, *Organic Glasses of High Glass Transition Temperatures Due To Substitution with Nitrile Groups* J. Phys. Chem. B **2019**, *123*, 10286-10293.
- [2] T. Körber, F. Krohn, C. Neuber, H.-W. Schmidt, and E. A. Rössler, *Main and secondary relaxations of non-polymeric high- T_g glass formers as revealed by dielectric spectroscopy*, Phys. Chem. Chem. Phys. PCCP **2020**, *22*, 9086-9097
- [3] T. Körber, F. Krohn, C. Neuber, H.-W. Schmidt, and E. A. Rössler, *Reorientational dynamics of highly asymmetric binary non-polymeric mixtures – a dielectric spectroscopy study*, Phys. Chem. Chem. Phys. PCCP **2021**, *22*, 7200-7212
- [4] F. Krohn, A. W. Knoll, S. Bisig, F. Ruggeri, C. Neuber, and H.-W. Schmidt, *Poly(olefin sulfone)s as new resist materials for thermal scanning probe lithography*, to be submitted

The following publications and manuscripts arose from collaborations within the time frame of the thesis. They are related to topics beyond the scope of this thesis and hence are not considered further in this work.

- [5] C. Neuber, H.-W. Schmidt, P. Strohriegl, D. Wagner, F. Krohn, A. Schedl, S. Bonanni, F. Holzner, C. Rawlings, U. Dürig, and A. W. Knoll, *PVD prepared molecular glass resists for scanning probe lithography*, Proc. SPIE **2016**, *9779*, 97791C
- [6] F. Krohn, A. W. Knoll, S. Bisig, C. Neuber, H.-W. Schmidt, *Poly(olefin sulfones) for thermal scanning probe lithography*, Bayreuther Polymer Symposium **2019**

1. Introduction

1.1. The History of Glasses

Humans have used amorphous materials practically ever since they started manufacturing and using tools, such as knives from obsidian and arrow tips from natural originating glass.^{1,2} The knowledge of how to manufacture glass can be dated back to about 4,500 BC, when appropriate methods have been discovered in Mesopotamia. This glass consisted essentially of a $\text{Na}_2\text{O-CaO-SiO}_2$ composition, which is very close to that of our modern glasses that we are familiar with today.² The oldest glass objects that have been discovered so far can be dated back to 3,000 BC and have been manufactured by the Egyptians. In the following millennia, the knowledge and skills in handling and manufacturing objects made of glass evolved. The first glass industries were established in Egypt, followed by Syria and Mesopotamia and glass objects became important trade objects.³ An important advance in the manufacturing process was the invention of *glass blowing* in Phoenicia around 50 BC. In the Western World, the use of glass objects was spread by the Roman Empire. The proceedings in the glass technology, however, were rather driven by trial and error studies than by using the means of science, which have not yet existed in that time.⁴ Still it is an important note that many tools playing a role in events that can be considered the starting point of modern science were manufactured of glass. Examples include lenses that were needed by Galilei to study the motion of the planets, and prisms, lenses, and mirrors used by Isaac Newton in his studies of optics. The following centuries brought further technological advances and scientific background that enabled improvement of manufacturing processes and the chemical composition of glasses towards a variety of applications of our modern everyday life. In Figure 1.1.1 two examples of the use of glasses from different ages are exemplarily depicted.^{5,6}



Figure 1.1.1: A: Example of a medieval reading stone, reprinted under Creative Commons license.⁶ B: Modern high-tech bulletproof glass, reprinted under Creative Commons license.⁵

1.2. General Theory of Glasses

So far, however the term *glass* has only been used to describe silicate based glasses that we associate with windows and bottles. In the early 20th century, the term glass was slowly generalized to define a non-crystalline solid in scientific language. A scientific milestone in the definition of a glass was the work of Tammann in 1930,⁷ who was the first to postulate the *vitreous state*, i.e. glass as a *physical state of matter*. Today, in scientific language, we speak about glasses in general as amorphous materials, consisting of an unordered, solid phase. As such, a glass may be thought of as a *frozen liquid*, whose structure and order resemble that of a typical liquid that however shows the viscosity usually associated with solids. For the remainder of this work, the term *glass* will be used as a synonym for a non-crystalline solid. In the following paragraphs, general features and theories of glasses and glass transition will be briefly described.

1.2.1. Glass Formation and Glass Transition

Upon cooling of a liquid below its melting point T_m , the liquid will enter a metastable equilibrium. For many liquids a crystallization can be observed *via* nucleation and growth of crystallites.⁸ At this point, the volume (or enthalpy) of the system shows a non-continuous decrease.⁹ Thereby, atoms or molecules rearrange into their translationally periodic array with a long-range order.¹⁰ If, however, the thermodynamic barrier to nucleation cannot be overcome, the liquid will further cool down until the motions of atoms or molecules slow down and become trapped at their current position. This leads to a rapid increase of the viscosity to an order of $10^{12} \text{ Pa} \cdot \text{s}$. This process occurs over a range of temperatures and is called the *glass transition region*. During that process, the volume (or enthalpy) of the material shrinks continuously as opposed to the before mentioned crystallization. The volume expansion coefficient will rapidly decrease during the glass transition, until it reaches a value that is comparable to that of the corresponding crystalline solid.⁹ During glass transition, the properties of the liquid vary with time.¹ That means that many of the properties of the glass depend on the cooling rate at the glass transition region. The higher the cooling rate, the less time is available for the atoms or molecules to rearrange. This leads to a higher volume and an increase of the observed glass transition temperature. A scheme of the volume change

during crystallization and vitrification of a material is shown in Figure 1.2.1A. There, volume change during cooling of a liquid is depicted. Curve 1 is showing a crystallizing liquid exhibiting a distinct step in the volume upon crystallization, Curves 2 and 3 show a glass forming liquid with a higher cooling rate for curve 2. The observed glass transition temperature is shifted towards higher temperatures with higher cooling rates.⁹

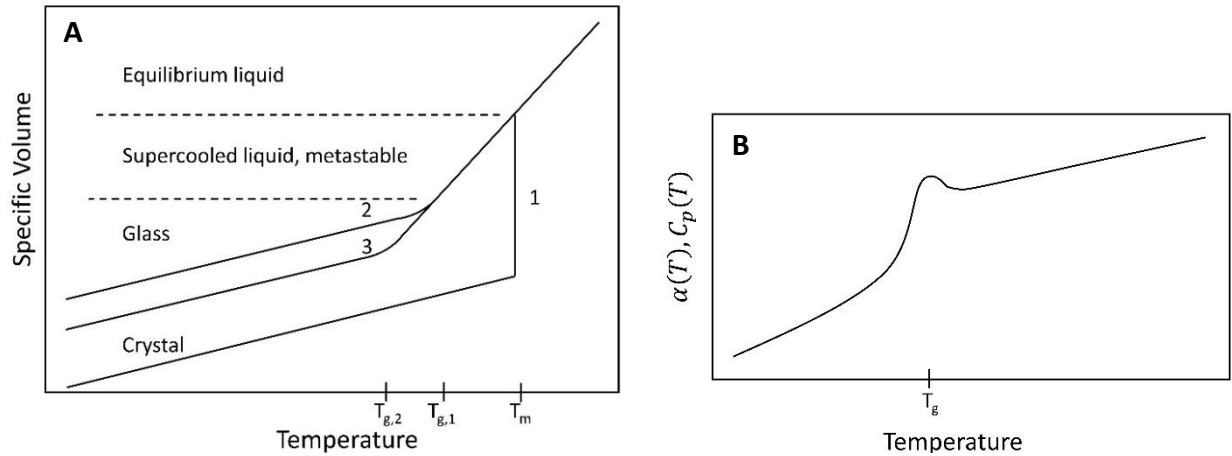


Figure 1.2.1: A: Volume change during cooling of a liquid. Path 1 shows a liquid that crystallizes, path 2 and 3 show the vitrification of a liquid with a higher cooling rate for path 2. Adapted from Ref. 1. B: $\alpha(T)$ and $C_p(T)$ during the glass transition.

Further addressing the phenomena associated with the glass transition requires a short excursion to the basics of thermodynamics. The term *first order transition* is derived from the Gibbs energy

$$\Delta G = \Delta H - T\Delta S \quad (1.2.1)$$

where volume and entropy are first order derivatives with respect to pressure or temperature.¹⁰ A phase transition is called first order if volume or entropy change in a discontinuous way.

In a *second order transition*, discontinuities in the second derivative of the Gibbs function, that is, in the slopes of $V(T)$ or $S(T)$, i.e. in $\alpha(T)$ (the volume expansion coefficient) or $C_p(T)$ (the specific heat capacity at constant pressure), are involved. Consequently, a phase transition is called n^{th} order if the n^{th} derivative of the Gibbs function is the first to show a discontinuity.¹⁰

For crystallization, as stated above, a discontinuity in the volume can be observed, making it an example of a first order transition. During glass transition, no discontinuity can be observed

for volume or entropy. However, as already mentioned, $\alpha(T)$ and $C_p(T)$ drastically change in the glass transition region. These transitions are, however, not sharp and discontinuous as they should be in an ideal second order transition, but they are rather diffuse and occur over a small temperature interval, as can be seen in Figure 1.2.1B. Still, as the change in $\alpha(T)$ and $C_p(T)$ are prominent, the glass transition is defined as an *apparent, diffuse, second order transition*.¹⁰

1.2.2. Fragility

When observing the viscosity during the passage of T_g , especially for systems with non-directional bonds (i.e. metals and van der Waals solids), small changes in temperature may result in a huge change of the viscosity.⁸ In particular, an abrupt fall of the viscosity can be observed for these materials immediately above T_g suggesting that the system's architecture is very *fragile*. Still it is to emphasize that the change of the viscosity during vitrification remains continuous as opposed to crystallization.³ The opposite of a fragile glass is a glass with directional bonds such as SiO_2 . Upon passing T_g , the structural units essentially keep their medium range order and the change in the viscosity is essentially linear in a semi-logarithmic plot. These systems are hence called *strong* glasses. This classification was proposed by Angell in 1995.¹¹ A typical *Angell-Plot* is depicted in Figure 1.2.2. Here, the logarithmic viscosity is plotted against the reduced glass transition temperature T_g/T for SiO_2 as an example of a mineral glass with directional bonds, for a metallic glass and for *o*-terphenyl as an example of a van-der-Waals glass. Whereas a strong glass such as SiO_2 shows a linear increase in the viscosity, *o*-terphenyl exhibits a low increase at low temperatures, but upon approaching T_g , the viscosity drastically increases.

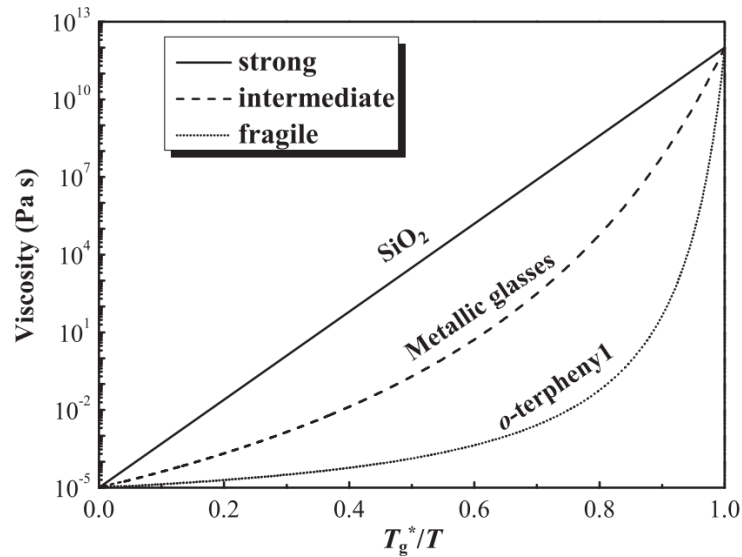


Figure 1.2.2: Angell-Plot for strong (SiO_2), intermediate (metallic glasses) and fragile (*o*-terphenyl) liquids. Reprinted from Ref. 12 with permission from Elsevier, © 2014.

A mathematical description of this behavior is given by the Vogel-Fulcher-Tammann (VFT) equation by

$$\eta = \eta_0 \exp \left[\frac{B}{T - T_0} \right] \quad (1.2.2)$$

with η_0 and B being constants. If T_0 becomes zero, the function becomes the Arrhenius-equation where B becomes the activation barrier E/k_B .⁸ As viscosity and relaxation time are directly connected as can be seen from equation 1.2.3, the VFT-equation can also be used to describe the relaxation times in the glass transition region as measured by e.g. dielectric spectroscopy.

1.2.3. Relaxation

In a typical liquid, the motion of atoms or molecules is fast enough to ensure that the system can react to any changes in temperature by adjusting the relative positions in order to minimize the free energy.³ That is to say that the time for readjustment (the *relaxation time*) is not too large as compared to the external stimuli and the liquid is hence in an equilibrium. It has to be noted at this point, that the relaxation time is proportional to the viscosity via^{13}

$$\tau_p = \frac{\eta}{K_p} \quad (1.2.3)$$

with K_p being a constant and τ_p being the relaxation time for the property p that is measured.⁹ Upon cooling through T_g (i.e. vitrification), the viscosity of the liquid increases dramatically and slows down the motion of structural units, which means that the relaxation time to ensure equilibrium is too large in comparison to the speed of the external stimulus. The positions of the structural units can now be considered frozen, and it can easily be understood that their arrangement depends on the conditions under which vitrification occurred. This is what is generally called the *thermal history*.³

The α -relaxation is the main process of molecular rearrangement in a sample exhibiting a structural relaxation. Here, an isotropic and cooperative rearrangement of the molecules or, in the case of polymers, structural units takes place, which is attributed to the glass transition. In addition to the main α -relaxation, secondary processes such as an excess wing (EW) or a second peak, called the β -relaxation, can be observed in mechanical or dielectric studies in supercooled liquids, as shown in Figure 1.2.3.^{14,15} These relaxations are typically attributed to sterically hindered, anisotropic motions or motions involving only parts of the structural units at $T < T_g$.¹⁶ Systems exhibiting an EW but no β -relaxation are called type A glass formers, whereas systems exhibiting a clearly discernible β -relaxation are called type B glass formers.¹⁶ The secondary processes are shifted to lower temperatures or higher frequencies, respectively. They persist below T_g , thus they are still observable in the glassy state. Contrary to the α -relaxation, the maximum shifts with temperature according to an Arrhenius law and merges with the α -process above T_g .¹⁷ A more detailed explanation of dynamics and relaxation processes as observed in dielectric spectroscopy will be presented in 1.3.3.

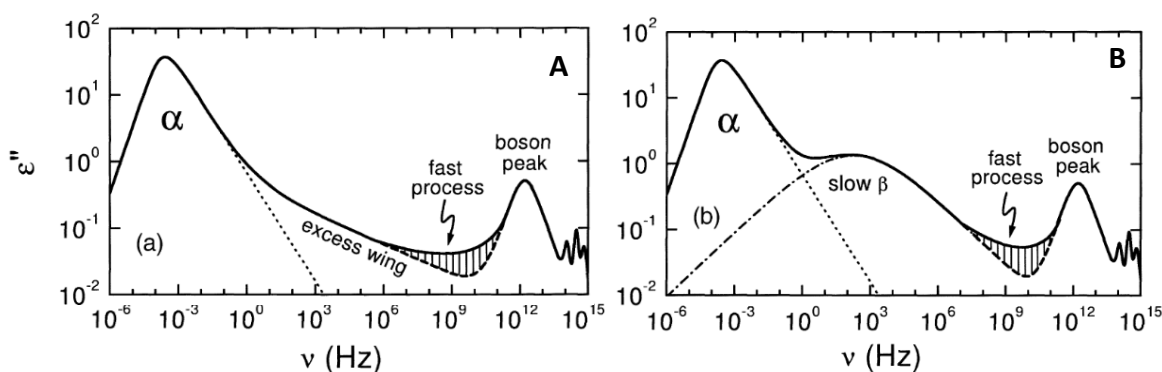


Figure 1.2.3: Schematic depiction of the frequency dependent dielectric loss. A: In type A glass formers; B: In type B glass formers. Reprinted by permission from Springer, ref. 15, © 2003.

1.2.4. Theories of Glass Transition

The exact description of the microscopic mechanisms controlling glass transition are still not completely resolved and represent a highly debated field in solid state physics.⁸ As a detailed analysis would be beyond the scope of this (chemical) work, only the most important theories shall be briefly and qualitatively described.

In 1948, Kauzmann pointed out that upon extrapolation of the entropy of a supercooled liquid during cooling the resulting entropy would, at a certain point, be lower than that of corresponding crystal and the entropy would become zero at finite temperatures.¹⁸ The intersection temperature was thus named Kauzmann temperature T_K . An experimental answer to that paradox cannot be found, as τ would increase above any experimentally accessible time scales already above T_K . Thus, several theories have since been developed, the most important of which are the *free volume model* and the *theory of cooperative relaxations*.

The *free volume theory* was developed by Turnbull and Cohen in the late 1950s.¹⁹⁻²¹ In their idealized approach the structure units exist as hard spheres. They base their theory on the hypothesis of Fox and Flory that the glass transition results from a decrease in the free volume²² and the findings of Williams, Landel, and Ferry who showed that the fluidity φ in the glass transition region depending on the temperature can be described by the Doolittle equation^{23,24}

$$\varphi = A * \exp \left[-\frac{qv_0}{v_f} \right] \quad (1.2.4)$$

with q being a constant, v_0 being the volume, and v_f being the free volume defined by $v_f = \bar{v} - v_0$ and \bar{v} being the specific volume. Turnbull and Cohen postulated that molecules can only diffuse if the total free volume is larger than a critical value $v_{0,c}$. At low temperatures, thermal expansion of a material is derived from vibratory motions of the molecules, thus the added volume will basically be uniformly distributed and the corresponding volume expansion will be near the expansion of the crystalline material, thus no free volume will be added. For higher temperatures, however, more of the added volume will be free creating randomly distributed voids. This reduces the free energy of the system by increasing the configuration

entropy.³ At a certain point, the free volume reaches $v_{0,c}$ where an increase in the diffusion takes place. Thus, the point where $v_{0,c}$ is reached is the glass transition temperature.

A thermodynamic approach was conducted by Gibbs and DiMarzio and Adam and Gibbs that postulated a second order transition below T_g where the configurational entropy disappears instead of taking negative values.^{25,26}

1.2.5. Glassy Materials

There is a huge variety of chemical compositions that glasses can be made of: While only few elements can be brought into the vitreous state, many inorganic minerals are known to form glasses, for example oxides such as SiO_2 or B_2O_3 , Chalcogenides or Halides such as As-S, P-Se, BeF_2 , or ZnCl_2 .³ There is also a number of salts and metal alloys known in the vitreous state, the latter of which is also a very important branch of today's glass research and fabrication. However, all of the before mentioned materials will not play a role in the proceedings of this work and will thus not be further discussed here.

Beside inorganic materials, there has been extensive research and progress on organic glasses that can be divided into two main categories: organic polymers and organic non-polymeric glasses, also called "*molecular glasses*". Organic glasses are of very high importance in several fields of research and industry, from commodity to nanotechnology and pharmaceuticals. Thus, in the following part, organic glasses are discussed in detail.

1.3. Organic glasses - applications and properties

1.3.1. From polymeric to non-polymeric glasses

Beside their evident application as materials to produce discrete goods that we handle every day (from plastic glasses to the CD), polymeric organic glasses have widespread applications in more technological fields. In thin-film processing the amorphous nature of glasses yields uniform films from few nanometers to several micrometers of layer thickness. Organic polymeric glasses have been intensively studied in the last decades as resist materials for several lithographic techniques.²⁷⁻²⁹ Anti-reflective coatings can be realized using amorphous thin films.³⁰ Tunable high refractive-index polymers can be used for several optical elements and waveguide cladding materials.³¹ The incorporation of dyes enables the use as sensor materials in biochemical applications.³²

Polymers were preferentially used as vitrification was long time regarded a privilege of polymeric materials.³³ Due to their long chains and entanglements, crystallization is sterically hindered, thus crystallinity in polymers usually does not exceed 80 %. The presence of sidegroups dramatically influences the crystallization behavior of polymers, where isotactic polymers show a higher tendency to crystallize as opposed to atactic polymers, which often are completely amorphous. Molecular glasses, however, do not consist of long chains of repeating structural motifs, they are rather defined, small organic molecules. Due to the lower stability of the amorphous phase they were hardly used in technological applications until the 1980s. Some pioneering work on stable molecular glasses has been done in 1976, when Sano *et al.* showed that 1,3,5-triaryl-2-pyrazolines are able to form a stable glassy phase at room temperature and well above. The interest in these materials then grew in the late 1980s when Shirota and co-workers examined the use of molecular glasses for electronic and optoelectronic applications.³⁴⁻³⁶ This pioneering work draw the interest of more researchers towards molecular glasses, and since the late 1990s, they are intensively investigated e.g. as photoresists by Matsui *et al.*,³⁷ Ueda *et al.*,³⁸ and Ober *et al.*³⁹⁻⁴¹ As many molecular glasses show favorable electrochemical properties, they have been thoroughly investigated as material for electronic applications, such as OLEDs⁴²⁻⁴⁴ and OFETs⁴⁵. Many drugs have been found to be accessible in the glassy state⁴⁶ increasing their bio-availability.⁴⁷

Some differences are usually attributed to polymeric and non-polymeric glass formers. In general, polymeric glass-formers show a much lower tendency to crystallize, which facilitates their use in applications where amorphous properties are crucial. In lithography applications, polymeric glass formers show a higher pattern stability, whereas molecular glass formers show surface flow at temperatures well below their bulk T_g thereby reducing pattern quality.⁴⁸ However, some advantages of molecular glasses over polymers are based on the simple and defined structure of the molecules as opposed to polydisperse polymers. Molecular glasses can be purified by standard adsorption chromatography. The accessibility of the gaseous phase makes the use of physical vapor deposition (PVD) possible, which enables solvent free processing. Using vaporizable and cross-linkable molecular glasses, all-dry photolithography has been demonstrated by Kryszak, Kolb, *et al.* in 2010.⁴⁹ For nano-lithography it is discussed that the use of non-polymeric glasses will be favorable as macromolecules have a root-mean-square end-to-end distances of 6 – 10 nm which inherently yields defects in the pattern edges of greater than 3 – 5 nm,⁵⁰ being a major issue in current semi-conductor fabrication where the 7 nm node has already been introduced.^{51,52} With non-polymeric building blocks it is supposed to decrease line-edge roughness as compared to polymeric materials.^{53,54} As can be seen, the question of which material is to favor for a certain application has to be answered according to its specific requirements.

1.3.2. The design of molecular glasses – glass transition temperature and glass forming ability

While most polymers can be easily brought into the amorphous state, molecular glasses show an inherent tendency to crystallize. In the past 30 years, a lot of effort has been put into the understanding of how to design molecules in order to obtain a stable, high- T_g amorphous phase. A general rule of thumb has been found early on for many systems forming a stable amorphous state (including polymeric and inorganic systems) that $T_g/T_m \approx 2/3$ in absolute temperature,^{55,56} although deviations were found. It is generally agreed upon that increasing this ratio increases the stability of the amorphous state.⁵⁷ However, these observations are mainly phenomenological. A more fundamental approach was conducted by Naito and Miura in 1993 and 1994, respectively. Based on thermodynamic calculations they worked out

guidelines for the design of molecular glasses and demonstrated that highly symmetric, globular, rigid, and dense molecules form stable organic glasses with a high T_g .^{56,58} While asymmetric molecules would reduce the maximum crystal-growth velocity (MCV) thereby increasing the stability of the amorphous phase, they also increase the entropy of phase transitions between T_g and T_m , $\sum \Delta S_{tr,m}$ which consequently decreases T_g . Furthermore, intramolecular dipole-dipole interactions should be minimized for low MCV . Nevertheless, highly interacting groups may also contribute to a high T_g , however, this usually goes hand-in-hand with a higher tendency for crystallization.^{59–62} Usually, an increase in molar mass and the introduction of rigid substituents is associated to increase the T_g of a corresponding material.

The interdependence of glass transition temperature and molar mass M for a given polymer was reported by Fox and Flory in 1950: They observed that T_g increases with increasing M for low values of M , saturating at a certain point.²² In contrast to polymers, T_g of molecular glasses does not show any saturation as reported by Novikov and Rössler.⁶³ This is shown in Figure 1.3.1. Furthermore, a general trend that T_g and M are linked by a power-law function of the form

$$T_g \propto M^\alpha \quad (1.3.1)$$

with $\alpha \approx 0.5$ was observed. While this trend holds as an approximation for the *entirety* of molecular glasses, it generalizes over many different architectures and substituents resulting in a large scatter of data. However, specific interaction cannot be ignored. The influence of specific, especially polar moieties on T_g has so far not been investigated in detail. If one extracts T_g and M data of systematic investigations of molecular glasses, one finds that the correlation of $T_g \propto M^{0.5}$ is approximately consistent. Examples include tris(aryl)benzene glasses, where $\alpha \approx 0.3$ for naphthyl and $\alpha \approx 0.7$ for anthracyl substituents,⁶⁴ or a group of cyclic stilbenes, where T_g increases with increasing ring size, resulting in $\alpha \approx 0.5$.⁶⁵ For several applications, it would be beneficial to increase T_g while at the same time keeping the molar mass low. This is especially the case where the accessibility of the gaseous phase is required. However, in current literature a study of how to obtain stable high- T_g glasses with little increase in M is missing. This might be achieved by the introduction of highly polar moieties. In this case, however, the material has to be optimized in order to maintain a good glass forming ability, as strongly interacting groups favor crystallization.

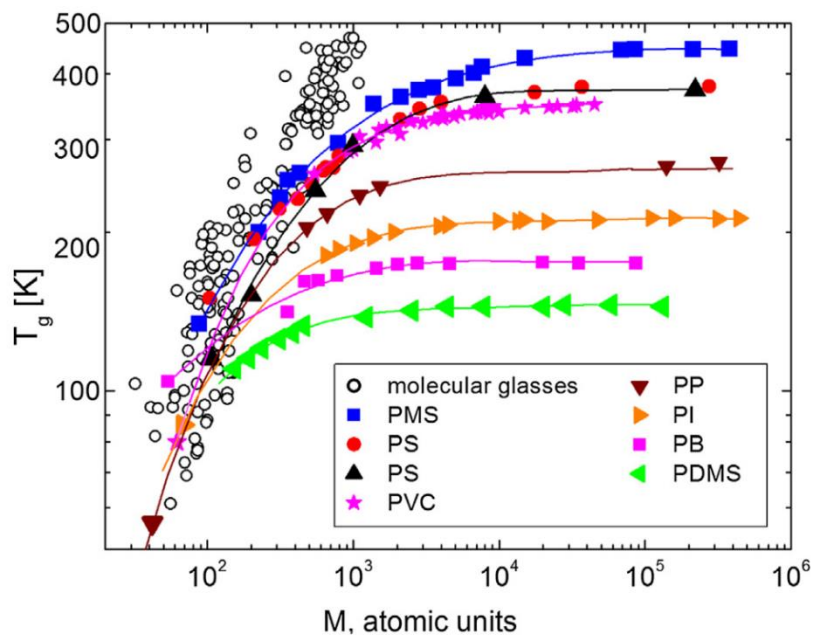


Figure 1.3.1: Dependence of T_g on M for selected polymers and a comprehensive amount of molecular glasses. A linear relationship is observed for molecular glasses. Reprinted from Ref. 63 with permission from Elsevier, ©2013.

1.3.3. Dynamics in organic glasses as studied by dielectric spectroscopy – from neat to binary systems

In the following, a fundamental overview of the most important relaxation features that can be observed in dielectric spectroscopy of organic glasses is presented with a special attention to characteristics that are important for the proceedings of this work.

1.3.3.1. Relaxations in dielectric spectroscopy

Due to its capability to cover a frequency range of up to 16 decades, broadband dielectric spectroscopy (DS) has played a major role in examining the dynamics of liquids. Its principle was first described by Debye 1927.⁶⁶

The interaction of an electromagnetic field with matter yields fluctuations of the molecular dipoles. The response of these dipolar systems is a complex function of the form^{67,68}

$$\varepsilon^*(\omega) = \varepsilon'(\omega) - i\varepsilon''(\omega) = \varepsilon_\infty + \Delta\varepsilon \int_0^\infty -\frac{d\phi(t)}{dt} e^{-i\omega t} dt \quad (1.3.2)$$

where ε^* is the complex dielectric function, with ε' being the real part or the dielectric storage and ε'' being the imaginary part or the dielectric loss. $\omega = 2\pi\nu$ is the angular frequency, ε_∞ the high frequency permittivity, and $\phi(t)$ the step-response function.

As already mentioned in 1.2.2, relaxation can be understood as the readjustment of a system to an external stimulus. If this stimulus, however, is fast as compared to the relaxation time, the system is too slow to follow the stimulus. For a very slowly changing electric field, the dipoles of the involved molecules may rearrange along with the external field. This goes along with a plateau in ε' with the value ε_s . With an increasing frequency, the dipoles may not follow anymore, resulting in a step-wise decrease in ε' to a lower plateau, ε_∞ . The dielectric relaxation strength $\Delta\varepsilon$ is defined as $\varepsilon_s - \varepsilon_\infty$ and is linked to the molecular dipole moment.

Along with the step in $\varepsilon'(\omega)$ a peak occurs in the dielectric loss spectrum $\varepsilon''(\omega)$. As $\varepsilon'(\omega)$ and $\varepsilon''(\omega)$ are interrelated both carry the same information, thus the relaxation strength may also be calculated by the area under the loss peak.⁶⁹ Figure 1.3.2 schematically shows $\varepsilon'(\omega)$ and

$\epsilon''(\omega)$ for a Debye relaxation. The Debye relaxation time τ_D for a given temperature can then be calculated with the frequency of the peak maximum of the dielectric loss function ω_p according to

$$\omega_p = 2\pi\nu_p = 1/\tau_D \quad (1.3.3)$$

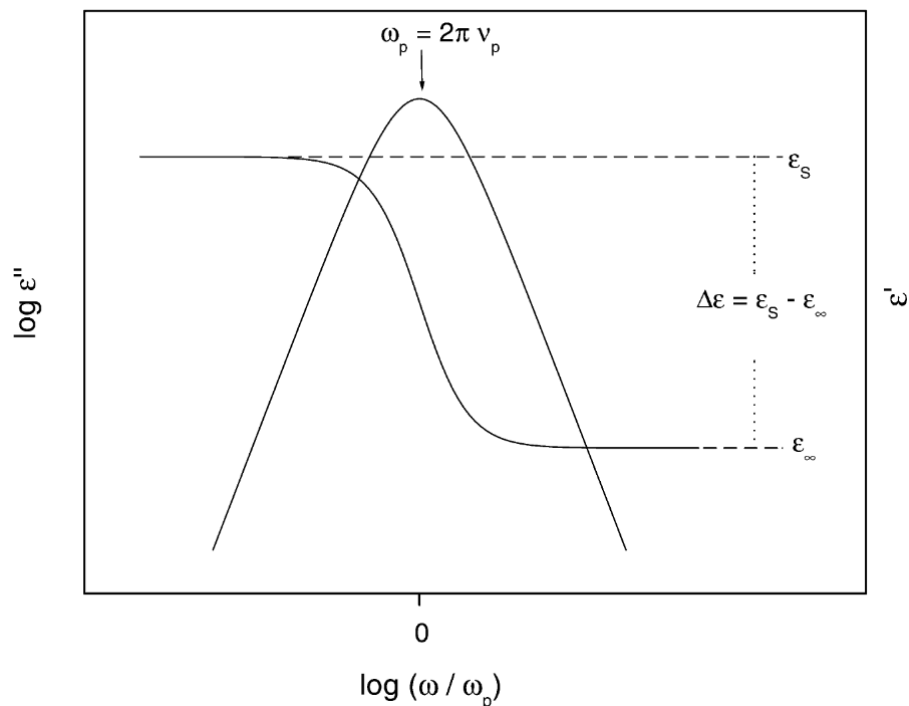


Figure 1.3.2: Dielectric storage (ϵ') and dielectric loss (ϵ'') as a function of the normalized frequency for a Debye-relaxation. Reprinted by permission from Springer, ref. 69, ©2003.

1.3.3.2. Main relaxations

For the Debye relaxation as depicted in Figure 1.3.2, a step-response function $\Phi(\tau)$ according to the exponential function⁶⁸

$$\Phi(\tau) = \exp\left(-\frac{t}{\tau_p}\right) \quad (1.3.4)$$

can be found. However, a Debye-relaxation is usually not observed in dielectric measurements. In main relaxations (also referred to as α -relaxations), a broadening especially on the high-frequency flank changes the appearance of the dielectric loss peak. The corresponding function can then be described by a stretched exponential function of the form⁶⁸

$$\Phi(\tau) = \exp\left(-\frac{t}{\tau_p}\right)^{\beta_{KWW}} \quad (1.3.5)$$

where β_{KWW} is the stretching parameter being between 0 and 1 and typically between 0.4 and 0.85 for neat glass formers.⁷⁰ For $\beta_{KWW} = 1$ this function becomes the Debye function. It was originally developed by Kohlrausch in 1847 to describe the creep of metals⁷¹ and later rediscovered by Williams and Watts to describe the relaxation as observed in dielectric spectroscopy.⁷² Examples of dielectric loss peaks that can be described with the Fourier transform of a Kohlrausch function are presented in Figure 1.3.3A.

Further functions have been developed in order to describe the distribution of relaxation times by Cole and Cole,^{73,74} Cole and Davidson,⁷⁵ and Havriliak and Negami,⁷⁶ but their detailed explanation would go far beyond the scope of this work.

In general, frequency-time superposition (FTS) applies for the α -process itself. That means that the shape of the process and thus the obtained function does not change with temperature. The curves can be superimposed to a master curve by shifting along the X-axis and slightly along the Y-axis to adjust for the Curie law.⁷⁷ An observed change with temperature is only because of the occurrence of secondary processes and its different relative weights so that the curve of the α -process gets spoiled.⁷⁸

In the recent decades a broad range of organic glasses has been analyzed. Still, a clear correlation between the structure of a compound and the shape of its relaxation process cannot be drawn, although several theories have been postulated recently. Nielsen *et al.* in 2009⁷⁹ and later Paluch *et al.* in 2016⁸⁰ reported a correlation between the dielectric strength (i.e. the dipole moment) and the stretching parameter in a study of “almost all” organic glasses studied by dielectric spectroscopy so far: The higher the dielectric strength, the higher is the stretching parameter, as schematically shown in Figure 1.3.3. Figure 1.3.3A shows this correlation exemplarily for Propylene carbonate and toluene along with the shape of the alpha relaxation in ϵ'' . For propylene carbonate showing a high dipole moment of 4.9 D and thus a high relaxation strength, β_{KWW} is 0.78, whereas for toluene with a low dipole moment of 0.36 D, β_{KWW} is 0.50. The collection as presented in ref⁸⁰ is shown in Figure 1.3.3B as a plot of $\Delta\epsilon$ vs. β_{KWW} .

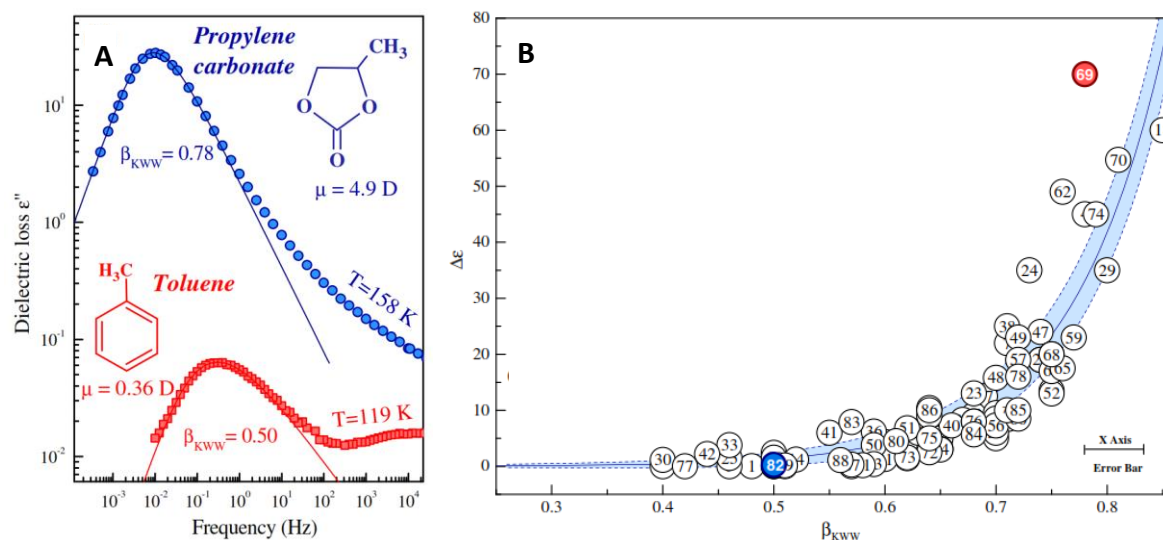


Figure 1.3.3: A: Dielectric loss and stretching parameter shown exemplarily for propylene carbonate and toluene, B: Correlation between dielectric strength ΔE and Kohlrausch stretching parameter β_{KWW} for a collection of “almost all” organic glasses studied so far. Reprinted figures with permission from ref. 80, ©2016 by the American Physical Society.

A further study of the shape of the alpha relaxation was done by Gainaru in 2019.⁸¹ Originally comparing viscoelastic relaxation data for simple materials (i.e. materials that do not form superstructures) it was seen that simple scaling by ω_α (with $\omega_\alpha = 1/\tau_\alpha$) and $F(0)$ (being the steady-state flow at low temperatures) results in a generic master curve up to frequencies that are four decades above ω_α . These results were then connected to the findings of Paluch *et al.* proposing a generic high-frequency flank of the susceptibility data (Figure 1.3.4). As can be seen, the susceptibility data of several compounds follows a master curve on the high frequency flank. All compounds follow that master curve until the occurrence of the α -relaxation peak. As a decreasing slope on the high-frequency flank is observed one can understand why compounds exhibiting a higher dielectric strength show a higher value for β_{KWW} , i.e. a higher initial slope.

Only recently, a study focusing on differently polar endgroups (namely OCH_3 and CF_3) attached to a stiff and big core-unit showed that these endgroups mainly determine the dielectric behavior of the whole molecule.⁸² However, this study only involved two compounds, therefore more data is needed before a generalized assertion on the influence of polar endgroups on the dielectric response of large and stiff molecular glasses can be made. Clearly, the relaxation process is still a highly debated topic in current literature and more data and insights are still needed for a thorough understanding.

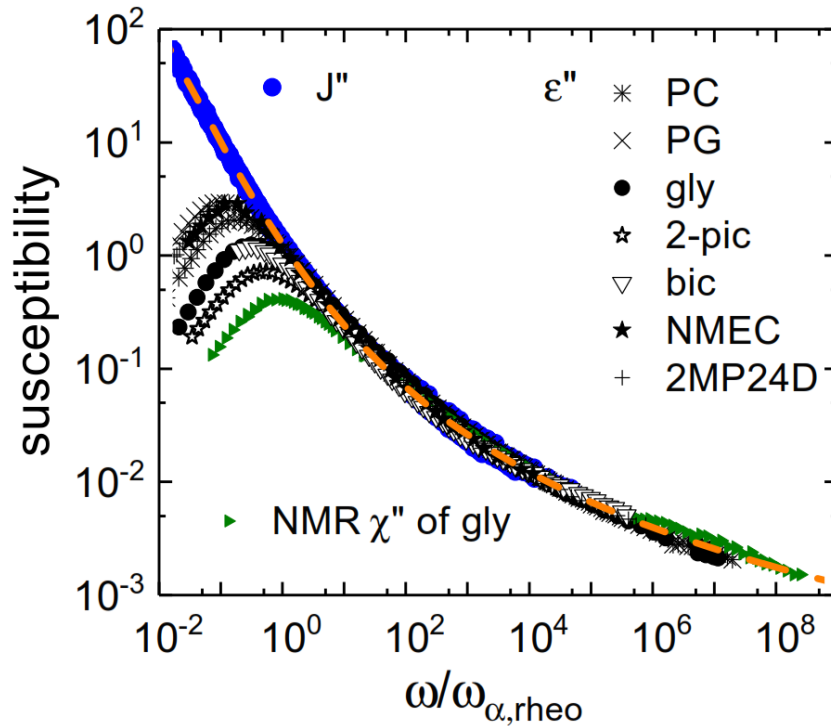


Figure 1.3.4: Generic α -relaxation of several simple glass-formers. Reprinted figure with permission from ref. 81, ©2019 by the American Physical Society.

1.3.3.3. Secondary relaxations

As already pointed out in 1.2.2, beside the α -relaxation secondary relaxations may appear in relaxation spectra. These occur at shorter time-scales or lower temperatures, respectively, and may include an excess wing (EW), a β -relaxation, or fast dynamics and the boson peak (see also Figure 1.2.3). This section focuses on the occurrence of the EW and the β -relaxation.

In comparison to the well-researched α -relaxation, fewer attention has been paid to the β -relaxation. In contrast to the α -relaxation, β -relaxations exhibit a thermally activated Arrhenius behavior below T_g , i.e.

$$\tau_\beta = \tau_\infty \exp(E_A/RT) \quad (1.3.6)$$

with τ_∞ being a prefactor usually in the range of $10^{-13} - 10^{-16}$ s.^{16,83} The process shows a wide and symmetric, temperature-independent distribution of relaxation times $g(E)$. While below T_g , $\Delta\varepsilon_\beta(T)$ is almost constant, it shows a strong increase at temperatures above T_g .⁸⁴ Furthermore, at temperatures above T_g , a tendency of the β -process to merge with the α -

process is observed. The behavior of the β -process below and above T_g is shown in Figure 1.3.5 for Tripropyl phosphate (TPP), a well-investigated molecular glass former with a T_g ($\tau_{T_g} = 100$ s) of 134 K.^{85,86} Below T_g , the β -process is very broad, clearly separated from the α -process, and its intensity is only weakly increasing with temperature. Above T_g , however, its intensity drastically increases and the separation from the α -process gets weaker until, eventually, no discernible β -process can be observed anymore.

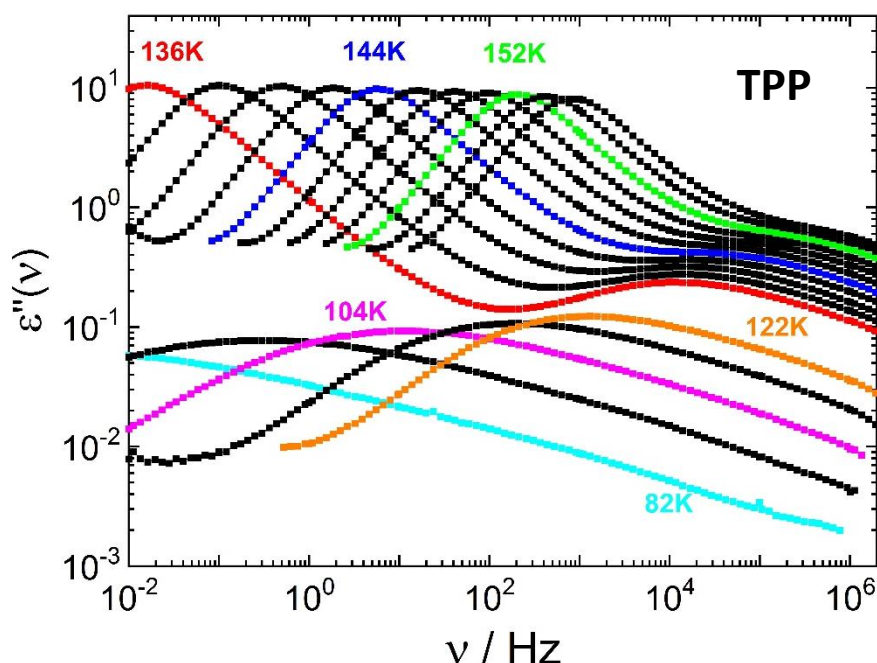


Figure 1.3.5: Dielectric susceptibility spectra of TPP with selected temperatures shown in color as indicated.

The origin of the β -process is still a debated topic in literature. Early studies in glasses suggested hindered internal molecular modes as the source of these relaxations. This is true for some glass formers like some polymers but also molecular glasses such as 1,1'-bis(methoxyphenyl)cyclohexane where the rotation of the methoxyphenyl moiety causes the observed β -relaxation.⁸⁷ However, in 1970 Johari and Goldstein discovered clearly discernible secondary relaxations in rigid molecules such as chlorobenzenes or *o*-terphenyl.⁸⁸ Thus it was concluded that these secondary relaxations are an intrinsic feature of the glassy state. The corresponding kind of relaxation that could be seen in rigid molecules was hence called *Johari-Goldstein (JG) β -relaxation* and the term was later employed to any secondary relaxation involving the whole structural unit. Loosely packed regions in the glass, i.e. heterogeneities of the material may account for this relaxation. These *islands of mobility* have been discussed by

Johari.⁸⁹ Also, local vibrational modes have been considered from Goldstein⁹⁰ and Johari and Goldstein.⁸⁸ However, NMR experiments proved that all molecules take part in this process making it a cooperative process.⁹¹ Furthermore, a small amplitude ($< 10^\circ$) reorientation was revealed as the origin of this relaxation in toluene, a so-called wobbling within-a-cone.⁹¹

Measurements under elevated pressure showed that the “generic” JG β -process shows the same $T - p$ dependence as the α -process, in contrast to β -processes reflecting peculiarities of the respective structural unit. Therefore, it is concluded that the JG β -relaxation is a precursor of the α -relaxation, the slower dynamics of the latter being linked to a higher cooperativity or restricted motion.^{83,92} Physical aging of the sample results in a decrease of the relative strength of the JG β -relaxation in comparison to the α -relaxation.⁸⁸

Notably, the apparent activation energy of the β -process is in the order of $24 T_g$ for many investigated systems.¹⁶ Although several exceptions were found after the initial reports by Kudlik *et al.*,⁹³ it is still remarkable that completely different systems, such as e.g. toluene and poly(butadiene), share this property. However, it is still not clear if there is any factor, e.g. the structure of the molecule or the origin of the β -process, which plays a role in the apparent activation energy of the β -process.

While the β -process can be investigated quite well below T_g , many questions still arise for its merging behavior with the α -process at temperatures above T_g . Due to the increasing superimposition of both processes, a separate evaluation becomes difficult. Clearly, the Arrhenius behavior as observed in the glassy state is not continued. In contrast, a stronger temperature dependence can be observed.⁹⁴ Due to the strong increase of the relative relaxation strength, it is discussed that the β -relaxation takes over the entire relaxation strength upon merging.⁹⁵ However, no widely accepted model for the merging behavior of both processes has been proposed yet.

The excess wing manifests itself as a decreasing slope of the high-frequency flank of susceptibility spectra (see also Figure 1.2.3). Its origin may either be hidden secondary relaxations that may be separated by aging or pressure^{96,97} or it can be regarded as an intrinsic feature of the α -process.⁹⁸

1.3.3.4. Relaxations in asymmetric binary systems

Asymmetric binary systems can be understood as mixtures of two completely miscible materials with a big contrast in T_g . A typical example would be a polymer / plasticizer mixture, in which a low molecular weight component is mixed with a polymer to decrease T_g of the polymer, or a miscible polymer blend with a high T_g -contrast of the investigated polymers. In early works, only one T_g was observed in DSC measurements which was then claimed to be a necessity for miscibility.⁹⁹ Later works, however, demonstrated the occurrence of two distinct T_g s.¹⁰⁰ An example of this is depicted in Figure 1.3.6 from Pizzoli *et al.* who studied the glass transition of a system consisting of Polystyrene (PS) and Tritolylphosphate (TTP).¹⁰¹ DSC curves for low concentrations of PS reveal two steps corresponding to two T_g s. The plot of the respective T_g s attributes two characteristics of such binary systems: For the high- T_g component, a strong plasticizer effect occurs as identified by the strong decrease of its T_g with increasing amount of plasticizer. In contrast, the opposite occurs for the low T_g component, albeit in a weaker fashion: With increasing amount of the high- T_g component, the T_g of the low- T_g component increases in the sense of an anti-plasticizer effect.

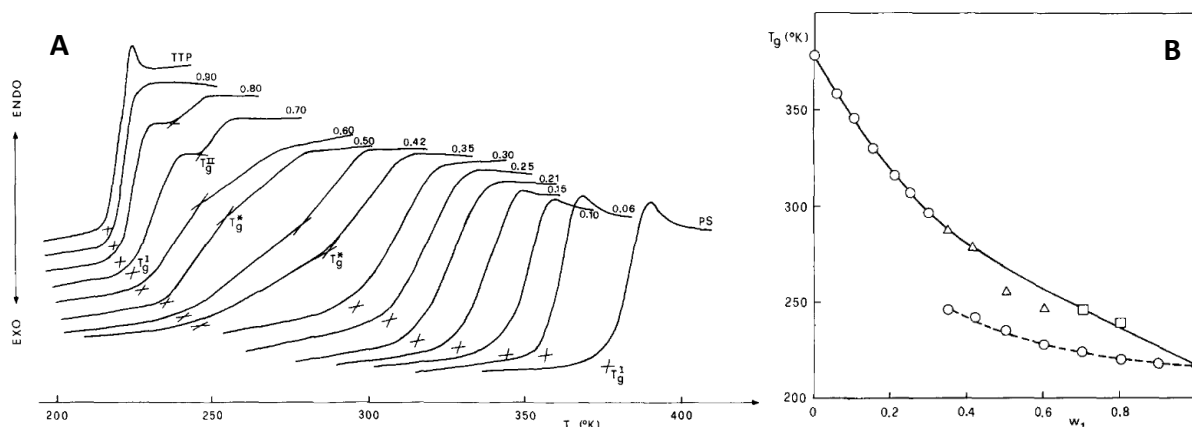


Figure 1.3.6: A: DSC-curves for the system Polystyrene (PS) and Tritolylphosphate (TTP) at different concentrations. B: Plot of respective T_g s. The lower curve corresponds to the T_g of TTP, the upper curve to the T_g of PS. Reprinted from ref. 101 © 1987 with permission from Elsevier.

Several studies on the dynamics of such systems have been carried out in the last decades.^{102–105} In general, two independent relaxations can be discovered in such systems. Furthermore, a broadening of the relaxation peaks is usually observed. This was first shown in the early work of Hains and Williams for non-polar Polystyrene mixed with a highly polar, small “probe”

molecule such as tripropyl phosphate (TPP) or dioctyl phthalate (DOP). Revealing only the dynamics of the probe molecule in DS due to its high polarity, two clearly separated α -processes could be observed for small probe concentration $< 50\%$.¹⁰² Adachi and Ishida revealed a similar behavior for the system Poly(methyl acrylate) / Toluene.¹⁰⁶ Beirnes and Burns demonstrated at the same time that these effects can also be detected calorimetrically.¹⁰⁷ In general, strong dynamic heterogeneities can be found in such systems.¹⁰⁸ Since no macroscopic phase separation is observed, it has been proposed that thermally driven concentration fluctuations^{109–111} or a *self-concentration effect*^{111,112} arise. The latter emerges because in polymers a structural unit is always connected to two other structural units. This leads to a localized concentration shift, which is different from the macroscopic concentration.^{104,112} Consequently, this behavior can be out-ruled for non-polymeric glass formers due to the absence of covalently bonded structural repeating units.¹¹³

Asymmetric, binary system were intensively studied by Blochowicz *et al.*^{114,115} and Bock, Kahlau, *et al.*^{105,116} who discussed intrinsic confinement effects, in which small probe molecules exhibit their own, fast dynamics in a frozen matrix, the latter being below its respective T_g . Such behavior was already reported previously for liquids being confined in porous space such as silica.^{117–119} In all dielectric studies reported by Blochowicz, Bock, and Kahlau the dynamics were exclusively probed for the additive as it showed significantly higher dipole moment as compared to the matrix. Still, two α -relaxation peaks for the additive could be identified. This means that there exist two sub-ensembles of additive molecules one of which is coupled to the matrix and thus slaved to its slow dynamics (α_1 -process, long time-scale), the other of which is highly decoupled exhibiting its own fast dynamics (α_2 -process, short time-scale). Furthermore, a strong broadening of the DS spectra for the α_2 -process is observed with decreasing additive concentration. Accordingly, two-phase spectra can be identified in NMR-spectroscopy over a broad temperature range, which are a sign for pronounced dynamic heterogeneities that are usually not observed in neat glass formers.^{120,121}

A thorough insight was given by Kahlau, Bock *et al.* in a study using deuterated Polystyrene (PS) as matrix and Tripropyl phosphate (TPP) as additive. Using DS, the dynamics of the additive could be revealed. Using ^2H -NMR to selectively probe the α_1 -process of the matrix it was shown that its dynamics essentially remain the same except for a temperature shift due

to a plasticizer effect. The α_2 -process, however, shows a different behavior such as the failure of FTS in DS spectra. Furthermore, the α_2 -process shows a transition of a Vogel-Fulcher behavior to an Arrhenius behavior for low additive concentrations below the respective T_g of the matrix, a so-called *fragile-to-strong* transition. Since the activation energy of this process decreases with decreasing additive content also T_g decreases upon extrapolation to $\tau_{T_g} = 100$ s.¹⁰⁵ This means that a maximum in T_g of the additive within the investigated concentration range is found, as can be seen in Figure 1.3.7. ^2H - and ^{31}P -NMR spectroscopy selectively probing one of each components proved this process to be of isotropic nature, thus clearly distinguishing it from a sterically hindered β -process.¹¹⁶ Furthermore, two-phase spectra were observed within an interval of about 100 K revealing pronounced dynamic heterogeneities for TPP. The features that are observed in these binary system such as the pronounced dynamic heterogeneities and the *fragile-to-strong* transition are also observed in experiments and simulations in confined space^{122–125} Also, mode-coupling theory predicts such a dynamic decoupling of large and small particles when differing enough in size.^{126–128}

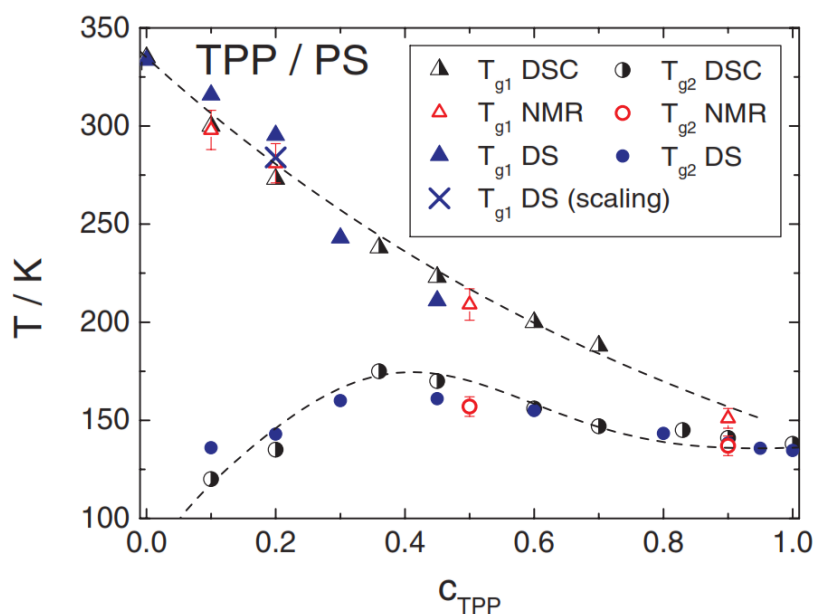


Figure 1.3.7: T_g s of mixtures of PS and TPP with various concentrations as observed by DS, DSC, and NMR as shown in Ref. 105.

The local maximum of the concentration-dependent $T_{g,2}$ -curve was later confirmed for mixtures of a high- T_g molecular glass former with a low-molecular additive. However, demixing and crystallization effects of the matrix prevented the measurement of the entire

temperature and concentration range.^{129,130} Nevertheless it could be shown that the crossover from the super-Arrhenius Vogel-Fulcher behavior to an Arrhenius behavior for the α_2 -process occurs at temperatures around T_g of the α_1 -process, thus at the moment where the dynamics of the matrix become frozen. Still, establishing a system of highly asymmetric molecular glass formers that show neither crystallization nor demixing is necessary to confirm the observed behavior and to gather data over the entire concentration and temperature range.

The local maximum of the concentration-dependent $T_{g,2}$ -curve is still a highly debated topic in the scientific community. Conducting experiments at elevated pressure, Ngai *et al.* interpreted the α_2 -process at lower additive concentrations as a JG β -relaxation of the matrix with the *true* α_2 -process being hidden below.^{131,132} Accordingly, in their interpretation $T_{g,2}$ shows a monotonous increase with decreasing additive concentration.

Regarding the β -process of the additive in such asymmetric, binary systems it was shown in the case of PS/TPP as well as of a molecular glass/TPP that the time constants of the β -process do not change upon mixing. Furthermore, a participation of the high- T_g matrix in the β -process of the additive was observed. In other words: The small additive molecules “*enslave*” the big matrix molecule to perform some highly restricted reorientation at temperatures far below the respective T_g of the matrix.^{116,121,133}

1.4. Micro- and Nanolithography

1.4.1. Photolithography from 1960 until today

As photolithography is the main process of micro- and nanomanufacturing from the very beginnings of the semiconductor industry until today, its principles are briefly described in this section.

The history of the manufacturing of integrated circuits is closely connected to the evolution in micro- and nanolithography. As the technology of computation advanced through World War II, some devices reached a level of complexity that was too high for the techniques being used. Devices consisting of thousands of vacuum tubes suffered failures and downtimes whose losses exceeded the benefits.¹³⁴ The need to reduce the number of components of such systems was apparent. In 1947, the first transistor was built at the Bell Laboratories.¹³⁵ 12 years later, Jack Kilby, who was awarded the Nobel Prize in 2000, built the first working integrated circuit.¹³⁶ At the same time photolithography was invented. The first to use this term were Lathrop and Nall, who at this time were working for US military to improve proximity fuses.¹³⁷ From that day onwards, photolithography with subsequent pattern transfer was the main method in the production of Integrated Circuits (ICs).¹³⁸ The general scheme of this process is shown in Figure 1.4.1. Here, exemplarily, a Silicon wafer with an oxide layer (A) is coated with a negative-tone resist (B). Upon exposure to UV-light (C), this resist material undergoes a change in its chemical structure, making it insoluble for a certain solvent. This solvent is called *developer* and washes unexposed photoresist off the wafer (D). The now bare SiO₂ can then be etched with HF (E) and the exposed resist is afterwards washed away with e.g. an acid such as H₂SO₄ (F). While SiO₂ is the most common substrate material in lithography, also other materials are used depending on the application, such as Si₃N₄¹³⁹ or semiconductors from other elements as silicon such as Gallium (in form of GaAs, GaN, GaP, GaSb) or Indium (in form of InAs, InSb, or InP). Positive-tone photoresists can also be used, in this case the exposed photoresist is dissolved and thus removed by the developer.

Negative-tone photoresists usually work on the principle of UV-polymerization, where a photo-induced polymerization forms a polymer that is insoluble in the developer. Examples include the widespread SU-8 consisting of an epoxy resin that crosslinks upon irradiation with

the help of an acid, generated by a photo-acid generator (PAG), or Kodak KTFR which is an azide-sensitized poly(isoprene) rubber.¹³⁸

A typical positive-tone resist is poly(methylmethacrylate) (PMMA), where the polymer depolymerizes due to photo-induced chain scission leaving easier soluble oligomer or monomer behind.^{140,141} Another typical positive-tone resist is the two component system of a Novolak Resin with a photoactive diazoquinone ester. Here, the diazoquinone ester is acting as a dissolution inhibitor for the resin in aqueous solvents. However, after exposure the generated carboxylic acid enhances the solubility of the novolak resin in basic developers.¹⁴²

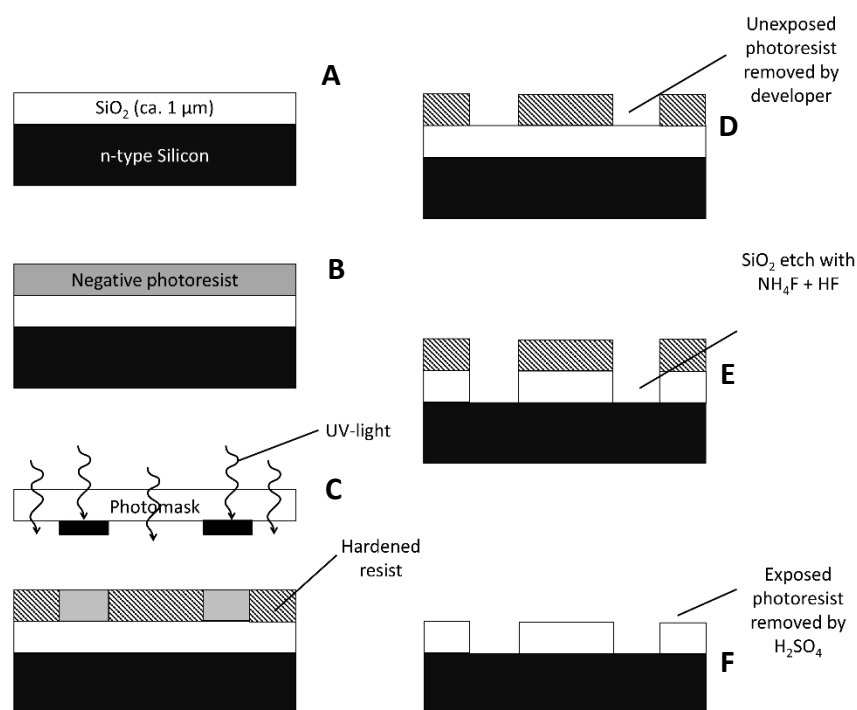


Figure 1.4.1: Scheme of a photolithographic process using SiO_2 and a negative tone photoresist.

Soon after the invention of the integrated circuit, Gordon Moore of Fairchild found that for chip production there is an optimum cost of a single component of an IC with respect to the total number of components in the IC.¹⁴³ This optimum is the best compromise between higher fabrication costs for smaller structures and non-effective material exploitation if the structures are too large. In his first publication, he predicted an annual doubling of the components per IC, which later was corrected to a doubling every 18 months. This became

known as *Moore's Law* and is regarded as a self-fulfilling prophecy based on empirical observations rather than a natural law.

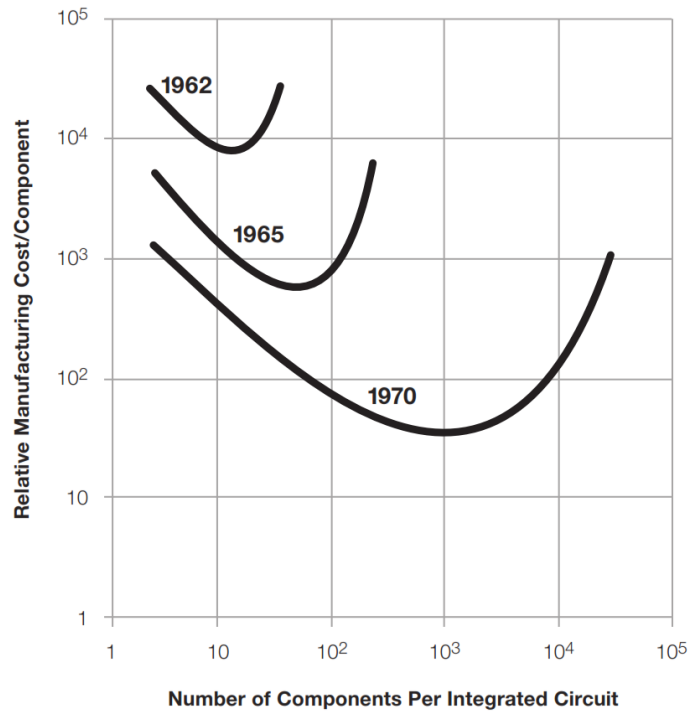


Figure 1.4.2: Moore's Law: Original plot of relative manufacturing costs per component versus number of components per IC with respect to the year. Reprinted from ref. 143.

The fulfilling of Moore's Law would not have been possible in the recent decades if advances in lithographic technology had not enabled the fabrication of ever smaller feature sizes. For the widely used project lithography, the resolution limit R is given by the Raleigh equation¹⁴⁴

$$R = k_1 \frac{\lambda}{NA} \quad (1.4.1)$$

with k_1 being a constant dependent on the photoresist, optics, and process conditions, λ being the wavelength of the light and NA the numerical aperture of the lens. That means that for a higher resolution, k_1 and λ have to be minimized and NA to be maximized. As for k_1 , 0.25 is seen as the limit with 0.28 being used as of 2010.¹³⁸ The wavelength that has been used for the lithography since the mid 2000's was 193 nm being generated by an ArF excimer laser. As the resolution limit of this technique was foreseeable, immersion lithography was introduced allowing for higher NA than 1 with 1.35 being used in 2010.^{142,145} With this technique, an overall resolution of 40 nm was achieved for a single pattern. Using multi steps with several layers, the limits of 193 nm lithography were further pushed to the 10 nm process being used

by Samsung and Intel since 2017 and 2018, respectively, for the production of the 10 nm node.¹⁴⁶ As classical 193 nm lithography has already exceeded the expected resolution limits, the need for a new lithography technique was apparent. Currently, extreme ultra-violet (EUV) lithography is introduced into the market and already used for the production of the 7 nm node.¹⁴⁷ EUV-Lithography uses plasma to create 13.5 nm photons. The extreme shift in the wavelength from 193 nm to 13.5 nm brought many challenges. As lens materials are opaque for these low wavelengths, no conventional masks can be used. The technique rather requires a series of mirrors.¹⁴⁸ Also, the mean free path for photons of this wavelength in air is only a few millimeters, requiring exposure in vacuum. All these new challenges drastically increase the costs for the production process.

An inherent disadvantage in EUV lithography is the trade-off between resolution, line-edge roughness, and sensitivity.^{149–151} In order to improve the process, current research puts a lot of effort into the development of new materials. Currently, many resist types are being investigated, such as molecular resists, inorganic resists, or chemically amplified resists.¹⁵² A promising resist material has been introduced by the group of Ober.^{50,150} Here, a ZrO₂-methacrylic acid nanocluster with a size of only 1.7 nm serves as resist material exhibiting a high sensitivity towards EUV, a low line-edge roughness and superior etch resistance. Due to its small size, it overcomes the issue of a high mean end-to-end distance as present in polymeric resists.

1.4.2. Alternative lithographic techniques

Due the need of expensive optical systems such as masks (for classical photolithography) or mirrors (for EUV lithography) the prototyping of devices becomes a time and cost-consuming process. The high costs for their production can make low-volume production of certain devices unfeasible. Therefore, other lithographic techniques are needed to address this issue. In the following, the most important regularly used alternative lithography techniques are briefly described.

1.4.2.1. Nanoimprint Lithography

Nanoimprint lithography (NIL) was invented by Princeton professor Stephen Chou in 1996.¹⁵³ Here, a nanopatterned stamp is pressed onto a viscous material. Typically, the material is either above T_g and cooled before the stamp is removed (hot embossing), or the material is cured by e.g. UV radiation to maintain its shape after stamp removal (UV-based NIL). NIL only plays a minor role in today's nanomanufacturing, although it has some advantages such as cost-effectiveness and simplicity by not requiring expensive optics and being capable of creating extremely small structures down to 5 nm. It is mostly used for some non-semiconductor applications¹⁵⁴ due to limitations in defectivity, overlay, and throughput, preventing it from becoming a challenger for EUV lithography. For hot-embossing, PMMA was the first reported material to be patterned by NIL. UV-based NIL uses UV-curable photo resists being based on the same mechanism as UV photolithography. A different approach was used by Probst *et al.* who used Azobenzene-containing molecular glasses in a non-thermal approach.¹⁵⁵ Using a PDMS-stamp and UV-light, the azo-group was reversibly switched from cis- to trans-configuration at room temperature, i.e. below T_g of the material. This lowers the viscosity of the film by transferring it into a photofluidic state, allowing the filling of the stamp's cavities.

As a disadvantage of NIL, the stamp has to be produced by another lithographic method such as optical or e-beam lithography. Furthermore, due to repeated contact with the resist, the stamp is subject to wear and tear, which may require replacement after a certain number of patternings.

1.4.2.2. E-beam lithography

E-beam lithography is a maskless technique where an electron beam is used to induce changes in a material. As such, the mechanisms behind e-beam lithography are very similar to those in conventional photolithography. Although e-beam lithography is capable of creating structures with single-nanometer resolution, its applicability is limited as high-throughput and sub-20 nm resolution cannot be achieved at the same time.¹⁵⁶ Furthermore, due to scattered electrons, the proximity effect creates errors in written structures¹⁵⁷ and due to limited field size, stitching errors in the order of written structures (i.e. 10 nm) may occur.¹⁵⁸ Due to these

drawbacks, the application of e-beam lithography is mainly limited to mask production, low-volume fabrication, as well as research and development where rapid prototyping is required.

PMMA is used as a standard resist material for e-beam lithography. Upon UV-exposure, chain scission of the polymer increases its solubility in organic solvents. At the same time, a polymerization process occurs in areas of very high intensity of exposure which crosslinks the polymer to an insoluble network.¹⁵⁹ This opens the opportunity for PMMA to be used as a dual-tone resist: With low doses, the chain scission is the dominant reaction occurring, and PMMA can be used as a negative tone resist. With high doses, the crosslinking reaction becomes dominant enabling the use of PMMA as a positive tone resist. Sub 10 nm features have already been demonstrated using PMMA.¹⁶⁰ Another frequently used material is hydrogen silsesquioxane (HSQ), a silicon-based amorphous material that crosslinks upon exposure, making it a positive tone resist with promising patterning behavior.¹⁵⁹

1.4.2.3. Scanning Probe Lithography

The history of scanning probes dates back to the year 1981 when Binnig and Rohrer invented the Scanning Tunneling Microscope (STM)¹⁶¹ earning them the Nobel Prize in physics in 1986. Using an STM, imaging of a surface was now possible with unprecedented accuracy. The achieved lateral resolution is down to 1 Å and the vertical resolution down to 0.1 Å.¹⁶² The invention of the STM was followed by the invention of the Atomic Force Microscope (AFM), by Binnig and coworkers, in 1986.¹⁶³ Soon it became apparent, that Scanning Probes are not only able to detect features on the nanoscale, but also to manipulate features on the nanoscale. This was demonstrated in 1990 when the logo “IBM” was written by an STM using 35 Xe-atoms by scientists of IBM’s Almaden laboratory.¹⁶⁴

Due to the variety of processes that can be controlled using a sharp tip, several approaches have been examined for Scanning Probe Lithography (SPL) in recent years, most of which are based on an AFM.¹⁶⁵ The different methods can be classified by the nature of the process that they are based on, such as electric field,¹⁶⁶ thermal,¹⁶⁷ mechanical, thermomechanical, or oxidative processes.¹⁶⁸ From those, thermal scanning probe lithography (t-SPL) stands out in terms of resolution and throughput. As t-SPL is relevant in this work it is described in detail in the next paragraph.

1.4.3. Thermal Scanning Probe Lithography

Thermal scanning probe lithography (t-SPL) is based on an AFM, where the tip is heated to induce thermal processes in the treated material. A first paper was published in 1992 by Mamin and Rugar, who used an infrared laser to heat an AFM tip that subsequently softens a PMMA layer. This, however, was rather a method of nano-indentation and not yet a kind of t-SPL as it is used today. This method was further exploited for the use of data-storage, reaching megabit-per-second writing rates and terabit-per-square-inch densities.^{169,170} In the early 2010's t-SPL was extensively developed and commercialized by IBM and SwissLitho (later Heidelberg Instruments Nano). In their approach, the tip of the modified AFM is heated to 700 – 1000 °C and thus evaporates the resist material by pushing the hot tip into the resist layer. This is schematically shown in Figure 1.4.3.

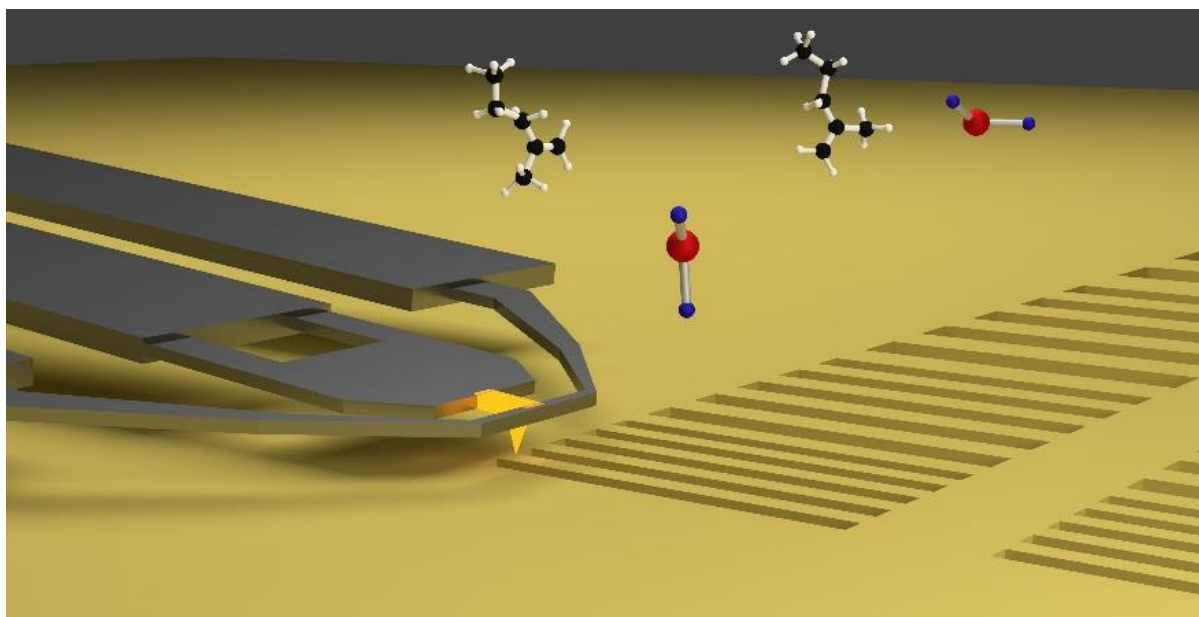


Figure 1.4.3: Schematic representation of the writing procedure in t-SPL.

Contrary to field-emission lithography, t-SPL does not require a conductive substrate in proximity to the tip. Furthermore, no piling up of excess material is observed. The immediate removal of the resist material by evaporation makes a subsequent development step unnecessary. As the AFM can be used for non-destructive surface characterization, samples can be inspected *in-situ* allowing for the reduction of stitching-errors as present i.e. in E-beam lithography or finding buried features beneath resist films. Rawlings et al. demonstrated a 3 nm precise overlay accuracy in 2015.¹⁷¹ Furthermore, the *in-situ* metrology, together with

the nature of a 'direct-development' enables a closed-loop control where the writing parameters can be adjusted during patterning enabling correction for errors during the writing procedure.¹⁷² As the depth to which the tip is pushed into the material determines the depth of the pattern, any arbitrary shape can be written into the resist. In 2010, a replica of the Matterhorn with a lateral size of $2 \times 2 \mu\text{m}$ was written into a 100 nm thick resist film.¹⁷³

As materials for t-SPL, both polymeric and molecular glass resists have been investigated. In one of the first approaches, a thermally triggered Diels-Alder polymer consisting of tris(furane) and bis(maleimide) moieties was used.¹⁷⁴ While initially examining the possibility to crosslink the polymer at medium temperatures to increase wear-resistance for data-storage application using the thermal nano-indentation method, it was observed that with increasing tip-temperature removal of the material was possible. However, this mechanism requires the cleavage of many covalent bonds in the polymer. The large energetic barrier of that process drastically influences the depolymerization rate slowing down the entire writing process. Thus molecular glass resists were seen as an alternative material, as for the evaporation only secondary interactions such as hydrogen bonds had to be overcome.¹⁷³ Molecular glasses, however, show a significantly higher mobility in thin films as compared to the bulk material. Thus, the flow of material back into written structures was found to be an issue for the stability of patterns, even with materials exhibiting a T_g of more than 100 °C. Furthermore, the size of molecular glasses with such a high T_g affects their possibility to *fly away* from the patterning site, rather landing next to the written structures and hence decreasing pattern quality.^{175,176}

The dilemma between energy consumption and pattern stability was resolved when Poly(phthal aldehyde) (PPA) was introduced as a resist material.¹⁷⁷ PPA is a heat sensitive polymer with a low ceiling temperature of ca. -40 °C.¹⁷⁸ Upon endcapping, the material is stable up to 150 °C. If, however, one bond within the polymer chain is cleaved, the entire chain will depolymerize in an *unzipping* process. This *self-amplified depolymerization* behavior opens up the possibility for a fast writing process. 20 mm s⁻¹ writing speeds at 40 nm pixel size have been demonstrated.¹⁷² Today, t-SPL is capable of producing features with 9 nm half-pitch and 14 nm half-pitch transferred into silicone.¹⁷⁹

Besides *classical* lithography, the applications of t-SPL are mainly driven by the capability to manufacture arbitrary 3D structures. The fabrication of nano-fluidic devices was reported by

Schwemmer *et al.* and Skaug *et al.*^{180,181} Tang *et al.* reported the use of t-SPL for the generation of tissue microenvironment for cell-culture.¹⁸² Further applications of t-SPL include the generation of guide patterns for directed self-assembly of block-copolymers¹⁸³ or the creation of fluorescence patterns in stimuli-responsive supramolecular polymers.¹⁸⁴ The applications reported by Schwemmer *et al.* and Tang *et al.* require the patterned structures to be in contact with or even immersed in aqueous media. While PPA shows sufficient stability to aqueous media, it decomposes under acidic conditions¹⁸⁵ in an *unzipping* process that resembles the process observed under thermal stimulus.¹⁸⁶

1.4.4. Etching

An issue that is faced in many lithographic applications is the transfer of the generated patterns into the substrate. In order to keep the aspect ratio of those structures reasonable, the resist thickness has to scale with the pattern size. Furthermore, it has to be compatible with the short depth-of-focus required by high resolution lithography. Therefore, an amplification of the achieved aspect ratio is usually required during etching for final application. This amplification is achieved with a high selectivity of the etch-process by etching the substrate at a higher rate than the remaining resist material. For current EUV and e-beam resists, this can be achieved by hybrid metal-organic resists where the metal atoms increase the etch-resistance whereas the organic ligands ensure processability with standard solvent based techniques. Examples include hydrogen silsesquioxanes containing silicon,¹⁵⁹ the before-mentioned Zn-nanocluster developed by Ober and co-workers for EUV lithography⁵⁰ or a $\text{Cr}_8\text{F}_8(\text{pivalate})_{16}$ cluster for e-beam lithography, the latter achieving a selectivity of 6.2:1 into silicone.¹⁸⁷

While metal-organic resists seem to be an appealing concept for solvent-based development lithography, t-SPL requires the resist to evaporate at ambient pressure and moderate temperatures. This is certainly impossible for such metal-organic clusters. Here, other techniques such as a complex stack of hard masks with subsequent etch cycles or metal lift-off processes are used. For t-SPL using PPA as resist material, a 65 nm etch into silicone was achieved from a 9 nm pattern thickness using an SiO_2 intermediate layer on a 50 nm HM8006 organic hardmask.¹⁸⁸

An elegant answer to that issue was developed by Darling, Elam, and co-workers using a standard atomic layer deposition (ALD) process. The metal precursors used in ALD such as TiCl_4 or $\text{Al}(\text{CH}_3)_3$ can interact with carbonyl groups in a Lewis-acid-base reaction which was used to selectively nucleate the ALD process inside a PMMA block of a PS-*b*-PMMA copolymer.¹⁸⁹ This process was hence called sequential infiltration synthesis (SIS). Using Al_2O_3 -SIS, the etch resistance of PMMA could be increased by the factor 37¹⁹⁰ and a 60-fold increase was achieved for a commercial 193 nm photoresist.¹⁹¹ The latter result exhibited the versatility of SIS towards a variety of resist materials, the only limitation of which would be the ability of the resist to react with and immobilize the ALD precursor, i.e. exhibiting a Lewis-base behavior. Consequently, this process was applied for PPA in t-SPL. Using a hardmask stack out of a cross-linked polystyrene (X-PS) buffer layer due to the inertness of PS to SIS and a Si_3N_4 layer on Si substrate, an 8-fold amplification of the written structures could be achieved while keeping the stack architecture more simple as compared to previously used hardmask stack.¹⁹²

1.5. References

- [1] J. Zarzycki, ed., *Materials Science and Technology, Volume 9: Glasses and Amorphous Materials*, VCH, Weinheim, **1991**.
- [2] Douglas, R.W., Frank, S., *A history of glass making*, G. T. Foulis & co., Henley-on-thames, **1972**.
- [3] J. Zarzycki, *Glasses and the vitreous state*, Cambridge University Press, Cambridge, **1991**.
- [4] M. Cable in *Materials Science and Technology, Volume 9: Glasses and Amorphous Materials*, ed. J. Zarzycki, VCH, Weinheim, **1991**.
- [5] Stahlkocher,
https://commons.wikimedia.org/wiki/File:Panzerglas_Beschussprobe.jpg.
- [6] Z. van Dijk, https://commons.wikimedia.org/wiki/File:2015-08_archeon_reading_stone.JPG.
- [7] G. Tammann, *Der Glaszustand*, Voss, Leipzig, **1930**.
- [8] P. M. Ossi, *Disordered Materials: An Introduction*, Springer, Heidelberg, **2006**.
- [9] G. W. Scherer in *Materials Science and Technology, Volume 9: Glasses and Amorphous Materials*, ed. J. Zarzycki, VCH, Weinheim, **1991**.
- [10] R. Zallen, *Physics of amorphous materials book*, WILEY-VCH, Weinheim, **2004**.
- [11] C. A. Angell, *Formation of Glasses from Liquids and Biopolymers*, *Science*, **1995**, 267, 1924–1935.
- [12] L. Hu and F. Ye, *Liquid fragility calculations from thermal analyses for metallic glasses*, *Journal of Non-Crystalline Solids*, **2014**, 386, 46–50.
- [13] S. M. Rekhson, A. V. Bulaeva and O. V. Mazurin, *Sov. J. Inorg. Mater.*, 7, 622–623.

- [14] P. Lunkenheimer, U. Schneider, R. Brand and A. Loid, *Glassy dynamics*, Contemporary Physics, **2000**, *41*, 15–36.
- [15] P. Lunkenheimer and A. Loidl in *Broadband Dielectric Spectroscopy*, ed. F. Kremer and A. Schönhal, Springer, Berlin, **2003**, 131–169.
- [16] Kudlik, A., Benkhof, S., T. Blochowicz, C. Tschirwitz and E. A. Rössler, *The dielectric response of simple organic glass formers*, J. Mol. Struct., **1999**, *479*, 201–218.
- [17] E. A. Rössler and H. Sillescu in *Materials Science and Technology, Volume 9: Glasses and Amorphous Materials*, ed. J. Zarzycki, VCH, Weinheim, **1991**.
- [18] W. Kauzmann, *The Nature of the Glassy State and the Behavior of Liquids at Low Temperatures*.
- [19] D. Turnbull and M. H. Cohen, *Concerning Reconstructive Transformation and Formation of Glass*, The Journal of chemical physics, **1958**, *29*, 1049–1054.
- [20] M. H. Cohen and D. Turnbull, *Molecular Transport in Liquids and Glasses*, The Journal of chemical physics, **1959**, *31*, 1164–1169.
- [21] D. Turnbull and M. H. Cohen, *Free-Volume Model of the Amorphous Phase: Glass Transition*, The Journal of chemical physics, **1961**, *34*, 120–125.
- [22] T. G. Fox and P. J. Flory, *Second-Order Transition Temperatures and Related Properties of Polystyrene. I. Influence of Molecular Weight*, Journal of Applied Physics, **1950**, *21*, 581–591.
- [23] Malcolm L. Williams, Robert F. Landel and John D. Ferry, *The Temperature Dependence of Relaxation Mechanisms in Amorphous Polymers and Other Glass-forming Liquids*.
- [24] A. K. Doolittle, *Studies in Newtonian Flow. II. The Dependence of the Viscosity of Liquids on Free-Space*, Journal of Applied Physics, **1951**, *22*, 1471–1475.
- [25] J. H. Gibbs and E. A. DiMarzio, *Nature of the Glass Transition and the Glassy State*, The Journal of chemical physics, **1958**, *28*, 373–383.

- [26] G. Adam and J. H. Gibbs, *On the Temperature Dependence of Cooperative Relaxation Properties in Glass-Forming Liquids*, *The Journal of chemical physics*, **1965**, *43*, 139–146.
- [27] M. Endo, Y. Tani, M. Sasago, K. Ogawa and N. Nomura, *Novel positive deep UV resist for KrF excimer laser lithography*, *Polym. Eng. Sci.*, **1989**, *29*, 859–862.
- [28] H.-W. Kim, S. Lee, S.-J. Choi, S.-G. Woo, Y.-S. Chao, J. Kim, J.-T. Moon, R. Kavanagh and G. Barclay, *Application of VEMA type ArF Resist to Sub-100nm lithography*, *J. Photopolym. Sci. Technol.*, **2002**, *15*, 529–534.
- [29] D. J. Carbaugh, S. Kaya and F. Rahman, *Lithographic tone reversal in optical exposure of polymethyl methacrylate (PMMA) resist*, *Mater. Res. Express*, **2019**, *6*, 45308.
- [30] X. Li, X. Yu and Y. Han, *Polymer thin films for antireflection coatings*, *J. Mater. Chem. C*, **2013**, *1*, 2266.
- [31] L. L. Beecroft and C. K. Ober, *High Refractive Index Polymers for Optical Applications*, *J. Macromol. Sci. A*, **1997**, *34*, 573–586.
- [32] A. Vollrath, D. Pretzel, C. Pietsch, I. Perevyazko, S. Schubert, G. M. Pavlov and U. S. Schubert, *Preparation, cellular internalization, and biocompatibility of highly fluorescent PMMA nanoparticles*, *Macromol. Rapid Commun.*, **2012**, *33*, 1791–1797.
- [33] P. Stroehriegl and J. V. Grazulevicius, *Charge-Transporting Molecular Glasses*, *Adv. Mater.*, **2002**, *14*, 1439–1452.
- [34] Y. Shirota, T. Kobata and N. Noma, *Starburst Molecules for Amorphous Materials. 4,4',4''-Tris(N,N-diphenylamino)triphenylamine and 4,4',4''-Tris[N-(3-methylphenyl)-N-phenylamino]triphenylamine*, *Chem. Lett.*, **1989**, 1145–1148.
- [35] A. Higuchi, H. Inada, T. Kobata and Y. Shirota, *Amorphous molecular materials: Synthesis and properties of a novel starburst molecule, 4,4[prime],4[Prime] -Tri(N-phenothiazinyl)triphenylamine*, *Adv. Mater.*, **1991**, *3*, 549–550.

- [36] W. Ishikawa, H. Inada, H. Nakano and Y. Shirota, *Starburst Molecules for Amorphous Molecular Materials: Synthesis and Morphology of 1,3,5-Tris(diphenylamino)benzene and Its Methyl-substituted Derivatives*, Molecular Crystals and Liquid Crystals Science and Technology. Section A. Molecular Crystals and Liquid Crystals, **1992**, *211*, 431–438.
- [37] J. Fujita, Y. Ohnishi, Y. Ochiai and S. Matsui, *Ultrahigh resolution of calixarene negative resist in electron beam lithography*, Appl. Phys. Lett., **1996**, *68*, 1297–1299.
- [38] K. Young-Gil, J. B. Kin, T. Fujigaya, Y. Shibasaki and M. Ueda, *A positive-working alkaline developable photoresist based on partially tert-Boc-protected calix[4]resorcinarene and a photoacid generator*, J. Mater. Chem., **2002**, *12*, 53–57.
- [39] N. M. Felix, A. de Silva and C. K. Ober, *Calix[4]resorcinarene Derivatives as High-Resolution Resist Materials for Supercritical CO₂ Processing*, Adv. Mater., **2008**, *20*, 1303–1309.
- [40] K. Tsuchiya, S. W. Chang, N. M. Felix, M. Ueda and C. K. Ober, *Lithography Based on Molecular Glasses*, Journal of Photopolymer Science and Technology, **2005**, *18*, 431–434.
- [41] D. Yang, S. W. Chang and C. K. Ober, *Molecular glass photoresists for advanced lithography*, J. Mater. Chem., **2006**, *16*, 1693.
- [42] J. Salbeck and F. Weissörtel, *Spiro linked Compounds for Use as Active Materials in Organic Light Emitting Diodes*, Macromol. Symp., **1997**, *125*, 121–132.
- [43] Q. Niu, Q. Zhang, W. Xu, Y. Jiang, R. Xia, D. D.C. Bradley, D. Li and X. Wen, *Solution-processed anthracene-based molecular glasses as stable blue-light-emission laser gain media*, Organic Electronics, **2015**, *18*, 95–100.
- [44] J. Pang, Y. Tao, S. Freiberg, X.-P. Yang, M. D'Iorio and S. Wang, *Syntheses, structures, and electroluminescence of new blue luminescent star-shaped compounds based on 1,3,5-triazine and 1,3,5-trisubstituted benzene*, J. Mater. Chem., **2002**, *12*, 206–212.

- [45] M. Sonntag, K. Kreger, D. Hanft, P. Strohrriegl, S. Setayesh and D. de Leeuw, *Novel Star-Shaped Triphenylamine-Based Molecular Glasses and Their Use in OFETs*, Chem. Mater., **2005**, *17*, 3031–3039.
- [46] D. Q.M. Craig, P. G. Royall, V. L. Kett and M. L. Hopton, *The relevance of the amorphous state to pharmaceutical dosage forms: glassy drugs and freeze dried systems*, Int. J. Pharm., **1999**, *179*, 179–207.
- [47] J. D. Mullins and T. J. Macek, *Some Pharmaceutical Properties of Novobiocin*, J. Am. Pharm. Assoc. Sci. Ed., **1960**, *49*, 245–248.
- [48] C. Neuber, A. Ringk, T. Kolb, F. Wieberger, P. Strohrriegl, H.-W. Schmidt, V. Fokkema, M. Cooke, C. Rawlings, U. Dürig, A. W. Knoll, J.-F. de Marneffe, P. de Schepper, M. Kaestner, Y. Krivoschapkina, M. Budden and I. W. Rangelow, *Molecular glass resists for scanning probe lithography*, Proc. SPIE, **2014**, 90491V.
- [49] M. Krysak, T. Kolb, C. Neuber, H.-W. Schmidt and C. K. Ober, ed. R. D. Allen, SPIE, **2010**, 76392C.
- [50] H. Xu, K. Sakai, K. Kasahara, V. Kosma, K. Yang, H. C. Herbol, J. Odent, P. Clancy, E. P. Giannelis and C. K. Ober, *Metal–Organic Framework-Inspired Metal-Containing Clusters for High-Resolution Patterning*, Chem. Mater., **2018**, *30*, 4124–4133.
- [51] D. de Simone, P. Vaneldereren and G. Vandenberghe, *Photo Material Readiness at the Eve of EUVL HVM*, Journal of Photopolymer Science and Technology, **2017**, *30*, 613–617.
- [52] <https://www.tsmc.com/english/dedicatedFoundry/technology/7nm.htm> (last accessed January 2020).
- [53] J. Dai, S. W. Chang, A. Hamad, D. Yang, N. Felix and C. K. Ober, *Molecular Glass Resists for High-Resolution Patterning*, Chem. Mater., **2006**, *18*, 3404–3411.
- [54] J. Chen, Q. Hao, S. Wang, S. Li, T. Yu, Y. Zeng, J. Zhao, S. Yang, Y. Wu, C. Xue, G. Yang and Y. Li, *Molecular Glass Resists Based on 9,9'-Spirobifluorene Derivatives: Pendant*

- Effect and Comprehensive Evaluation in Extreme Ultraviolet Lithography*, ACS Appl. Polym. Mater., **2019**, *1*, 526–534.
- [55] S. Sakka and J. D. MacKenzie, *Relation Between Apparent Glass Transition Temperature and Liquidus Temperature for Inorganic Glasses*, Journal of Non-Crystalline Solids, **1971**, *6*, 145–162.
- [56] K. Naito and A. Miura, *Molecular design for nonpolymeric organic dye glasses with thermal stability: relations between thermodynamic parameters and amorphous properties*, J. Phys. Chem., **1993**, *97*, 6240–6248.
- [57] J. A. Baird, B. van Eerdenbrugh and L. S. Taylor, *A classification system to assess the crystallization tendency of organic molecules from undercooled melts*, Journal of pharmaceutical sciences, **2010**, *99*, 3787–3806.
- [58] K. Naito, *Quantitative Relations between Glass Transition Temperatures and Thermodynamic Parameters for Various Materials: Molecular Design for Nonpolymeric Organic Dye Glasses with Thermal Stability*, Chem. Mater., **1994**, *6*, 2343–2350.
- [59] Y. Shirota, *Organic materials for electronic and optoelectronic devices*, J. Mater. Chem., **2000**, *10*, 1–25.
- [60] Y. Shirota, *Photo- and electroactive amorphous molecular materials—molecular design, syntheses, reactions, properties, and applications*, J. Mater. Chem., **2005**, *15*, 75–93.
- [61] O. Lebel, T. Maris, M.-E. Perron, E. Demers and J. D. Wuest, *The dark side of crystal engineering: creating glasses from small symmetric molecules that form multiple hydrogen bonds*, J. Am. Chem. Soc., **2006**, *128*, 10372–10373.
- [62] C. Alba-Simionesco, J. Fan and C. A. Angell, *Thermodynamic aspects of the glass transition phenomenon. II. Molecular liquids with variable interactions*, J. Chem. Phys., **1999**, *110*, 5262–5272.

- [63] V. N. Novikov and E. A. Rössler, *Correlation between glass transition temperature and molecular mass in non-polymeric and polymer glass formers*, *Polymer*, **2013**, *54*, 6987–6991.
- [64] T. Liu, K. Cheng, E. Salami-Ranjbaran, F. Gao, E. C. Glor, M. Li, P. J. Walsh and Z. Fakhraai, *Synthesis and high-throughput characterization of structural analogues of molecular glassformers: 1,3,5-trisarylbenzenes*, *Soft matter*, **2015**, *11*, 7558–7566.
- [65] W. Ping, D. Paraska, R. Baker, P. Harrowell and C. A. Angell, *Molecular engineering of the glass transition: glass-forming ability across a homologous series of cyclic stilbenes*, *J. Phys. Chem. B*, **2011**, *115*, 4696–4702.
- [66] F. Kremer and A. Schönals, eds., *Broadband Dielectric Spectroscopy*, Springer, Berlin, **2003**.
- [67] C. J. F. Böttcher and P. Bordewijk, *Theory of electric polarization*, Elsevier, Amsterdam, **1996**.
- [68] A. Schönals and F. Kremer in *Broadband Dielectric Spectroscopy*, ed. F. Kremer and A. Schönals, Springer, Berlin, **2003**, 1–34.
- [69] A. Schönals and F. Kremer in *Broadband Dielectric Spectroscopy*, ed. F. Kremer and A. Schönals, Springer, Berlin, **2003**, 59–98.
- [70] B. Schmidtke, N. Petzold, B. Pötzschner, H. Weingärtner and E. A. Rössler, *Relaxation stretching, fast dynamics, and activation energy: a comparison of molecular and ionic liquids as revealed by depolarized light scattering*, *J. Phys. Chem. B*, **2014**, *118*, 7108–7118.
- [71] R. Kohlrausch, *Ueber das Dellmann'sche Elektrometer*, *Ann. Phys. Chem.*, **1847**, *72*, 353–405.
- [72] G. Williams and D. C. Watts, *Non-Symmetrical Dielectric Relaxation Behaviour Arising from a Simple Empirical Decay Function*, *J. Chem. Soc. Faraday Trans.*, **1970**, *66*, 80–85.

- [73] K. S. Cole and R. H. Cole, *Dispersion and Absorption in Dielectrics I. Alternating Current Characteristics*, J. Chem. Phys., **1941**, *9*, 341–351.
- [74] K. S. Cole and R. H. Cole, *Dispersion and Absorption in Dielectrics II. Direct Current Characteristics*, J. Chem. Phys., **1942**, *10*, 98–105.
- [75] D. W. Davidson and R. H. Cole, *Dielectric Relaxation in Glycerol, Propylene Glycol, and n-Propanol*, J. Chem. Phys., **1951**, *19*, 1484–1490.
- [76] S. Havriliak and S. Negami, *A complex plane representation of dielectric and mechanical relaxation processes in some polymers*, Polymer, **1967**, *8*, 161–210.
- [77] B. Bochu, M. N. Deschizeaux, J. C. Joubert, A. Collomb, J. Chenavas and M. Marezio, *Synthèse et caractérisation d'une série de titanates pérowskites isotypes de [CaCu₃](Mn₄)O₁₂*, J. Solid State Chem., **1979**, *29*, 291–298.
- [78] C. Gainaru, *Dielectric Properties of Molecular Glass Formers; from the Liquid State to the Tunneling Regime*, **2008**.
- [79] A. I. Nielsen, T. Christensen, B. Jakobsen, K. Niss, N. B. Olsen, R. Richert and J. C. Dyre, *Prevalence of approximate square root(t) relaxation for the dielectric alpha process in viscous organic liquids*, J. Chem. Phys., **2009**, *130*, 154508.
- [80] M. Paluch, J. Knapik, Z. Wojnarowska, A. Grzybowski and K. L. Ngai, *Universal Behavior of Dielectric Responses of Glass Formers: Role of Dipole-Dipole Interactions*, Phys. Rev. Lett., **2016**, *116*, 25702.
- [81] C. Gainaru, *Spectral shape simplicity of viscous materials*, Phys. Rev. E, **2019**, *100*, 20601.
- [82] A. Jedrzejowska, M. Matussek, K. L. Ngai, K. Grzybowska, K. Jurkiewicz and M. Paluch, *New paradigm of dielectric relaxation of sizable and rigid molecular glass formers*, Physical review. E, **2020**, *101*, 10603.

- [83] K. L. Ngai, *Relation between some secondary relaxations and the α relaxations in glass-forming materials according to the coupling model*, J. Chem. Phys., **1998**, *109*, 6982–6994.
- [84] T. Blochowicz, C. Tschirwitz, St. Benkhof and E. A. Rössler, *Susceptibility functions for slow relaxation processes in supercooled liquids and the search for universal relaxation patterns*, J. Chem. Phys., **2003**, *118*, 7544.
- [85] S. Adishchev, D. Bock, C. Gainaru, R. Kahlau, B. Micko, N. Petzold, B. Pötzschner and E. A. Rössler, *Reorientational Dynamics of Organophosphate Glass Formers – a Joint Study by ^{31}P NMR, Dielectric Spectroscopy and Light Scattering*, Z. Phys. Chem., **2012**, *226*, 1149–1168.
- [86] R. Kahlau, T. Dörfler and E. A. Rössler, *Secondary relaxations in a series of organic phosphate glasses revealed by dielectric spectroscopy*, J. Chem. Phys., **2013**, *139*, 134504.
- [87] G. Meier, B. Gerharz, D. Boese and E. W. Fischer, *Dynamical processes in organic glassforming van der Waals liquids*, J. Chem. Phys., **1991**, *94*, 3050–3059.
- [88] G. P. Johari and M. Goldstein, *Viscous Liquids and the Glass Transition. II. Secondary Relaxations in Glasses of Rigid Molecules*, J. Chem. Phys., **1970**, *53*, 2372–2388.
- [89] G. P. Johari, *Glass Transition and Secondary Relaxations in Molecular Liquids and Crystals*, Ann. N.Y. Acad. of Sci., **1976**, *279*, 117–140.
- [90] M. Goldstein, *Viscous Liquids and the Glass Transition: A Potential Energy Barrier Picture*, J. Chem. Phys., **1969**, *51*, 3728–3739.
- [91] M. Vogel and E. Rössler, *Slow β process in simple organic glass formers studied by one- and two-dimensional ^2H nuclear magnetic resonance. I*, J. Chem. Phys., **2001**, *114*, 5802–5815.
- [92] F. Caporaletti, S. Capaccioli, S. Valenti, M. Mikolasek, A. I. Chumakov and G. Monaco, *A microscopic look at the Johari-Goldstein relaxation in a hydrogen-bonded glass-former*, Sci. Rep., **2019**, *9*, 14319.

- [93] C. Gainaru, R. Kahlau, E. A. Rössler and R. Böhmer, *Evolution of excess wing and beta-process in simple glass formers*, J. Chem. Phys., **2009**, *131*, 184510.
- [94] K. L. Ngai and M. Paluch, *Classification of secondary relaxation in glass-formers based on dynamic properties*, J. Chem. Phys., **2004**, *120*, 857–873.
- [95] H. Wagner and R. Richert, *Dielectric beta relaxations in the glassy state of salol?*, J. Chem. Phys., **1999**, *110*, 11660–11663.
- [96] U. Schneider, R. Brand, P. Lunkenheimer and A. Loidl, *Excess Wing in the Dielectric Loss of Glass Formers: A Johari-Goldstein β -relaxation?*, Phys. Rev. Lett., **2000**, *84*, 5560–5563.
- [97] H. Wagner and R. Richert, *Equilibrium and Non-Equilibrium Type β -Relaxations: d -Sorbitol versus o -Terphenyl*, J. Phys. Chem. B, **1999**, *103*, 4071–4077.
- [98] N. Petzold, B. Schmidtke, R. Kahlau, D. Bock, R. Meier, B. Micko, D. Kruk and E. A. Rössler, *Evolution of the dynamic susceptibility in molecular glass formers: results from light scattering, dielectric spectroscopy, and NMR*, J. Chem. Phys., **2013**, *138*, 12A510.
- [99] L. A. Utracki, *Polymer Alloys and Blends: Thermodynamics and Rheology*, Hanser, München, **1990**.
- [100] T. Sakaguchi, N. Taniguchi, O. Urakawa and K. Adachi, *Calorimetric Study of Dynamical Heterogeneity in Blends of Polyisoprene and Poly(vinylethylene)*, Macromolecules, **2005**, *38*, 422–428.
- [101] M. Pizzoli, M. Scandola and G. Ceccorulli, *Molecular motion in polymer-diluent systems: polystyrene tritolylphosphate*, Eur. Polym. J., **1987**, *23*, 843–846.
- [102] P. J. Hains and G. Williams, *Molecular motion in polystyrene-plasticizer systems as studied by dielectric relaxation*, Polymer, **1975**, *16*, 725–729.
- [103] M. Scandola, G. Ceccorulli and M. Pizzoli, *Composition dependence of the glass transition of polymer diluent mixtures: 2. Two concomitant glass transition processes as a general feature of plasticized polymers*, Polymer, **1987**, *28*, 2081–2084.

- [104] D. Cangialosi, A. Alegría and J. Colmenero, "Self-concentration" effects on the dynamics of a polychlorinated biphenyl diluted in 1,4-polybutadiene, *J. Chem. Phys.*, **2007**, *126*, 204904.
- [105] R. Kahlau, D. Bock, B. Schmidtke and E. A. Rössler, *Dynamics of asymmetric binary glass formers. I. A dielectric and nuclear magnetic resonance spectroscopy study*, *J. Chem. Phys.*, **2014**, *140*, 44509.
- [106] K. Adachi and Y. Ishida, *Effect of Diluent on Molecular Motion and Glass Transition in Polymers. IV. The system Poly(methyl acrylate)-Toluene*, *Polym. J.*, **1979**, *11*, 233–239.
- [107] K. J. Beirnes and C. M. Burns, *Thermal analysis of the glass transition of plasticized poly(vinyl chloride)*, *J. Appl. Polym. Sci.*, **1986**, *31*, 2561–2567.
- [108] D. Bock, *Molekulare Dynamik in binären Glasbildnern studiert mittels ³¹P- und ²H-NMR*, Bayreuth, **2015**.
- [109] S. K. Kumar, R. H. Colby, S. H. Anastasiadis and G. Fytas, *Concentration fluctuation induced dynamic heterogeneities in polymer blends*, *J. Chem. Phys.*, **1996**, *105*, 3777–3788.
- [110] R. Kant, S. K. Kumar and R. H. Colby, *What Length Scales Control the Dynamics of Miscible Polymer Blends?*, *Macromolecules*, **2003**, *36*, 10087–10094.
- [111] J. Colmenero and A. Arbe, *Segmental dynamics in miscible polymer blends: recent results and open questions*, *Soft matter*, **2007**, *3*, 1474.
- [112] T. P. Lodge and T. C. B. McLeish, *Self-Concentrations and Effective Glass Transition Temperatures in Polymer Blends*, *Macromolecules*, **2000**, *33*, 5278–5284.
- [113] M. D. Ediger, T. R. Lutz and Y. He, *Dynamics in glass-forming mixtures: Comparison of behavior of polymeric and non-polymeric components*, *J. Non-Cryst. Solids*, **2006**, *352*, 4718–4723.

- [114] T. Blochowicz, S. A. Lusceac, P. Gutfreund, S. Schramm and B. Stühn, *Two glass transitions and secondary relaxations of methyltetrahydrofuran in a binary mixture*, J. Phys. Chem. B, **2011**, *115*, 1623–1637.
- [115] T. Blochowicz, S. Schramm, S. Lusceac, M. Vogel, B. Stühn, P. Gutfreund and B. Frick, *Signature of a type-A glass transition and intrinsic confinement effects in a binary glass-forming system*, Phys. Rev. Lett, **2012**, *109*, 35702.
- [116] D. Bock, R. Kahlau, B. Pötzschner, T. Körber, E. Wagner and E. A. Rössler, *Dynamics of asymmetric binary glass formers. II. Results from nuclear magnetic resonance spectroscopy*, J. Chem. Phys., **2014**, *140*, 94505.
- [117] M. Arndt, R. Stannarius, H. Groothues, E. Hempel and F. Kremer, *Length Scale of Cooperativity in the Dynamic Glass Transition*, Phys. Rev. Lett., **1997**, *79*, 2077–2080.
- [118] G. Dosseh, C. Le Quellec, N. Brodie-linder, C. Alba-simionesco, W. Haeussler and P. Levitz, *Fluid–wall interactions effects on the dynamical properties of confined orthoterphenyl*, J. Non-Cryst. Solids, **2006**, *352*, 4964–4968.
- [119] S. Gradmann, P. Medick and E. A. Rössler, *Glassy dynamics in nanoconfinement as revealed by ^{31}P NMR*, J. Phys. Chem. B, **2009**, *113*, 8443–8445.
- [120] D. Bock, N. Petzold, R. Kahlau, S. Gradmann, B. Schmidtke, N. Benoit and E. A. Rössler, *Dynamic heterogeneities in glass-forming systems*, J. Non-Cryst. Solids, **2015**, *407*, 88–97.
- [121] D. Bock, T. Körber, F. Mohamed, B. Pötzschner and E. A. Rössler in *Kremer, Loidl (Hg.) 2018 – Scaling of Relaxation Processes*, 173–201.
- [122] C. R. Nugent, K. V. Edmond, H. N. Patel and E. R. Weeks, *Colloidal glass transition observed in confinement*, Phys. Rev. Lett., **2007**, *99*, 25702.
- [123] J. Koppensteiner, W. Schranz and M. R. Puica, *Confinement effects on glass forming liquids probed by dynamic mechanical analysis*, Phys. Rev. B, **2008**, *78*, 219.

- [124] G. Szklarz, K. Adrjanowicz, M. Tarnacka, J. Pionteck and M. Paluch, *Confinement-Induced Changes in the Glassy Dynamics and Crystallization Behavior of Supercooled Fenofibrate*, J. Phys. Chem. C, **2018**, *122*, 1384–1395.
- [125] A. Schönhals, H. Goering, C. Schick, B. Frick, M. Mayorova and R. Zorn, *Segmental dynamics of poly(methyl phenyl siloxane) confined to nanoporous glasses*, Eur. Phys. J. Spec. Top., **2007**, *141*, 255–259.
- [126] Bosse and Thakur, *Delocalization of small particles in a glassy matrix*, Phys. Rev. Lett., **1987**, *59*, 998–1001.
- [127] Bosse and Kaneko, *Self-Diffusion in Supercooled Binary Liquids*, Phys. Rev. Lett., **1995**, *74*, 4023–4026.
- [128] Y. Kaneko and J. Bosse, *Dynamics of binary liquids near the glass transition: a mode-coupling theory*, J. Non-Cryst. Solids, **1996**, *205-207*, 472–475.
- [129] B. Pötzschner, F. Mohamed, A. Lichtinger, D. Bock and E. A. Rössler, *Dynamics of asymmetric non-polymeric binary glass formers-A nuclear magnetic resonance and dielectric spectroscopy study*, J. Chem. Phys., **2015**, *143*, 154506.
- [130] B. Pötzschner, F. Mohamed, C. Bächer, E. Wagner, A. Lichtinger, R. Minikejew, K. Kreger, H.-W. Schmidt and E. A. Rössler, *Non-polymeric asymmetric binary glass-formers. I. Main relaxation studied by dielectric, ²H NMR, and ³¹P NMR spectroscopy*, J. Chem. Phys., **2017**, *146*, 1–12.
- [131] S. Valenti, S. Capaccioli and K. L. Ngai, *Contrasting two different interpretations of the dynamics in binary glass forming mixtures*, J. Chem. Phys., **2018**, *148*, 54504.
- [132] K. L. Ngai, S. Valenti and S. Capaccioli, *Molecular dynamic in binary mixtures and polymer blends with large difference in glass transition temperatures of the two components: A critical review*, J. Non-Cryst. Solids, **2019**, 119573.
- [133] B. Pötzschner, F. Mohamed, C. Bächer, E. Wagner, A. Lichtinger, D. Bock, K. Kreger, H.-W. Schmidt and E. A. Rössler, *Non-polymeric asymmetric binary glass-formers. II.*

- Secondary relaxation studied by dielectric, 2H NMR, and 31P NMR spectroscopy*, J. Chem. Phys., **2017**, 146.
- [134] F. Kaplan, 1959. *The Year Everything Changed*, John Wiley & Sons, Hoboken, NJ, USA, **2009**.
- [135] T. Scherer, <https://www.elektormagazine.de/news/vor-70-jahren-der-erste-transistor-der-welt> (last accessed April 2020).
- [136] M. Kabel, <https://www.eetimes.com/kilby-surprised-to-win-nobel-prize-as-ic-inventor/> (last accessed April 2020).
- [137] G. Weightman, *Eureka: How Invention Happens*, Yale University press, New Haven, **2015**.
- [138] M. J. Madou, *Fundamentals of Microfabrication: The Science of Miniaturization*, CRC Press, Boca Raton, **2002**.
- [139] J. W. Kim, B. Chmielak, H. Lerch and U. Plachetka, *Fabrication of photonic integrated circuits in silicon nitride using substrate conformal imprint lithography*, Microelectron. Eng., **2017**, 176, 11–14.
- [140] A. R. Shultz, *Degradation of Polymethyl Methacrylate by Ultraviolet Light*, J. Mater. Chem. C, **1961**, 65, 967–972.
- [141] A. Torikai, M. Ohno and K. Fueki, *Photodegradation of poly(methyl methacrylate) by monochromatic light: Quantum yield, effect of wavelengths, and light intensity*, J. Appl. Polym. Sci., **1990**, 41, 1023–1032.
- [142] C. A. Mack, [http://w.lithoguru.com/scientist/litho_tutor/TUTOR05%20\(Winter%2094\).pdf](http://w.lithoguru.com/scientist/litho_tutor/TUTOR05%20(Winter%2094).pdf) (last accessed January 2020).
- [143] G. E. Moore, *Cramming more components onto integrated circuits*, Electronics, **1965**, 38.
- [144] S. Okazaki, *Resolution limits of optical lithography*, J. Vac. Sci. Technol. B, **1991**, 9, 2829.

- [145] C. A. Mack, *Field Guide to Optical Lithography*, SPIE Press, Bellingham, WA, USA, **2006**.
- [146] https://en.wikichip.org/wiki/10_nm_lithography_process (last accessed January 2020).
- [147] Samsung Newsroom, <https://news.samsung.com/global/samsung-electronics-starts-production-of-euv-based-7nm-lpp-process> (last accessed June 2020).
- [148] R. M. M. Hasan and X. Luo, *Promising Lithography Techniques for Next-Generation Logic Devices*, *Nanomanuf. Metrol.*, **2018**, *1*, 67–81.
- [149] K. Matsuzawa, T. Fujii, S. Matsumara, T. Yamada, Y. Komuro, D. Kawana and K. Ohmori, *Challenges to Overcome Trade-Off between High-Resolution and High-Sensitivity in EUV lithography*, *J. Photopolym. Sci. Technol.*, **2016**, *29*, 489–493.
- [150] C. K. Ober, H. Xu, V. Kosma, K. Sakai and E. Giannelis, *EUV photolithography: resist progress and challenges*, *Proc. SPIE*, **2018**.
- [151] H. Yamamoto, Y. Vesters, J. Jiang, D. de Simone, G. Vandenberghe and T. Kozawa, *Role of Metal Sensitizers for Sensitivity Improvement in EUC Chemically Amplified Resist*, *J. Photopolym. Sci. Techn.*, **2018**, *31*, 747–751.
- [152] X. Wang, L.-T. Tseng, I. Mochi, M. Vockenhuber, L. van Lent-Protasova, R. Custers, G. Rispens, R. Hoefnagels and Y. Ekinici in *International Conference on Extreme Ultraviolet Lithography 2019*, ed. K. G. Ronse, P. A. Gargini, P. P. Naulleau and T. Itani, SPIE, **2019** - **2019**, 35.
- [153] S. Y. Chou, P. R. Krauss and P. J. Renstrom, *Nanoimprint Lithography*, *J. Vac. Sci. Techn. B*, **1996**, *14*, 4129–4133.
- [154] M. Lapedus, <https://semiengineering.com/what-happened-to-nanoimprint-litho/> (last accessed January 2020).
- [155] C. Probst, C. Meichner, K. Kreger, L. Kador, C. Neuber and H.-W. Schmidt, *Athermal Azobenzene-Based Nanoimprint Lithography*, *Adv. Mater.*, **2016**, *28*, 2624–2628.

- [156] T. R. Groves, D. Pickard, B. Rafferty, N. Crosland, G. Adam and G. Schubert, *Maskless electron beam lithography: prospects, progress, and challenges*, *Microelectron. Eng.*, **2002**, 61-62, 285–293.
- [157] W. Mi and P. Nillius, *Efficient proximity effect correction method based on multivariate adaptive regression splines for grayscale e-beam lithography*, *J. Vac. Sci. Technol. B*, **2014**, 32, 31602.
- [158] R. K. Dey and B. Cui, *Stitching error reduction in electron beam lithography with in-situ feedback using self-developing resist*, *J. Vac. Sci. Technol. B*, **2013**, 31, 06F409.
- [159] A. E. Grigorescu and C. W. Hagen, *Resists for sub-20-nm electron beam lithography with a focus on HSQ: state of the art*, *Nanotechnology*, **2009**, 20, 292001.
- [160] D. Küpper, D. Küpper, T. Wahlbrink, J. Bolten, M. C. Lemme, Y. M. Georgiev and H. Kurz, *Megasonic-assisted development of nanostructures*, *J. Vac. Sci. Technol. B*, **2006**, 24, 1827.
- [161] G. Binnig, H. Rohrer, C. Gerber and E. Weibel, *Tunneling through a controllable vacuum gap*, *Appl. Phys. Lett.*, **1982**, 40, 178–180.
- [162] G. Binnig, H. Rohrer, C. Gerber and E. Weibel, *Surface Studies by Scanning Tunneling Microscopy*, *Phys. Rev. Lett.*, **1982**, 49, 57–61.
- [163] G. Binnig, C. F. Quate and C. Gerber, *Atomic Force Microscope*, *Phys. Rev. Lett.*, **1986**, 56, 930–934.
- [164] D. M. Eigler and E. K. Schweizer, *Positioning single atoms with a scanning tunneling microscope*, *Nature*, **1990**, 344, 524–526.
- [165] R. Garcia, A. W. Knoll and E. Riedo, *Advanced scanning probe lithography*, *Nat. Nanotechnol.*, **2014**, 9, 577–587.
- [166] M. Kaestner, M. Hofer and I. W. Rangelow, *Nanolithography by scanning probes on calixarene molecular glass resist using mix-and-match lithography*, *J. Micro/Nanolith. MEMS MOEMS (Journal of Micro/Nanolithography, MEMS, and MOEMS)*, **2013**, 12.

- [167] A. W. Knoll, D. Pires, O. Coulembier, P. Dubois, J. L. Hedrick, J. Frommer and U. Duerig, *Probe-based 3-D nanolithography using self-amplified depolymerization polymers*, *Adv. Mat.*, **2010**, *22*, 3361–3365.
- [168] A. I. Dago, Y. K. Ryu, F. J. Palomares and R. Garcia, *Direct Patterning of p-Type-Doped Few-layer WSe₂ Nanoelectronic Devices by Oxidation Scanning Probe Lithography*, *ACS applied materials & interfaces*, **2018**, *10*, 40054–40061.
- [169] R. J. Cannara, B. Gotsmann, A. Knoll and U. Dürig, *Thermo-mechanical probe storage at Mbps single-probe data rates and Tbit in(-2) densities*, *Nanotechnology*, **2008**, *19*, 395305.
- [170] A. Pantazzi, A. Sebastian, T. A. Antonakopoulos, P. Bächtold, A. R. Bonaccio, J. Bonan, G. Cherubini, M. Despont, R. A. DiPietro, U. Drechsler, U. Dürig, B. Gotsmann, W. Häberle, C. Hagleitner, J. L. Hedrick, D. Jubin, A. W. Knoll, M. A. Lantz, J. Pentarakis, H. Pozidis, R. C. Pratt, H. Rothuizen, R. Stutz, M. Varsamou, D. Wiesmann and E. Eleftheriou, *Probe-based ultrahigh-density storage technology*, *IBM J. Res. & Dev.*, **2008**, *52*, 493–511.
- [171] C. Rawlings, H. Wolf, J. L. Hedrick, D. J. Coady, U. Duerig and A. W. Knoll, *Accurate Location and Manipulation of Nanoscaled Objects Buried under Spin-Coated Films*, *ACS nano*, **2015**, *9*, 6188–6195.
- [172] P. C. Paul, A. W. Knoll, F. Holzner, M. Despont and U. Duerig, *Rapid turnaround scanning probe nanolithography*, *Nanotechnology*, **2011**, *22*, 275306.
- [173] D. Pires, J. L. Hedrick, A. de Silva, J. Frommer, B. Gotsmann, H. Wolf, M. Despont, U. Duerig and A. W. Knoll, *Nanoscale Three-Dimensional Patterning of Molecular Resists by Scanning Probes*, *Science*, **2010**, *328*, 732–735.
- [174] B. Gotsmann, U. Duerig, J. Frommer and C. J. Hawker, *Exploiting Chemical Switching in a Diels–Alder Polymer for Nanoscale Probe Lithography and Data Storage*, *Adv. Funct. Mater.*, **2006**, *16*, 1499–1505.

- [175] C. Neuber, H.-W. Schmidt, P. Strohrriegl, A. Ringk, T. Kolb, A. Schedl, V. Fokkema, M. G. A. van Veghel, M. Cooke, C. Rawlings, U. Dürig, A. Knoll, J.-F. d. Marneffe, Z. el Otell, M. Kaestner, Y. Krivoshapkina, M. Budden and I. W. Rangelow, *Tailored molecular glass resists for scanning probe lithography*, Proc. SPIE, **2015**, 94250E.
- [176] C. Neuber, H.-W. Schmidt, P. Strohrriegl, D. Wagner, F. Krohn, A. Schedl, S. Bonanni, F. Holzner, C. Rawlings, U. Dürig and A. W. Knoll, *PVD prepared molecular glass resists for scanning probe lithography*, Proc. SPIE, **2016**, 97791C.
- [177] O. Coulembier, A. Knoll, D. Pires, B. Gotsmann, U. Duerig, J. Frommer, R. D. Miller, P. Dubois and J. L. Hedrick, *Probe-Based Nanolithography: Self-Amplified Depolymerization Media for Dry Lithography*, Macromolecules, **2010**, *43*, 572–574.
- [178] C. G. Willson, H. Ito, J. M.J. Fréchet, T. G. Tessier and F. M. Houlihan, *Approaches to the Design of Radiation-Sensitive Polymeric Imaging Systems with Improved Sensitivity and Resolution*, J. Electrochem. Soc., **1986**, *133*, 181–187.
- [179] Y. K. Ryu Cho, C. D. Rawlings, H. Wolf, M. Spieser, S. Bisig, S. Reidt, M. Sousa, S. R. Khanal, T. D. B. Jacobs and A. W. Knoll, *Sub-10 Nanometer Feature Size in Silicon Using Thermal Scanning Probe Lithography*, ACS nano, **2017**, *11*, 11890–11897.
- [180] C. Schwemmer, S. Fringes, U. Duerig, Y. K. Ryu and A. W. Knoll, *Experimental Observation of Current Reversal in a Rocking Brownian Motor*, Phys. Rev. Lett., **2018**, *121*, 104102.
- [181] M. J. Skaug, C. Schwemmer, S. Fringes, C. D. Rawlings and A. W. Knoll, *Nanofluidic rocking Brownian motors*, Science (New York, N.Y.), **2018**, *359*, 1505–1508.
- [182] S. W. Tang, M. H. Uddin, W. Y. Tong, P. Pasic, W. Yuen, H. Thissen, Y. W. Lam and N. H. Voelcker, *Replication of a Tissue Microenvironment by Thermal Scanning Probe Lithography*, ACS Appl. Mat. Inter., **2019**, *11*, 18988–18994.
- [183] S. Gottlieb, M. Lorenzoni, L. Evangelio, M. Fernández-Regúlez, Y. K. Ryu, C. Rawlings, M. Spieser, A. Knoll and F. Perez-Murano, *Corrigendum: Thermal scanning probe*

- lithography for the directed self-assembly of block copolymers (2017 Nanotechnology 28 175301)*, *Nanotechnology*, **2017**, *28*, 289501.
- [184] S. T. Zimmermann, D. W. R. Balkenende, A. Lavrenova, C. Weder and J. Brugger, *Nanopatterning of a Stimuli-Responsive Fluorescent Supramolecular Polymer by Thermal Scanning Probe Lithography*, *ACS Appl. Mat. Inter.*, **2017**, *9*, 41454–41461.
- [185] J. M. Schwartz, O. Phillips, A. Engler, A. Sutlief, J. Lee and P. A. Kohl, *Stable, High-Molecular-Weight Poly(phthalaldehyde)*, *J. Polym. Sci. Part A: Polym. Chem.*, **2017**, *55*, 1166–1172.
- [186] H. Ito and C. G. Willson, *Chemical Amplification in the Design of Dry Developing Resist Materials*, *Poly. Eng. Sci.*, **1983**, *23*, 1012–1018.
- [187] S. M. Lewis, M. S. Hunt, G. A. DeRose, H. R. Alty, J. Li, A. Wertheim, L. de Rose, G. A. Timco, A. Scherer, S. G. Yeates and R. E. P. Winpenny, *Plasma-Etched Pattern Transfer of Sub-10 nm Structures Using a Metal-Organic Resist and Helium Ion Beam Lithography*, *Nano Lett.*, **2019**, *19*, 6043–6048.
- [188] H. Wolf, C. Rawlings, P. Mensch, J. L. Hedrick, D. J. Coady, U. Duerig and A. W. Knoll, *Sub 20 nm Silicon Patterning and Metal Lift-Off Using Thermal Scanning Probe Lithography*, *J. Vac. Sci. Technol. B*, **2015**, *33*.
- [189] Q. Peng, Y.-C. Tseng, S. B. Darling and J. W. Elam, *Nanoscopic patterned materials with tunable dimensions via atomic layer deposition on block copolymers*, *Adv. Mat.*, **2010**, *22*, 5129–5133.
- [190] Y.-C. Tseng, Q. Peng, L. E. Ocola, D. A. Czaplewski, J. W. Elam and S. B. Darling, *Enhanced polymeric lithography resists via sequential infiltration synthesis*, *J. Mater. Chem.*, **2011**, *21*, 11722.
- [191] Y.-C. Tseng, A. U. Mane, J. W. Elam and S. B. Darling, *Enhanced lithographic imaging layer meets semiconductor manufacturing specification a decade early*, *Adv. Mat.*, **2012**, *24*, 2608–2613.

- [192] J.-F. d. Marneffe, B. T. Chan, M. Spieser, G. Vereecke, S. Naumov, D. Vanhaeren, H. Wolf and A. W. Knoll, *Conversion of a Patterned Organic Resist into a High Performance Inorganic Hard Mask for High Resolution Pattern Transfer*, ACS nano, **2018**, *12*, 11152–11160.

2. Objective of the Thesis

The main objectives of this thesis are the design and synthesis of new high- T_g molecular glass formers based on 9,9'-spirobi[9H]fluorene and their evaluation in terms of T_g and glass-forming ability as well as the investigation of their dynamics in neat and binary systems. Furthermore, poly(olefin sulfone)s shall be investigated as possible novel amorphous resist materials for thermal scanning probe lithography (t-SPL).

I. Influence of dipole containing substituents on the thermal properties of molecular glasses

Molecular glasses are widely used in industry for resist materials, pharmaceuticals, or as active materials in optoelectronic devices. For all applications, a stable amorphous state is required. Therefore, a high T_g is beneficial as crystallization is heavily suppressed below T_g . As especially in thin films surface properties dominate and thus e.g. mobility of surface molecules is increased as compared to its bulk material, a T_g far above process temperatures is desirable. This is especially the case for the use as resist materials, where surface mobility of molecules decreases the stability of inscribed patterns already well below T_g . However, for solvent free techniques such as PVD a reasonably low molecular weight is required for vaporization. Therefore, highly interacting groups such as nitriles may be attached to the molecules to increase T_g while keeping the molar mass still low. However, current literature lacks detailed studies on the influence of specific substituents and their respective position on T_g and on the stability of the amorphous state. Therefore, in the *first topic* of this thesis, the influence of nitrile groups on these material properties shall be investigated for a series of synthesized molecular glasses based on the stiff core molecule 9,9'-spirobi[9H]fluorene.

II. Dynamics in neat and asymmetric binary molecular glass formers

The dynamics of glass forming systems in terms of i.e. the occurrence or absence of a β -relaxation, its relative strength, and the distribution of relaxation times for both, the α - and β -relaxation are still a highly debated field in solid state physics. Recent literature discusses the effect of dipolar side-groups on the relaxation behavior of otherwise non-polar, stiff core molecules, however with only two molecules. In the *second topic* of this thesis, a series of selected novel molecular glasses shall be characterized by dielectric spectroscopy in order to determine the influence of presence or absence and the substitution position of highly dipolar

nitrile groups on the relaxation behavior of these systems. New insights on the interdependence of relaxation strength and stretching behavior shall be gained by comparison with other already well-investigated glass formers. Furthermore, presence or absence of a β -relaxation and its distribution of relaxation times shall be investigated in more detail.

While the dynamics for a wide variety of neat glass formers have been investigated by several techniques such as dielectric and NMR-spectroscopy, asymmetric binary glass/plasticizer systems are by far not as thoroughly investigated. Recent investigations reveal highly decoupled dynamics and pronounced dynamic heterogeneities in such systems, which resemble dynamics in confined space. A local maximum in the concentration dependent T_g -curve of the low- T_g component at intermediate concentrations is observed. The latter phenomenon, however, is currently highly debated, as the apparent relaxation of the plasticizer may be regarded as a β -process of the matrix. Still it is not completely understood whether these observations are mainly due the structure of the involved species or their T_g -contrast. A further understanding of these phenomena is anticipated when investigating molecular glasses as high- T_g components in such systems. However, the tendency to demix or crystallize in the presence of plasticizers hampered the analysis in the whole composition and temperature range of such systems so far.

In the *third topic* of this thesis, a novel asymmetric binary system being composed of a molecular glass and a plasticizer with a T_g difference of at least 200 K showing neither demixing nor crystallization over the whole temperature range including all T_g s and the whole concentration range shall be developed. Therefore, materials and knowledge gained in the *first* and *second topic* of this thesis will be used. The dynamics of this binary system shall be investigated by dielectric and NMR-spectroscopy revealing insight in all relaxation processes of both components. A thorough characterization of the relaxations in terms of relaxation times, distribution functions, and glass transition temperatures shall be performed as well as a comparison with other studies of glass / plasticizer systems from literature.

III. Poly(olefin sulfone)s as new resist materials for thermal scanning probe lithography

For thermal scanning probe lithography (t-SPL) molecular glasses showed limited application potential as resist materials due to their surface mobility even of high- T_g materials leading to reflux of material into written structures. Thus, the use of polymers is inevitable. So far, only

poly(phthal aldehyde) (PPA) has met the requirements of residue-free decomposition in the required temperature range. However, PPA shows limited shelf life and its sensitivity towards acidic conditions limits possible application of written structures.

Poly(olefin sulfone)s are a class of polymers showing very low ceiling temperatures and thus offer a high potential for the use as resist materials for t-SPL. Therefore, in the *fourth topic* a series of poly(olefin sulfone)s should be synthesized and characterized regarding their potential application as resist materials for t-SPL. For promising candidates, t-SPL should be carried out and the performance of the material in terms of sensitivity and resolution be evaluated. The etch resistance should be investigated along with the focus to prepare a highly etch-resistant hard mask. Furthermore, investigations on the acid resistivity should be performed.

3. Synopsis

3.1. Overview of the thesis

This thesis focuses on the synthesis of novel organic glasses and investigations on their thermal properties, relaxation behavior, and possible applications. It consists of four topics, three of which involve novel synthesized molecular glasses based on 9,9'-spirobi[9H]fluorene, while the fourth topic involves synthesized poly(olefin sulfone)s. A graphical illustration of these topics is given in Figure 3.1.1.

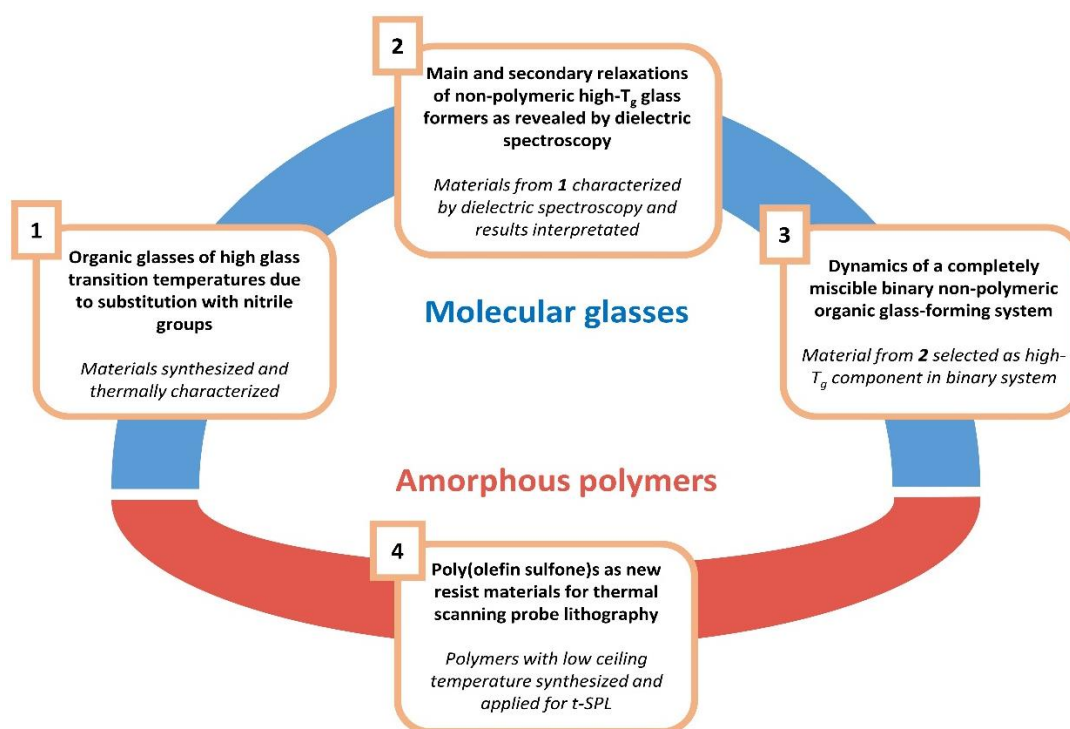


Figure 3.1.1: Overview of the four topics presented in the thesis: 1) The T_g of molecular glasses is drastically increased by the introduction of nitrile groups. 2) The dielectric properties of molecular glasses are investigated with respect to the presence and substitution position of nitrile groups. 3) A stable binary mixture of a compound investigated in 2 and a low-molecular weight additive is investigated with dielectric spectroscopy, DMA, and DSC. 4) Poly(olefin sulfone)s are investigated as new resist materials for thermal scanning probe lithography.

The *first topic* features a series of novel synthesized 9,9'-spirobi[9H]fluorenes substituted with highly dipolar nitrile groups at different positions. Depending on the substitution position of the nitrile group, they show with respect to their molar mass a much higher increase of T_g as compared to less interacting side-groups previously published in literature. Furthermore, the influence of the nitrile groups on the stability of the amorphous state is evaluated for several architectures. The findings of this topic are published as a full paper.

Due to the fact that for unpolar core molecules with a highly dipolar substituents only the substituent dynamics are probed in dielectric spectroscopy, the *second topic* focuses on dielectric relaxations of selected compounds synthesized and characterized in the first topic. Furthermore, these findings are compared to other well-studied glass formers. It can be demonstrated that for molecules with nitrile groups that show possible intra-molecular rotatability with respect to the core a prominent β -relaxation can be found. In contrast, no well-resolved β -relaxation is observed when the nitrile group is fixed relative to the core. However, in the latter case, secondary relaxations exhibiting constant widths at different temperatures occur, a phenomenon that has not been observed before. The results of this topic are published as a full paper.

In the *third topic* one of the glass formers examined in the second topic is mixed with a small, polar probe molecule acting as a plasticizer in order to determine the dynamics of this binary system. The compounds show neither demixing nor crystallization behavior throughout the concentration and temperature range. Utilizing dielectric spectroscopy, the dynamics of the highly polar probe molecule are determined, whereas ^2H - and ^{31}P -NMR will be carried out to probe the dynamics for each of the compounds separately. Whereas for the high- T_g component a decreasing T_g with increasing plasticizer concentration is observed, the plasticizer itself shows a T_g -maximum at about 40 wt%, a highly debated phenomenon. The findings of these topic are presented in a full paper manuscript that will be submitted for publication shortly.

In the *fourth topic*, poly(olefin sulfone)s are synthesized in order to examine their possible application as resist materials for thermal scanning probe lithography (t-SPL). With promising candidates, t-SPL is carried out and the performance of the polymer is compared to the workhorse resist used in t-SPL, poly(phthal aldehyde) (PPA). 3D- and high-resolution 2D-patterns are prepared. The sensitivity of the poly(olefin sulfone) resist is similar as for PPA. 10 nm half-pitch lines are obtained. Sequential infiltration synthesis is used to create etch-resistant hard masks and the patterns are planned to be transferred into SiO_2 shortly. The findings of this topic are presented as a manuscript of a full paper and intended for publication at ACS Nano.

3.2. Organic Glasses of High Glass Transition Temperatures Due To Substitution with Nitrile Groups

The glass transition temperature of a molecular glass usually scales with its molar mass. This increase correlates to a power-law of the form $T_g \propto M^\alpha$ with $\alpha \approx 0.5$ as shown in 1.3.2. For several applications, however, a highly increased T_g with only a moderate increase in M is desirable. As current literature lacks detailed studies on how highly dipolar substituents influence the thermal properties, we evaluated the influence of nitrile groups on T_g utilizing different substituted 9,9'-spirobi[9H]fluorenes. For that, we synthesized three different series of molecules based on three different architectures that can be distinguished by the amounts of phenyl rings bonded to the spiro-core. The three architectures are shown in Figure 3.2.1. The substituents R and R' can be hydrogen atoms or CN groups, respectively, with the CN groups attached to the additional substituted phenyl ring being in *ortho*, *meta*, or *para* position.

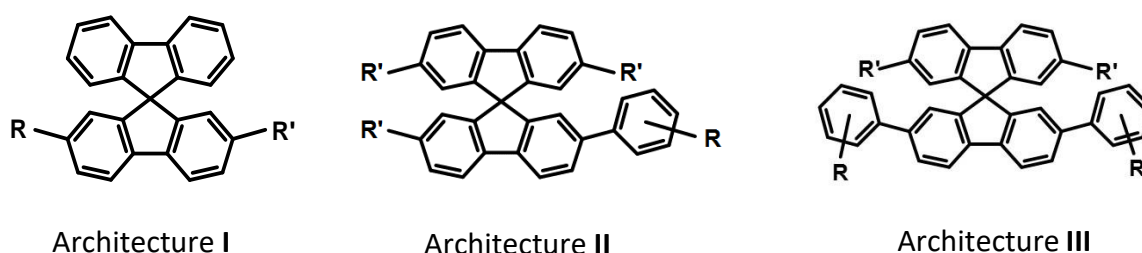


Figure 3.2.1: Three different architectures based on the 9,9'-spirobi[9H]fluorenes used as core unit in this study. R and R' can be H or CN moieties. Reproduced with permission from Publication 4.2, © 2019, American Chemical Society.

It was observed that for architecture II and III the T_g increases in the sense of *ortho* – *meta* – *para*, with the compound possessing the nitrile group in *para*-position showing a much higher T_g than when the nitrile group is positioned in *ortho*- or *meta*-location. The increase in T_g is generally higher the more nitrile groups are directly bonded to the spiro-core. Thus α of investigated molecules is highest for architecture I with 1.65. For architecture II and III with nitrile groups in *para*-position, still values above 1.00 are calculated. In conclusion, the relative increase of T_g with respect to M is about two to three times as high as the average value of the “entirety” of molecular glasses, if highly interacting nitrile groups are present. T_m shows a higher increase for molecules of architecture II as compared to those of architecture III. The

3.2 ORGANIC GLASSES OF HIGH GLASS TRANSITION TEMPERATURES DUE TO SUBSTITUTION WITH NITRILE GROUPS

relation of T_g and M in dependence of the substitution position of the nitrile group is shown in Figure 3.2.2 for architecture II and architecture III.

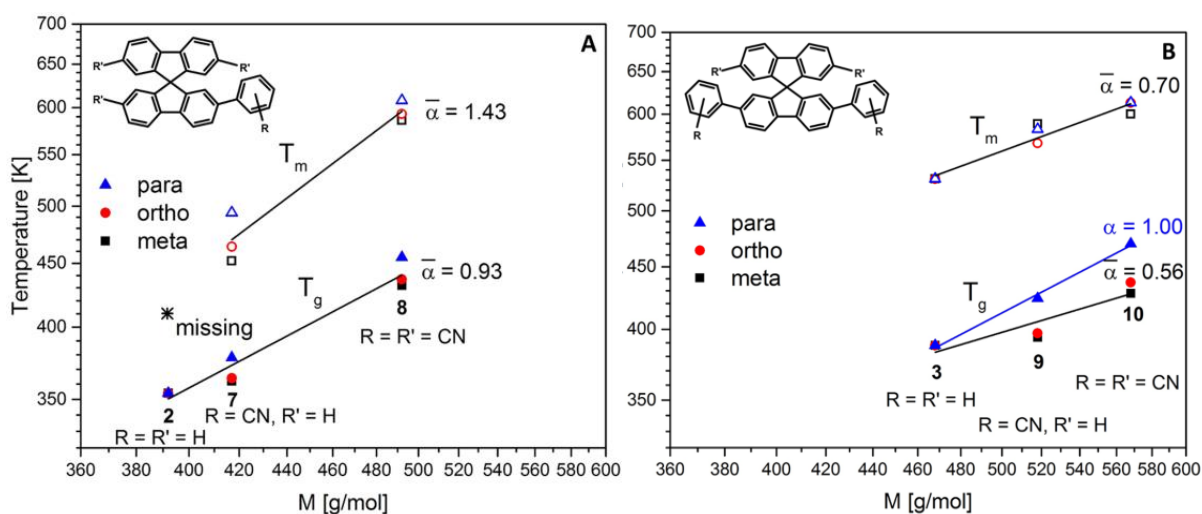


Figure 3.2.2: T_g and T_m for synthesized 9,9'-spiro[9H]fluorene compounds with architecture II (A) and III (B). The lines show respective power-law fits. Reproduced with permission from Publication 4.2, © 2019, American Chemical Society.

$\frac{T_g}{T_m}$ ratios were determined to evaluate the stability of the amorphous phase, as highly interacting groups might decrease this ratio. Values between 0.7 and 0.8 are observed, indicating good to excellent stability of the amorphous state.

The findings presented here are guidelines for the synthesis of novel high- T_g materials with tailored properties. This may be beneficial for several applications such as lithography or in general in thin film processing.

3.3. Main and secondary relaxations of non-polymeric high- T_g glass formers as revealed by dielectric spectroscopy

Although the dynamics of many glass formers have been extensively studied in the past decades by means of i.e. dielectric or NMR-spectroscopy, still a general understanding of the correlation between molecular structure and relaxation features is missing. Some studies in literature focus on the influence of substitution position or general constitution of isomers on the relaxation behavior, obtaining assumptions on i.e. fragility in dependence of steric hindrance. However, a lot of work still needs to be done in order to get a thorough understanding of several observed relaxation features. In 3.2 a series of structurally similar novel high- T_g molecular glasses was synthesized and characterized which distinguish by absence or presence and substitution position of nitrile groups. Due to their strong polarity the signal in dielectric spectroscopy is determined by the reorientation of the nitrile moieties, which allows new insight in the dependence of substitution position on the dynamics of such molecules. Hence, in this topic, a number of molecular glasses was investigated by means of dielectric spectroscopy to reveal relaxation features with respect to the position of the nitrile group. In addition, the observed relaxation features are compared to those of other known glass formers. Figure 3.3.1 shows the dielectric master curves of selected investigated glass-formers as well as their respective molecular structures.

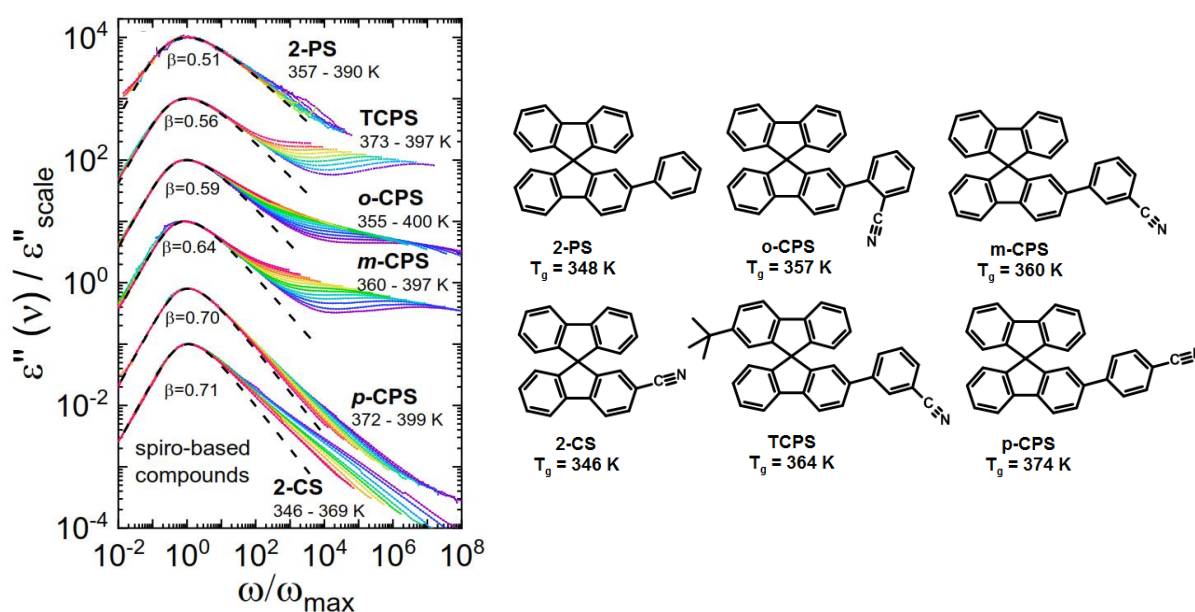


Figure 3.3.1: Dielectric master curves of the α -relaxation of selected investigated molecular glasses with molecular structures and respective stretching parameters. Reproduced by permission of the PCCP Owner Societies from Publication 4.3.

Our results reveal a dependence of the presence of a discernible β -relaxation on the position of the nitrile group: For nitrile groups with a certain degree of freedom of movement in relation to the core a clearly discernible β -process can be observed and evaluated in corresponding relaxation spectra. If, however, the nitrile groups are in a fixed position to the core, no clearly resolved β -relaxation is found. The behavior of the high-frequency flank of the α -relaxation, however, reveals that a broad, low-intensity secondary relaxation is underlying the main peak. Furthermore, a secondary relaxation is observed, which occurs at much lower temperatures. While the Arrhenius-behavior is very similar to usual β -processes observed in glass-formers, contrary to them this relaxation shows no broadening with temperature. Calculations of the apparent activation energies of the typical β -processes yield values of ca. $24 T_g$, a phenomenon discussed previously in literature. More general, values between $20 - 30 T_g$ are observed. The unusual processes, however, show apparent activation energies of ca. $14 T_g$. These values are usually observed for glasses where the β -process shows a strong separation from the α -process, as shown with examples from literature. Calculated activation energies of the observed β -processes of selected glass-formers are shown in Figure 3.3.2.

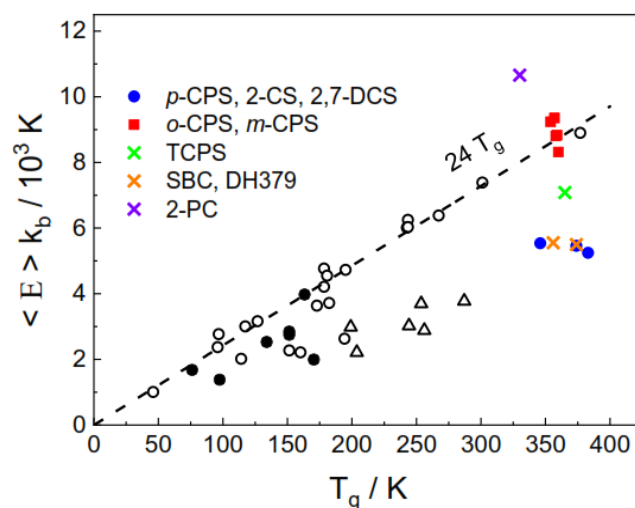


Figure 3.3.2: Calculated activation energies of β -processes of here investigated glass-formers in comparison with systems previously reported in literature. Reproduced by permission of the PCCP Owner Societies from from Publication 4.3.

The results, published in a full paper, reveal new insights in dynamics of high- T_g glass formers, distribution of relaxation times, and merging behavior of α - and β -process. Clearly, an influence of the substitution position of the probed nitrile group is observed.

3.4. Dynamics of a completely miscible binary non-polymeric organic glass-forming system

The investigation of the dynamics in asymmetric, binary glass-forming systems (i.e. solid/plasticizer systems) such as poly(styrene)/tripropyl phosphate (PS/TPP) revealed highly decoupled dynamics and pronounced dynamic heterogeneities for low additive concentrations as well as a local maximum in the concentration dependent T_g -curve of the additive for intermediate concentrations. Using molecular glasses as high- T_g component, demixing and crystallization hampered a thorough investigation over the entire temperature and concentration range of these systems. Thus, in this topic, a binary glass-forming system based on a molecular glass as high- T_g component and the additive TPP showing neither crystallization nor demixing was established. This investigated system is shown in Figure 3.4.1. In order to enable selective ^2H -NMR spectroscopy of the matrix, a synthesis route allowing the labelling of the matrix with deuterium atoms at the core unit was developed. The dynamics of this mixture were investigated using dielectric spectroscopy (DS), dynamic scanning calorimetry (DSC), and dynamic mechanical analysis (DMA), while NMR-investigations are pending.

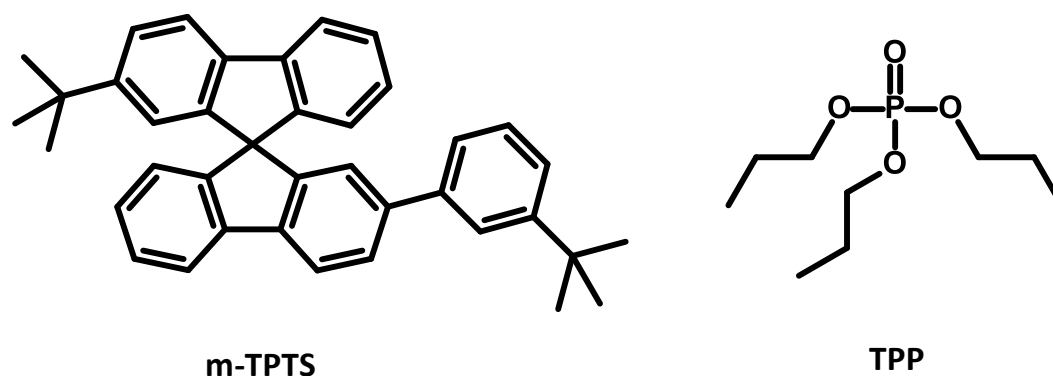


Figure 3.4.1: Asymmetric, binary glass-forming system investigated in this chapter.

In general, many features of other, previously investigated asymmetric binary systems are rediscovered, such as a strong broadening of the α_2 -relaxation (belonging to the additive) indicating a broad distribution of relaxation times $G(\ln\tau_\alpha)$ and a failure of frequency-time-superposition (FTS). Also, a weaker broadening of the α_1 -relaxation on the high-frequency flank is observed. In contrast to other investigations, FTS also fails in general for the α_1 -process (belonging to the high- T_g component). Furthermore, the β -process of the additive shows an

anti-plasticizer effect and a decrease of its apparent activation energy with decreasing additive content. Figure 3.4.2 shows the dielectric susceptibility spectra of 60 % m-TPTS / 40 % TPP (A) and 90 % m-TPTS / 10 % TPP (B). For the mixture containing 40 % TPP, clearly two relaxations can be observed being attributed to the α_1 - and the α_2 -relaxation, respectively. The α_1 -relaxation shows a broadening on the high-frequency flank, while the low-frequency flank still follows $\chi''(\omega) \propto \omega^{-1}$. The α_2 -relaxation, in contrast, is mainly broadened on the low-frequency flank. With increasing temperature, the amplitude of the α_2 -relaxation increases accompanied by a decrease of the α_1 -amplitude. In the mixture containing 10 % TPP, the α_1 -relaxation follows a similar trend with a broadening on the high-frequency flank. The α_2 -relaxation appears as a very broad process with low amplitude which still increases upon increasing temperature.

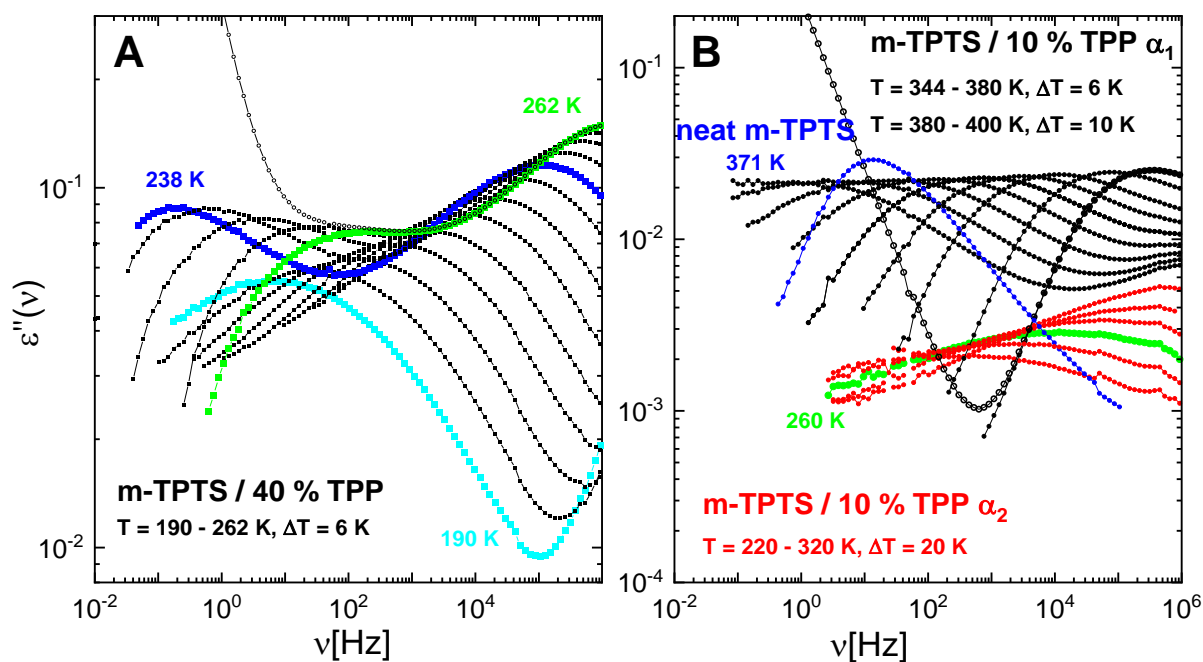


Figure 3.4.2: A: Dielectric susceptibility spectra of 60 % m-TPTS / 40 % TPP. Selected temperatures are shown in color as indicated. B: Dielectric susceptibility spectra 90 % m-TPTS / 10 % TPP with α_1 -process shown in black and α_2 -process shown in red. Spectrum of neat m-TPTS in blue is shown for comparison.

Figure 3.4.3 shows all measured T_g s of the m-TPTS / TPP-system as a function of weight fraction of TPP. For m-TPTS (i.e. the α_1 -process), the well-known monotonous plasticizer effect is observed, thus the respective T_g (assigned as $T_{g,1}$) decreases upon increasing TPP content. For TPP (i.e. the α_2 -process), with up to 50 % m-TPTS added, an anti-plasticizer effect is observed. When further decreasing the TPP content $T_{g,2}$ shows a maximum and decreases again. This behavior is observed due to a transition of the respective time-constants of the α_2 -

process from a VFT-behavior above $T_{g,1}$ to an Arrhenius-behavior below $T_{g,1}$ with a decreasing apparent activation energy with decreasing TPP content. Thus, upon extrapolating to $\tau(T_g) = 100$ s the apparent T_g decreases. This decrease of $T_{g,2}$ is confirmed with corresponding DSC measurements detecting the respective transition calorimetrically. We suggest an intrinsic confinement effect of the additive in the frozen matrix, as the revealed dynamics resemble those dynamics found in confined space such as pores and as predicted by mode-coupling theory.

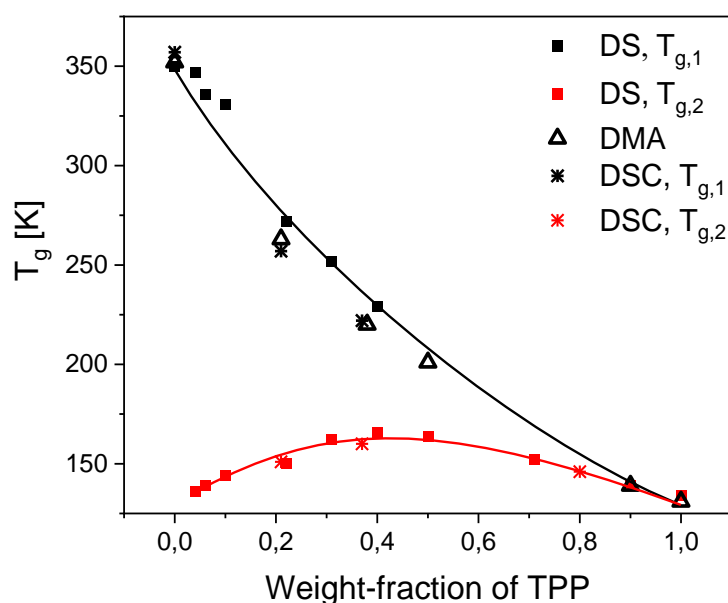


Figure 3.4.3: T_g s as measured by DS, DSC, and DMA for all m -TPTS / TPP systems. Black indicates $T_{g,1}$, red $T_{g,2}$. Squares indicated the T_g as determined by DS, stars indicate T_g as determined by DSC and open triangles indicate T_g as determined by DMA. Lines: guide for the eye. Reproduced by permission of the PCCP Owner Societies from Publication 4.3.

The results of this chapter, published as a full paper, reveal new insight in the dynamics of asymmetric, binary glass-forming systems. It becomes clear that the observed phenomena are mainly affected by the T_g -contrast of such systems rather than by their structure. In general, no big difference can be seen between polymeric and non-polymeric glass formers in such systems.

3.5. Poly(olefin sulfone)s as new resist materials for thermal scanning probe lithography.

In thermal scanning probe lithography (t-SPL), a heated AFM-tip evaporates the resist material to generate a pattern in a direct-write approach. Polymers depolymerizing under the influence of thermal energy and molecular glasses that can be evaporated have been considered as resist materials in the past. However, molecular glasses have been proven less applicable for t-SPL due to limited removal of high molecular weight glasses and the increased surface mobility. So far, only poly(phthal aldehyde) (PPA) is commercially used as a resist for t-SPL as it meets all important requirements such as high sensitivity, stable pattern formation, and transferability into the substrate. This, however, limits possible applications of patterned structures to conditions where PPA shows sufficient stability. In conclusion, the development of alternative novel resist materials will play an important role in establishing t-SPL for further applications.

In this work, we present poly(olefin sulfone)s as a new promising class of resist materials for t-SPL. Poly(2-methylpentene sulfone) (PMPS) and poly(cyclohexene sulfone) (PCHS) were synthesized and their writing capability investigated. Both polymers show similar sensitivity in the writing process as compared to PPA. Furthermore, the obtained images are stable in acidic conditions ($\text{pH} = 1$), as opposed to PPA films that dissolve instantly in solution of $\text{pH} = 1$. A patterned example is shown in Figure 3.5.1, where an image of the Bayreuth Festspielhaus in PMPS is shown before and after 1 h immersion into 0.1 M HCl solution. No observable difference can be found between both images.

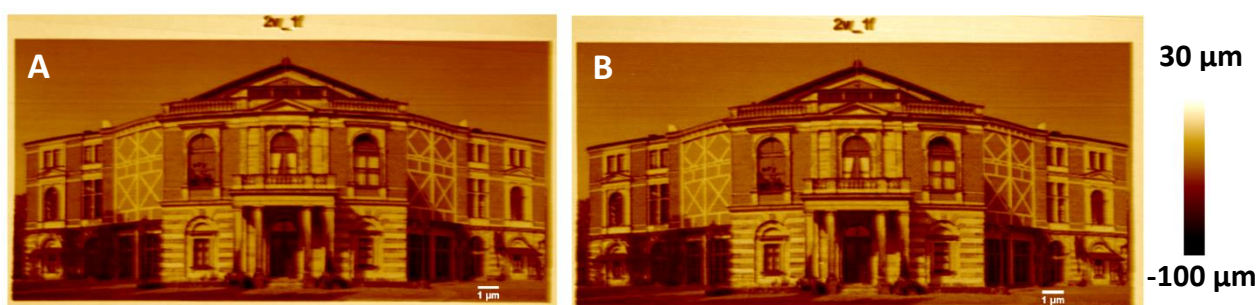


Figure 3.5.1: Image of the Bayreuth Festspielhaus written by t-SPL into PMPS before (A) and after (B) 1 h immersion into 0.1 M HCl solution. Original Photo © Guido Radig under CC BY-SA 3.0.

Furthermore, the high-resolution capabilities of PMPS were investigated. Therefore, line-and-space patterns were written into a 7 nm thin PMPS film. The results are shown in Figure 3.5.2. 10 nm half-pitch lines could be written with a depth of 3 nm into the resist, whereas complete resist removal with 7 nm depth was obtained for 27 nm half-pitch.

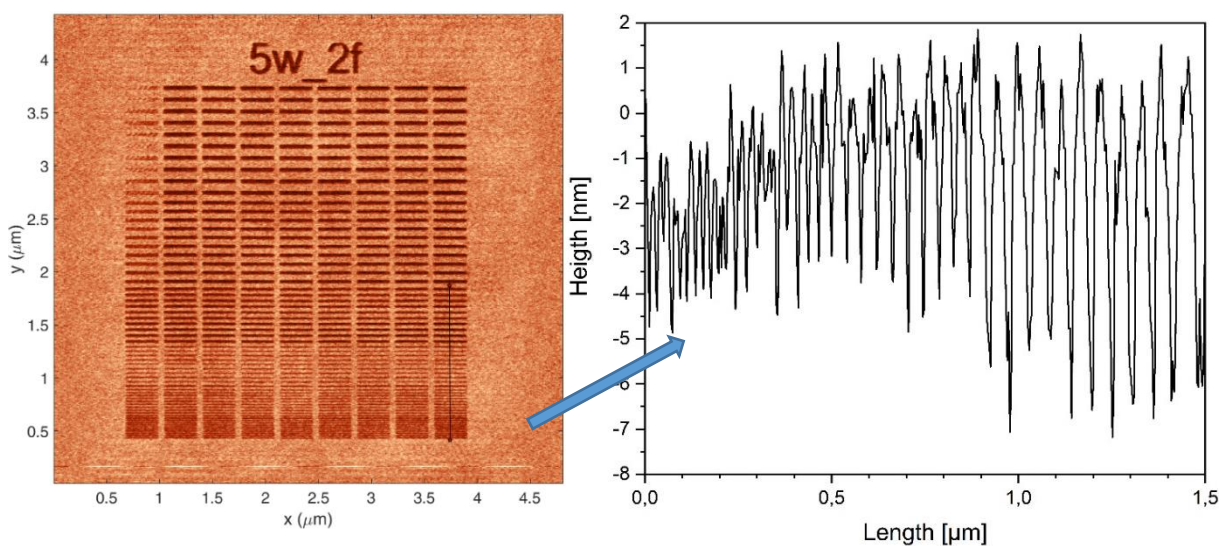


Figure 3.5.2: Line and space patterns written by t-SPL into a 7 nm thin PMPS film and cross section of the highlighted area.

Using Sequential Infiltration Synthesis the polymer was infiltrated with aluminum resulting in an enhanced etch resistance which is required for a possible pattern transfer into the substrate. A selectivity of 3.75 against SiO_2 is demonstrated.

In conclusion, poly(olefin sulfone)s can be used as resist materials for t-SPL offering similar writing sensitivity and resolution as compared to PPA. A clear advantage of poly(olefin sulfone) resists is their acid resistance which offers new options for the application of these t-SPL written patterns. The results of this chapter are intended for publication once pattern transfer has been achieved.

4. Publications and manuscripts

4.1. Individual contributions to joint publications

The publications and manuscripts in this thesis emerged from collaborations with scientists of different departments and facilities. In the following, the individual contributions of each author are presented. The work done by myself was performed at the chair of Macromolecular Chemistry I at the University of Bayreuth under supervision of Prof. Dr. Hans-Werner Schmidt.

Publication 1: Organic Glasses of High Glass Transition Temperatures Due To Substitution with Nitrile Groups

J. Phys. Chem. B **2019**, 123, 10286-10293.

Felix Krohn, Christian Neuber, Ernst A. Rössler, and Hans-Werner Schmidt

In this contribution, a series of nitrile containing molecular glasses based on 9,9'-spirobi[9H]fluorene is investigated with respect to the influence of nitrile groups on T_g and glass forming ability. I designed the molecules that were selected for this study and performed synthesis, analysis, and thermal characterization. I evaluated the measured data and found the strong correlation of M and T_g in the presence of nitrile groups. The draft of the manuscript was written by me with the help of Dr. Christian Neuber (Macromolecular Chemistry I, University of Bayreuth). Prof. Dr. Ernst A. Rössler (Inorganic Chemistry III, University of Bayreuth) gave valuable input in the presentation of the data and the preparation of the manuscript. Prof. Dr. Hans-Werner Schmidt (Macromolecular Chemistry I, University of Bayreuth) conceived the topic and supervised the project. The manuscript was jointly finalized with the contribution of all co-authors.

Publication 2: Main and secondary relaxations of non-polymeric high- T_g glass formers as revealed by dielectric spectroscopy

Phys. Chem. Chem. Phys. **2020**, 22, 9086-9097

Thomas Körber, Felix Krohn, Christian Neuber, Hans-Werner Schmidt, and Ernst A. Rössler

In this contribution, a series of molecular glasses based on 9,9'-spirobi[9H]fluorene is investigated with respect to the influence of selected side groups, mainly nitrile groups, on the nature of their relaxation behaviors. I synthesized all molecules and performed DSC and dielectric measurements as well as the basic evaluation of the dielectric spectroscopy data. Thomas Körber (Inorganic Chemistry III, University of Bayreuth) performed the detailed evaluation of the dielectric spectroscopy data. Prof. Dr. Ernst A. Rössler (Inorganic Chemistry III, University of Bayreuth) supervised the project and was involved in scientific discussion. Prof. Dr. Hans-Werner Schmidt and Dr. Christian Neuber (Macromolecular Chemistry I, University of Bayreuth) were involved in scientific discussion. The paper draft was partly written by myself, Thomas Körber, and Ernst A. Rössler and jointly finalized with the contribution of all co-authors.

Publication 3: Reorientational Dynamics of highly asymmetric binary non-polymeric mixtures – a dielectric spectroscopy study

Thomas Körber, Felix Krohn, Christian Neuber, Hans-Werner Schmidt, and Ernst A. Rössler

In this contribution, a new binary asymmetric glass-forming system based on a non-polymeric high- T_g component and the additive tripropyl phosphate is established. The dynamics of these mixtures are thoroughly investigated by dielectric spectroscopy, DSC, and DMA. I designed and synthesized the high- T_g component. I performed and evaluated DMA measurements, prepared the DSC samples and evaluated the results that were obtained from Mettler. Dielectric spectroscopy and evaluation of the obtained data was done by me. Thomas Körber (Inorganic Chemistry III, University of Bayreuth) performed the detailed evaluation and fitting of the obtained data. Dr. Christian Neuber (Macromolecular Chemistry I, University of Bayreuth) was involved in scientific discussion with his expertise in synthesis and molecular glasses and gave valuable input in molecular design and synthesis. Prof. Dr. Ernst A. Rössler (Inorganic Chemistry III, University of Bayreuth) co-conceived the topic, supervised the project

from the side of the Inorganic Chemistry III group, gave valuable input required for the understanding of this complex system and was involved in scientific discussion. Prof. Dr. Hans-Werner Schmidt (Macromolecular Chemistry I, University of Bayreuth) co-conceived the topic, supervised the project from the side of Macromolecular Chemistry I, and was also involved in scientific discussion. The paper was written by me and Thomas Körber with the help of Dr. Christian Neuber and Prof. Dr. Ernst A. Rössler and jointly finalized with the contribution of all co-authors.

Publication 4: Poly(olefin sulfone)s as new resist materials for thermal scanning probe lithography

Felix Krohn, Armin W. Knoll, Samuel Bisig, Francesca Ruggeri, Christian Neuber, and Hans-Werner Schmidt

In this contribution, poly(olefin sulfone)s are investigated as new resist material for thermal scanning probe lithography. I synthesized the polymers and performed the characterization. I developed and investigated the possible use of tetraalkyl-ammonium salts as thermal base generators and carried out the mixing of the polymers with the salts. The patterning using t-SPL was partly carried out by myself at IBM Research Zurich with the help of Dr. Armin W. Knoll. Sequential Infiltration Synthesis and AFM imaging were done by myself. Dr. Armin W. Knoll (IBM Research Zurich) helped with the project from the side of IBM, gave valuable input in discussions, and performed and helped with t-SPL patterning. Samuel Bisig (Heidelberg Instruments Nano) helped within the project from the side of SwissLitho / Heidelberg Instruments Nano, gave valuable input in discussions, and carried out some t-SPL patterning and the SEM measurements. Dr. Francesca Ruggeri (IBM Research Zurich) performed and evaluated the RIE. Dr. Christian Neuber (Macromolecular Chemistry I, University of Bayreuth) helped with polymer synthesis and characterization and gave valuable input in discussions. Prof. Dr. Hans-Werner Schmidt (Macromolecular Chemistry I, University of Bayreuth) supervised the project from the side of the University of Bayreuth. The draft of the manuscript was written by myself with the help of Dr. Christian Neuber, Dr. Armin W. Knoll, and Samuel Bisig. It was jointly finalized with the contribution of all co-authors.

4.2. Organic Glasses of High Glass Transition Temperatures Due To Substitution with Nitrile Groups

Felix Krohn[†], Christian Neuber^{,†}, Ernst A. Rössler[‡] and Hans-Werner Schmidt^{*,†}*

[†]Department of Macromolecular Chemistry I and Bavarian Polymer Institute, University of Bayreuth, 95440 Bayreuth, Germany

[‡]Department of Inorganic Chemistry III and North Bavarian NMR Center, University of Bayreuth, 95440 Bayreuth, Germany

The results have been published as a full paper in

J. Phys. Chem. B **2019**, 123, 10286-10293.

Copyright © 2019, American Chemical Society.

DOI: 10.1021/acs.jpcc.9b08792

4.2.1. Abstract

The glass transition temperature (T_g) of a molecular glass depends on its molar mass. However, the nature of intermolecular interactions also plays a major role in both the glass transition temperature and its glass-forming ability. In this context, we report on novel molecular glasses containing nitrile groups and investigate the influence of this highly polar group on T_g and the glass-forming ability. As reference compounds, we studied the thermal properties of synthesized molecular glasses with C–C-bonded phenyl rings. The molar mass of the studied compounds ranges from 341 to 568 g/mol. Despite their relatively low molar mass, glass transition temperatures from 347 K (74 °C) to 471 K (198 °C) were observed. Most of the compounds possess high T_g/T_m ratios between 0.7 and 0.8. By introducing highly interacting nitrile groups, the dependence of the molar mass on T_g could be increased by a factor of 2–3.

4.2.2. Introduction

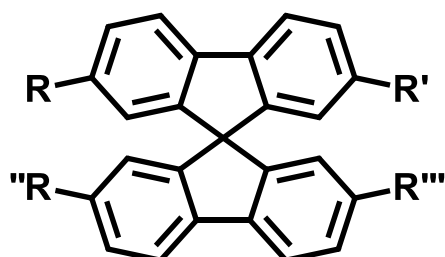
Amorphous non-polymeric organic materials have gained increasing interest in research over the past decades. Applications range from the use in electronic devices such as OLEDs¹⁻⁴ and OFETs⁵ to resist materials for lithography⁶⁻⁸ and pharmaceutical applications.^{9,10} Their advantages are based on the combination of specific properties usually observed in polymers, such as a high T_g , allowing the formation of stable thin films. Furthermore, they offer the benefits of a well-defined molecular structure, the use of standard chromatographic purification techniques, and the accessibility of the gaseous phase, thereby enabling solvent-free vapor processing.^{11,12} However, their application is limited due to the typically low stability of the amorphous state with respect to crystallization as compared to polymeric glass formers.^{9,13} To quantify the stability of a molecular glass, some researchers introduced the quotient T_g/T_m .^{14,15} It was reported that for many amorphous compounds, $T_g/T_m \approx \frac{2}{3}$, although higher and lower values have been reported as well.^{16,17} As a consequence, the glass-forming ability of a molecular glass is often correlated to this ratio: the higher T_g/T_m , the higher is the glass-forming ability.^{18,19} Based on this observation, one may even ask if T_g/T_m may approach 1, which could lead to a thermodynamically stable glass.

Many researchers have investigated the glass-forming abilities and T_g s of various molecular glasses in order to identify guidelines for a molecular design. As a result, a stable molecular glass should possess a nonplanar molecular structure (such as a star shape), bulky substituents, the ability to form different conformers, and usually a particularly high molar mass.^{20,21} In order to increase T_g , it is commonly proposed to introduce inflexible units into the molecule as well as to increase the molar mass.²⁰ Substituents that form strong intermolecular interactions, such as large aromatic systems, which develop π - π -interactions and dipolar groups, are also known to increase T_g . However, they also increase the tendency for crystallization, making them less favorable for applications.¹⁹ Naito and Miura reported that a strong asymmetric shape increases the entropy of the phase transitions, which results in a lower T_g . This means that, counterintuitively, a symmetric shape is required for a stable high- T_g molecular glass formation.¹⁶ Certain applications such as nano-lithography require the use of high- T_g materials to increase pattern resolution for ultra-thin films.²² The required bulky substituents and increased molar mass may, however, limit their applicability in processes such as physical vapor deposition. A deep knowledge of how to adjust the T_g of molecular glasses is therefore crucial in order to fine tune the material properties for the respective application.

Although there has been some research on the interdependence of molar mass (M) and T_g , detailed investigations of the influence of functional groups on T_g are rather rare. For polymers, the relation of M and T_g is well known as the Flory-Fox equation, where T_g approaches a certain value at high M. For molecular glasses, however, no such saturation is observed.¹⁷ Novikov and Rössler examined a vast number of molecular glasses and found that the T_g is linked to the molar mass of a compound via a power law of the form $T_g \sim M^\alpha$, $\alpha = 0.5$.¹⁷ This trend, however, was obtained by generalizing over many different architectures and functional groups, resulting in a large scatter of the T_g data (see also Figure 4.2.7). This is supported by an R^2 value of only 0.87 for the corresponding fit. Liu et al. investigated, amongst other properties, T_g and T_m of a series of trisnaphthylbenzene derivatives.¹⁹ Fitting their provided data, we calculated $\alpha = 0.31$ for naphthyl substituents, and $\alpha = 0.69$ for anthracyl substituents. Ping et al. investigated the glass-forming abilities of cyclic stilbene derivatives.²³ Their investigation focused on the glass-forming ability; however, when we extracted M and T_g in this homologous series, we obtained a value of $\alpha = 0.52$. Wuest and

Lebel examined the influence of different functional groups and alkyl chains attached on 4,6-bis(methylamino)-1,3,5-triazines on the T_g , but except for a trend of decreasing T_g with increasing length of the attached alkyl chain (internal plasticizer effect), their investigations remained rather qualitative.²⁴ Clearly, besides the influence of M, specific interaction cannot be ignored. To the best of our knowledge, the influence on the T_g by adding other (especially polar) moieties to an aromatic core molecule and of their specific substitution position has not yet been investigated in detail.

Herein, we present a series of novel, high- T_g molecular glasses based on the 9,9'-spirobi[9H]fluorene core. We varied M by adding C-C-bonded phenyl rings, and attached nitrile groups at selected positions to quantify the influence on the T_g as compared to non-nitrile-containing systems of the same architecture. The general structure of 9,9'-spirobi[9H]fluorene is shown in Figure 4.2.1. In order to compare the influence of different substituents, we limited the positions of the substituents to the 2,2',7,7' positions of the spiro core. Substituents of the investigated molecular glasses include hydrogen, nitrile groups, phenyl rings, and/or cyanophenyl moieties.



R, R', R'', R''' = H, CN, Ph, Ph-CN

Figure 4.2.1: General structure of investigated 9,9'-spirobi[9H]fluorene and the positions of installed substituents.

9,9'-spirobi[9H]fluorene was selected as it has already been extensively investigated as a core molecule for high- T_g materials, especially for opto-electronic devices.^{25–28} In addition, we selected nitrile groups as functional groups, as they are known to readily undergo self-association with bonding energies of about 20 kJ/mole.^{29,30} Attaching these small, strongly interacting groups into structurally related molecules should yield a much higher T_g dependence of the molar mass and thus a higher value for α . Further, we evaluate T_g/T_m of these synthesized compounds and present their correlation to the molecular symmetry and the attached nitrile groups.

4.2.3. Materials and Methods

Thermogravimetric analysis (TGA) was conducted on a Mettler TGA/DSC3 with a heating rate of 10 K/min under nitrogen flow. Differential scanning calorimetry was performed with a Mettler DSC3+ in pierced Al pans at 10 K/min under nitrogen flow. The T_g was determined as the onset temperature of the step. T_m was determined as the peak temperature of the melting peak. These calculations were performed by Mettler STARe 15.00a software. Magnetic resonance spectra were recorded on a Bruker Avance 300 with CDCl_3 as solvent. Commercial solvents and reagents were used without further purification.

4.2.4. Results

In order to obtain reference data, pure and phenyl-substituted 9,9'-spirobi[9H]fluorenes **1-4**, as shown in Figure 4.2.2, were investigated first. These reference compounds possess a fully aromatic architecture without nitrile-containing substituents, which will be considered later in this work. They all feature similar interactions, most importantly, π - π -interactions. Therefore, they are ideal model compounds to investigate the influence of added phenyl rings on T_g and T_g/T_m . These compounds have already been discussed in literature;^{28,31-34} however, due to different measurement techniques and sample preparation, reported values of T_g differ considerably, i.e. from 420 K to 457 K for **4**. Therefore, we performed our own measurements for a more reliable comparability of the obtained data.

Table 4.2.1 lists M and thermal properties of the reference compounds **1-4**. Despite several quenching attempts, no amorphous phase of **1** was observed. Remarkably, no crystalline phase of **2** was observed; therefore no T_g , T_m , or T_g/T_m could be determined for **1** and **2**. However, Thiery et al. reported a broad melting range of 100-108 °C for **2**.²⁸ Using this melting temperature, the resulting T_g/T_m would be a tremendously high value of 0.93. Within **2-4**, T_g increases with M, as expected, and **4** shows a remarkably high T_g/T_m value of almost 0.8. The temperature of 5 % weight loss in the TGA ($T_{-5 \text{ wt}\%}$) of all compounds is significantly higher than the melting point, indicating sufficient thermal stability against decomposition in the measured range.

4.2 ORGANIC GLASSES OF HIGH GLASS TRANSITION TEMPERATURES DUE TO SUBSTITUTION WITH NITRILE GROUPS

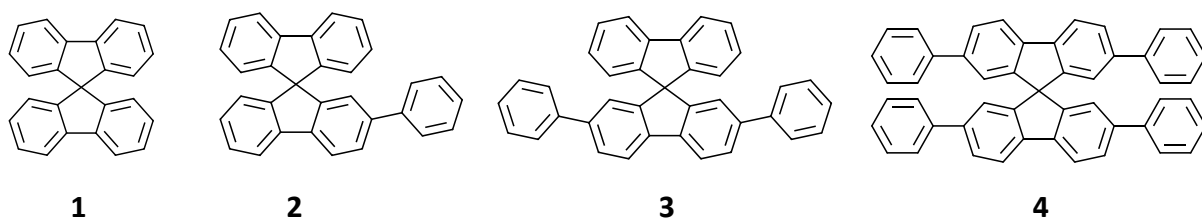


Figure 4.2.2: Reference structures **1-4** of phenyl-substituted spirobifluorenes used in this investigation.

Table 4.2.1: Molar mass (*M*) and thermal properties of phenyl-containing molecular glasses

| Compound | <i>M</i> | $T_g^{a)}$ | $T_m^{a)}$ | T_g/T_m | $T_{-5 \text{ wt}\%}^{b)}$ |
|----------|-----------|------------|---------------------------------------|---------------------------|----------------------------|
| 1 | 316 g/mol | - | 475 K | - | 526 K |
| 2 | 392 g/mol | 355 K | 373 K – 381 K (Lit.) ²⁸ | 0.93 (Lit.) ²⁸ | 577 K |
| 3 | 468 g/mol | 389 K | 531 K | 0.73 | 641 K |
| 4 | 620 g/mol | 447 K | 568 K | 0.79 | 705 K |

Measured by DSC, 2nd heating run, heating rate of 10 K/min, N₂; b) measured by TGA, heating rate of 10 K/min, N₂.

Figure 4.2.3 shows T_g and T_m vs. *M* for compounds **1**, **2**, **3**, and **4** in a double logarithmic plot. As discussed in the introduction, we observe an increasing T_g with increasing *M* that seems to follow a power law. Fitting this data yields $T_g \sim M^{0.50}$, which is in good agreement with previously published results.^{17,19,23} As can also be seen, T_m of **1**, **3**, and **4** exhibits a similar relationship; however, T_m of **2**, which was taken from the literature, is more than 100 K lower than expected by this trend and was thus not taken into account. The fit of the melting points of **1**, **3**, and **4**, however, shows a weaker dependence on *M* than that of the T_g data. If these trends continued to higher *M*, T_g/T_m could reach unity at sufficiently high *M*, thereby enabling a thermodynamically stable glass. In order to verify this trend, data from two further systems taken from literature with the same core but larger aromatic substituents, spiro sexiphenyl and 4-spiro^{2,27,34} are added to Figure 4.2.3. Clearly, the trend of **2-4** concerning T_g is not continued, and the influence of increasing *M* on T_g is lower than observed regarding the systems investigated here. The trend concerning T_m continues and essentially parallels that of T_g . There is still a rather high degree of scattering between the different works. This scattering, however, is small with respect to the entirety of molecular glasses considered by Novikov and Rössler due to less scatter of specific interaction (compare also to Figure 4.2.7), yielding an R^2 of the fit of 0.96. However, the observed dependence of T_g on *M* is much lower as compared to previously published work.^{17,19,23}

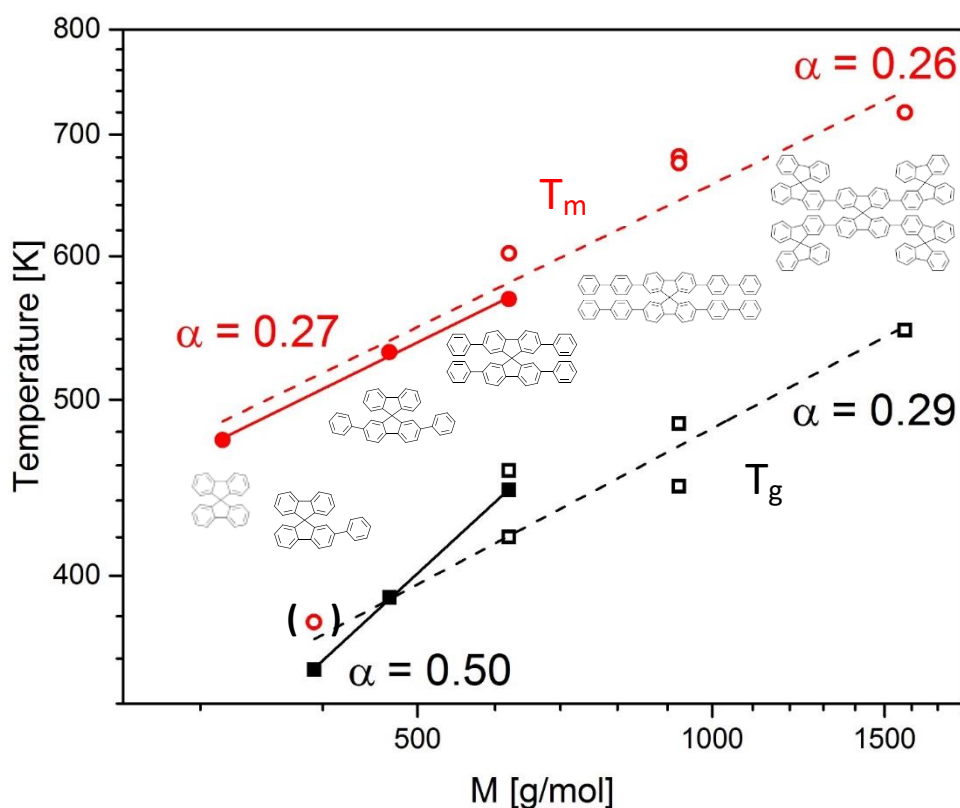


Figure 4.2.3: Double logarithmic plot for glass transition temperatures (black) and melting points (red) vs. M . Our own measurements are indicated by solid symbols, literature values by open symbols. Power-law fits of our own measurement data are shown as solid lines, power-law fits of all data of T_g or T_m are indicated by dashed lines. Brackets indicate the literature value for T_m of **2** which was not taken into account. Literature values of **4** and spiro-sexiphenyl:^{27,34} Literature values of spiro-4:^{2,27}

In order to study the influence of strongly interacting substituents (in this case, nitrile groups) attached to 9,9'-spirobi[9H]fluorene on T_g and T_m , compounds **1-3** (see Figure 4.2.2) were selected.

In the following, compounds based on pure 9,9'-spirobi[9H]fluorene (**1**) will be denoted as architecture I, compounds based on 2-phenyl-9,9'-spirobi[9H]fluorene (**2**) will be denoted as architecture II, and the compounds based on 2,7-biphenyl-9,9'-spirobi[9H]fluorene (**3**) will be denoted as architecture III. The structures of all nitrile-containing compounds used are shown in Figure 4.2.4. The molar masses and thermal properties of these compounds are summarized in Table 4.2.2.

Table 4.2.2: Molar masses and thermal properties for all nitrile compounds investigated in this study.

| Compound | Architecture | M | $T_g^{a)}$ | $T_m^{a)}$ | T_g/T_m | $T_{-5\text{ wt}\%}^{b)}$ |
|-----------------|--------------|-----------|------------|------------|-----------|---------------------------|
| 5 | I | 341 g/mol | 347 K | 508 K | 0.68 | 568 K |
| 6 | | 366 g/mol | 390 K | 540 K | 0.72 | 598 K |
| 7-ortho | II | 417 g/mol | 363 K | 452 K | 0.80 | 568 K |
| 7-meta | | | 368 K | 464 K | 0.79 | 603 K |
| 7-para | | | 380 K | 494 K | 0.77 | 598 K |
| 8-ortho | II | 492 g/mol | 435 K | 586 K | 0.74 | 668 K |
| 8-meta | | | 438 K | 593 K | 0.74 | 693 K |
| 8-para | | | 458 K | 620 K | 0.74 | 703 K |
| 9-ortho | III | 518 g/mol | 400 K | 589 K | 0.68 | 658 K |
| 9-meta | | | 400 K | 568 K | 0.70 | 662 K |
| 9-para | | | 427 K | 583 K | 0.73 | 683 K |
| 10-ortho | III | 568 g/mol | 429 K | 600 K | 0.72 | 688 K |
| 10-meta | | | 437 K | 613 K | 0.71 | 733 K |
| 10-para | | | 471 K | 613 K | 0.77 | 723 K |

Measured by DSC, 2nd heating run, heating rate of 10 K/min, N₂; b) measured by TGA, heating rate of 10 K/min, N₂.

Table 4.2.3 shows the calculated values for α with respect to the architecture of the molecule and the position of the nitrile group. In all cases, a strong effect of M on T_g can be observed. Architecture I shows the highest value with $\alpha = 1.65$. For architecture II, the values are in the order of 1 whereas for architecture III this only applies if the nitrile groups are in para-position. If the nitrile groups are in *ortho*- or *meta*-position, α is about halved to 0.5 – 0.6. The trend seen in Table 4.2.2 concerning T_g increasing in the sense of *ortho* – *meta* – *para* is reflected in Table 4.2.3 with increasing α in the same sense.

Table 4.2.3: Calculated values for α for the different architectures and nitrile positions.

| Architecture | I | II ortho | II meta | II para | III ortho | III meta | III para |
|--------------|----------|-----------------|----------------|----------------|------------------|-----------------|-----------------|
| α | 1.65 | 0.93 | 0.98 | 1.11 | 0.51 | 0.62 | 1.00 |

4.2 ORGANIC GLASSES OF HIGH GLASS TRANSITION TEMPERATURES DUE TO SUBSTITUTION WITH NITRILE GROUPS

In order to compare the influence of the position of the nitrile group, a more detailed look on the data is needed. Therefore, Figure 4.2.5 shows the T_m and T_g for all compounds of architecture II and III, including the reference compounds 2 and 3, in a double logarithmic plot. In Figure 4.2.5A, the plot for architecture II, and in Figure 4.2.5B, the plot for architecture III, is shown.

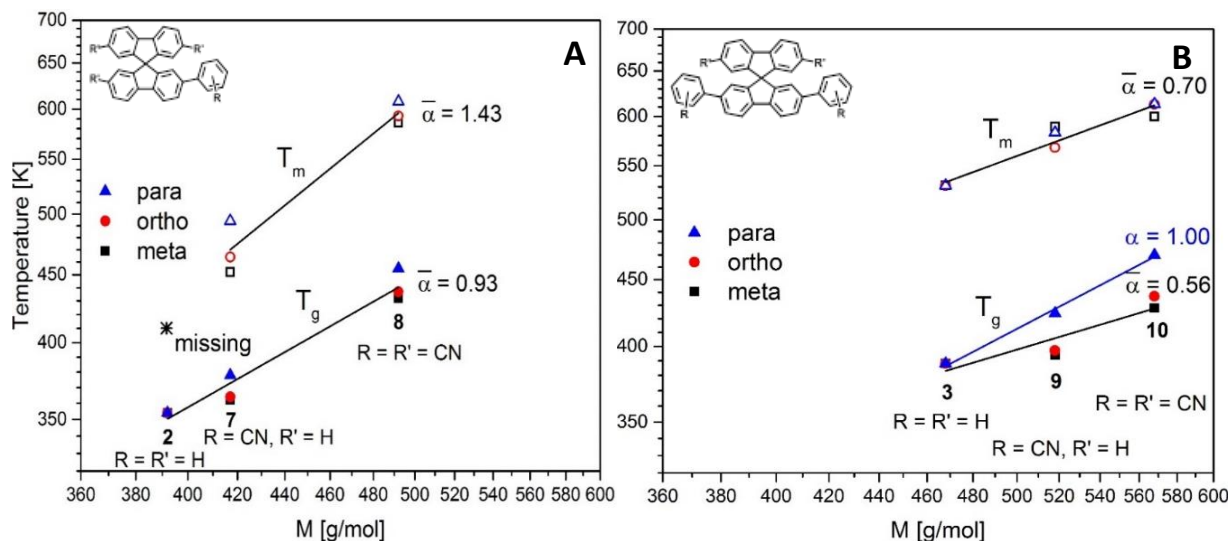


Figure 4.2.5: T_g (solid symbols) as a function of M with power-law fit (lines) and T_m (open symbols) with power-law fit (lines) for nitrile-containing compounds with architecture II (Figure 4.2.5A, left) and architecture III (Figure 4.2.5B, right), $\bar{\alpha}$ indicates average value of fits, position of the substituents R is indicated by the symbols: ortho (black square), meta (red circle), and para (blue triangle).

The influence of M on T_g has already been noted in Table 4.2.3. Regarding T_m for architecture II, the increase is much higher as compared to the T_g increase, resulting in decreasing T_g/T_m with increasing M. For architecture III, the trend concerning T_m essentially parallels that of T_g for the *ortho*- and *meta*-substituted compounds. However, the slope for T_g is clearly steeper than for T_m for *para*-substituted compounds, which results in an increase of T_g/T_m with increasing M. Looking in more detail at the measured data, it can be observed that for *para*-substitution, all three points are essentially on a straight line, whereas for *meta*- and *ortho*-substitution, the middle point of the line is always below the fit.

Figure 4.2.6 shows the T_g/T_m ratios for the investigated molecular glasses with architecture I (star, dotted lines), architecture II (solid symbols and lines) and architecture III (open symbols, dashed lines).

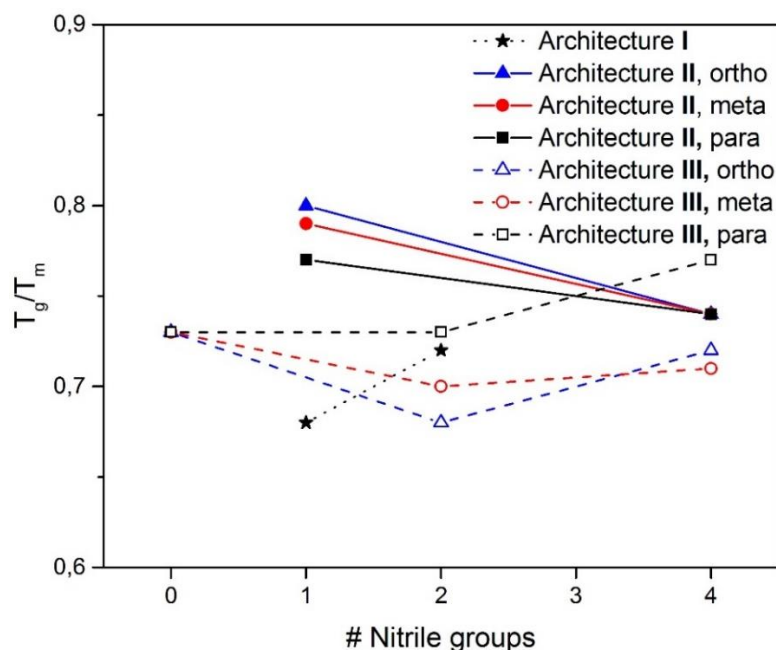


Figure 4.2.6: T_g/T_m dependence on architecture and number of added nitrile groups.

For architecture II, T_g/T_m of the compounds decreases with increasing number of attached nitrile groups. This is consistent with the observation of Naito and Miura, that strong intermolecular cohesion – as is present with the introduction of nitrile groups – reduces the stability of the amorphous state.¹⁶ With one nitrile group attached, T_g/T_m decreases in the sense of *ortho* – *meta* – *para*, whereas with four attached nitrile groups, T_g/T_m is the same for all three isomers. For architecture III, T_g/T_m decreases or, in the case of *para*-substitution, remains constant even with two nitrile groups. Two additional nitrile groups, however, cause an increase in T_g/T_m . Contrary to architecture II, the highest T_g/T_m can be observed for *para*-substitution. For architecture I, $\frac{T_g}{T_m}$ also increases from one to two nitrile groups.

4.2.5. Discussion

For further discussion, we refer to the nitrile groups that are directly bonded to the spiro-core as *inner* nitrile groups, and those that are attached to an additional C-C-bonded phenyl ring as *outer* nitrile groups. As already mentioned in the Results, the steepest slope of lines (i.e., the highest value for α) can be observed when the outer nitrile groups are in the *para*-position. In this case, $\alpha = 1.12$ for architecture II and $\alpha = 1.00$ for architecture III. These values, however, are significantly lower than for architecture I, where $\alpha = 1.65$. The molecules with

architecture I only possess *inner* nitrile groups. Therefore, we attribute this high value for α to the fact that any interaction between two nitrile groups directly links two spiro-cores together, whereas in molecules of architecture II or III, some interactions will always have *outer* nitrile groups involved. Here, we assume that some of the rigidity of the system gets lost because of the additionally attached phenyl ring. This observation is supported as α is usually higher for architecture II than for architecture III, especially in the case of the outer nitrile groups being in *ortho*- or *meta*-position. For architecture II, only one outer nitrile group is present, whereas in architecture III two outer nitrile groups are present. Therefore, the ratio of interactions involving one of the outer nitrile groups will increase for architecture III, hence α will decrease.

When the outer nitrile groups are in the *ortho*- or *meta*-position, α drastically decreases from 1.12 to about 0.95 in the case of architecture II, and from 1.00 to only 0.50 to 0.60 in the case of architecture III as compared to *para*-substituted nitriles. As stated above, it can also be observed that for the *ortho*- or *meta*-position, any middle point of the dataset, i.e., the point where only the *outer* nitrile groups were added, is below the respective power-law fit. In conclusion, those *ortho*- or *meta*-substituted outer nitrile groups influence the thermal properties considerably less than the *inner* or outer *para*-substituted nitrile groups.

Most literature favors a perfect antiparallel alignment for nitrile groups in order to achieve high association energy.^{29,30,35} However, especially in compounds with bulky moieties, this perfect alignment can often not be achieved. As discussed above, the increase in T_g is a measure of intermolecular interaction, hence it can be stated that the intermolecular interaction is in the order *ortho* < *meta* < *para* substitution for *outer* nitrile groups. We assume two effects taking part in this observation: The first is the fact that nitrile groups in the *ortho*-position point towards the central fluorene unit, which, with its high steric demand, might prevent perfect alignment of the nitrile groups. The second point is the fact that the phenyl ring attached to the spiro-core may be able to rotate, or, as free rotation may be hindered, at least to flip back and forth. For a nitrile group in *para*-substitution, a flipping phenyl ring does not alter its position, as these nitrile groups are placed in line with the rotational axis. Therefore it is concluded that, in order to increase the T_g of a molecular glass, it is not sufficient to introduce only strongly interacting groups, but it is also very important for these groups to be attached to a rigid core of the molecule or at least be in the rotational axis of the respective moiety.

Furthermore, the dipole moment of the compounds should be considered, as it will change drastically with the introduction of highly polar groups. Sun et al. performed DFT calculations for a set of spiro[fluorene-9,9'-xanthenes], also possessing nitrile-substitutions at the 2 or 2,7-positions of the fluorene unit.³⁶ Their calculations yielded a dipole moment μ of 1.00 D for the unsubstituted, 5.51 D for the mono-substituted, and 1.59 D for the di-substituted compound. Clearly, unsymmetrical substitution with nitrile groups yields a high overall dipole moment, whereas symmetrical substitution cancels this dipole moment yielding a quadrupole moment. In our work, for architecture **I** measured T_g s of **5** and **6** with monosubstituted and disubstituted nitrile groups, correspondingly, increase from 347 K to 390 K and for architecture **II** measured T_g s of **2**, **7-para** and **9-para** with unsubstituted, mono-substituted, and tetra-substituted nitrile groups, correspondingly, increase independent of the corresponding dipole moment from 355 K to 380 K to 427 K. In conclusion the increase in T_g is mainly driven by the numbers of the nitrile groups due to locally strong dipole-dipole interactions rather than the overall dipole moment of the molecule.

In Figure 4.2.6, a decreasing T_g/T_m can be seen with increasing number of nitrile groups in architecture **II**. Here, it can be assumed that, in the crystalline state, nitrile groups are arranged in perfect anti-parallel orientation, unlike in the unordered amorphous glass. Therefore, the interactions between the nitrile groups are more perfect in the crystalline than in the amorphous state, hence the increase in T_m is stronger than the increase in T_g . Liu et al.¹⁹ observed a similar trend when they compared the influence of phenyl, naphthyl, and anthracyl groups. The larger the side groups, the more pronounced are their π - π -interactions, with a higher impact on T_m than on T_g , thereby reducing T_g/T_m . For architecture **III**, T_g/T_m is lower than for architecture **II**, except for compound **10-para** which shows the highest T_g/T_m ratio in all compounds containing four nitrile groups. In contrast to architecture **II**, T_g/T_m is increased for all compounds of **10** as compared to their **9** analogue, i.e. the ratio is increased by increasing the number of nitrile groups. This may be due to a more globular shape of the molecule, i.e. by increasing the symmetry in the sense of Naito and Miura.¹⁶ In accordance **10-para** offers the highest symmetry among all of the compounds with four nitrile groups and consequently exhibits the highest T_g/T_m ratio. But considering these conclusions, the T_g/T_m ratios of all compounds of **7** (0.77 – 0.8) seem to be remarkably high. Here, all compounds of **7** offer an unsymmetrical shape and strong dipole moment because of the

mono-substituted nitrile group. However, these features are also offered by **5**, which only shows a T_g/T_m ratio of 0.68. Therefore, we think the specific asymmetry and the overall dipole moment have little influence on the T_g/T_m ratio. We rather think that an obvious explanation for the high T_g/T_m for all compounds of **7** is based on the attached phenyl ring, which contributes to different conformers.

Figure 4.2.7 shows an M versus T_g plot as well as the power-law fit from Novikov and Rössler¹⁷ and the added data points and power-law fits for the investigated compounds. For clarity, only those compounds without nitrile groups and with the outer nitrile groups in para-substitution are shown. In summary, all these investigated molecular glasses show a very high T_g as compared to the reported comprehensive amount of molecular glasses of similar M . As this observation is also valid for compounds **2-4** that do not contain nitrile groups, this is mainly attributed to the rigid core of the utilized 9,9'-spirobi[9H]fluorene. However, for non-nitrile-containing compounds, the slope of the power-law fit essentially parallels the general trend observed by Novikov and Rössler. With the addition of nitrile groups into structurally related molecules, α increases to 1.65 for architecture **I**, 1.11 for architecture **II**, and 1.00 for architecture **III** and thereby reaches values that are about two to three times as high as previously observed in literature.

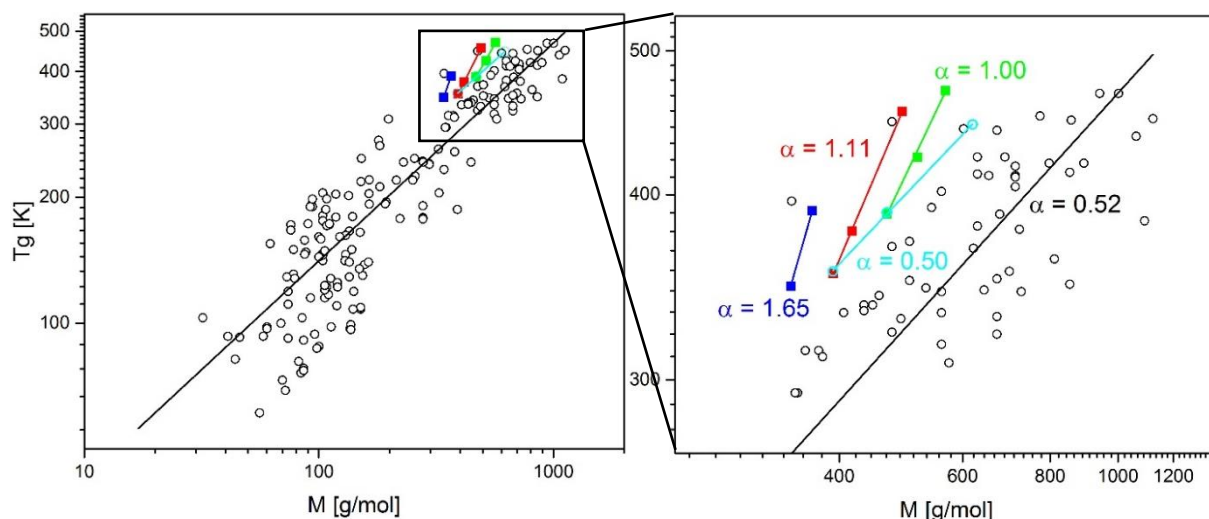


Figure 4.2.7: M vs. T_g plot and zoomed-in view from Novikov and Rössler¹⁷ (black circles and line), with points, power-law fits, and calculated exponents α for the non-nitrile containing compounds **2**, **3**, and **4** (cyan), as well as for architecture **I** (**5** and **6**, blue), architecture **II** (**2**, **7-para**, and **8-para**, red) and architecture **III** (**3**, **9-para**, and **10-para**, green).

4.2.6. Conclusion

A novel series of nitrile-containing molecular glasses featuring very high T_g s and good glass-forming abilities was synthesized and characterized. T_g/T_m of most compounds is between 0.7 and 0.8. By reducing the scatter of specific interaction, the scatter of the T_g -M dependence could be drastically reduced. As a consequence, the influence of phenyl rings and nitrile groups attached to 9,9'-spirobi[9H]fluorene could be quantified. The impact of attached nitrile groups is quantified by a power law of the form $T_g \sim M^\alpha$, with α being about twice to three times as high as for studies previously published in the literature. Attaching nitrile groups increases the T_g to more of an extent when the nitrile groups are either directly attached to the rigid core of the molecule or at the para-position of a C-C-bonded phenyl ring, whereas substitution in *ortho*- or *meta*-position only shows little influence on T_g . The T_g/T_m ratio is not only affected by the amount of nitrile groups, but also by the shape of the whole molecule with higher ratios for more globular, symmetrical shapes. The reported findings and interpretations allow new insight with respect to the impact of added very polar nitrile groups on T_g as well as the glass-forming ability of molecular glasses. Furthermore, it is assumed that the results are guidelines for tailoring glass-forming properties of novel molecular glasses in order to improve their application in fields such as pharmaceuticals, photo resists, or in general for thin film processing.

4.2.7. Acknowledgement

This research was funded by the Deutsche Forschungsgemeinschaft (DFG), grant numbers Schm 703/9-1 and RO 907/19. F.K. acknowledges support from the Elite Network of Bavaria (ENB) within the Elite study program Macromolecular Science.

4.2.8. References

- [1] Niu, Q.; Zhang, Q.; Xu, W.; Jiang, Y.; Xia, R.; Bradley, D. D.C.; Li, D.; Wen, X. *Solution-processed Anthracene-based Molecular Glasses as Stable Blue-light-emission Laser Gain Media*. *Organic Electronics*, **2015**, *18*, 95–100.
- [2] Salbeck, J.; Weissörtel, F.; Bauer, J. *Spiro Linked Compounds for Use as Active Materials in Organic Light Emitting Diodes*. *Macromol. Symp.*, **1997**, 121–132.
- [3] Pang, J.; Tao, Y.; Freiberg, S.; Yang, X.-P.; D'lorio, M.; Wang, S. *Syntheses, Structures, and Electroluminescence of New Blue Luminescent Star-shaped Compounds Based on 1,3,5-triazine and 1,3,5-trisubstituted Benzene*. *J. Mater. Chem.*, **2002**, *12*, 206–212.
- [4] Shen, J. Y.; Lee, C. Y.; Huang, T.-H.; Lin, J. T.; Tao, Y.-T.; Chien, C.-H.; Tsai, C. *High T_g Blue Emitting Materials for Electroluminescent Devices*. *J. Mater. Chem.*, **2005**, *15*, 2455.
- [5] Sonntag, M.; Kreger, K.; Hanft, D.; Strohriegl, P.; Setayesh, S.; Leeuw, D. de. *Novel Star-Shaped Triphenylamine-Based Molecular Glasses and Their Use in OFETs*. *Chem. Mater.*, **2005**, *17*, 3031–3039.
- [6] Tsuchiya, K.; Chang, S. W.; Felix, N. M.; Ueda, M.; Ober, C. K. *Lithography Based on Molecular Glasses*. *J. Photopolym. Sci. Technol.*, **2005**, *18*, 431–434.
- [7] Murotani, E.; Lee, J.-K.; Chatzichristidi, M.; Zakhidov, A. A.; Taylor, P. G.; Schwartz, E. L.; Malliaras, G. G.; Ober, C. K. *Cross-linkable Molecular Glasses: Low Dielectric Constant Materials Patternable in Hydrofluoroethers*. *ACS Appl. Mat. Interfaces*, **2009**, *1*, 2363–2370.
- [8] Felix, N. M.; Silva, A. de; Ober, C. K. *Calix[4]resorcinarene Derivatives as High-Resolution Resist Materials for Supercritical CO₂ Processing*. *Adv. Mater.*, **2008**, *20*, 1303–1309.
- [9] Kissi, E. O.; Grohganz, H.; Löbmann, K.; Ruggiero, M. T.; Zeitler, J. A.; Rades, T. *Glass-Transition Temperature of the β -Relaxation as the Major Predictive Parameter for Recrystallization of Neat Amorphous Drugs*. *J. Phys. Chem. B*, **2018**, *122*, 2803–2808.

- [10] Afzal, A.; Shahin Thayyil, M.; Sulaiman, M. K.; Kulkarni, A. R. *Dielectric Relaxation Studies in Super-cooled Liquid and Glassy Phases of Anti-cancerous Alkaloid: Brucine*. Indian J. Phys., **2018**, *92*, 565–573.
- [11] Pfeiffer, F.; Felix, N. M.; Neuber, C.; Ober, C. K.; Schmidt, H.-W. *Physical Vapor Deposition of Molecular Glass Photoresists: A New Route to Chemically Amplified Patterning*. Adv. Funct. Mater., **2007**, *17*, 2336–2342.
- [12] Pfeiffer, F.; Felix, N. M.; Neuber, C.; Ober, C. K.; Schmidt, H.-W. *Towards Environmentally Friendly, Dry Deposited, Water Developable Molecular Glass Photoresists*. PCCP, **2008**, *10*, 1257–1262.
- [13] Hasebe, M.; Musumeci, D.; Yu, L. *Fast Surface Crystallization of Molecular Glasses: Creation of Depletion Zones by Surface Diffusion and Crystallization Flux*. J. Phys. Chem. B, **2015**, *119*, 3304–3311.
- [14] Turnbull, D. *Under what Conditions Can a Glass be Formed?* Contemp. Phys., **1969**, *10*, 473–488.
- [15] Fedors, R. F. *A Universal Reduced Glass Transition Temperature for Liquids*. J. Polym. Sci. B Polym. Lett. Ed., **1979**, *17*, 719–722.
- [16] Naito, K.; Miura, A. *Molecular Design for Nonpolymeric Organic Dye Glasses with Thermal Stability: Relations between Thermodynamic Parameters and Amorphous Properties*. J. Phys. Chem., **1993**, *97*, 6240–6248.
- [17] Novikov, V. N.; Rössler, E. A. *Correlation between Glass Transition Temperature and Molecular Mass in Non-polymeric and Polymer Glass Formers*. Polymer **2013**, *54*, 6987–6991.
- [18] Baird, J. A.; van Eerdenbrugh, B.; Taylor, L. S. *A Classification System to Assess the Crystallization Tendency of Organic Molecules from Undercooled Melts*. J. Pharm. Sci., **2010**, *99*, 3787–3806.
- [19] Liu, T.; Cheng, K.; Salami-Ranjbaran, E.; Gao, F.; Glor, E. C.; Li, M.; Walsh, P. J.; Fakhraai, Z. *Synthesis and High-throughput Characterization of Structural Analogues of Molecular Glassformers: 1,3,5-trisarylbenzenes*. Soft Matter **2015**, *11*, 7558–7566.

- [20] Shirota, Y. *Photo- and electroactive Amorphous Molecular Materials—Molecular Design, Syntheses, Reactions, Properties, and Applications*. J. Mater. Chem., **2005**, *15*, 75–93.
- [21] Bratton, D.; Yang, D.; Dai, J.; Ober, C. K. *Recent Progress in High Resolution Lithography*. Polym. Adv. Technol., **2006**, *17*, 94–103.
- [22] Silva, A. de; Ober, C. K. *Hydroxyphenylbenzene Derivatives as Glass Forming Molecules for High Resolution Photoresists*. J. Mater. Chem., **2008**, *18*, 1903.
- [23] Ping, W.; Paraska, D.; Baker, R.; Harrowell, P.; Angell, C. A. *Molecular Engineering of the Glass Transition: Glass-Forming Ability across a Homologous Series of Cyclic Stilbenes*. J. Phys. Chem. B, **2011**, *115*, 4696–4702.
- [24] Wuest, J. D.; Lebel, O. *Anarchy in the Solid State: Structural Dependence on Glass-Forming Ability in Triazine-based Molecular Glasses*. Tetrahedron, **2009**, *65*, 7393–7402.
- [25] Lin, Y.; Chen, Z.-K.; Ye, T.-L.; Dai, Y.-F.; Ma, D.-G.; Ma, Z.; Liu, Q.-D.; Chen, Y. *Conjugated Copolymers Comprised Cyanophenyl-Substituted Spirobifluorene and Tricarbazole-Triphenylamine Repeat Units for Blue-Light-Emitting Diodes*. J. Polym. Sci. A Polym. Chem., **2010**, *48*, 292–301.
- [26] Pei, J.; Ni, J.; Zhou, X.-H.; Cao, X.-Y.; Lai, Y.-H. *Head-to-Tail Regioregular Oligothiophene-Functionalized 9,9'-Spirobifluorene Derivatives. 1. Synthesis*. J. Org. Chem., **2002**, *67*, 4924–4936.
- [27] Saragi, T. P. I.; Spehr, T.; Siebert, A.; Fuhrmann-Lieker, T.; Salbeck, J. *Spiro Compounds for Organic Optoelectronics*. Chem. Rev., **2007**, *107*, 1011–1065.
- [28] Thierry, S.; Declairieux, C.; Tondelier, D.; Seo, G.; Geffroy, B.; Jeannin, O.; Métivier, R.; Rault-Berthelot, J.; Poriel, C. *2-Substituted vs 4-substituted-9,9'-spirobifluorene Host Materials for Green and Blue Phosphorescent OLEDs: A Structure-Property Relationship Study*. Tetrahedron, **2014**, *70*, 6337–6351.
- [29] Murray, F. E.; Schneider, W. G. *On the Intermolecular Force Field of Nitriles*. Can. J. Chem., **1955**, *33*, 797–803.

- [30] Saum, A. M. *Intermolecular Association in Organic Nitriles; the CN Dipole-Pair Bond*. J. Polym. Sci., **1960**, *42*, 57–66.
- [31] Kobin, B.; Behren, S.; Braun-Cula, B.; Hecht, S. *Photochemical Degradation of Various Bridge-Substituted Fluorene-Based Materials*. J. Phys. Chem. A, **2016**, *120*, 5474–5480.
- [32] Johansson, N.; Salbeck, J.; Bauer, J.; Weissörtel, F.; Bröms, P.; Andersson, A.; Salaneck, W. R. *Solid-State Amplified Spontaneous Emission in Some Spiro-Type Molecules: A New Concept for the Design of Solid-State Lasing Molecules*. Adv. Mater., **1998**, *10*, 1136–1141.
- [33] Salbeck, J.; Yu, N.; Bauer, J.; Weissörtel, F.; Bestgen, H. *Low Molecular Organic Glasses for Blue Electroluminescence*. Synth. Met., **1997**, *91*, 209–215.
- [34] Schartel, B.; Stümpflen, V.; Wendling, J.; Wendorff, J. H. *Rigid Cross-shaped Multipodes: Molecules Designed for Molecular Reinforcement*. Polym. Adv. Technol., **1996**, *7*, 160–167.
- [35] Lee, S.; Mallik, A. B.; Fredrickson, D. C. *Dipolar-Dipolar Interactions and the Crystal Packing of Nitriles, Ketones, Aldehydes, and C(sp²)–F Groups*. Cryst. Growth Des., **2004**, *4*, 279–290.
- [36] Sun, C.; Lin, Z.; Xu, W.; Xie, L.; Ling, H.; Chen, M.; Wang, J.; Wei, Y.; Yi, M.; Huang, W. *Dipole Moment Effect of Cyano-Substituted Spirofluorenes on Charge Storage for Organic Transistor Memory*. J. Phys. Chem. C, **2015**, *119*, 18014–18021.

4.2.9. Supporting information

4.2.9.1. Synthetic details

2-cyano-9,9'-spirobi[9H]fluorene (**5**) and 2,7-dicyano-9,9'-spirobi[9H]fluorene (**6**) were prepared according to literature procedures.¹ 2,7-dibromo-9,9'-spirobi[9H]fluorene was prepared according to literature procedures.²

General procedure for Suzuki-Miyaura cross coupling: 5 mmol of bromo-substituted 9,9'-spirobi[9H]fluorene are dissolved in 100 mL THF with 1.25 equivalents of the respective phenyl boronic acid. 60 mL 2 M K₂CO₃ are added and argon is flushed through the solution for 30 min. 2 mole-% (according to the boronic acid) of Pd(PPh₃)₄ are added to the mixture and argon is flushed for another 30 min. Subsequently, the mixture is heated to 80 °C for 17 h. After cooling, the phases are separated, the organic phase is washed with brine, dried over MgSO₄, and the solvent is removed under reduced pressure. The crude product is further purified by column chromatography (cyclohexane/ethyl acetate).

General procedure for a Rosenmund-von-Braun reaction: 1 g of bromo-substituted 9,9'-spirobi[9H]fluorene are dissolved in 15 mL of dry DMF under inert atmosphere. Two equivalents of CuCN are added and the mixture is heated to 170 °C for 17 h. After cooling, 40 mL H₂O, 4 mL of 32 % HCl and 5 g FeCl₃ are added and the mixture is kept at 70 °C for another 30 min. After cooling, the mixture is extracted three times with toluene, the organic phases are combined, dried over MgSO₄, and the solvent is evaporated under reduced pressure. The crude product is further purified by column chromatography (cyclohexane/ethyl acetate).

2,7-dibromo-2',7'-dicyano-9,9'-spirobi[9H]fluorene: 2 g (5.47 mmol) of 2,7-dicyano-9,9'-Spirobi[9H]fluorene (**6**) are dissolved in 20 mL DCM with 45 mg (5 mole-%) FeCl₃. 3.5 g (22 mmol) of Br₂ are dissolved in another 4 mL DCM and slowly added to the educts. The mixture is subsequently heated to reflux for 24 h. After cooling, 10 % aqueous Na₂SO₃ is added to the mixture which is subsequently extracted three times with DCM. The combined organic phases are dried over MgSO₄ and the solvent is evaporated under reduced pressure to yield 2.11 g (74 %) of an off-white powder. M_p: 326 °C (under decomposition), ¹H NMR (300 MHz, CDCl₃): δ = 6.77 (d, 2H, Ar-H), 7.06 (m, 2H, Ar-H), 7.59 (dd, 2H, Ar-H), 7.73 (d, 1H, Ar-H), 7.77 (dd, 1H, Ar-H), 8.00 (dd, 1H, Ar-H)

2-phenyl-9,9'-spirobi[9H]fluorene (**2**): The product was obtained as a white solid, yield: 82 %, $^1\text{H NMR}$ (300 MHz, CDCl_3): δ = 6.74 (m, 1H, Ar-H), 6.78 (m, 2H, Ar-H), 6.94 (dd, 1H, Ar-H), 7.08 – 7.15 (m, 3H, Ar-H), 7.20 – 7.44 (m, 7H, Ar-H), 7.62 (dd, 1H, Ar-H), 7.83 – 7.89 (m, 3H, Ar-H), 7.91 (dd, 1H, Ar-H).

2,7-diphenyl-9,9'-spirobi[9H]fluorene (**3**): After recrystallization, the product was obtained as white crystals, yield: 50 %, Mp: 258 °C, $^1\text{H NMR}$ (300 MHz, CDCl_3): δ = 6.82 (m, 2H, Ar-H), 6.94 (m, 2H, Ar-H), 7.12 (dt, 2H, Ar-H), 7.20 – 7.45 (m, 12H, Ar-H), 7.65 (dd, 1H, Ar-H), 7.86 (m, 2H, Ar-H), 7.92 (m, 2H, Ar-H).

General procedure for the bromination of **7a-c**: 1.04 g of 4a-c (2.49 mmol) are dissolved in 18 mL of DCM with a spatula tip of I_2 . 1.5 g (9.4 mmol) of Br_2 are dissolved in 3 mL of DCM and slowly added to the educts. The mixture is stirred at room temperature for 72 h. After the reaction is complete, 10 % aqueous Na_2SO_3 is added to the mixture, which is subsequently extracted three times with DCM. The combined organic phases are dried over MgSO_4 and the solvent is evaporated under reduced pressure.

2-(2-cyanophenyl)-9,9'-spirobi[9H]fluorene (**7-ortho**): The product remained as a white powder. Yield: 73 %. Mp: 179 °C, $^1\text{H NMR}$ (300 MHz, CDCl_3): δ = 6.73-6.86 (m, 4H, Ar-H), 7.10-7.18 (m, 3H, Ar-H), 7.28-7.43 (m, 5H, Ar-H), 7.49 (m, 1H, Ar-H), 7.65 (dd, 2H, Ar-H), 7.81-7.91 (m, 3H, Ar-H), 7.95 (d, 1H, Ar-H).

2-(3-cyanophenyl)-9,9'-Spirobi[9H]fluorene (**7-meta**): After recrystallization in $\text{CHCl}_3/\text{MeOH}$, the product remained as off-white crystals. Yield: 78 %, Mp: 191 °C, $^1\text{H NMR}$ (300 MHz, CDCl_3): δ = 6.72-6.79 (m, 3H, Ar-H), 6.89 (d, 1H, Ar-H), 7.90-7.17 (m, 3H, Ar-H), 7.36-7.44 (m, 4H, Ar-H), 7.52 (dt, 1H, Ar-H), 7.58 (dd, 1H, Ar-H), 7.64 (dt, 1H, Ar-H), 7.67 (dt, 1H, Ar-H), 7.88 (d, 2H, Ar-H), 7.94 (d, 1H, Ar-H).

2-(4-cyanophenyl)-9,9'-spirobi[9H]fluorene (**7-para**): The product remained as white flakes. Yield: 78 %, Mp: 221 °C, $^1\text{H NMR}$ (300 MHz, CDCl_3): δ = 6.75 (m, 3H, Ar-H), 6.93 (d, 1H, Ar-H), 7.08-7.18 (m, 3H, Ar-H), 7.35-7.44 (m, 3H, Ar-H), 7.51 (dt, 2H, Ar-H), 7.56-7.64 (m, 3H, Ar-H), 7.64 (dt, 1H, Ar-H), 7.84-7.90 (m, 3H, Ar-H), 7.95 (d, 1H, Ar-H).

2-(2-cyanophenyl)-2',7,7'-tribromo-9,9'-spirobi[9H]fluorene: The product was obtained as off-white crystals. Yield: 96 %, $^1\text{H NMR}$ (300 MHz, CDCl_3): δ = 6.85 (dd, 2H, Ar-H), 6.90 (d, 2H, Ar-

4.2 ORGANIC GLASSES OF HIGH GLASS TRANSITION TEMPERATURES DUE TO SUBSTITUTION WITH NITRILE GROUPS

H), 7.33-7.39 (m, 2H, Ar-H), 7.50 – 7.59 (m, 4H, Ar-H), 7.65 – 7.78 (m, 5H, Ar-H), 7.94 (d, 1H, Ar-H).

2-(3-cyanophenyl)-2',7,7'-tribromo-9,9'-spirobi[9H]fluorene: The product remained as an off-white powder, yield: 99 %, ¹H NMR (300 MHz, CDCl₃): δ = 6.86 (m, 4H, Ar-H), 7.45 (dt, 1H, Ar-H), 7.50-7.78 (m, 10H, Ar-H), 7.91 (dd, 1H, Ar-H).

2-(4-cyanophenyl)-2',7,7'-tribromo-9,9'-Spirobi[9H]fluorene: The product was obtained as an off-white solid, yield: 98 %, ¹H NMR (300 MHz, CDCl₃): δ = 6,86-6,93 (m, 3H, Ar-H), 7,52-7,80 (m, 11H, Ar-H), 7,94 (m, 1H, Ar-H).

2-(2-cyanophenyl)-2',7,7'-tricyano-9,9'-spirobi[9H]fluorene (**8-ortho**): The product was obtained as a white powder, yield: 34 %, M_p: 313 °C, ¹H NMR (300 MHz, CDCl₃): δ = 6.89 (d, 1H, Ar-H), 6.98 (d, 1H, Ar-H), 7.11 (d, 2H, Ar-H), 7.40 (m, 2H, Ar-H) 7.57 (m, 1H, Ar-H) 7.68 (dd, 1H, Ar-H), 7.73 – 7.82 (m, 4H, Ar-H), 7.99 – 8.10 (m, 4H, Ar-H).

2-(3-cyanophenyl)-2',7,7'-tricyano-9,9'-spirobi[9H]fluorene (**8-meta**): The product remained as a white solid, yield: 62 %, M_p: 320 °C, ¹H NMR (300 MHz, CDCl₃): δ = 6.86 (dd, 1H, Ar-H), 6.96 (dd, 1H, Ar-H), 7.07 (dd, 2H, Ar-H), 7.48 (m, 1H, Ar-H), 7.59 (dt, 1H, Ar-H), 7.66-7.70 (m, 2H, Ar-H), 7.74 (dd, 1H, Ar-H), 7.77-7.83 (m, 3H, Ar-H), 8.01-8.09 (m, 4H, Ar-H).

2-(4-cyanophenyl)-2',7,7'-tricyano-9,9'-spirobi[9H]fluorene (**8-para**): The product remained as an off-white powder, yield: 37 %, M_p: 347 °C ¹H NMR (300 MHz, CDCl₃): δ = 6.92 (dd, 2H, Ar-H), 7.07 (d, 2H, Ar-H), 7.53 (d, 2H, Ar-H), 7.65 (d, 2H, Ar-H) 7.73 – 7.82 (m, 4H, Ar-H), 7.99 – 8.09 (m, 4H, Ar-H).

2,7-bis-(2-cyanophenyl)-9,9'-spirobi[9H]fluorene (**9-ortho**): After recrystallization, the product was obtained as white crystals, yield: 68 %, M_p: 316 °C, ¹H NMR (300 MHz, CDCl₃): δ = 6.85 – 6.90 (m, 4H, Ar-H), 7.17 (dt, 2H, Ar-H), 7.30 – 7.42 (m, 6H, Ar-H), 7.46 – 7.54 (m, 4H, Ar-H), 7.63 – 7.70 (m, 4H, Ar-H), 7.84 (m, 2H, Ar-H), 8.00 (dd, 2H, Ar-H).

2,7-bis-(3-cyanophenyl)-9,9'-spirobi[9H]fluorene (**9-meta**): The product remained as white crystals, yield: 26 %, M_p: °C, ¹H NMR (300 MHz, CDCl₃): δ = 6.80 (m, 2H, Ar-H), 6.91 (dd, 2H, Ar-H), 7.15 (td, 2H, Ar-H), 7.38-7.46 (m, 4H, Ar-H), 7.53 (td, 2H, Ar-H), 7.59-7.72 (m, 6H, Ar-H), 7.91 (m, 2H, Ar-H), 7.98 (dd, 2H, Ar-H).

2,7-bis-(4-cyanophenyl)-9,9'-spirobi[9H]fluorene (**9-para**): The product was obtained as an off-white solid, yield: 80 %, M_p : 310 °C, 1H NMR (300 MHz, $CDCl_3$): δ = 6.80 (dt, 1H, Ar-H), 6.94 (dd, 1H, Ar-H), 7.14 (m, 1H, Ar-H), 7.41 (m, 1H, Ar-H), 7.52 (m, 2H, Ar-H), 7.60 (m, 2H, Ar-H), 7.65 (dd, 1H, Ar-H), 7.89 (m, 1H, Ar-H), 7.98 (dd, 1H, Ar-H).

2,7-bis-(2-cyanophenyl)-2',7'-dicyano-9,9'-spirobi[9H]fluorene (**10-ortho**): After recrystallization, the product was obtained as an off-white solid, yield: 67 %, M_p : 327 °C, 1H NMR (300 MHz, $CDCl_3$): δ = 6.87 (d, 2H, Ar-H), 7.21 (d, 2H, Ar-H), 7.34-7.43 (m, 4H, Ar-H), 7.56 (td, 2H, Ar-H), 7.65 – 7.76 (m, 6H, Ar-H), 7.98 (d, 2H, Ar-H), 8.06 (d, 2H, Ar-H).

2,7-bis-(3-cyanophenyl)-2',7'-dicyano-9,9'-spirobi[9H]fluorene (**10-meta**): After recrystallization, a white powder was obtained, yield: 40 %, M_p : 340 °C, 1H NMR (300 MHz, $CDCl_3$): δ = 6.82 (d, 2H, Ar-H), 7.13 (d, 2H, Ar-H), 7.47 (td, 2H, Ar-H), 7.58 (dt, 2H, Ar-H), 7.70 (m, 6H, Ar-H), 7.79 (dd, 2H, Ar-H), 8.05 (m, 4H, Ar-H).

2,7-bis-(4-cyanophenyl)-2',7'-dicyano-9,9'-spirobi[9H]fluorene (**10-para**): After recrystallization, off-white crystals were obtained, yield: 36 %, M_p : 340 °C, 1H NMR (300 MHz, $CDCl_3$): δ = 6.84 (d, 2H, Ar-H), 7.13 (d, 2H, Ar-H), 7.53 (dt, 4H, Ar-H), 7.64 (dt, 4H, Ar-H), 7.70 – 7.80 (m, 4H, Ar-H), 8.04 (d, 4H, Ar-H).

4.2.9.2. References

- (1) K.-T. Wong, S.-Y. Ku, Y.-M. Cheng, X.-Y. Lin, Y.-Y. Hung, S.-C. Pu, P.-T. Chou, G.-H. Lee, S.-M. Peng, *Synthesis, structures, and photoinduced electron transfer reaction in the 9,9'-spirobifluorene-bridged bipolar systems*, *The Journal of organic chemistry* **71** (2006) 456–465.
- (2) W.Y. Huang, M.Y. Chang, Y.K. Han, P.T. Huang, *Sterically encumbered poly(arylene ether)s containing spiro-annulated substituents: Synthesis and thermal properties*, *J. Polym. Sci. A Polym. Chem.* **48** (2010) 5872–5884.

4.3. Main and secondary relaxation of non-polymeric high-T_g glass formers as revealed by dielectric spectroscopy

Thomas Körber,^{a†} Felix Krohn,^{b†} Christian Neuber,^b Hans-Werner Schmidt,^b and Ernst A. Rössler^{*a}

^aDepartment of Inorganic Chemistry III and Northern Bavarian NMR Center, University of Bayreuth, 95440 Bayreuth, Germany

^bDepartment of Macromolecular Chemistry I and Bavarian Polymer Institute, University of Bayreuth, 95440 Bayreuth, Germany

The results have been published as a full paper.

Reproduced by permission of the PCCP Owner Societies from *Phys. Chem. Chem. Phys.* **2020**, 22, 9086-9097.

DOI: 10.1039/D0CP00930J

† Both authors contributed equally to this manuscript.

4.3.1. Abstract

A series of high- T_g glass formers with T_g values varying between 347 and 390 K and molar masses in the range of 341 and 504 g/mol are investigated by dielectric spectroscopy. They are compared to paradigmatic reference systems. Differently polar side groups are attached to a stiff non-polar core unit at different positions. Thereby, the dielectric relaxation strength varies over more than two decades. All the relaxation features typical of molecular glass formers are rediscovered, i.e. stretching of the main (α -) relaxation, a more or less pronounced secondary (β -) process, and a fragility index quite similar to that of other molecular systems. The position of the polar nitrile side group influences the manifestation of the β -relaxation. The α -relaxation stretching displays the trend to become less with higher relaxation strength $\Delta\varepsilon_\alpha$, confirming recent reports. Typical for a generic β -process is the increase of its amplitude above T_g which is found to follow a power-law behaviour as a function of the ratio τ_α/τ_β with a universal exponent; yet, its relative amplitude to that of the α -relaxation varies as does the temporal separation of both processes. The mean activation energy of the β -process as well as the width of the energy distribution $g_\beta(E)$ increases more or less systematically with T_g . The latter is determined from the dielectric spectra subjected to a scaling procedure assuming a thermally activated process. Plotting $g_\beta(E)$ as a function of the reduced energy scale E/T_g the distributions are centred between 20 – 30 and their widths differ by a factor 2 - 3.

4.3.2. Introduction

Investigating the dynamics in super-cooled molecular liquids, most studies have focused on systems with their glass transition temperature T_g below ambient temperatures.¹⁻⁵ Most prominently, covering a wide frequency range of up to 16 decades, dielectric spectroscopy (DS) has revealed the spectral evolution of the dynamic susceptibility regarding molecular reorientation. Likewise, depolarized light scattering (DLS)⁶⁻⁹ and optical Kerr effect (OKE)^{10,11} have also provided information on molecular reorientation, however over a smaller time or frequency range. Clearly, a non-exponential (stretched) correlation function or equivalently a non-Lorentzian spectral density underlies the main (α -) relaxation. Yet, there is no full agreement on the details or generic features of its spectral shape due to the interference of additional spectral contributions on the high-frequency flank of the relaxation peak. Typically,

secondary relaxations like the Johari β -relaxation^{1,12-15} and the excess wing^{1,2,16-18} show up close to T_g , or contributions of microscopic dynamics occur, the latter hampering an analysis of the susceptibility spectra collected in the GHz range by DLS or OKE.

Attempts were made to correlate some spectral parameters with other quantities characterizing “glassy dynamics”. For example, scrutinizing organic and inorganic glass formers, the stretching parameter was found to be correlated with the extent of fragility, the latter describing the steepness of the logarithm of the time constant τ_α at T_g on the reduced temperature scale T_g/T .¹⁹ The more fragile the glass former, the larger the stretching. However, a study on molecular systems as well as ionic liquids did not find any correlations.²⁰ Recently, collecting data on “almost all” molecular glass formers studied so far, the authors established a trend between the molecular dipole moment in terms of the dielectric relaxation strength $\Delta\varepsilon_\alpha$ and the stretching parameter β_K of the α -process.²¹ The higher $\Delta\varepsilon_\alpha$, the weaker is the stretching, i.e. the higher is the Kohlrausch stretching parameter β_K . Actually, this relationship was already reported before.²² Regarding the more or less ubiquitous presence of a secondary (β -) process emerging close to T_g and persisting below T_g ,^{1,12-15} the corresponding activation energy follows in many cases a relation $E_\beta = 24 T_g$ (in K).¹ Although several exceptions were found,^{1,23,24} still it is a non-trivial fact that quite different system like for instance polybutadiene and toluene display this relation.

Polymer glass formers with T_g values well above ambient temperatures are well studied and widely employed in innumerable technical applications. In recent years, interest in non-polymeric high- T_g glass formers, so-called molecular glasses, has grown. Their applications range from the use in electronic devices,²⁵⁻²⁸ resist materials for lithography,²⁹⁻³¹ to pharmaceutical formulations.^{32,33} It is the combination of properties usually observed in polymers with the benefits of a low molecular nature that makes these glasses ideal materials for specific applications. Just as polymers, molecular glasses allow the formation of stable thin films. In contrast to polymers, however, they possess a well-defined molecular structure and purification can be done using standard chromatographic techniques. Solvent-free vapour processing has been demonstrated for a variety of molecular glasses.^{34,35} Their application, however, is limited due to their high tendency to crystallize as compared to polymeric glass former.^{32,36}

In the present contribution we characterized a series of high- T_g systems in terms of their dielectric response above as well as below T_g . The systems are based on a non-polar 9,9'-Spirobi[9H]fluorene core unit and by introducing more or less polar substituents, a variety of high- T_g materials were synthesized.³⁷ This "spiro core" consists of two planar fluorene units linked at the bridging C_9 atom with a 90° twist angle. This results in a rigid structure yielding molecular glasses with high T_g values. The systems considered here are part of a long-running research project specially synthesising non-polymeric high- T_g glass formers.^{38,39} Regarding the possibility to enhance T_g by introducing polar side groups, a first study was recently published.³⁷

It is of fundamental interest to examine the influence of substituents on the dynamics of the molecules. The present substituents include *tert*-butyl groups, phenyl rings, and nitrile groups. Absence or presence and position of a nitrile group control the relaxation strength $\Delta\epsilon_\alpha$ as well as the manifestation of the β -relaxation. The T_g values lie in the range of 347 – 390 K. Usually, a T_g increase is caused by a higher molar mass. Averaging over T_g data of many systems, a relation $T_g \propto M^{0.5}$ was found,⁴⁰ yet, the exponent can be increased by introducing highly polar side moieties.³⁷

Here, we analyse in detail the spectral shapes of α - and β -relaxation, corresponding time constants, and fragility. We check the above-mentioned correlation between stretching parameter and relaxation strength. As high T_g values are involved, we also investigate the relation for the (mean) activation energy of the β -process $E_\beta = f(T_g)$. Furthermore, a comparison with typical low- T_g glass formers as reference systems is performed. As will be demonstrated, beyond the more or less systematic growth of the activation energy E_β and the width of energy distribution $g_\beta(E)$ with T_g , we analyse the increase of the relaxation strength above T_g as a characteristic feature of the generic β -process. It turns out that the relative amplitude of the β -relaxation increases along a power-law behaviour with the separation of the two processes becoming smaller. The increase appears to be universal though the amplitude is different.

4.3.3. Experimental

4.3.3.1. Systems studied

In Figure 4.3.1, the chemical formulae of the investigated glass formers are shown together with their abbreviations used throughout the text. In general, the “S” is used for the core unit spirobifluorene, “C” stands for an attached cyano group, “P” for an attached phenyl group, and “T” for an attached *tert*-butyl group. The combination “CP” is used for an attached cyanophenyl group. In detail, the abbreviations of the compounds are derived from their structure as follows: *o*-CPS, *m*-CPS, and *p*-CPS are all 2-(cyanophenyl)-spirobifluorenes, with the cyano-group being in ortho, meta, or para-position, respectively. 2-CS and 2-PS are 2-cyano- and 2-phenylspirobifluorene, respectively. 2,7-DCS stands for the disubstituted 2,7-dicyanospirobifluorene. The compound TCPS corresponds to 2-tert-butyl-2'-(3-cyanophenyl)-spirobifluorene, and *m*-TPTS to 2-(meta-tert-butylphenyl)-2'-tert-butyl-spirobifluorene. The synthesis and DSC characterization of *o*-CPS, *m*-CPS, *p*-CPS, 2-CS, 2,7-DCS, and 2-PS can be found elsewhere.³⁷ The synthesis route and characterization of the deuterated isomers of *o*-CPS and *m*-CPS as well as of TCPS and *m*-TPTS can be found in the ESI. The obtained products were purified by sublimation prior to DS measurements. The here considered glass formers can be distinguished by the presence or the absence of strongly dipolar nitrile groups, its position (*o*, *m*, and *p*, appearing before) and as a consequence its dielectric relaxation strength $\Delta\varepsilon_\alpha$. Table 4.3.1 lists molar masses M , glass transition temperatures T_g , either determined by DSC measurements or by dielectric spectroscopy, and in addition parameters of the analyses presented in the following. Furthermore, we include in Table 4.3.1 some properties of two other high T_g glass formers previously characterized (SBC³⁹ and DH 379³⁸).

In addition, we compare selected systems with mainly low T_g values as paradigmatic reference systems which well display the characteristic spectral features of molecular glass formers: polybutadiene (PB, $M = 35.3$ kg/mol),⁴¹ toluene (Tol; unpublished work,⁴² cf. also ref. 1), tripropyl phosphate (TPP),^{43,44} decahydroisoquinoline (DHIQ),²⁴ 3,3',4,4'-benzophenone tetracarboxylic dianhydride (2-PC, unpublished work⁴²) and felodipine (FD, unpublished work⁴⁵).

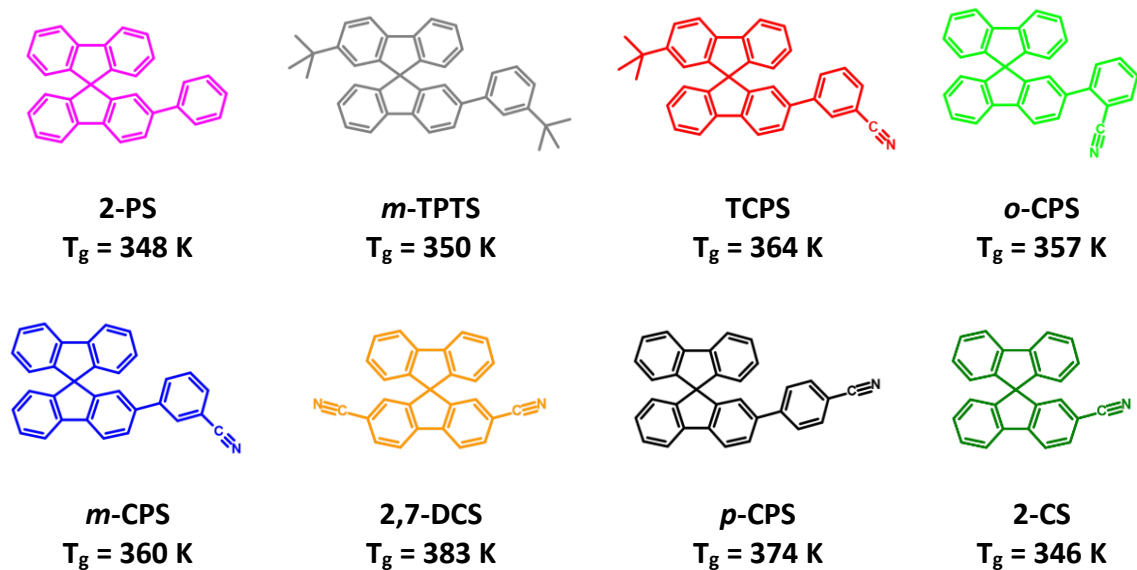


Figure 4.3.1: Structure and glass transition temperature T_g of the investigated glass formers.

4.3.3.2. Differential Scanning Calorimetry

Differential scanning calorimetry was performed with a Mettler DSC3+ in pierced Aluminium pans at 10 K min⁻¹ under nitrogen flow. The glass transition temperature T_g was determined as the onset temperature of the step as calculated by Mettler STARe 15.00a software. Results are found in Table 4.3.1.

4.3.3.3. Dielectric spectroscopy

The dielectric permittivity is given by the equation^{46,47}

$$\varepsilon^*(\omega) = \varepsilon'(\omega) - i\varepsilon''(\omega) = \varepsilon_\infty + \Delta\varepsilon \int_0^\infty -\frac{d\phi(t)}{dt} e^{-i\omega t} dt \quad (4.3.1)$$

where $\varepsilon^*(\omega)$ is the complex dielectric constant, $\omega = 2\pi\nu$ the angular frequency, ε_∞ the high frequency permittivity, and $\phi(t)$ the step-response function. The quantity $\Delta\varepsilon$ is the relaxation strength being linked to the molecular dipole moment.

The main (α -) dielectric response in glass forming systems is often described either by a Cole-Davidson or Kohlrausch function.⁴⁶ In this work, the Kohlrausch function

$$\phi_K(t) = \exp \left[- \left(\frac{t}{\tau_K} \right)^{\beta_K} \right] \quad (4.3.2)$$

was applied in terms of its Fourier transform (FT). Here, τ_K is the time constant and β_K the stretching parameter. The average relaxation time τ_α is then defined by:⁴⁶

$$\tau_\alpha = \frac{\tau_K}{\beta_K} \Gamma \left(\frac{1}{\beta_K} \right) \quad (4.3.3)$$

while above T_g the time constants of the α -relaxation are extracted via the FT of eqn (4.3.2), below T_g with the persisting β -process, we extract the time constants τ_β either via peak-picking $\tau_\beta = (2\pi\nu_{\max})^{-1}$ for clearly recognizable peaks or we apply a distribution of correlation times $G_\beta(\ln \tau)$ previously introduced for describing the step-response function of a secondary relaxation process. Explicitly, we take⁴⁸

$$G_\beta(\ln \tau) = N_\beta(a, b) \frac{1}{b \left(\frac{\tau}{\tau_m} \right)^a + \left(\frac{\tau}{\tau_m} \right)^{-ab}} \quad (4.3.4)$$

with the normalization factor

$$N_\beta(a, b) = \frac{a(1+b)}{\pi} b^{\frac{b}{1+b}} \sin \left(\frac{\pi b}{1+b} \right) \quad (4.3.5)$$

and with τ_m being the time constant at the maximum of $G_\beta(\ln \tau)$ which is the same as via peak-picking. The parameter a controls the symmetric broadening of the distribution and susceptibility, respectively, while the ‘‘asymmetry parameter’’ b only affects its high-frequency. Assuming that a distribution of activation energies $g_\beta(E)$ underlies $G_\beta(\ln \tau)$, and that the time constant at each site in the structurally disordered glass follows an Arrhenius-like temperature dependence, $\tau_\beta = \tau_0 \exp \left(\frac{E}{RT} \right)$, the temperature dependent distribution $G_\beta(\ln \tau)$ eqn (4.3.4) can be mapped to a temperature independent distribution $g_\beta(E)$:⁴⁸

$$g_\beta(E) = N_\beta(c, b) \frac{1}{b \exp(c(E - E_m)) + \exp(-cb(E - E_m))} \quad (4.3.6)$$

Independent of assuming a particular shape for $G_\beta(\ln \tau)$, one can directly apply a scaling procedure on the experimental dielectric spectra compiled at different temperatures which compensates for the broadening of $G_\beta(\ln \tau)$ introduced by the underlying distribution $g_\beta(E)$.^{44,49-52}

$$g_{\beta}(E) = g\left(T \ln\left(\frac{\nu_0}{\nu}\right)\right) = \frac{2}{\pi} \frac{\varepsilon''(\nu)}{T\Delta\varepsilon} \quad (4.3.7)$$

In words, by plotting the dielectric loss $\varepsilon''(\nu)$ divided by the temperature T as a function of the natural logarithm of the inverse frequency multiplied by T , one gets an estimate of the activation energy distribution of the β -process. In the present analysis, we take the attempt frequency $\nu_0 = 1/2\pi\tau_0$ from the intercept of plotting the mean time constant vs. the reciprocal temperature at infinite temperature (cf. Figure 4.3.6A).

For describing the dielectric loss $\varepsilon''(\nu)$ in the temperature regime, where both, α - and β -relaxation occur together, we use a Williams-Watts approach.^{1,13,53} Thereby, one assumes that the step-response function ϕ is partly decaying by ϕ_{β} and then completely decaying via ϕ_{α} in the following manner:

$$\phi = [(1 - S)\phi_{\beta} + S]\phi_{\alpha} \quad (4.3.8)$$

Hereby, $(1 - S)$ gives the maximum amount of correlation decaying by ϕ_{β} (order parameter S). Here, the function ϕ_{α} is given by a Kohlrausch decay (FT of eqn (4.3.2)), and ϕ_{β} is described by the distribution of eqn (4.3.4).

The dielectric measurements were carried out with an Alpha-A Analyzer from Novocontrol in the frequency range $\nu = 10^{-2} - 10^6$ Hz. Temperature was kept constant within ± 0.2 K by using a Quattro-H temperature controller from Novocontrol yielding an absolute accuracy better than ± 0.2 K. The temperature ranges from 100 up to 400 K. The sample cell was constructed by a design of Wagner and Richert and assures a constant sample volume.⁵⁴ The relaxation strength $\Delta\varepsilon_{\alpha}$ is determined by a single Kohlrausch fit of the main relaxation close to T_g without consideration of any further processes and is listed in Table 4.3.1.

4.3.4. Results

4.3.4.1. Relaxation spectra

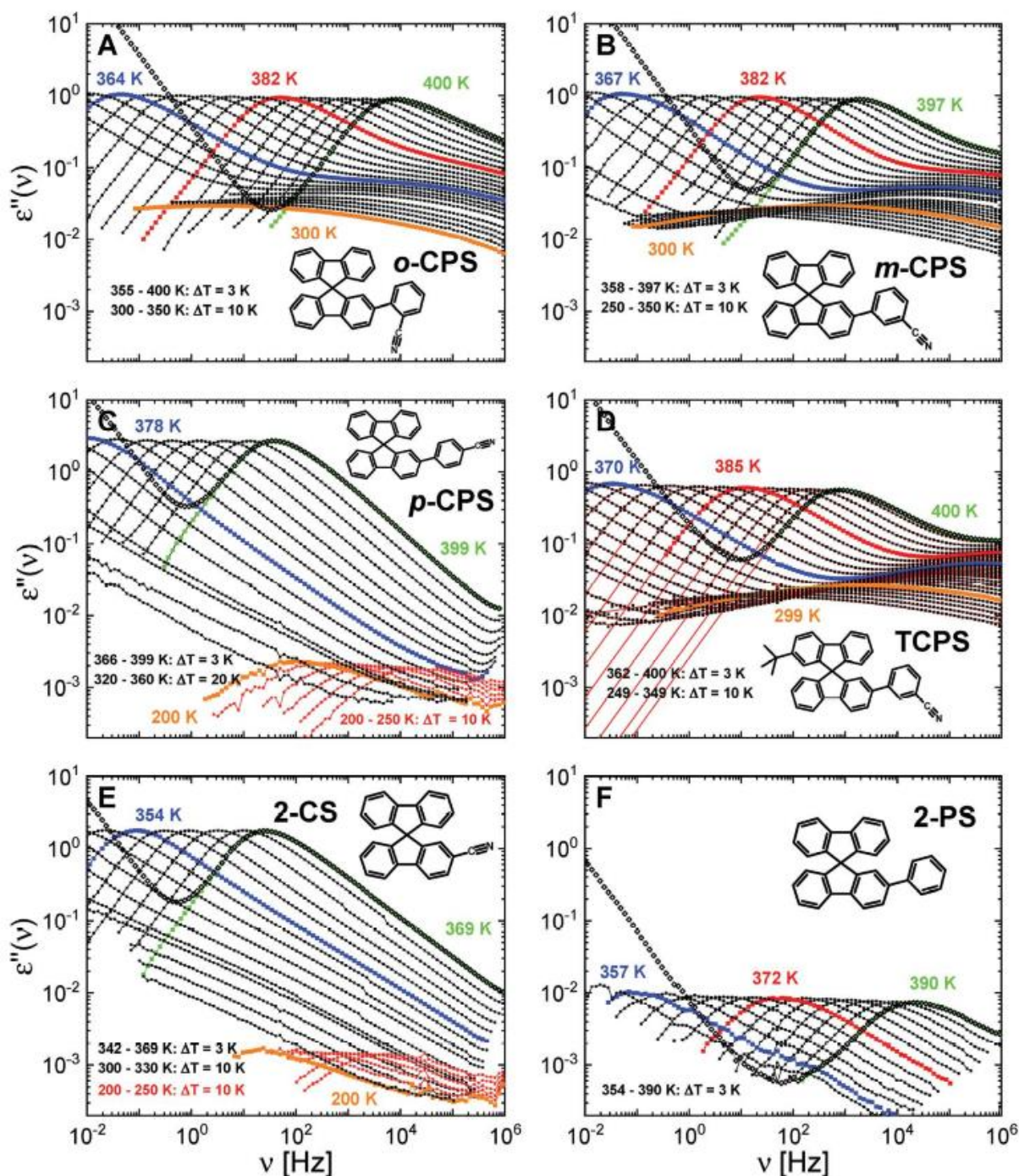


Figure 4.3.2: Dielectric loss spectra of *o*-CPS (A), *m*-CPS (B), *p*-CPS (C), TCPS (D), 2-CS (E), and 2-PS (F). DC conductivity contribution is subtracted; original data is shown in open symbols for the highest temperature. Temperature range and increments are given; coloured curves highlight selected temperatures. Red lines in (D): Interpolations along a Williams-Watts approach with a Kohlrausch function for the α -relaxation and a symmetric distribution of correlation times for the β -relaxation.

Figure 4.3.2A - D show the dielectric loss spectra of *o*-CPS, *m*-CPS, *p*-CPS, and TCPS, all of which possess a nitrile group that is attached via a phenyl ring at the spiro core, however, at different positions on the phenyl ring. In the case of TCPS, the core contains in addition a non-polar *tert*-butyl group. The system 2-CS (Figure 4.3.2E) carries one nitrile group directly at the core unit as does 2,7-DCS with two nitrile groups attached (Appendix, Figure 4.3.10A), implying that both molecules are completely rigid. In the case of *p*-CPS, and 2-PS (containing only a phenyl group attached to the core, Figure 4.3.2F), 180 degree jumps of the phenyl ring are expected to occur, yet, this process is dielectrically inactive. Due to the introduced highly polar nitrile groups the dielectric loss of the first five systems (Figure 4.3.2A - E) is rather large. In contrast, the systems 2-PS and *m*-TPTS (see Appendix Figure 4.3.10C) without nitrile groups show a low loss. As 2,7-DCS possesses two nitrile groups symmetrically attached to the core, the partial dipole moments cancel partly, leading to the dielectric loss being somewhat smaller than that of the other nitrile group containing systems. We also measured a mixture of the isomers *o*-CPS and *m*-CPS (*o*-/*m*-CPS, Appendix Figure 4.3.10B). No broadening of the main relaxation is observed; thus it appears to behave like a pure glass former. This is of special interest for applications where a crystallization tendency has to be suppressed. In addition, we also measured systems *o*-CPS-*d*₄ and *m*-CPS-*d*₄ with one ring of the core deuterated; their spectra (not shown) are equal to those of their protonated counterpart (synthesis route provided in the ESI).

All liquids exhibit a more or less pronounced DC conductivity which is shown only for one temperature (open squares) in each system and subtracted otherwise for all spectra shown in the Figure 4.3.2A - E, and no more shown for simplicity in Figure 4.3.2F. The systems *o*-CPS and *m*-CPS, and TCPS as well as the mixture *o*-/*m*-CPS are type B glass formers with a pronounced and typical β -process.¹ Interestingly, the β -relaxation appears to be absent when the nitrile group is in the *para*-position (*p*-CPS). Instead, one finds a well separated secondary relaxation process at much lower temperatures. A similar behaviour is also found for 2-CS and 2,7-DCS, where the nitrile group is attached directly to the spiro core.

Table 4.3.1: Comparison of molar mass M , T_g as determined by dielectric spectroscopy (DS; $\tau_\alpha(T_g) = 100\text{s}$) and DSC³⁷, dielectric strength $\Delta\varepsilon_\alpha$ at $1.02 T_g$, Kohlrausch stretching parameter β_K , and time constant τ_0 as well as activation energy E_β of β -process in units of T_g for the investigated systems and reference systems (polybutadiene (PB), toluene (Tol), tripropyl phosphate (TPP), decahydro isoquinoline (DHIQ), 3,3',4,4'-benzophenonetetracarboxylic dianhydride (2-PC) and felodipine (FD)); in addition, data for SBC and DH 379.

| System | M [g/mol] | T_g^{DS} [K] | T_g^{DSC} [K] | $\Delta\varepsilon_\alpha$ | β_K | E_β [K] | τ_0 [s] |
|---------------------------------------|-------------|----------------|-----------------|----------------------------|-----------|---------------|----------------------|
| 2-PS | 392 | 348 | 355 | 0.034 | 0.51 | --- | --- |
| <i>m</i> -TPTS | 504 | 350 | 357 | 0.11 | 0.52 | --- | --- |
| TCPS | 473 | 364 | 365 | 2.21 | 0.56 | 19.4 | $3.3 \cdot 10^{-15}$ |
| <i>o</i> -CPS (- d_4) ^a | 417 (421) | 357 (354) | 363 (359) | 3.24 | 0.59 | 26.2 | $1.3 \cdot 10^{-15}$ |
| <i>o</i> -/ <i>m</i> -CPS | 417 | 359 | 363 | 1.9 | 0.62 | 24.6 | $3.4 \cdot 10^{-15}$ |
| <i>m</i> -CPS (- d_4) | 417 (421) | 360 (358) | 368 (363) | 2.7 | 0.64 | 23.1 | $8 \cdot 10^{-16}$ |
| 2,7-DCS | 366 | 383 | 390 | 0.75 | 0.65 | 13.7 | $6.5 \cdot 10^{-15}$ |
| <i>p</i> -CPS | 417 | 374 | 380 | 7.65 | 0.70 | 14.6 | $2.1 \cdot 10^{-15}$ |
| 2-CS | 341 | 346 | 347 | 4.8 | 0.71 | 16.0 | $6.6 \cdot 10^{-15}$ |
| SBC ³⁹ | 809 | 356 | --- | 0.72 | 0.50 | 15.6 | $6.3 \cdot 10^{-16}$ |
| DH 379 ^{38,55} | 1205 | 374 | 382 | 0.66 | 0.45 | 14.7 | $1.7 \cdot 10^{-15}$ |
| Toluene ⁴² | 92 | 117 | --- | 0.25 | --- | 26.1 | $4.7 \cdot 10^{-17}$ |
| TPP ^{43,44} | 224 | 134 | --- | 24.3 | --- | 23.2 | $1.6 \cdot 10^{-15}$ |
| PB ⁴¹ | 35.3k | 174.5 | --- | 0.082 | --- | 24.1 | $5.0 \cdot 10^{-16}$ |
| DHIQ ²⁴ | 139 | 179.5 | --- | 1.7 | --- | 28.3 | $2.1 \cdot 10^{-16}$ |
| FD ⁴⁵ | 384 | 313 | --- | 1.12 | --- | --- | --- |
| 2-PC ⁴² | 322 | 330 | --- | 6.93 | --- | 32.3 | $2.0 \cdot 10^{-16}$ |

^a (- d_4): Compound marked with four deuterium atoms at the spiro core. Details: ESI

4.3.4.2. Main relaxation

In order to demonstrate the evolution of the spectra with temperatures above T_g and to compare the different systems, Figure 4.3.3A shows the relaxation spectra scaled by the maximum of the α -relaxation peak and its frequency, respectively, for selected glass formers, 2-PS, TCPS, *o*-CPS, *m*-CPS, *p*-CPS, and 2-CS in a stacked plot. For comparison, some typical (“reference”) systems like polybutadiene (PB), toluene (Tol), tripropyl phosphate (TPP), decahydroisoquinoline (DHIQ), 3,3',4,4'-benzophenone tetracarboxylic dianhydride (2-PC) and felodipine (FD) are presented in Figure 4.3.3B. The temperature is color-coded, starting in red for the highest temperature and ending in violet for the lowest temperature.

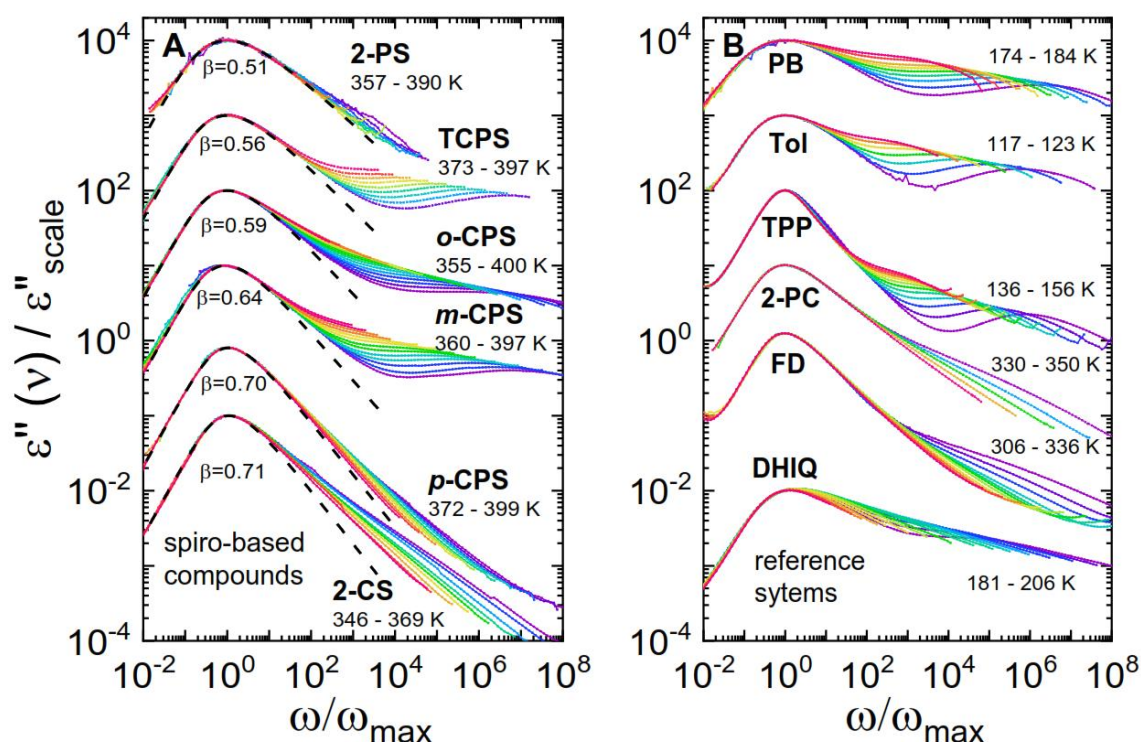


Figure 4.3.3: Master curves (coloured symbols) and respective Kohlrausch fits (dashed black lines, stretching parameter β_K indicated) for (A) 2-PS, TCPS, *o*-CPS, *m*-CPS, *p*-CPS, and 2-CS (top to bottom) and for reference systems (B) polybutadiene (PB), toluene (Tol), tripropylphosphate (TPP), 3,3',4,4'-benzophenone tetracarboxylic dianhydride (2-PC), felodipine (FD), and decahydroisoquinoline (DHIQ) (top to bottom). Master curves constructed by scaling axes by peak amplitude and frequency, respectively; they are shifted to an arbitrary height. Temperature of the curves increases from violet to red.

Regarding the α -relaxation, frequency-temperature superposition (FTS) appears to apply around the peak. Whether it covers also the full high-frequency flank cannot be decided due to the occurrence of a β -relaxation which “spoils” the master curve at these frequencies. The α -relaxation peaks are describable by a Kohlrausch function (eqn (4.3.2)), the stretching parameter β_K values are found in the range 0.51 for 2-PS and 0.71 for 2-CS (*cf.* Table 4.3.1)

and Figure 4.3.3A). In general, it increases with increasing polarity of the system, a relation which will be discussed below.

Looking in more detail on the spectra exhibiting a β -relaxation in Figure 4.3.3, i.e., the corresponding curves of TCPS, *o*-CPS, and *m*-CPS, and those of the three reference systems PB, Tol, and TPP, a common relaxation pattern is observed: The higher the temperature, the more a broadening of the main relaxation peak is observed due to the merging of α - and β -relaxation. *Vice versa*, the lower the temperature the narrower is the α -peak because the β -relaxation peak separates more and more. This similar spectral evolution is reflected by a colour-coding changing from red at high temperature to violet at low temperature. The systems are distinguished by a different relaxation strength of the β -relaxation with respect to that of the α -relaxation and by a different spectral separation of the two processes. Whereas in the case of PB or toluene, the β -relaxation displays a rather high relative strength and thus appears to take over the α -process when merging at high temperatures, for other systems such as TPP or *o*-CPS and *m*-CPS, the β -process exhibits a low strength and thus would rather be “consumed” by the α -process upon merging. We will come back to this point.

Considering *p*-CPS, 2-CS as well as FD and 2-PC no clear evidence of a β -relaxation is found, still, at high frequencies no master curve is recognised. In these cases, the curves measured at higher temperatures (marked in red) exhibit a narrower spectrum than those measured at lower temperatures (marked in violet). In other words, an opposite evolution of the color-coding with temperature is found with respect to the spectra discussed before. Assuming FTS still holds for the α -process, this relaxation pattern can be explained by a broad β -relaxation with a low relaxation strength and a time constant τ_β being very close to that of the α -process. This is clearly recognizable for the lowest temperatures in FD and 2-PC, when the ratio τ_β/τ_α becomes large leading to the beginning formation a separate peak.

A special relaxation pattern is observed for DHIQ. Here, the peak is the narrowest at the highest temperature, gets broader with decreasing temperatures until a second peak starts to separate out of the main peak and leads for lowest temperatures again to a narrower α -relaxation peak in combination with a clearly separated β -peak. Therefore, DHIQ is a rare example, where the full merging of the α - and β -relaxation is observable in the experimental frequency window given by the present spectrometer.

Figure 4.3.4A presents the time constants $\tau_\alpha(T)$ for all investigated glass formers as a function of the inverse temperature as given by a Kohlrausch fit (*cf.* Figure 4.3.3A). The glass transition temperature T_g (*cf.* Table 4.3.1) was determined along the definition of $\tau_\alpha(T_g) = 100\text{s}$, applying a Vogel-Fulcher-Tammann (VFT) fit for extrapolating $\tau_\alpha(T)$ to low temperatures (lines in Figure 4.3.4A). The so obtained T_g values agree within few degrees with those determined by DSC (Table 4.3.1). There is a slight difference between the deuterated and non-deuterated system of 2 - 3 K concerning the T_g . In the inset of Figure 4.3.4A, the time constants are plotted *versus* the reduced reciprocal temperature T_g/T . Clearly, the fragility of all investigated systems is essentially the same. In the case of 2-PS, the curve is less curved although displaying the same fragility indicating that more than one parameter is needed to characterize $\tau_\alpha(T_g/T)$.

As mentioned, the spectra presented in Figure 4.3.3 show the trend that the α -relaxation is broader, the lower the relaxation strength $\Delta\varepsilon_\alpha$ is, a trend first recognised by Nielsen *et al.*²² and recently considered by Paluch *et al.*²¹. Figure 4.3.4B displays the Kohlrausch stretching parameter β_K as a function of the relaxation strength (*cf.* Table 4.3.1) in a semi-logarithmic plot (instead of a linear plot as done by Paluch *et al.*²¹) as collected in ref. 21. We added the data of the herein investigated glass formers as well as those of ref. 38 and 39. They follow the overall trend.

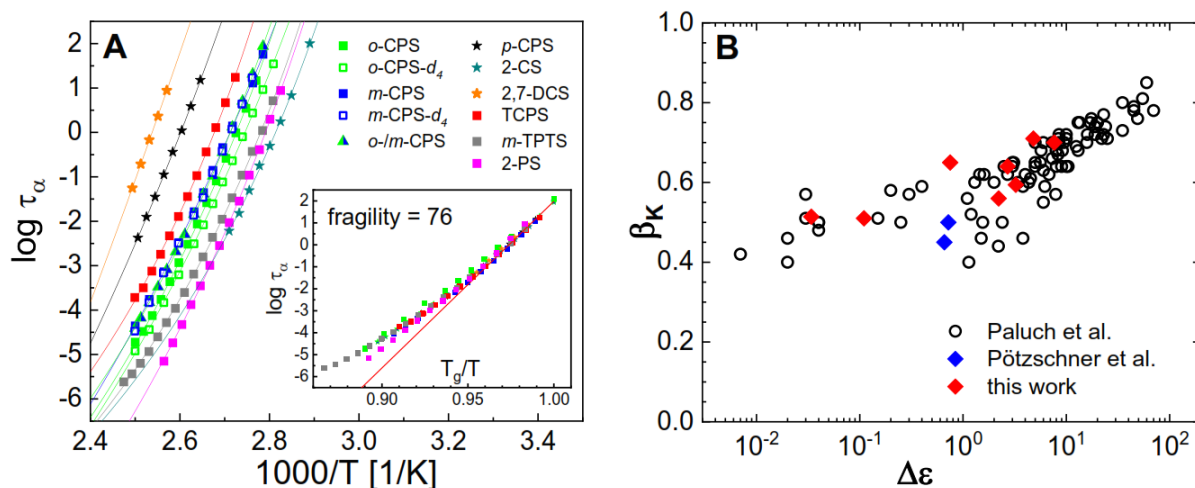


Figure 4.3.4: (A) Time constants τ_α as function of inverse temperature for all investigated systems. Lines are VFT extrapolations to determine T_g . Colour and symbol determine system. Inset: Time constants as function of reduced temperature T_g/T . (B) Stretching parameter β_K as function of the dielectric relaxation strength $\Delta\varepsilon$ for a large collection of systems from Paluch *et al.*²¹ (open black circles), the two high- T_g glass formers SBC and DH 379 from Pötzschner *et al.*^{38,39} blue diamonds), and the herein investigated systems (red diamonds, *cf.* Table 4.3.1).

4.3.4.3. Secondary relaxation

In order to characterize the merging behaviour of the α - and β -process, we took the ratio of the amplitude of the β -relaxation peak to that of the α -peak $\varepsilon''_{max,\beta}/\varepsilon''_{max,\alpha}$ at a given temperature above T_g and plotted it against the ratio of the frequency of the β -peak and the α -peak $\nu_{max,\beta}/\nu_{max,\alpha}$ in a double-logarithmic plot (see Figure 4.3.5A). For all investigated systems, a linear relationship in this representation showing essentially the same slope of $m = 0.1 \pm 0.01$ can be found whereas the relative amplitude varies significantly. Quantitatively this yields a power-law relationship, explicitly:

$$\varepsilon''_{max,\beta}/\varepsilon''_{max,\alpha} \propto (\nu_{max,\beta}/\nu_{max,\alpha})^{-m} \quad (4.3.9)$$

Interestingly, one finds a high relative strength of the β -relaxation for non-polar systems like PB or toluene, whereas the amplitude is small for polar systems like TPP. Moreover, one gets a rough estimate of the relative strength of the β -process at the merging. For example, in the case of PB, the β -process appears to take all the relaxation strength of the α -process, i.e., applying a Williams-Watts approach^{1,13,53} it literally consumes the α -process. While in the case of TPP, the amplitude of the β -relaxation at the merging becomes only about 10 % of that of the α -process.

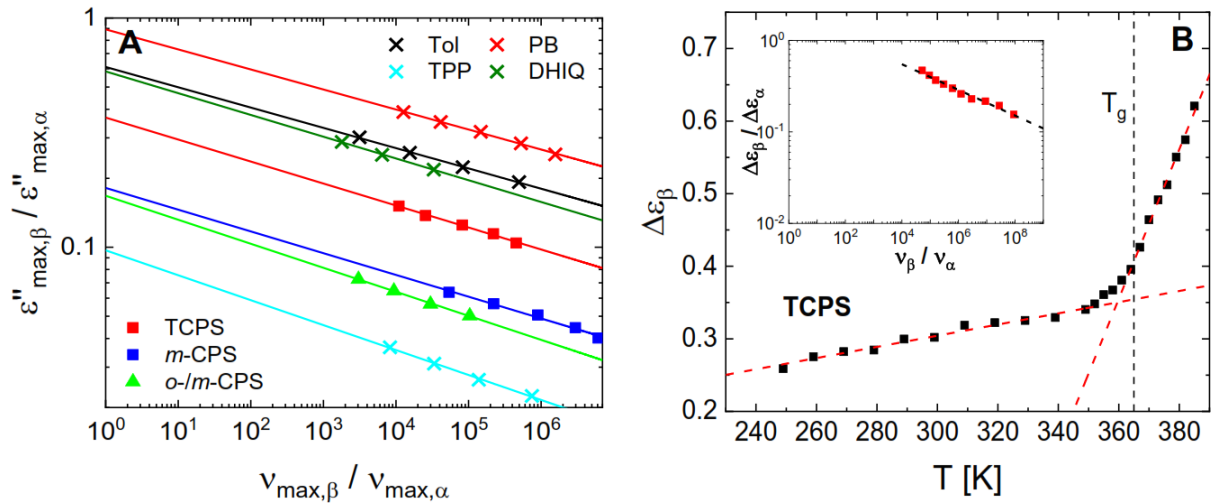


Figure 4.3.5: (A) Relative amplitude of the β -process $\varepsilon''_{max,\beta}$ with respect to that of the α -process $\varepsilon''_{max,\alpha}$ plotted against the relative relaxation frequency $\nu_{max,\beta}/\nu_{max,\alpha}$. Colour and symbol define system. Lines are linear fits. (B) Relaxation strength $\Delta\varepsilon_\beta(T)$ of TCPS determined from a Williams-Watts approach (cf. Figure 4.3.2D for fits). Dashed red lines indicate the crossover at T_g . Inset: Relative relaxation strength $\Delta\varepsilon_\beta/\Delta\varepsilon_\alpha$ above T_g as function of ν_β/ν_α , which is comparable to (A); a linear but different trend is observed.

We emphasize that eqn (4.3.9) is of phenomenological nature, and above we assumed that a linear extrapolation to full merging is permissible. In order to model the merging of both, α - and β - relaxation in detail, no single model has been generally accepted. Here, we stick to a Williams-Watts approach^{1,13,53} which assumes that the full relaxation function is given by a product of the relaxation functions of the two processes (*cf.* Experimental 4.3.2.3, eqn (4.3.8)). We applied this model for the case of the spectra of TCPS (*cf.* Figure 4.3.2D) and 2-PC (Appendix Figure 4.3.10D): The first system displays a rather well resolved β -relaxation, whereas the second is interesting as it shows a comparatively slow β -relaxation strongly submerged under a large α -relaxation. We assumed for the α -process a Kohlrausch step-response function and for the β -process a temperature independent symmetric distribution of correlation times (*cf.* eqn (4.3.4) with $b = 1$), which were then combined along eqn (4.3.8). As result, we get the relaxation strength of the β -process $\Delta\varepsilon_\beta(T)$ of TCPS (Figure 4.3.5B) as well as the ratio of time constants, $\tau_\alpha(T)/\tau_\beta(T) = \nu_\beta/\nu_\alpha$ and the relative relaxation strength $\frac{\Delta\varepsilon_\beta}{\Delta\varepsilon_\alpha} = \frac{1}{S} - 1$ (*cf.* eqn (4.3.8)) at temperatures above T_g (Figure 4.3.5B inset). Approximately, again, a power-law is observed but the relative relaxation strength displays higher values compared to the ratio of the amplitudes plotted in Figure 4.3.5A. Regarding the time constants $\tau_\beta(T)$ of 2-PC and TCPS, both show a stronger temperature dependence above T_g than below, a phenomenon best recognised when plotted against T/T_g and well known from literature (Figure 4.3.6B).⁴ Such an analysis also yields different stretching parameters of the α -relaxation compared to that of a simple Kohlrausch fit mainly determined by the relaxation peak. Actually, stretching turns out to be temperature dependent. For example, in the case of TCPS we find $\beta_K = 0.51$ at T_g and $\beta_K = 0.59$ at 400 K under consideration of the β -process. Overall, some care has to be taken when presenting stretching parameters (as in Figure 4.3.4B) just obtained from a single Kohlrausch fit at T_g without taking the β -relaxation into account. Still, the Williams-Watts approach needs justification within a final theory of the glass transition.

We now focus on temperatures below T_g . In Figure 4.3.6A, the logarithm of the time constants τ_β of the investigated (stars, squares, and triangle) and of the reference systems (crosses) are plotted *versus* the inverse temperature. All β -relaxations display an Arrhenius temperature behaviour, with an exponential pre-factor τ_0 in the range 10^{-15} s – 10^{-16} s consistent with

previous reports,^{1,56,57} except for toluene, for which it is about 10^{-17} s and therefore slightly lower. The values of the activation energies (together with those of the attempt time τ_0) are listed in Table 4.3.1. Figure 4.3.6B shows the time constant of the β -process as a function of the reduced temperature T_g/T together with those of the α -process of the high- T_g systems (the latter as a single line). Whereas the high- T_g systems *o*-CPS, *m*-CPS, TCPS and the reference systems Tol, PB, DHIQ, and TPP display almost parallel straight lines with a slope close to $24 T_g$ (cf. Table 4.3.1) except for 2-PC which displays a somewhat higher slope, the time constants of the systems *p*-CPS, 2-CS, 2,7-DCS, DH 379, and SBC are found at higher T_g/T values and show slopes around $14 T_g$. However, as we will demonstrate below, the secondary relaxation spectra of *p*-CPS, 2-CS, 2,7-DCS (in contrast to DH 379 and SBC) exhibit an atypical evolution with temperature.

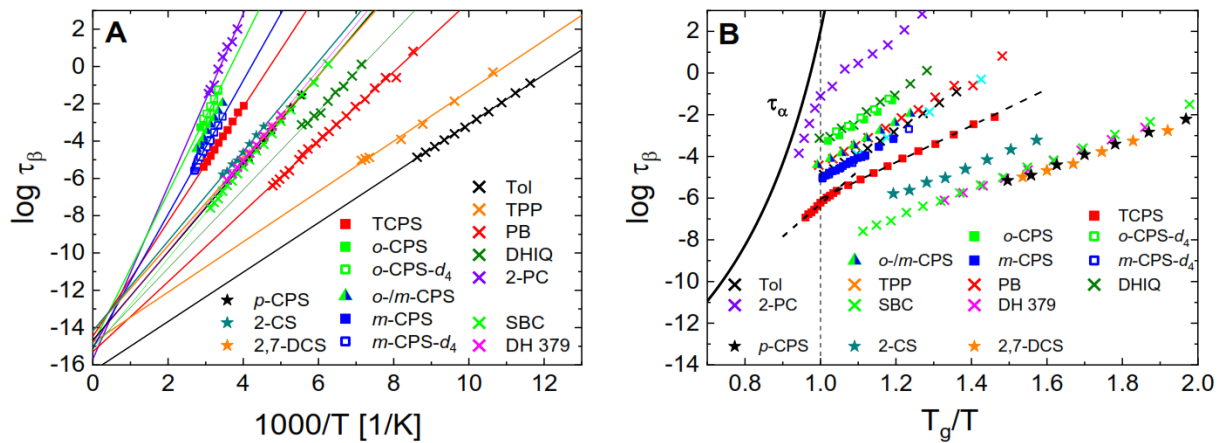


Figure 4.3.6: (A) Time constants τ_β of the β -process ($T < T_g$) as a function of inverse temperature with linear extrapolation to τ_0 . Stars: *p*-CPS, 2-CS, 2,7-DCS (atypical β -process); squares and triangles: *o*-CPS(- d_4), *m*-CPS(- d_4), mixture *o*/*m*-CPS, TCPS; crosses: reference systems (Tol, TPP, PB, DHIQ, and 2-PC) as well as SBC³⁹, and DH 379.³⁸ (B) Time constant τ_β as a function of reduced temperature T_g/T with “average” α -process (black line) of herein investigated glass formers. Systems like in (A). τ_β was determined with a Williams-Watts approach for TCPS (red squares, cf. Figure 4.3.2D) and 2-PC (purple crosses, cf. Appendix Figure 4.3.10D) also above T_g .

As can be noticed from inspecting Figure 4.3.2, below T_g the spectra of the β -relaxation broaden with lowering temperature, a phenomenon well known.^{1,12,14} The spectral broadening can be traced back to an underlying temperature independent distribution of activation energies $g_\beta(E)$.^{1,14,44,48} Given this and referring to the Experimental section 2.3, the spectra of the β -process measured at the different temperatures can be rescaled along eqn (4.3.7) to directly provide the distribution $g_\beta(E)$. This was done in Figure 4.3.7A by using the exponential pre-factor provided by the extrapolation in Figure 4.3.6A (cf. Table 4.3.1). We also

included the spectra of 2-PC (see Appendix) which displays a β -relaxation highly submerged with the α -relaxation, as said. First of all, rather symmetric master curves, i.e., the distributions $g_\beta(E)$, are obtained. Second, the distributions shift to higher energies for glass formers with higher T_g , of course, not surprising due to the trend $E_\beta \cong 24 T_g$ in many cases. The distributions displayed in Figure 4.3.7A are not normalized, instead they refer to some reference temperature ($0.9 T_g$ as indicated). Thus, they still reflect the absolute relaxation strength of the β -relaxation, which, like the α -relaxation, is large in the case of TPP or DHIQ, for example, but rather small for the system TCPS, *o*-CPS, *m*-CPS, and Tol.

In order to estimate the relative contribution of the β -relaxation with respect to that of the α -relaxation we scaled the amplitudes in Figure 4.3.7A by the corresponding values of the relaxation strengths $\Delta\varepsilon_\alpha(T_g)$ – see Figure 4.3.7B, where the $\Delta\varepsilon_\alpha(T_g)$ values were taken from a Kohlrausch fit of the α -relaxation peak (*cf.* Table 4.3.1). Only the fits of $g_\beta(E)$ along eqn (4.3.6) from Figure 4.3.7A are shown. Now a completely different picture emerges. Whereas due to the large $\Delta\varepsilon_\alpha$ of TPP the β -relaxation shown in Figure 4.3.7A is strong, it shows as a relatively weak contribution in the representation of Figure 4.3.7B. The numbers indicate the integral of the distribution and thus the relative strength of the β -relaxation, i.e. $\Delta\varepsilon_\beta(0.9 T_g)/\Delta\varepsilon_\alpha(T_g)$.

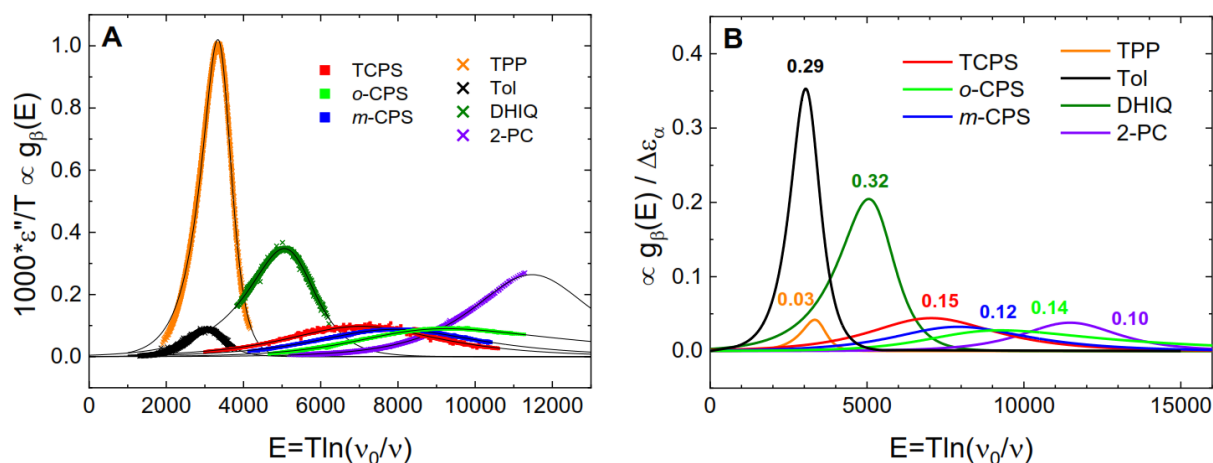


Figure 4.3.7: (A) Relaxation spectra of β -process ($T < T_g$) scaled along eqn (4.3.7) on an absolute scale for TCPS, *o*-CPS, *m*-CPS as well as TPP, Tol, DHIQ, and 2-PC. Lines are fits along eqn (4.3.6) without normalisation. (B) Relative contribution of the β -process at $0.9 T_g$ compared to that of α -process by plotting fits of (A) divided by $\Delta\varepsilon_\alpha(T_g)$ (*cf.* Table 4.3.1). Numbers indicate integral over the distribution and thus the relative strength $\Delta\varepsilon_\beta(0.9 T_g)/\Delta\varepsilon_\alpha(T_g)$.

The secondary relaxations observed in the systems p -CPS, 2-CS, and 2,7-DCS exhibit a different evolution with temperature, as already mentioned. Master curves result just by shifting the spectra at different temperatures along the frequency axis and applying small factors in amplitude to match one at a reference temperature (220 K) as shown in Figure 4.3.8. The missing temperature dependence of the width of the spectra prohibits to map these spectra onto a temperature independent distribution of activation energies as done for the typical secondary (β -) relaxations discussed before. Yet, the spectral shape is asymmetric: the low-frequency flank follows a power-law exponent of about 0.8, whereas the high-frequency flank decays with an exponent of about 0.2 by magnitude. The master curves can be interpolated with a distribution of correlation times according to eqn (4.3.4). Important to note, the exponential pre-factors of these atypical secondary relaxation processes are quite similar to those regarded as typical (see Figure 4.3.6A).

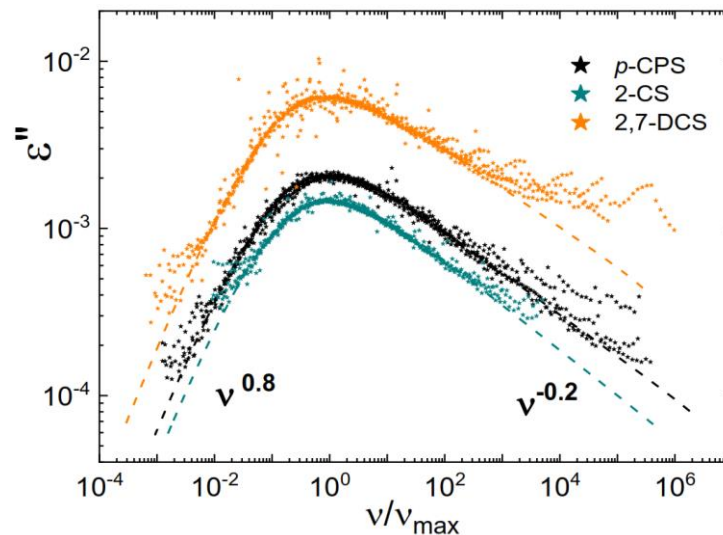


Figure 4.3.8: Master curves of the atypical secondary process in p -CPS, 2-CS, and 2,7-DCS, scaled to the maximum of the curve at 220 K solely by shifting along the frequency axis and small adaptations in the amplitude. Dashed lines: interpolation by eqn (4.3.4).

The distribution of activation energies $g_{\beta}(E)$ shown in Figure 4.3.7A, but now normalised, can also be plotted as a function of the reduced energy scale T/T_g what is found in Figure 4.3.9A. As expected, the distributions are centred between 19 – 35 and of similar width; only in the case of TPP the width is somewhat narrower. In other words, also the width of the β -relaxation increases with T_g .

Finally, we present in Figure 4.3.9B a collection of activation energy data of the β -process plotted vs. $T_g^{1,23}$ extended by the data compiled by the present study (*cf.* Table 4.3.1). Whereas the typical secondary processes essentially show an activation energy between 19 and 35 T_g , the atypical relaxations observed in the present study are closer to the relationship $14 T_g$. In the case of SBC, a typical β -relaxation, which shows a broadening of the spectra below T_g , still a value $E_\beta = 15.6 T_g$ was reported (Table 4.3.1), as for several other systems found in Figure 4.3.9B.

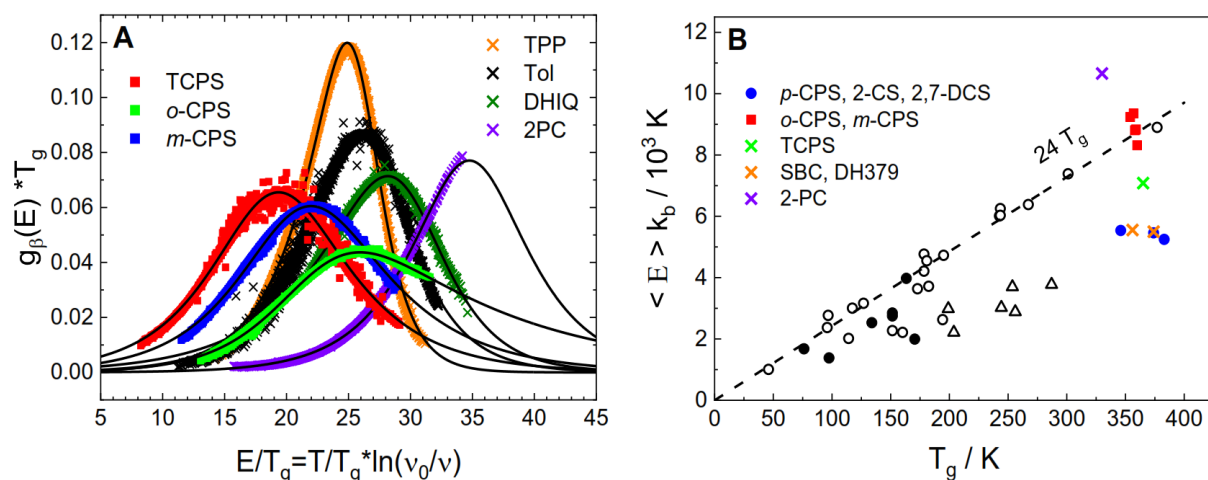


Figure 4.3.9: (A) Normalised distribution $g_\beta(E)$ scaled by T_g for TCPS, o-CPS, and m-CPS (squares) as well as for the reference systems TPP, Tol, DHIQ, and 2-PC (crosses). System is represented by colour and symbol. Black lines are fits along eqn (4.3.6). (B) Apparent activation energy of the secondary processes for the herein investigated glass formers (coloured symbols) in comparison to that of other glass formers investigated in ref. 1 and 23 (black symbols). Glass formers showing atypical β -processes are marked in blue. Dashed line gives $24 T_g$.

4.3.5. Discussion and conclusion

The dielectric spectra of a collection of specially synthesized high- T_g glass formers with a rather large, non-polar spiro core and more or less polar side groups leading to varying high T_g values are investigated. All the relaxation features typical of molecular low- T_g systems are rediscovered, that is, relaxation stretching, a more or less pronounced β -process, and a fragility index quite similar to that of other molecular low- T_g glass formers.¹⁹ As in many other glass formers, the appearance of a strong β -process hampers the identification of a possible generic relaxation pattern including α -peak and excess wing. For example, considering here systems with a rather high (mean) activation of the β -process and thus a low spectral separation of α - and β -process above T_g , no traces of an excess wing are found in contrast to systems with a lower activation energy.^{17,52} The relaxation stretching in terms of β_K of the α -relaxation displays the trend to become less with higher relaxation strength $\Delta\varepsilon_\alpha$, a relationship revealed recently.^{21,22} Yet, we do not find any outlier when the direction of the dipole moment introduced by the nitrile group is changed with respect to some molecular axis, a recent finding.⁵⁸ Also, the local positioning of the polar nitrile group at the rather large core interacting only *via* van-der-Waals forces - potentially having an effect on the stretching⁵⁸ - does not change the trend β_K vs. $\Delta\varepsilon_\alpha$ reported by Paluch et al.²¹

Well resolved β -relaxations are only found for those glass formers investigated here for which a nitrile group is attached in *o*- or *m*-position of the phenyl ring linked to the rigid spiro core. In the *p*-position no clearly resolved β -relaxation is observed. Likewise, no discernible β -relaxation peak is observed when one or two nitrile groups are directly attached to the spiro core as in 2-CS and 2,7-DCS. Absence of any nitrile group lowers the relaxation strength $\Delta\varepsilon_\alpha$ significantly, and no typical β -relaxation pattern is recognized, either. Typical for a generic secondary relaxation, *i.e.* a β -process, is the increase of its relaxation amplitude above T_g , which is found to follow a power-law behaviour with an universal exponent (*cf.* eqn (4.3.9)), yet, its relative amplitude, *i.e.* with respect to that of the α -relaxation, varies strongly. In addition, the separation of α - and β -process varies significantly because of the fact that E_β varies between 19 and 35 T_g , whereas fragility remains essentially the same. However, the power-law behaviour of the amplitudes is a phenomenological finding; a detailed spectral analysis in the frame of the Williams-Watts approach provides quantitative relaxation

strengths and time constants. In particular, the temperature dependence of $\tau_\beta(T)$ shows a crossover to a stronger temperature dependence above T_g , a phenomenon well known,^{1,4,56,59} and the relative strength of the β -process becomes stronger compared to its amplitude (Figure 4.3.5B). The latter can be understood by the fact that the β -relaxation shows a broader spectrum compared to that of the α -relaxation.

Generally speaking, on the one hand, there exist systems which clearly show traces of a weak β -process, yet, due to the closeness to the α -relaxation no two clearly resolved relaxation peaks are observable above T_g . On the other hand, there are glass formers which display well resolved secondary relaxation peaks which, given the frequency window of the Alpha-A Analyzer, are only well discernible below T_g . They belong to the group displaying a mean activation energy close to $12 - 15 T_g$, whereas the first group shows values around $24 T_g$. In the case of DHIQ, the relaxation strength is comparatively strong and the separation of both α - and β -process is sufficiently large, so that a clear-cut merging from two separate relaxations at low temperature to a single (α -) peak at high temperatures is observable in the present frequency window. In any case, E_β increases more or less systematically with T_g , as does the width of the distribution $g_\beta(E)$. Plotting $g_\beta(E)$ as a function of the reduced energy scale E/T_g , not identical but similar distributions are found with widths changing about a factor 2. As the actual manifestation of the β -relaxation depends on the temporal separation of α - and β -process, on amplitude, and width, it is not straight forward to estimate its relative relaxation strength $\Delta\varepsilon_\beta/\Delta\varepsilon_\alpha$ from its apparent manifestation in the relaxation spectra. Nevertheless, our results show that $\Delta\varepsilon_\beta/\Delta\varepsilon_\alpha$ ranges in the interval 0.03 (TPP) – 0.32 (DHIQ).

Applying multi-pulse echo techniques, NMR analyses of neat glasses have identified the β -process as a spatially highly restricted motion of essentially all molecules (a characteristics which might be different in binary glasses^{60,61} or polymers⁵⁶).^{62,63} Above T_g , the extent of this spatial restriction becomes less and less which can explain the quick increase of the relaxation strength $\Delta\varepsilon_\beta$ above T_g .⁶³⁻⁶⁵ Importantly, the NMR relaxation pattern displays rather universal features, which are difficult to reconcile with the quite different relative dielectric relaxation strength $\Delta\varepsilon_\beta/\Delta\varepsilon_\alpha$. These facts appear to challenge a direct mapping of dielectric and NMR results; it is not clear what determines the dielectric relaxation strength of the β -process. Also, on the basis of the NMR results compiled so far, we find it difficult to distinguish between a

generic (Johari-Goldstein) and non-generic secondary relaxation except for the two cases reported here, for which the evolution of the dielectric spectra display a completely different pattern.¹⁵ To the best of our knowledge, the latter kind of secondary process was not reported before.

Given the universal relaxation pattern revealed by NMR, we so far interpreted the β -process as a generic cooperative phenomenon.⁶¹⁻⁶³ Independent of molecular details, the β -process involves an essentially spatially isotropic reorientation of the molecules, though highly hindered. Yet, a possible anisotropic character was discussed by Li-Min Wang & Ngai.⁶⁶ In the case of the present glass formers *o*-, *m*-, and *p*-CPS, with a nitrile group in *ortho*-, *meta*-, and *para*-position, respectively, clear-cut differences are observed: With the nitrile group in the *para*-position, only a weak β -process is observed, in contrast to the other two cases with pronounced β -relaxation. Whether this difference of the manifestation of the β -process is an indication of an anisotropic character or a “localized” β -relaxation restricted to the motion of the phenyl ring alone, can be checked by investigating a deuterated core, by ²H NMR for example – a future task. In the case of toluene, a small, rigid molecule displaying a strong β -process (*cf.* Figure 4.3.3B), labelling the *para*-position by deuterium revealed no difference in the NMR relaxation pattern compared to that given by the fully deuterated phenyl ring.⁶⁷ Thus, reorientation around the pseudo C₂ axis alone can be ruled out. Still, there remains the theoretical possibility that the β -process involves an in-plane wobbling of the phenyl ring.

4.3.6. Appendix

Figure 4.3.10A-C show the dielectric loss spectra of 2,7-DCS, the 50:50 isomer mixture *o*-/*m*-CPS, and *m*-TPTS. For 3,3',4,4'-benzophenonetetracarboxylic dianhydride (2-PC), the Williams-Watts analysis of the dielectric loss data (*cf.* eqn (4.3.8)) with a Kohlrausch function (eqn (4.3.2)) for the α -relaxation and a symmetric distribution of correlation times (eqn (4.3.4)) for the β -relaxation is demonstrated in Figure 4.3.10D (*cf.* Experimental 4.3.2.3).

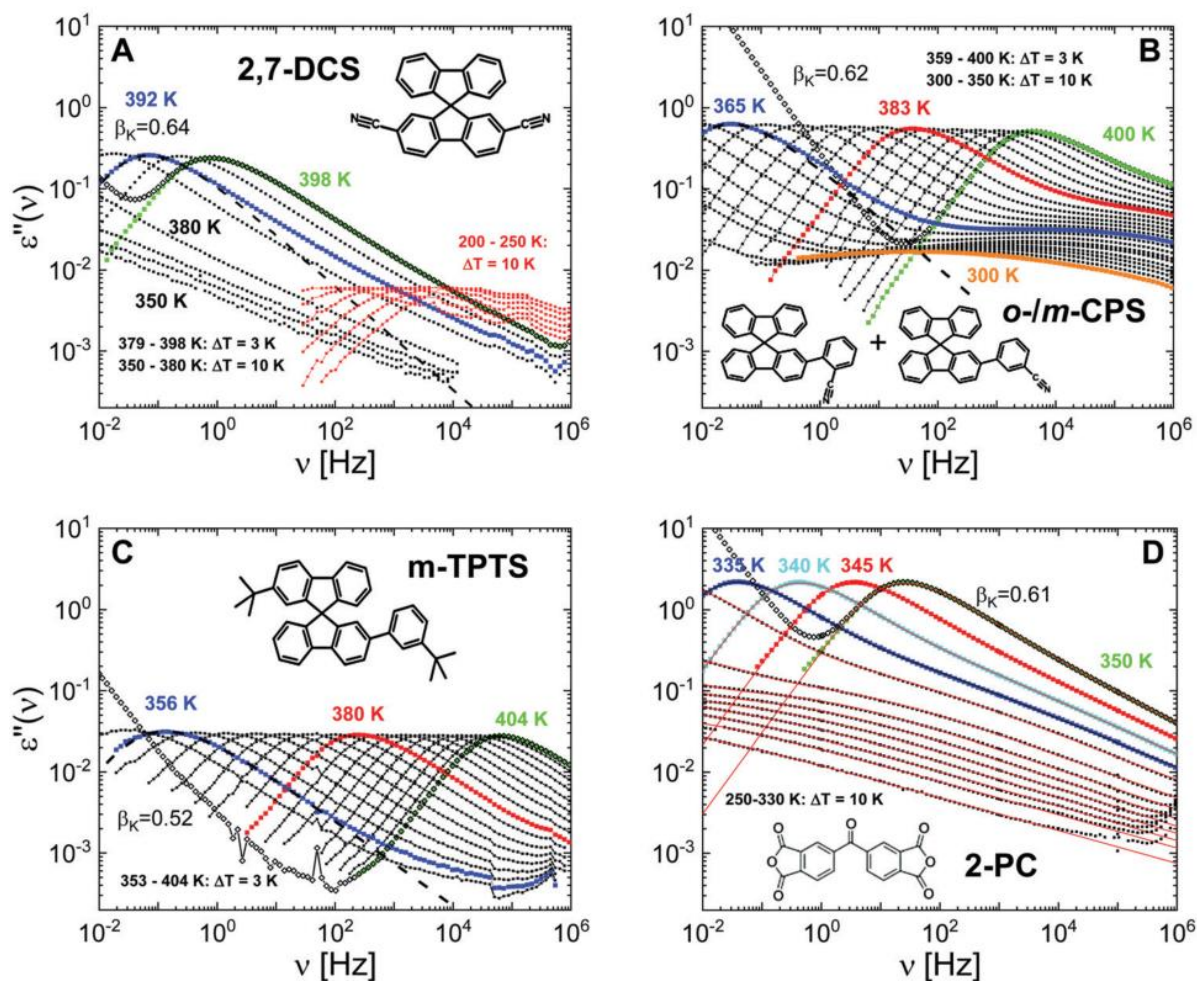


Figure 4.3.10: Dielectric loss spectra of 2,7-DCS (A), 50:50 isomer mixture *o*-/m-CPS (B), m-TPTS (C), and 3,3',4,4'-benzophenonetetracarboxylic dianhydride (2-PC). (D) DC conductivity contribution is subtracted; original data is shown in open symbols for the highest temperature. Coloured curves highlight selected temperatures. In (A)-(C), the dashed black lines show Kohlrausch fits at low temperatures with β_K being indicated. In (D), the red lines show interpolations along a Williams-Watts approach with a Kohlrausch function for the α -relaxation and a symmetric distribution of correlation times for the β -relaxation. (cf. Experimental 4.3.2.3)

4.3.7. Acknowledgement

This research was funded by the Deutsche Forschungsgemeinschaft (DFG, German Research Foundation), Grant Numbers Schm 703/9-1, RO 907/19, and SFB 840. F.K. acknowledges support from the Elite Network of Bavaria (ENB) within the Elite Study Program Macromolecular Science. TK and ER also acknowledge the support by Jürgen Senker to proceed in the experimental work.

4.3.8. References

- [1] A. Kudlik, S. Benkhof, T. Blochowicz, C. Tschirwitz and E. A. Rössler, *The dielectric response of simple organic glass formers*, J. Mol. Struct., **1999**, 479, 201–218.
- [2] P. Lunkenheimer, U. Schneider, R. Brand and A. Loidl, *Glassy dynamics*, Contemp. Phys., **2000**, 41, 15–36.
- [3] T. Blochowicz, A. Brodin and E. A. Rössler in *Advances in Chemical Physics*, ed. S. A. Rice, John Wiley and Sons, Inc., Hoboken, **2006**, 127–256.
- [4] G. Floudas, M. Paluch, A. Grzybowski and K. L. Ngai, *Molecular Dynamics of Glass-Forming Systems: Effects of Pressure*, Springer, Berlin, **2011**.
- [5] R. Richert in *Advances in Chemical Physics*, ed. A. R. Dinner and S. A. Rice, Wiley, Hoboken, **2014**, 101–195.
- [6] W. Götze, *Recent tests of the mode-coupling theory for glassy dynamics*, J. Phys.: Condens. Matter, **1999**, 11, A1-A45.
- [7] A. Aouadi, C. Dreyfus, M. Massot, R. M. Pick, T. Berger, W. Steffen, A. Patkowski and C. Alba-Simionesco, *Light scattering study of the liquid–glass transition of meta-toluidine*, J. Chem. Phys., **2000**, 112, 9860–9873.
- [8] H. Z. Cummins, *Dynamics of supercooled liquids: excess wings, β peaks, and rotation–translation coupling*, J. Phys.: Condens. Matter, **2005**, 17, 1457–1470.
- [9] F. Pabst, J. Gabriel, P. Weigl and T. Blochowicz, *Molecular dynamics of supercooled ionic liquids studied by light scattering and dielectric spectroscopy*, Chem. Phys., **2017**, 494, 103–110.
- [10] R. Torre, P. Bartolini and R. M. Pick, *Time-resolved optical Kerr effect in a fragile glass-forming liquid, salol*, Phys. Rev. E., **1998**, 57, 1912–1920.
- [11] H. Cang, V. N. Novikov and M. D. Fayer, *Experimental observation of a nearly logarithmic decay of the orientational correlation function in supercooled liquids on the picosecond-to-nanosecond time scales*, Phys. Rev. Lett., **2003**, 90, 197401.

- [12] G. P. Johari and M. Goldstein, *Viscous Liquids and the Glass Transition. II. Secondary Relaxations in Glasses of Rigid Molecules*, J. Chem. Phys., **1970**, *53*, 2372–2388.
- [13] L. Wu, *Relaxation mechanisms in a benzyl chloride-toluene glass*, Phys. Rev. B., **1991**, *43*, 9906–9915.
- [14] K. L. Ngai and M. Paluch, *Classification of secondary relaxation in glass-formers based on dynamic properties*, J. Chem. Phys., **2004**, *120*, 857–873.
- [15] G. Williams and D. C. Watts, *Molecular Motion in The Glassy State*, Trans. Faraday Soc., **1971**, *67*, 1971–1979.
- [16] A. Brodin, C. Gainaru, V. Porokhonsky and E. A. Rössler, *Evolution of dynamic susceptibility in molecular glass formers - a critical assessment*, J. Phys.: Condens. Matter, **2007**, *19*, 205104.
- [17] U. Schneider, R. Brand, P. Lunkenheimer and A. Loidl, *Excess wing in the dielectric loss of glass formers: A johari-goldstein beta relaxation?*, Phys. Rev. Lett., **2000**, *84*, 5560–5563.
- [18] N. Petzold, B. Schmidtke, R. Kahlau, D. Bock, R. Meier, B. Micko, D. Kruk and E. A. Rössler, *Evolution of the dynamic susceptibility in molecular glass formers: results from light scattering, dielectric spectroscopy, and NMR*, J. Chem. Phys., **2013**, *138*, 12A510.
- [19] R. Böhmer and C. A. Angell, *Correlations of the nonexponentiality and state dependence of mechanical relaxations with bond connectivity in Ge-As-Se supercooled liquids*, Phys. Rev. B, **1992**, *45*, 10091–10094.
- [20] B. Schmidtke, N. Petzold, B. Pötzschner, H. Weingärtner and E. A. Rössler, *Relaxation stretching, fast dynamics, and activation energy: a comparison of molecular and ionic liquids as revealed by depolarized light scattering*, J. Phys. Chem. B., **2014**, *118*, 7108–7118.
- [21] M. Paluch, J. Knapik, Z. Wojnarowska, A. Grzybowski and K. L. Ngai, *Universal Behavior of Dielectric Responses of Glass Formers: Role of Dipole-Dipole Interactions*, Phys. Rev. Lett., **2016**, *116*, 25702.

- [22] A. I. Nielsen, T. Christensen, B. Jakobsen, K. Niss, N. B. Olsen, R. Richert and J. C. Dyre, *Prevalence of approximate square root(t) relaxation for the dielectric alpha process in viscous organic liquids*, J. Chem. Phys., **2009**, *130*, 154508.
- [23] C. Tschirwitz, S. Benkhof, T. Blochowicz and E. Rössler, *Dielectric spectroscopy on the plastically crystalline phase of cyanocyclohexane*, J. Chem. Phys., **2002**, *117*, 6281–6288.
- [24] C. Gainaru, R. Kahlau, E. A. Rössler and R. Böhmer, *Evolution of excess wing and beta-process in simple glass formers*, J. Chem. Phys., **2009**, *131*, 184510.
- [25] Q. Niu, Q. Zhang, W. Xu, Y. Jiang, R. Xia, D. D.C. Bradley, D. Li and X. Wen, *Solution-processed anthracene-based molecular glasses as stable blue-light-emission laser gain media*, Org. Electron., **2015**, *18*, 95–100.
- [26] J. Salbeck and F. Weissörtel, *Spiro linked compounds for use as active materials in organic light emitting diodes*, Macromol. Symp., **1997**, *125*, 121–132.
- [27] J. Pang, Y. Tao, S. Freiberg, X.-P. Yang, M. D'lorio and S. Wang, *Syntheses, structures, and electroluminescence of new blue luminescent star-shaped compounds based on 1,3,5-triazine and 1,3,5-trisubstituted benzene*, J. Mater. Chem., **2002**, *12*, 206–212.
- [28] J. Y. Shen, C. Y. Lee, T.-H. Huang, J. T. Lin, Y.-T. Tao, C.-H. Chien and C. Tsai, *High- T_g blue emitting materials for electroluminescent devices*, J. Mater. Chem., **2005**, *15*, 2455–2463.
- [29] K. Tsuchiya, S. W. Chang, N. M. Felix, M. Ueda and C. K. Ober, *Lithography Based on Molecular Glasses*, J. Photopolym. Sci. Tech., **2005**, *18*, 431–434.
- [30] E. Murotani, J.-K. Lee, M. Chatzichristidi, A. A. Zakhidov, P. G. Taylor, E. L. Schwartz, G. G. Malliaras and C. K. Ober, *Cross-linkable molecular glasses: low dielectric constant materials patternable in hydrofluoroethers*, ACS Appl. Mater. Interfaces, **2009**, *1*, 2363–2370.
- [31] N. M. Felix, A. de Silva and C. K. Ober, *Calix[4]resorcinarene Derivatives as High-Resolution Resist Materials for Supercritical CO₂ Processing*, Adv. Mater., **2008**, *20*, 1303–1309.

- [32] E. O. Kissi, H. Grohganz, K. Löbmann, M. T. Ruggiero, J. A. Zeitler and T. Rades, *Glass-Transition Temperature of the β -Relaxation as the Major Predictive Parameter for Recrystallization of Neat Amorphous Drugs*, *J. Phys. Chem. B.*, **2018**, *122*, 2803–2808.
- [33] A. Afzal, M. Shahin Thayyil, M. K. Sulaiman and A. R. Kulkarni, *Dielectric relaxation studies in super-cooled liquid and glassy phases of anti-cancerous alkaloid: Brucine*, *Indian J. Phys.*, **2018**, *92*, 565–573.
- [34] F. Pfeiffer, N. M. Felix, C. Neuber, C. K. Ober and H.-W. Schmidt, *Physical Vapor Deposition of Molecular Glass Photoresists: A New Route to Chemically Amplified Patterning*, *Adv. Funct. Mater.*, **2007**, *17*, 2336–2342.
- [35] F. Pfeiffer, N. M. Felix, C. Neuber, C. K. Ober and H.-W. Schmidt, *Towards environmentally friendly, dry deposited, water developable molecular glass photoresists*, *PCCP*, **2008**, *10*, 1257–1262.
- [36] M. Hasebe, D. Musumeci and L. Yu, *Fast surface crystallization of molecular glasses: creation of depletion zones by surface diffusion and crystallization flux*, *J. Phys. Chem. B.*, **2015**, *119*, 3304–3311.
- [37] F. Krohn, C. Neuber, E. A. Rössler and H.-W. Schmidt, *Organic Glasses of High Glass Transition Temperatures Due To Substitution with Nitrile Groups*, *J. Phys. Chem. B.*, **2019**, *123*, 10286–10293.
- [38] B. Pötzschner, F. Mohamed, A. Lichtinger, D. Bock and E. A. Rössler, *Dynamics of asymmetric non-polymeric binary glass formers-A nuclear magnetic resonance and dielectric spectroscopy study*, *J. Chem. Phys.*, **2015**, *143*, 154506.
- [39] B. Pötzschner, F. Mohamed, C. Bächer, E. Wagner, A. Lichtinger, R. Minikejew, K. Kreger, H.-W. Schmidt and E. A. Rössler, *Non-polymeric asymmetric binary glass-formers. I. Main relaxations studied by dielectric, $^2\text{H-NMR}$, and ^{31}P spectroscopy*, *J. Chem. Phys.*, **2017**, *146*, 164503.
- [40] V. N. Novikov and E. A. Rössler, *Correlation between glass transition temperature and molecular mass in non-polymeric and polymer glass formers*, *Polymer*, **2013**, *54*, 6987–6991.

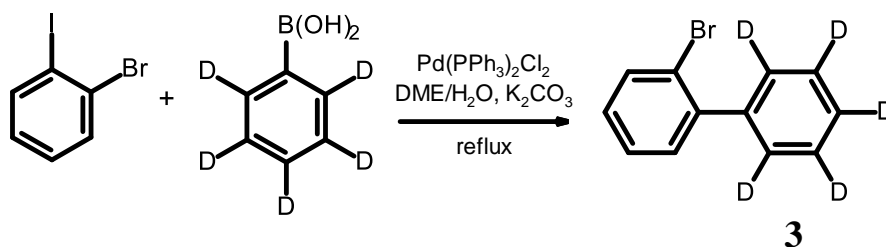
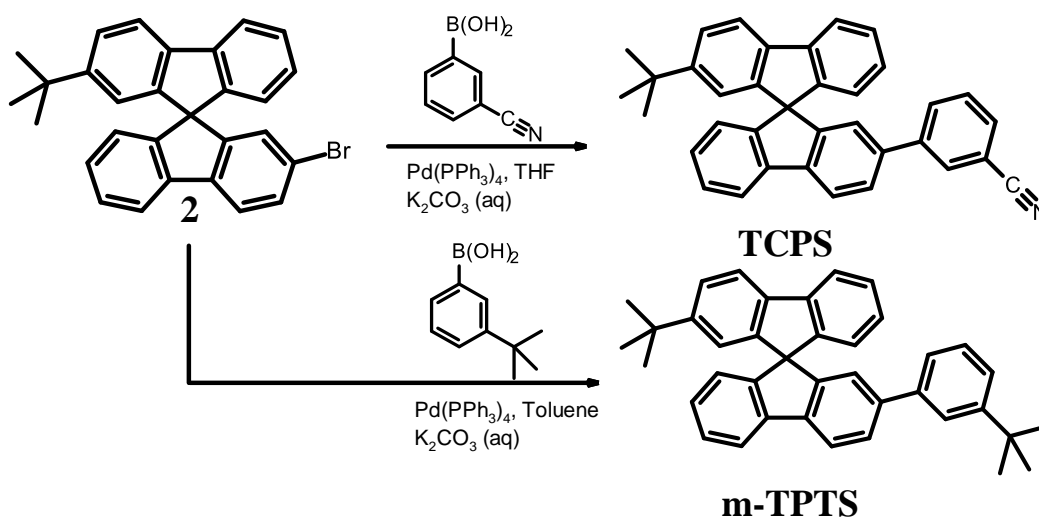
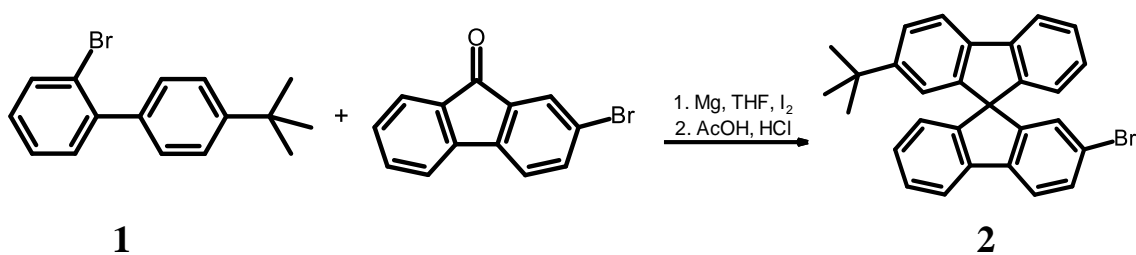
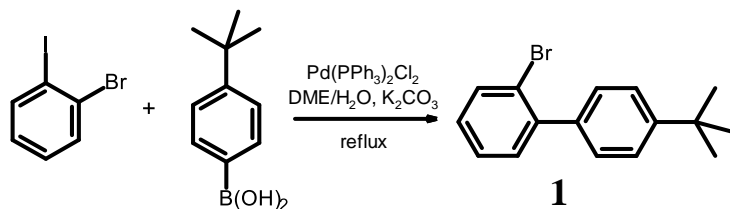
- [41] J. Hintermeyer, A. Herrmann, R. Kahlau, C. Goiceanu and E. A. Rössler, *Molecular Weight Dependence of Glassy Dynamics in Linear Polymers Revisited*, *Macromolecules*, **2008**, *41*, 9335-9344
- [42] R. Kahlau and E. A. Rössler, *unpublished work*.
- [43] S. Adishchev, D. Bock, C. Gainaru, R. Kahlau, B. Micko, N. Petzold, B. Pötzschner and E. A. Rössler, *Reorientational Dynamics of Organophosphate Glass Formers – a Joint Study by ^{31}P NMR, Dielectric Spectroscopy and Light Scattering*, *Z. Phys. Chem.*, **2012**, *226*, 1149–1168.
- [44] R. Kahlau, T. Dörler, and E. A. Rössler, *Secondary relaxations in a series of organic phosphate glasses revealed by dielectric spectroscopy*, *J. Chem. Phys.*, **2013**, *139*, 134504
- [45] S. Kachel and E. A. Rössler, *unpublished work*.
- [46] C. J. F. Böttcher and P. Bordewijk, *Dielectrics in Time-Dependent Fields*, Elsevier, Amsterdam, **1978**.
- [47] F. Kremer and A. Schönhal, *Broadband Dielectric Spectroscopy*, Springer, Berlin, **2003**
- [48] T. Blochowicz, C. Tschirwitz, St. Benkhof and E. A. Rössler, *Susceptibility functions for slow relaxation processes in supercooled liquids and the search for universal relaxation patterns*, *J. Chem. Phys.*, **2003**, *118*, 7544–7556.
- [49] K. S. Gilroy and W. A. Phillips, *An asymmetric double-well potential model for structural relaxation processes in amorphous materials*, *Philos. Mag. B*, **1981**, *43*, 735–746.
- [50] L. Wu and S. R. Nagel, *Secondary relaxation in o-terphenyl glass*, *Phys. Rev. B*, **1992**, *46*, 11198–11200.
- [51] J. Wiedersich, S. V. Adichtchev and E. A. Rössler, *Spectral Shape of Relaxations in Silica Glass*, *Phys. Rev. Lett.*, **2000**, *84*, 2718–2721.
- [52] C. Gainaru, R. Böhmer, R. Kahlau and E. Rössler, *Energy landscape in molecular glasses probed by high-resolution dielectric experiments*, *Phys. Rev. B*, **2010**, *82*, 104205.

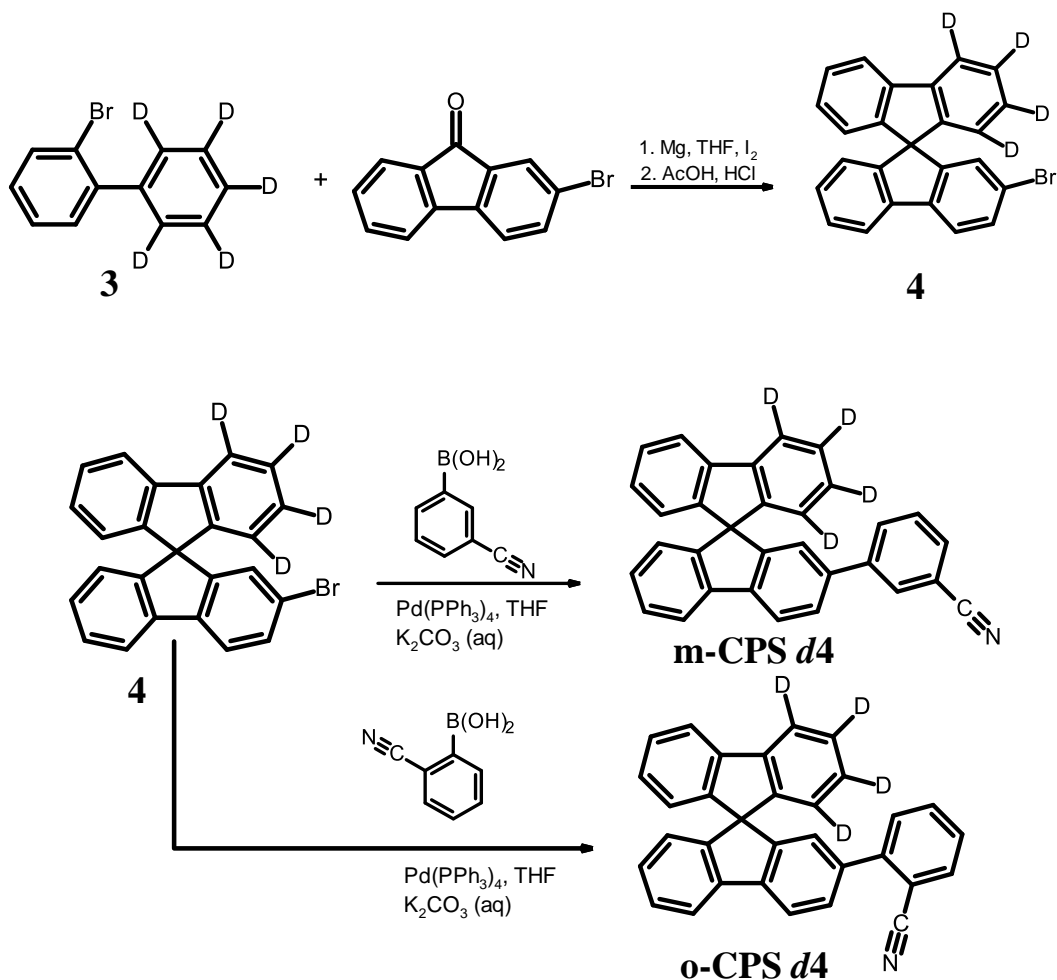
- [53] A. Arbe, D. Richter, J. Colmenero and B. Farago, *Merging of the α and β relaxations in polybutadiene: A neutron spin echo and dielectric study*, Phys. Rev. E., **1996**, *54*, 3853–3869.
- [54] H. Wagner and R. Richert, *Equilibrium and Non-Equilibrium Type β -Relaxations: d -Sorbitol versus o -Terphenyl*, J. Phys. Chem. B, **1999**, *103*, 4071–4077.
- [55] F. Mohamed, *Dynamics of Advanced Polymer Systems studied by Dielectric Spectroscopy and Rheology: From Binary Glass Formers to Nanocomposites*, Bayreuth, **2018**.
- [56] T. Körber, F. Mohamed, M. Hofmann, A. Lichtinger, L. Willner and E. A. Rössler, *The Nature of Secondary Relaxations: The Case of Poly(ethylene- alt -propylene) Studied by Dielectric and Deuteron NMR Spectroscopy*, Macromolecules, **2017**, *50*, 1554–1568.
- [57] A. Kudlik, C. Tschirwitz, T. Blochowicz, S. Benkhof and E. A. Rössler, *Slow secondary relaxation in simple glass formers*, J. Non-Cryst. Solids, **1998**, *235-237*, 406–411.
- [58] A. Jedrzejowska, M. Matussek, K. L. Ngai, K. Grzybowska, K. Jurkiewicz and M. Paluch, *New paradigm of dielectric relaxation of sizable and rigid molecular glass formers*, Phys. Rev. E, **2020**, *101*, 10603.
- [59] K. L. Ngai and M. Paluch, *Inference of the Evolution from Caged Dynamics to Cooperative Relaxation in Glass-Formers from Dielectric Relaxation Data*, J. Phys. Chem. B, **2003**, *107*, 6865–6872.
- [60] B. Micko, C. Tschirwitz and E. A. Rössler, *Secondary relaxation processes in binary glass formers: emergence of "islands of rigidity"*, J. Chem. Phys., **2013**, *138*, 154501.
- [61] D. Bock, R. Kahlau, B. Micko, B. Pötzschner, G. J. Schneider and E. A. Rössler, *On the cooperative nature of the β -process in neat and binary glasses: a dielectric and nuclear magnetic resonance spectroscopy study*, J. Chem. Phys., **2013**, *139*, 64508.
- [62] M. Vogel and E. Rössler, *Slow β process in simple organic glass formers studied by one- and two-dimensional ^2H nuclear magnetic resonance. I*, J. Chem. Phys., **2001**, *114*, 5802–5815.

- [63] M. Vogel, C. Tschirwitz, G. Schneider, C. Koplin, P. Medick and E. A. Rössler, *A ^2H NMR and dielectric spectroscopy study of the slow β -process in organic glass formers*, *J. Non-Cryst. Solids*, **2002**, 307-310, 326–335.
- [64] B. Micko, D. Kruk and E. A. Rössler, *Primary and secondary relaxation process in plastically crystalline cyanocyclohexane studied by ^2H nuclear magnetic resonance. II. Quantitative analysis*, *J. Chem. Phys.*, **2013**, 138, 74504.
- [65] M. Vogel, P. Medick and E. A. Rössler in *Annual Reports on NMR Spectroscopy*, ed. G. A. Webb, Academic Press, Amsterdam, **2005**, 231–299.
- [66] L.-M. Wang, Y. Tian, R. Liu and K. L. Ngai, *Anomalous component dynamics of a binary mixture of associating glass-forming liquids*, *J. Phys. Chem. B.*, **2011**, 115, 719–724.
- [67] D. Bock, T. Körber, F. Mohamed, B. Pötzschner and E. A. Rössler in *The Scaling of Relaxation Processes*, ed. F. Kremer and A. Loidl, Springer, Cham, **2018**.

4.3.9. Supporting Information

4.3.9.1. Synthetic route





4.3.9.2. Synthetic procedures and $^1\text{H-NMR}$ data

Synthesis of **1**: 7.00 g (24.8 mmol) Iodobromobenzene and 5.291 g (29.7 mmol) of 4-*tert*butylphenylboronic acid are solved in 60 mL of DME and 10 mL of H_2O . 8.55 g of K_2CO_3 are added, then the mixture is flushed with Argon under stirring for 30 minutes. 260 mg of $\text{PdCl}_2(\text{PPh}_3)_2$ are added and Argon is flushed for another 30 minutes. Afterwards the mixture is heated to 80°C for 18 h.

After cooling, DME is removed under reduced pressure, to the residue is given 80 mL of H_2O and 40 mL of Ether. The phases are separated, the aqueous phase is washed with Ether, the combined organic phases are dried over MgSO_4 and the solvent is removed under reduced pressure. The crude product is further purified by column chromatography with cyclohexane to yield 6.15 g (86 %) of a colourless liquid with a distinct odour.

^1H NMR (300 MHz, CDCl_3): δ = 1.40 (s, 9H, *t*-Bu-H), 7.21 (m, 1H, Ar-H), 7.38 (m, 4H, Ar-H), 7.47 (dt, 2H, Ar-H), 7.69 (m, 1H, Ar-H).

Synthesis of **2**: 6.15 g (21.4 mmol) of **1** are mixed with 625 mg of Mg and one spatula tip of I_2 in 50 mL of dry THF and heated under reflux. 4.66 g (18 mmol) 2-bromo-fluorenone are dissolved in 15 mL of dry THF. After 5 h, the Grignard reagent is transferred to the fluorenone solution with a syringe and stirred under reflux for further 17 h. Then a few drops of HCl are given to the solution upon which it clarifies. THF is removed under reduced pressure, the remaining material is dissolved in 50 mL AcOH and 2 mL of 32 % HCl and heated under reflux for 4 h. The precipitated product is then filtered, washed with hexane and EtOH, and dried to yield 5.04 g (62 %) of a colourless powder.

^1H NMR (300 MHz, CDCl_3): δ = 1.20 (s, 9H, *t*-Bu-H), 6.67 (m, 1H, Ar-H), 6.74 (m, 1H, Ar-H), 6.87 (dd, 1H, Ar-H), 7.12 (m, 2H, Ar-H), 7.37 (qd, 2H, Ar-H), 7.48 (m, 2H, Ar-H), 7.77 (m, 4H, Ar-H).

Synthesis of **TCPS**: 570 mg of **2** (1.3 mmol) are mixed with 240 mg 3-cyanophenylboronic acid (1.62 mmol, 1.25 n) in 100 mL of THF. 60 mL 2 M K_2CO_3 solution are added and the mixture is stirred under Ar stream for 30 minutes. 120 mg of $\text{Pd}(\text{PPh}_3)_4$ are added and the mixture is stirred under Ar for another 30 minutes and subsequently heated to reflux for 17 h.

After cooling the mixture is filtrated, the phases are separated, the organic phase is washed with brine, dried over MgSO_4 and the solvent is removed under reduced pressure. The crude product is further purified by column chromatography (cyclohexane / ethyl acetate 5:1) to yield 538 mg (85 %) of an off-white powder.

^1H NMR (300 MHz, CDCl_3): δ = 1.19 (s, 9H, *t*-Bu-H), 6.71 (m, 1H, Ar-H), 6,77 (m, 2H, Ar-H), 6.92 (dd, 1H, Ar-H), 7.13 (m, 2H, Ar-H), 7.43 (m, 4H, Ar-H), 7.54 (td, 1H, Ar-H), 7.64 (m, 2H, Ar-H), 7.72 (m, 1H, Ar-H), 7.80 – 7.99 (m, 4H, Ar-H).

Synthesis of **m-TPTS**: 4.5 g (10 mmol) of **2** are dissolved in 100 mL Toluene with 1.73 g (12.48 mmol) 3-tertbutylphenyl boronic acid. 60 mL 2M K₂CO₃ solution are added and the mixture is bubbled with Ar for 30 minutes. 336 mg Pd(PPh₃)₄ are added and Ar is bubbled for another 30 minutes. The mixture is then stirred at 100 °C for 17 h. After the reaction is complete, the phases are separated and the aqueous phase is washed with toluene. The combined organic phases are dried over MgSO₄ and the solvent is evaporated under reduced pressure. The crude product is purified via column chromatography (cyclohexane / ethyl acetate 5:1 and 100:1) to yield 2.07 g (41 %) of a white powder.

¹H NMR (300 MHz, CDCl₃): δ = 1.19 (s, 9H, *t*-Bu-H), 1.32 (s, 9H, *t*-Bu-H), 6.75 (m, 3H, Ar-H), 6.94 (dd, 1H, Ar-H), 7.10 (m, 2H, Ar-H), 7.18 – 7.48 (m, 7H, Ar-H), 7.64 (dd, 1H, Ar-H), 7.77 – 7.95 (m, 4H, Ar-H).

Synthesis of **3**: 3.81 g 2-Iodobromobenzene and 2.14 g of phenyl-*d*₅-boronic acid are dissolved in 40 mL of DME and 5 mL of H₂O. 3.64 g of K₂CO₃ are added, then the mixture is flushed with Argon under stirring for 30 minutes. 118 mg of PdCl₂(PPh₃)₄ are added and Argon is flushed for another 30 minutes. Afterwards the mixture is heated to 80 °C for 5 h.

After cooling, DME is removed under reduced pressure, to the residue is given 50 mL of H₂O and 30 mL of Ether. The phases are separated, the aqueous phase is washed with Ether, the combined organic phases are dried over MgSO₄ and the solvent is removed under reduced pressure. The crude product is further purified by column chromatography with hexane to yield 2.122 g (68 %) of a colourless liquid with a distinct odour.

¹H NMR (300 MHz, CDCl₃): δ = 7.23 (m, 1H, Ar-H), 7.33 – 7.42 (m, 2H, Ar-H), 7.70 (m, 1H, Ar-H).

Synthesis of **4**: 2.2 g of **3** are dissolved in 25 mL of dry THF. 0.271 g of Mg and a spatula tip of I₂ are added. The mixture is stirred under reflux for 3 h. 2.41 g of 2-Bromofluorenone are dissolved in 5 mL dry THF. The Grignard reagent is carefully transferred to the fluorenone solution using a syringe. The mixture is stirred for another 18 hours under reflux.

Afterwards, 2 mL of AcOH are added to the mixture, after which the opaque suspension clears. THF is removed under reduced pressure and to the mixture are added 20 mL of AcOH and 1 mL of HCl (32 %). The mixture is stirred under reflux for another 5 h. After cooling, DCM and water are added, the phases are separated and the aqueous phase is washed twice with DCM. The combined organic phase are dried over MgSO₄ and the solvent is removed under reduced pressure to yield 2.505 g (68 %) of a white solid.

¹H NMR (300 MHz, CDCl₃): δ = 6.74 (m, 2H, Ar-H), 6.87 (dd, 1H, Ar-H), 7.15 (dt, 2H, Ar-H), 7.40 (m, 2H, Ar-H), 7.50 (dd, 1H, Ar-H), 7.72 (dd, 1H, Ar-H), 7.85 (m, 2H, Ar-H).

Synthesis of **o-CPS d4** and **m-CPS d4**: The synthetic procedure to obtain both compounds from **4** is according to the undeuterated compounds and can be found elsewhere.¹

o-CPS d4: ¹H NMR (300 MHz, CDCl₃): δ = 6.80 (m, 2H, Ar-H), 6.87 (dd, 1H, Ar-H), 7.16 (qt, 2H, Ar-H), 7.30 – 7.44 (m, 4H, Ar-H), 7.51 (m, 1H, Ar-H), 7.67 (dd, 2H, Ar-H), 7.89 (m, 2H, Ar-H), 7.98 (dd, 1H, Ar-H).

m-CPS d4: ¹H NMR (300 MHz, CDCl₃): δ = 6.78 (m, 2H, Ar-H), 6.92 (dd, 1H, Ar-H), 7.15 (m, 2H, Ar-H), 7.42 (m, 3H, Ar-H), 7.53 (td, 1H, Ar-H), 7.58 – 7.73 (m, 3H, Ar-H), 7.90 (m, 2H, Ar-H), 7.96 (dd, 1H, Ar-H).

References:

1. F. Krohn, C. Neuber, E. A. Rössler and H.-W. Schmidt, J. Phys. Chem. B., **2019**, *123*, 10286–10293.

4.4. Reorientational Dynamics of highly asymmetric binary non-polymeric mixtures – a dielectric spectroscopy study

Thomas Körber,^a Felix Krohn,^b Christian Neuber,^b Hans-Werner Schmidt,^b and Ernst A. Rössler^{a*}

^a Department of Inorganic Chemistry III and Northern Bavarian NMR Center, University of Bayreuth, 95440 Bayreuth, Germany

^b Department of Macromolecular Chemistry and Bavarian Polymer Institute, University of Bayreuth, 95440 Bayreuth, Germany

The results have been published as a full paper.

Reproduced by permission of the PCCP Owner Societies from *Phys. Chem. Chem. Phys.* **2021**, *23*, 7200-7212.

<https://doi.org/10.1039/D0CP06652D>

4.4.1. Abstract

We present an analysis of dielectric spectra measured for a specially designed non-polymeric asymmetric glass former characterized by a large difference of the component's T_g ($\Delta T_g = 216\text{ K}$). We cover the whole additive concentration range from 4% up to 90 % (by mass). Two main relaxations α_1 and α_2 are identified, which are characterized by well-separated time scales and are attributed to the dynamics associated with the high- T_g component (α_1) and the low- T_g component (α_2). Frequency-temperature superposition does not apply. To cope with the extraordinary spectral broadening, we introduce a model consisting of a generalized Cole-Davidson (α_1) and a Havriliak-Negami function with a low frequency truncation (α_2). Whereas the α_1 -relaxation reflects essentially homogeneous dynamics and its spectra mainly broaden on the high-frequency flank of the relaxation peak, the α_2 -relaxation becomes broader and the low-frequency side reflecting pronounced dynamic heterogeneity in a more or less arrested matrix of high- T_g molecules. From the extracted time constants, two glass transition temperatures, T_{g_1} and T_{g_2} can be derived, showing a non-trivial concentration dependence for T_{g_2} . Supplementary, we find a β -relaxation. The total relaxation strength $\Delta\varepsilon$ strongly deviates from ideal mixing, and therefore care has to be taken interpreting the corresponding $\Delta\varepsilon_{\alpha_1}$ as representation of molecular populations.

4.4.2. Introduction

The dynamics of neat glass-formers was extensively investigated in the last decades, and a clear picture of the evolution of the dynamics has emerged.¹⁻⁵ Yet, a full understanding of the glass transition phenomenon has still to be accomplished. In recent years, interest has been drawn to the understanding of binary glass forming mixtures. A relevant technological field is a typical polymer-plasticizer system or a polymer blend, both of which were intensively reviewed.⁶⁻¹⁰ Significantly less is known about mixtures of non-polymeric compounds, especially dynamically asymmetric systems, that are systems having a high T_g -contrast. These mixtures may be taken as model systems for binary glass formers with significant molecular size disparity of their components and have also sparked the interest of molecular dynamics and theoretical studies.¹¹⁻¹⁷

While early studies suggested a single T_g to be a necessity in fully miscible systems,¹⁸ the existence of two T_g in dynamically asymmetric systems is now widely accepted which reflects

a decoupling of the component dynamics.^{19–21} For example, two glass transitions are observed in miscible polymer blends,²¹ polymer-plasticizer systems,^{19,22} and mixtures of non-polymeric organic glasses^{23–25} by means of dielectric spectroscopy (DS),^{22,26,27} nuclear magnetic resonance spectroscopy (NMR),^{28–30} differential scanning calorimetry (DSC),^{7,31} and neutron scattering.³² In such mixtures, a broadening of the underlying relaxation time distributions as compared to the neat materials is usually observed, and frequency temperature superposition (FTS) fails pronouncedly.^{22,33,34}

In a series of papers, we investigated component-selectively the dynamics in dynamically highly asymmetric binary glass formers, polymeric and non-polymeric, by dielectric as well as by ²H and ³¹P NMR spectroscopy.^{22,24,35} In particular, we started a program synthesizing stable non-polymeric high- T_g glass formers based on a spirobifluorene central unit.^{36,37} Mixtures with a T_g -contrast of their components up to $\Delta T_g \cong 250\text{ K}$ were studied. Two more or less separated main relaxations, α_1 associated with the slow dynamics of the high- T_g component and α_2 the faster one of the low- T_g component (additive) were observed. For the α_1 -process, the well-known plasticizer effect is observed, i.e. an acceleration of the dynamics upon mixing. The corresponding relaxation spectra appeared to broaden only weakly and frequency-time superposition (FTS) still applies approximately. Usually, they can be fitted with a Kohlrausch function. For the α_2 -process, an anti-plasticizer effect is observed. At low additive concentrations a crossover of the time constants τ_{α_2} to an Arrhenius-like temperature dependence is observed for $T \leq T_{g1}$. This “fragile-to-strong” transition was found in several other systems.^{22,31,38}

As confirmed by NMR, strong dynamic heterogeneities appear for the low- T_g component showing a quasi-logarithmic correlation loss and involving isotropic reorientation in a more or less arrested matrix of the high- T_g component.^{28,35} Thus, the α_2 -process was regarded as a second main (α -) relaxation. In DSC experiments, a second yet broadened glass step was found, allowing T_{g1} and T_{g2} to be determined in addition to DS. It turned out that the dynamic scenario does not differ significantly when taking a polymeric or non-polymeric high- T_g component. Recently, investigating systems with smaller T_g contrast ($\Delta T_g = 63 - 89\text{ K}$), we found indications that also the dynamics of the high- T_g component displays some extent of

dynamic heterogeneity.³⁴ In any case, given the broad and over-lapping relaxation spectra, their analysis becomes a challenge and their interpretation is still controversially debated.^{39,40}

Two features deserve to be particularly mentioned. First, interpreting the α_1 - and α_2 -process, respectively, as a separate glass transition, the mass concentration dependence $T_{g_1}(w_{additive})$ displays the well-established monotonously decrease starting with T_g of the high- T_g component. The peculiar trace of $T_{g_2}(w_{additive})$, however, showing a maximum at intermediate additive concentration was not reported before but found in all investigated systems with a high T_g -contrast.^{22,24,35} Yet, many studies on polymer-plasticizer did not investigate the full concentration range. Moreover, in the limit of low additive concentrations the second DSC step becomes highly broadened which may prevent a clear-cut determination of T_{g_2} . Second, the design of our experiments was such that the low- T_g component dominated the dielectric response. Thus, the dielectric spectra directly reflect its dynamics. Surprisingly, however, two dielectric relaxation peaks were observed, and comparing the respective relaxation strengths, we suggested that there exists a second sub-ensemble of additive molecules which follows the dynamics of the high- T_g molecules. Similar conclusions were drawn by Blochowicz and co-workers.^{23,31} Analysing the relaxation strength, it appeared that the fraction of additive molecules being linked to the α_1 -process continuously decreased upon increasing temperature until it finally disappears.

Our previous studies on non-polymeric asymmetric mixtures were hampered by the fact that the samples tend to de-mix and partly crystallize around room-temperature.²⁴ Furthermore, in order to probe the dynamics of the high- T_g component by ^2H NMR a deuterated phenyl group was attached to the spirobifluorene unit. However, the occurring phenyl-flip hampered a detailed analysis of the α_1 -process by NMR.³⁵ In the present contribution, we introduce a new non-polymeric asymmetric binary system not prone to de-mixing and crystallization. It is composed of the high- T_g component *m*-TPTS ($T_g = 350\text{ K}$) and the additive tripropyl phosphate (TPP; $T_g = 134\text{ K}$), thus featuring a T_g -contrast of 216 K (see Fig. 4.4.1 for chemical structure). One of the four phenyl rings constituting the spirobifluorene unit can be deuterated and thus, ^2H NMR can probe the dynamics of the rigid core of the glass former as will be demonstrated in a follow-up study. The additive TPP is already well-investigated as a neat glass-former^{41,42} and as the low- T_g component in our previous binary systems; its dynamics will be probed by ^{31}P NMR.^{22,35} The dielectric behaviour of neat *m*-TPTS was

reported recently.³⁷ In the present publication we report on the DSC and DS experiments. In the forthcoming paper, we will complement our investigations by presenting the results from the NMR investigations.⁴³

4.4.3. Experimental

4.4.3.1. Materials

Fig. 4.4.1 shows the chemical structures of the two used components in the present study. The high- T_g glass former 2-(*m*-*tert*butylphenyl)-2'-*tert*butyl-9,9'-spirobi[9*H*]fluorene (*m*-TPTS) was synthesized along the lines described in ref. 37. The compound was purified by sublimation. The low- T_g additive tripropyl phosphate (TPP; Sigma Aldrich) was rectified by the distillation over a vigreux column under reduced pressure before use. For dielectric measurements with 50 % or higher TPP content (by weight percentage), a solution was prepared in a vial and transferred into the sample-cell *via* a pipette. At 50 % and lower TPP content, a certain amount of *m*-TPTS amorphous powder was filled into the sample cell and re-vitrified. The amount of *m*-TPTS was chosen to yield 50 – 60 mg of the mixture in order to ensure a completely filled sample volume in the DS cell. Then, an appropriate amount of liquid TPP was added to the *m*-TPTS, the DS cell was tightly sealed and treated at elevated temperature (80 – 130 °C) for a prolonged time (1 – 3 days) to ensure complete mixing of both compounds in the cell. To prove the tightness of the cell, mass was controlled before and after tempering. DS measurements were conducted from highest to lowest temperature. Equilibrium of the mixture was ensured by a following measurement of selected temperatures from the lowest to the highest temperature, whereby the obtained spectra were identical in all cases. After the DS or DSC measurement was completed, the finally measured concentration of both compounds was determined by high-resolution NMR with an error of 1%. Mixtures with mass percentage $w_{TPP} = 4\%, 10\%, 20\%, 30\%, 40\%, 50\%, 70\%$ and 90% of TPP were measured. Like in polymer plasticizer systems, we call TPP throughout this work the plasticizer or additive.

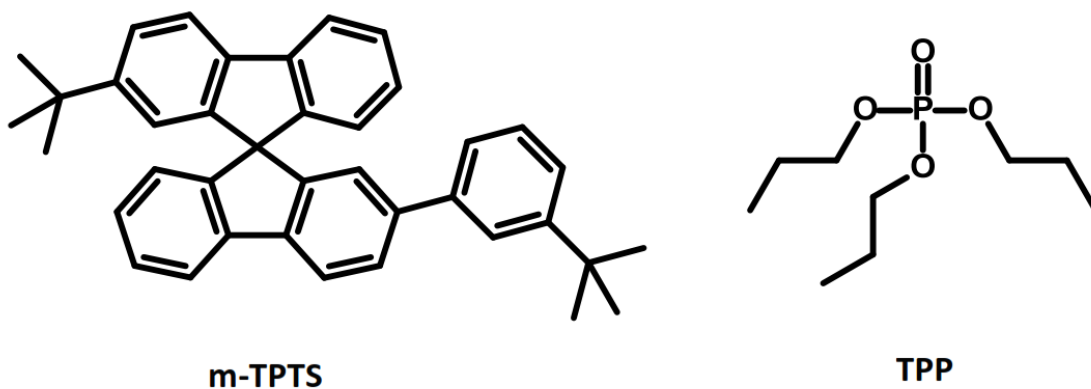


Figure 4.4.1: Chemical structures of of the high- T_g component m-TPTS and the low- T_g component tripropyl phosphate (TPP) used for the binary mixtures..

Differential scanning calorimetry (DSC) was performed at Mettler Laboratories in sealed Al-pans at a heating rate of 10 K/min. Sample preparation was according to the procedure established for DS measurements. In Fig. 4.4.2 DSC curves of the neat compounds and the mixtures $w_{TPP}=0.21, 0.37$ and 0.80 , scaled to a common baseline and comparable heights, are shown. In the mixtures, two steps are found. Corresponding T_g values are determined as onset of the observed step. The first step (1), coming from high temperatures, gets smaller and broader with increasing w_{TPP} , whereas the second one (2) decreases and broadens strongly with decreasing w_{TPP} . Therefore, the steps at low temperatures are attributed to the glass transition temperature of the α_2 -process (T_{g_2}), whereas the high temperature steps correspond to T_{g_1} . The concentration dependence of both T_g s is shown in Fig. 4.4.13 together with the DS results and will be discussed below. Such kind of DSC curves were already observed in previous investigations of binary glasses.^{22,23}

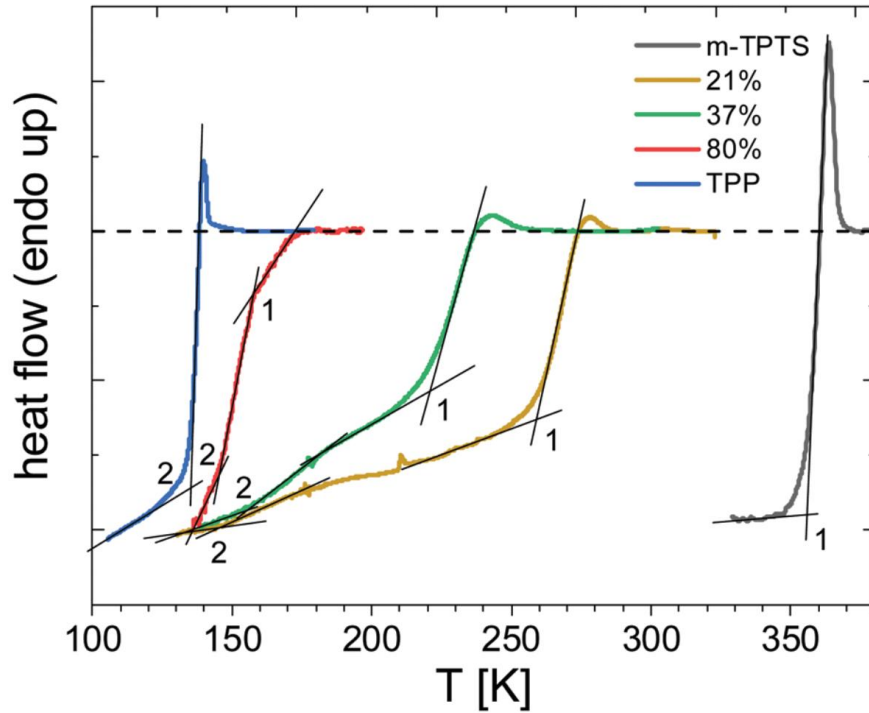


Figure 4.4.2: DSC measurements (colored lines) for the neat compounds *m*-TPTS (grey) and TPP (blue), as well as in the mixture with $w_{\text{TPP}} = 0.21$ (yellow), 0.37 (green) and 0.80 (red). All DSC measurements are scaled to a common baseline (dashed line) and comparable total heights. Lines indicate the crossing points determining the T_g s and the numbers denote the corresponding process (cf. Fig. 4.4.13).

4.4.3.2. Dielectric spectroscopy

The dielectric permittivity is described by the equation^{44,45}

$$\varepsilon^*(\omega) = \varepsilon'(\omega) - i\varepsilon''(\omega) = \varepsilon_\infty + \Delta\varepsilon \int_0^\infty -\frac{d\phi(t)}{dt} e^{-i\omega t} dt \quad (4.4.1)$$

where $\varepsilon^*(\omega)$ is the complex dielectric constant, $\omega = 2\pi\nu$ the angular frequency with ν being the frequency, ε_∞ the high frequency permittivity, and $\phi(t)$ the step-response function. The quantity of $\Delta\varepsilon$ denotes the relaxation strength which is linked to the molecular dipole moment.

The dielectric response of neat glass formers is often described either by a Cole-Davidson (CD) or Kohlrausch function.⁴⁴ In binary systems, however, these functions are no more applicable due to strongly varying peak shapes depending on concentration and temperature. Furthermore, at least in a certain concentration range, two relaxations α_1 (slow main relaxation) and α_2 (fast main relaxation) with different characteristic evolutions are found.^{22,24,35}

Therefore, we use the generalized Cole-Davidson relaxation function (GCD) introduced by Kahlau *et al.*,⁴⁶ to describe the α_1 -relaxation³⁴ and the widely used Havriliak–Negami relaxation function (HN) to describe the α_2 -relaxation.^{44,47} The step-response of the GCD can be numerically calculated along:

$$\phi_{GCD}(t) = \frac{\Gamma\left(\frac{b_{GCD}}{a_{GCD}}, \left(\frac{t}{\tau_{GCD}}\right)^a\right)}{\Gamma\left(\frac{b_{GCD}}{a_{GCD}}\right)} \quad (4.4.2)$$

This model function, which is used in terms of its Fourier Transform (cf. eq. (4.4.1)), consists of three parameters τ_{GCD} , defining the peak position, a_{GCD} giving a measure of the overall width of the peak and the high-frequency power law exponent b_{GCD} . The mean correlation time $\langle\tau_{GCD}\rangle$ of the GCD is well defined and a Debye like low-frequency behaviour ($\varepsilon'' \propto \omega^{-1}$) is granted.⁴⁶ The GCD includes also the cases of a Kohlrausch ($a = b$) and CD relaxation function ($a = 1$). The HN distribution, applied to describe the spectra associated with the low- T_g component, can be directly expressed as permittivity function:⁴⁴

$$\varepsilon^*(\omega) = \varepsilon_\infty + \frac{\Delta\varepsilon_{HN}}{(1 + (i\omega\tau_{HN})^{a_{HN}})^{b_{HN}}} \quad (4.4.3)$$

with the dielectric loss $\varepsilon''_{HN} = \Delta\varepsilon_{HN} \cdot \chi''_{HN}$:

$$\chi''_{HN}(\omega) = \frac{\sin(b_{HN}\phi)}{\left(1 + 2(\omega\tau_{HN})^{a_{HN}} \cos\left(\frac{\pi a_{HN}}{2}\right) + (\omega\tau_{HN})^{2(a_{HN})}\right)^{\frac{b_{HN}}{2}}} \quad (4.4.4)$$

$$\phi = \arctan\left(\frac{(\omega\tau_{HN})^{a_{HN}} \sin\left(\frac{\pi a_{HN}}{2}\right)}{1 + (\omega\tau_{HN})^{a_{HN}} \cos\left(\frac{\pi a_{HN}}{2}\right)}\right)$$

τ_{HN} is the characteristic relaxation time, a_{HN} the low-frequency limit power law exponent and $c_{HN} = a_{HN}b_{HN}$ the high-frequency power law exponent. No mean time constant can be defined because the integral over the corresponding relaxation function $\phi_{HN}(t)$ is not finite. The most probable time constant, which reflects the relaxation peak can be determined by peak-picking or from the fit parameters.^{44,47}

From a purely phenomenological point, one can safely state that the liquid-like dynamics of the low- T_g component is governed by a broad distribution of correlation times with essentially

two cut-offs τ_{α_2} and τ_{α_1} , which allow to define two T_g values, T_{g_1} and T_{g_2} . In between these limits the dynamics spans over a large time window, in particular at low additive concentrations.

Due to this fact and the problem, that the HN function does not display the correct low-frequency behaviour $\varepsilon'' \propto \omega^1$, we introduced a cut-off function. We calculated the pulse response function $\varphi_{HN} = -d\phi_{HN}(t)/dt$ of a HN relaxation function via numerical FT (applying some kind of Filon algorithm)⁴⁸ of χ''_{HN} and derivation. Then, we multiplied φ_{HN} with an exponential cut-off (τ_C), which is defined by the longest time constant in our system, the average time constant of the α_1 -relaxation ($\tau_C = \langle \tau_{\alpha_1} \rangle$).

$$\varphi_{HNC}(t) = \varphi_{HN}(t) \cdot \exp\left(-\frac{t}{\tau_C}\right) \quad (4.4.5)$$

The corresponding step-response function $\phi_{HNC}(t)$ is derived via numerical integration and normalization ($\phi_{HNC}(t=0) = 1$). Via FT we finally received our HN relaxation function with cut-off (HNC). This leads to a low-frequency power law with exponent a_{HNC} and a ω^1 behaviour at lowest frequencies. Whenever both relaxations α_1 and α_2 are observed in the dielectric spectra, we use an additive ansatz to describe the dielectric loss as combination of the GCD and HNC relaxation function:

$$\varepsilon''(\omega) = \Delta\varepsilon_{GCD} \cdot \chi''_{GCD}(\omega) + \Delta\varepsilon_{HNC} \cdot \chi''_{HNC}(\omega) \quad (4.4.6)$$

which we subsequently call "composite fit". If only one process is in the measurement window, we use either GCD or HN. In Fig. 4.4.3, we give some examples of the GCD (blue dashed lines) and the HNC function (red dashed lines, $\tau_C = \langle \tau_{GCD} \rangle$) and its superposition (composite fit, black lines) as it will be applied to interpolate the measured dielectric spectra of the mixtures.

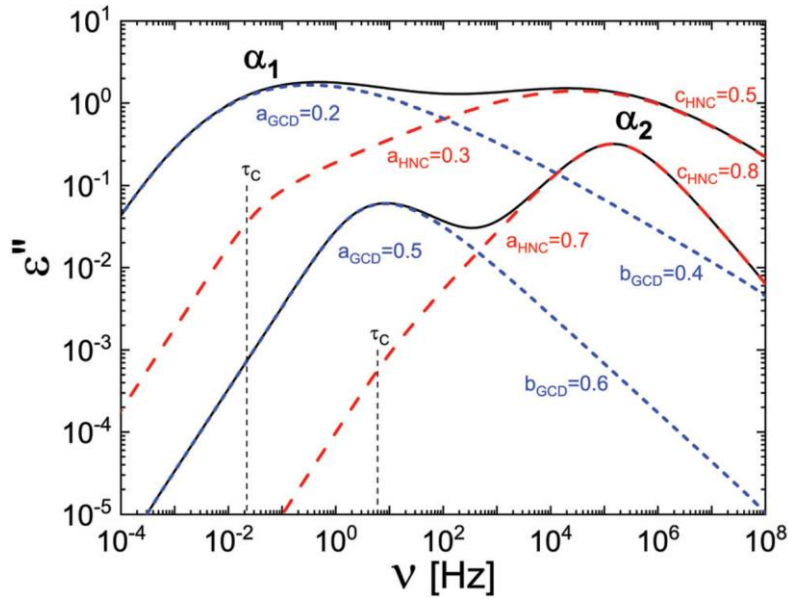


Figure 4.4.3: Calculated dielectric loss spectra for two sets of parameters ($\Delta\varepsilon_{GCD} = \Delta\varepsilon_{HNC}$ and $\Delta\varepsilon_{GCD} = 0.5 \cdot \Delta\varepsilon_{HNC}$, $\tau_{GCD} = 0.01s$, $\tau_{HNC} = 1 \cdot 10^{-6}s$). Blue dashed lines are GCD functions, red dashed lines are HNC functions with cut-off $\tau_c = \langle\tau_{GCD}\rangle$, and the black lines are the corresponding composite functions.

To get comparable time constants τ for both relaxations, we can only use the most probable time constant defined by the peak position via “peak-picking” ($\omega_p = 2\pi\nu_p = 1/\tau$).

Especially in systems with a high DC conductivity, relevant spectral contributions are often hidden under and sometimes even not visible after subtracting the DC conductivity contribution ($DC \propto \omega^{-1}$). Therefore, Wübbenhorst et. al.⁴⁹ introduced an Ohmic-conduction-free dielectric loss representation ($\partial\varepsilon'$) from the real part of the dielectric susceptibility ε' :

$$\partial\varepsilon' \equiv -\frac{\pi}{2} \frac{\partial\varepsilon'(\omega)}{\partial \ln \omega} \quad (4.4.7)$$

This representation results in peaks at the same peak position but somewhat different spectral shape. The exact used procedure and further details are described elsewhere.⁴⁹⁻⁵¹ Hence more subtle features can be resolved in $\partial\varepsilon'$ compared to ε'' . One has to mention, that for a complete description of $\partial\varepsilon'$, the corresponding interpolations must be calculated the same way (eq. (4.4.7)).

Dielectric measurements were carried out with an Alpha-A Analyzer from Novocontrol in the frequency range $\nu = 10^{-2} - 10^6$ Hz. Temperature was kept constant within ± 0.2 K by using a Quattro-H temperature controller from Novocontrol yielding an absolute accuracy better

than ± 0.2 K. Applied temperatures ranged from 100 up to 400 K. The completely sealed sample cell was adapted to a design assuring a constant sample volume.⁵²

4.4.4. Results

4.4.4.1. Pure components

Fig. 4.4.4 shows the dielectric spectra of the neat components TPP (black squares) and m-TPTS (black triangles) at selected temperatures. For both compounds the α -relaxation is observed which shifts to higher frequencies with increasing temperature. For TPP, a pronounced β -relaxation persisting below T_g is observed at high frequencies which was analysed earlier.^{37,53} For m-TPTS, no β -relaxation is observed, however, the high-frequency flank is made up of a crossover from one power-law behaviour to a second with a lower exponent, reflecting the so-called excess wing.^{2,5,54} The relaxation strength at $T \approx 1.02 T_g$ of m-TPTS ($\Delta\epsilon_{m-TPTS} \approx 0.1$) is about a factor of 240 smaller than that of TPP ($\Delta\epsilon_{TPP} \approx 24$), reflecting the non-polar nature of the hydrocarbon m-TPTS. Thus, DS predominately probes TPP in the present mixtures except for lowest TPP concentrations. For m-TPTS, no crystallization behaviour is observed, whereas crystallization may occur above 156 K for TPP.

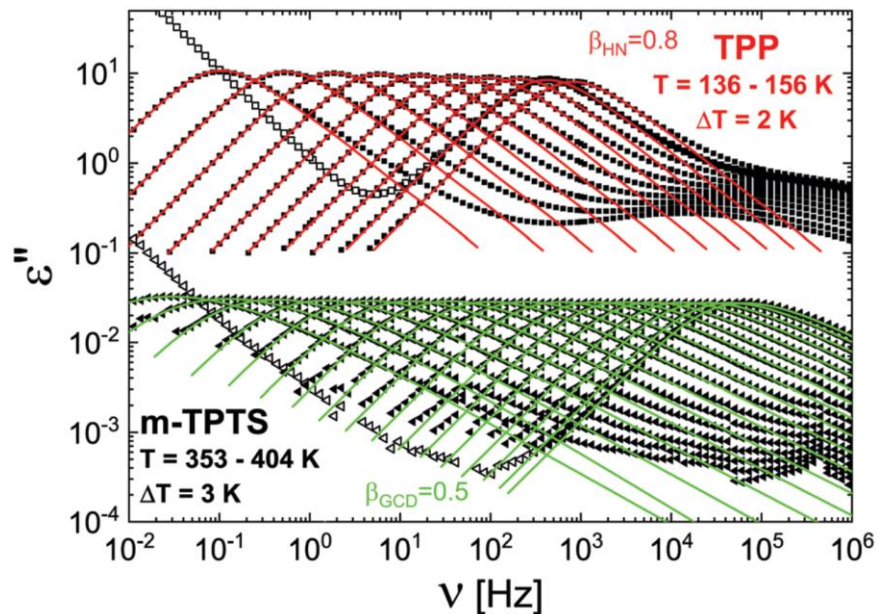


Figure 4.4.4: Selected dielectric spectra ϵ'' of neat TPP (squares) and neat m-TPTS (triangles). DC conductivity is shown only for one temperature for each system (open symbols) and subtracted for TPP. Fits by a HN function $\beta_{HN} = \beta_{CD} = 0.80$ are shown as red lines (parameters cf. Fig. 4.4.6) GCD fits as green lines (parameters cf. Fig. 4.4.9).

The TPP relaxation spectra are interpolated by a HN function (cf. eq. (4.4.5)) yielding $a_{HN} = 1$ and $b_{HN} = 0.80$ (red lines), which corresponds to a simple CD function. We disregard the contribution of the β -relaxation in the present context focusing on the two main relaxations. In the case of *m*-TPTS we apply a GCD function (green lines) with $b_{GCD} = 0.5$ and $a_{GCD}(T)$, changing slightly with temperature (cf. Fig 4.4.8). showing a spectral shape close to a Kohlrausch function. The resulting T_g value defined by $\tau(T_g) = 100$ s for *m*-TPTS is 350 K, that of TPP is $T_g = 134$ K, as reported prior.^{37,41}

4.4.4.2. High additive (TPP) concentrations ($w_{TPP} = 0.90$ and 0.70)

Mixtures with a strongly varying concentration of TPP in *m*-TPTS were measured. Starting with high TPP concentrations, Fig. 4.4.5(a) shows the dielectric spectra of $w_{TPP} = 0.90$ (black squares) and for comparison that of neat TPP at single temperature (green diamonds). The DC conductivity was subtracted; for $T = 162$ K, the original spectrum is shown (open squares). The HN fits of the relaxation spectra are shown as red lines.

As expected, the signal amplitude of the mixture is lower than that of neat TPP. Due to the anti-plasticizer effect, the spectra are shifted to lower frequencies. Furthermore, a strongly temperature dependant broadening on the low-frequency flank is observed, while the high-frequency is just slightly broader. Thus, FTS does not apply any longer in the mixture. Clearly, the spectra in Fig. 4.4.5(a) reflect the relaxation of the polar additive TPP and we denote it the α_2 -relaxation. The appearance of the β -process remains essentially the same but will be addressed later on separately (cf. section β -process).

As discussed in the Experimental section, our phenomenological approach assumes that the spectral contribution of the low- T_g additive stretches between the two cut-offs τ_{α_2} and τ_{α_1} , yet, the latter limit does not show up at high additive concentrations. Thus, we are left with an interpolation by a simple HN distribution which considers the additional broadening of the spectra at low frequencies. The corresponding parameters $a_{HN}(T)$ and c_{HN} are shown in Fig. 4.4.6. Whereas the high-frequency parameter $c_{HN} = 0.74$ is virtually temperature-independent and only slightly smaller compared to pure TPP ($c_{HN} = 0.8$), the low-frequency exponent $a_{HN}(T)$ decreases strongly from 0.81 to 0.52 with lowering temperature. Given the strong temperature dependence of $a_{HN}(T)$, one may speculate that at highest temperatures the CD limit $a_{HN} = 1$ is reached and the spectral form approaches that of neat TPP. Similar

features are observed for $w_{TPP} = 0.70$ (cf. Appendix Fig. 4.4.17). The FTS violation is even stronger with a_{HN} decreasing from 0.55 to 0.25 with decreasing temperature and a high frequency exponent of $c_{HN} = 0.65$.

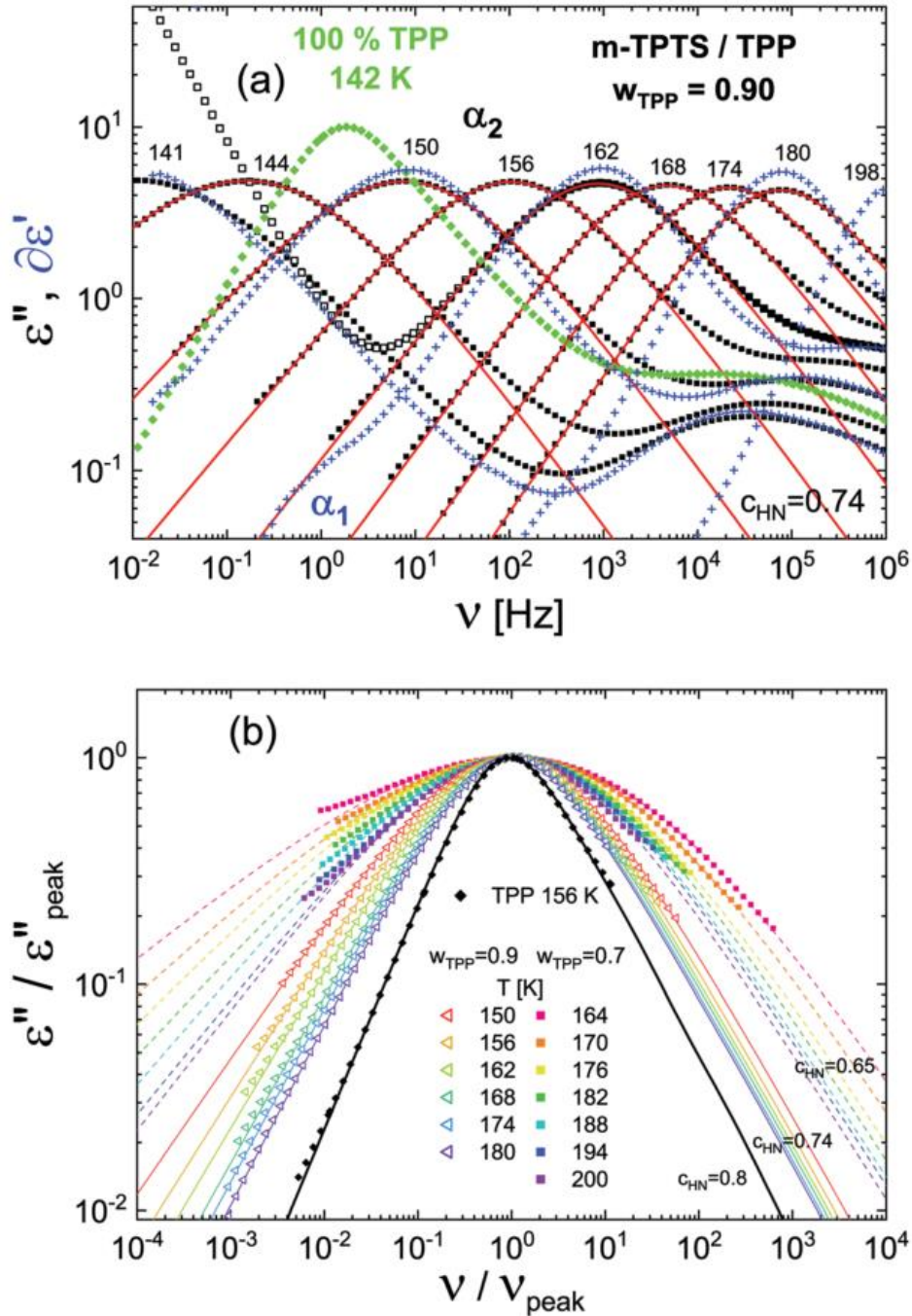


Figure 4.4.5: (a) Dielectric spectra ϵ'' of the mixture $w_{TPP} = 0.90$ (black squares, HN fits as red lines) and for comparison a spectrum of neat TPP (green diamonds). DC conductivity contribution is subtracted. For selected temperatures, derivative data $\partial\epsilon'$ (blue crosses) are shown. An additional relaxation contribution is recognized at lowest intensities (α_1), which cannot be resolved in ϵ'' . (b) Rescaled curves of $w_{TPP} = 0.90$ (open triangles) and 0.70 (squares) scaled on the peak position and amplitude for selected temperatures in comparison to neat TPP. β -relaxation and DC contributions are suppressed.

This is further demonstrated in Fig. 4.4.5(b) where selected spectra measured at different temperatures are scaled to the peak position and amplitude for the two mixtures $w_{TPP} = 0.90$ (open triangles, lines), 0.70 (squares, dashed lines) and compared to that of neat TPP (black diamonds). For both concentrations, the spectra clearly broaden with decreasing temperature mainly on the low-frequency flank but even the spectrum at highest temperature is significantly broader than that of neat TPP. The actual small changes in the high-frequency exponent c_{HN} are indicated. Evidently, the overall width drastically increases with decreasing TPP content.

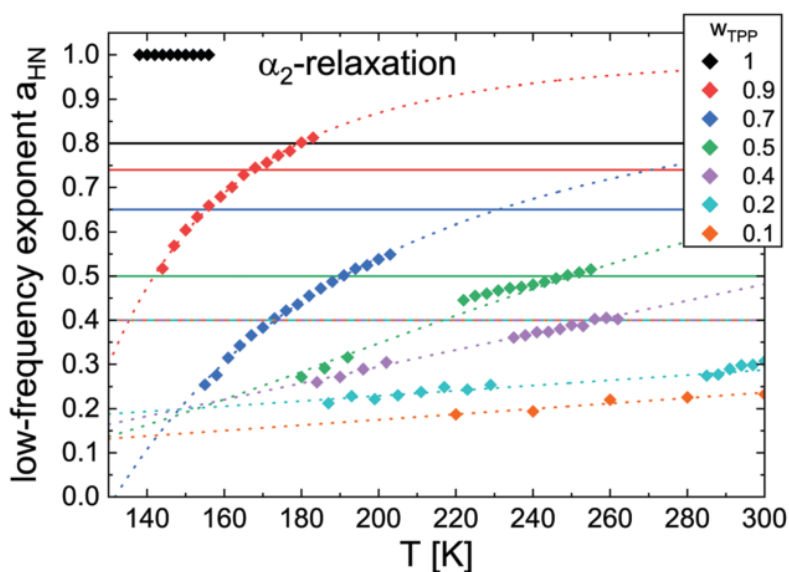


Figure 4.4.6: HN(C) fit parameters of the spectral analysis regarding the α_2 -relaxation. Low-frequency exponent $a_{HN(C)}$ as diamonds and constant high-frequency exponent $c_{HN(C)}$, determined at lowest temperatures, as solid lines. For $w_{TPP} \leq 0.4$, $c_{HN(C)}$ was kept constant at 0.4. Colour specifies the concentration and dotted lines are guides for the eye.

One of the challenges during the data analysis of $w_{TPP} = 0.70$ was the strong not addressable DC conductivity contribution. In order overcome this problem and to get a better resolution at low frequencies, where even subtracting the DC conductivity may still obscure some relaxation features, we took recourse to the derivative method $\partial \epsilon'$ outlined in the experimental section (eq. (4.4.7)). Indeed, one recognizes already for $w_{TPP} = 0.90$ a very weak shoulder at $T \leq 180$ K (blue crosses, Fig 4.4.5 (a)) which probably originates from a relaxation associated with the high- T_g component (a_1). However, a full quantitative analysis is not possible. Therefore, we estimate only the time constants τ_{α_1} via peak picking after subtracting the low-frequency power law behaviour of the a_2 -relaxation, as given by $\partial \epsilon'$. In the case of $w_{TPP} = 0.70$ (blue crosses, Appendix Fig. 4.4.17), the low-frequency contribution

is much larger, but still we refrain from quantitatively singling out this relaxation feature and determine only the time constants again *via* peak picking. All time constants determined for $w_{TPP} = 0.90$ and 0.70 are shown in Fig. 4.4.12 and will be discussed in the context of the results of all mixtures.

4.4.4.3. Low additive (TPP) concentrations - $w_{TPP} = 0.04$ and 0.10

Turning to the other end of the concentration range, in Fig. 4.4.7 the dielectric spectra of $w_{TPP} = 0.10$ are shown. The DC conductivity was subtracted, but original data is shown for $T = 390$ K (open diamonds). Clearly, now two separate relaxations can be identified, which we attribute to the α_1 -process (black squares, high temperatures) and the α_2 -process (open triangles, low temperatures). Additionally, at even lower temperatures, a β -relaxation is observed, but omitted for clarity and will be discussed separately. For selected temperatures, the derivative relaxation data $\partial\epsilon'$ is added (blue crosses), which is only slightly sharper as expected for broad peaks.⁴⁹

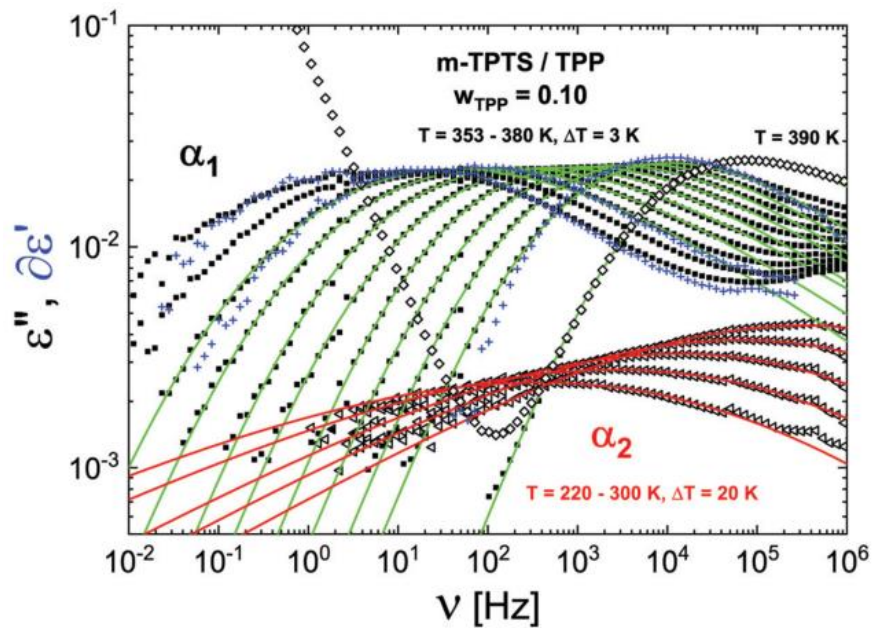


Figure 4.4.7: Dielectric spectra ϵ'' of the mixture $w_{TPP} = 0.10$ displaying two relaxations α_1 (squares) and α_2 (open triangles). DC conductivity contribution is subtracted; original data is shown for $T=390$ K (open diamonds). Temperatures are indicated. Green lines are GCD fits, red lines are HN fits. Fit parameters are included in Fig 4.4.6, Fig. 4.4.8, and Fig. 4.4.11. For selected temperatures, the derivative data $\partial\epsilon'$ is shown (blue crosses).

In contrast to the high-TPP concentration mixtures, the dominating α_1 -relaxation is associated with the high- T_g component whereas the α_2 -relaxation again with the additive component. We note that although the polarity of neat TPP is by a factor of about 240 larger than that of

m -TPTS, the amplitude of the corresponding a_2 -relaxation is significantly smaller; yet, it is extremely broad. Below we will consider the relaxation strength in detail (cf. Fig. 4.4.11). The a_1 -relaxation exhibits significant overall broadening, especially on the high-frequency flank, which increases with decreasing temperature. Thus, also for the high- T_g component FTS is violated. At low-frequencies, the expected ω^1 behaviour can be identified as expected for the slowest process of a liquid. Similar results are found for $w_{TPP} = 0.04$, which is shown in the Appendix (Fig. 4.4.18). Therefore, the spectral analysis will be discussed in the following for both concentrations.

To quantify the described relaxation features, the a_1 -relaxation is interpolated by a GCD function (green lines in Fig. 4.4.7 and Fig. 4.4.18), and the corresponding $a_{GCD}(T)$ and $b_{GCD}(T)$ are included in Fig. 4.4.8(a). We remind, that the GCD function always displays a Debye-behaviour ($\sim\omega^1$) at low frequencies, the high-frequency exponent is given by b_{GCD} and a_{GCD} specifies the overall width. In the mixtures, in addition to a_{GCD} , also b_{GCD} shows a significant temperature dependence and gets overall smaller with increasing w_{TPP} . In the case of $w_{TPP} = 0.10$ even a broad GCD function is unable to interpolate the broadest spectra at the two lowest temperatures ($T = 353K, 356K$), possibly indicating even a bimodal structure.

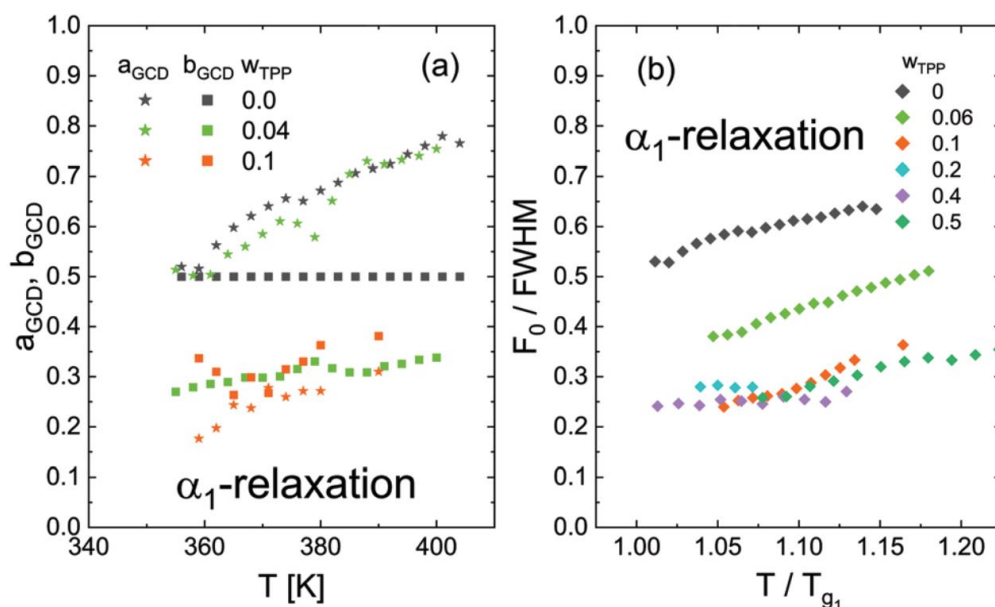


Figure 4.4.8: (a) Parameter of the GCD function interpolating α_1 -relaxation for the lowest concentrations as function of temperature. Peak width parameter a_{GCD} (stars) and b_{GCD} (diamonds). The concentration is colour coded. (b) Inverse logarithmic FWHM of the α_1 -process as function of the reduced temperature (T/T_{g_1}), normalized by the FWHM of a Debye function (F_0). The used DS glass transition temperatures are shown in Fig. 4.4.13.

As the parameters in Fig. 4.4.8(a) exhibit some scatter and it is difficult to fully grab the temperature evolution of the spectra, for convenience, we plot in Fig. 8(b) their inverse logarithmic half width ($1/FWHM$) in relation to that of a Debye function ($F_0 = 1.14$). Clearly, the spectra associated with the high- T_g component become broader with increasing w_{TPP} and exhibit a strong temperature dependence which is very similar when plotted on the reduced temperature scale T/T_{g1} . We added only up to 10% of TPP and already get α_1 -relaxation spectra by almost a factor of 3 broader compared to those of neat m -TPTS. Additionally, one has to discern, that the relaxation strength $\Delta\varepsilon_{\alpha_1}$ grows for increasing additive content w_{TPP} (cf. Fig. 4.4.11(b)) in contrast to a simple ideal mixing prospect.

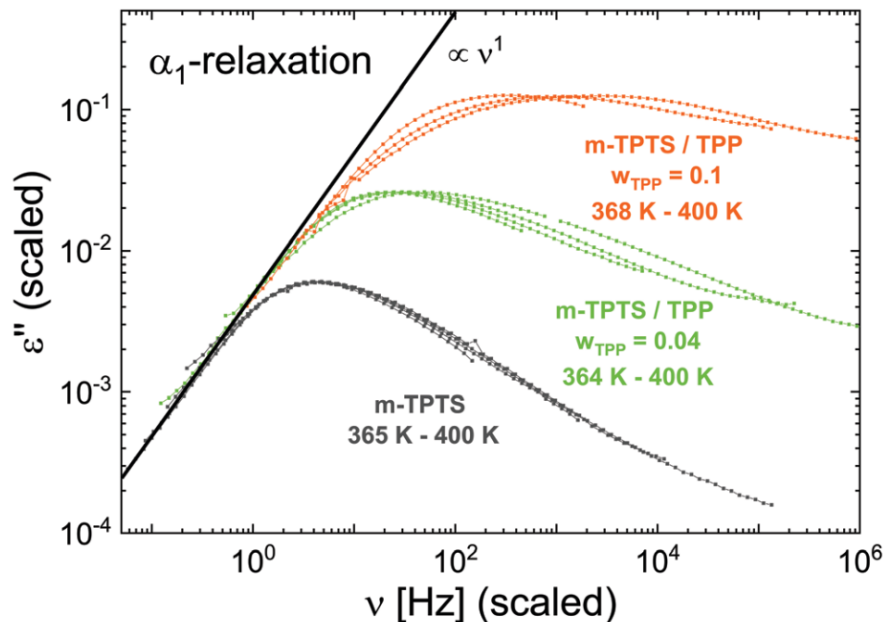


Figure 4.4.9: Master curves of the α_1 -relaxation, scaled to the low-frequency flank ($\propto \nu^1$), of neat m -TPTS (black) and mixtures with $w_{TPP} = 0.04$ (green) and 0.10 (orange), respectively. The mixture data is shifted in height for better visualization.

The described results can directly be observed, recasting the low w_{TPP} data in Fig. 4.4.9, scaled to provide the common low-frequency behavior $\varepsilon''(\omega) \sim \omega^1$. The temperature dependent spectral broadening in particular on the high-frequency flank compared to neat m -TPTS is obvious – a different behaviour compared to that of the spectra of TPP in the mixture (α_2 -relaxation) - and hence FTS fails, as said.

The α_2 -relaxation in Fig. 4.4.7 (open triangles) appears as a very broad relaxation with a very low amplitude, well separated from the α_1 -relaxation. In other words, an extremely broad distribution of relaxation times $G(\ln \tau_{\alpha_2})$ in the limit of low additive concentrations is found.

The spectra of $w_{TPP} = 0.10$ are fitted by simple HN functions (red lines), the corresponding parameters are included in Fig. 4.4.6. Extremely low values of the low-frequency exponent $a_{HN}(T)$ are found and FTS fails again. In the case of $w_{TPP} = 0.04$, the signal almost disappears in the background noise (cf. Appendix Fig. 4.4.18) and therefore we refrained from fitting the spectra and determined only the time constants *via* peak-picking (cf. Fig. 4.4.12).

4.4.4.4. Intermediate additive (TPP) concentrations ($w_{TPP} = 0.20, 0.40$ and 0.50)

We now focus on intermediate concentrations including the samples with $w_{TPP} = 0.20, 0.40$ and 0.50 . Fig. 4.4.10(a) – (c) show the corresponding dielectric spectra after subtraction of the DC conductivity. In all cases, two main relaxations can clearly be observed in a single spectrum, i.e., at high frequencies the α_2 -relaxation is recognized whereas at low frequencies the α_1 -relaxation is found. The relative intensity of the α_1 -relaxation to that of the α_2 -relaxation decreases from almost similar to much smaller with increasing w_{TPP} . Thereby, also the time constants of both processes come closer with increasing TPP concentration. Furthermore, the ratio of the amplitudes α_1/α_2 is strongly temperature dependent, decreasing with increasing temperature for all concentrations. As in the limiting cases discussed above, the α_2 -relaxation broadens on the low-frequency flank, whereas α_1 -relaxation mainly on the high-frequency flank. Again, as expected for the slowest relaxation of a liquid, its low-frequency flank still follows the relation $\varepsilon''(\omega) \propto \omega^1$.

As in all cases both α -relaxations overlap more or less strongly, we apply a composite fit (yellow lines) composed by a sum of a HN function (α_2 -relaxation) with a cut-off (HNC) at $\langle\tau_{\alpha_1}\rangle$ and a GCD function (α_1 -relaxation) – see eq. (4.4.6). Starting with $w_{TPP} = 0.20$ (Fig. 4.4.10(a), the high-temperature data (black squares) are well described. The low-temperature spectra (open triangles) displaying solely the α_2 -relaxation are interpolated by a simple HN-function (red lines). Here again, the low-frequency temperature dependent broadening is recognized. Analogous fits have been carried out for the other two concentrations (Fig. 4.4.10(b) and (c)). All shape parameters of the α_2 -relaxation are included in Fig. 4.4.6, showing that the overall stretching increases with decreasing w_{TPP} while the almost linear temperature dependence gets weaker. The FWHM of the α_1 -relaxation is added in Fig. 4.4.8(b), indicating some kind of

saturation in the overall width for $w_{TPP} \geq 0.10$ and similar temperature dependence for all concentrations on the reduced scale T/T_g .

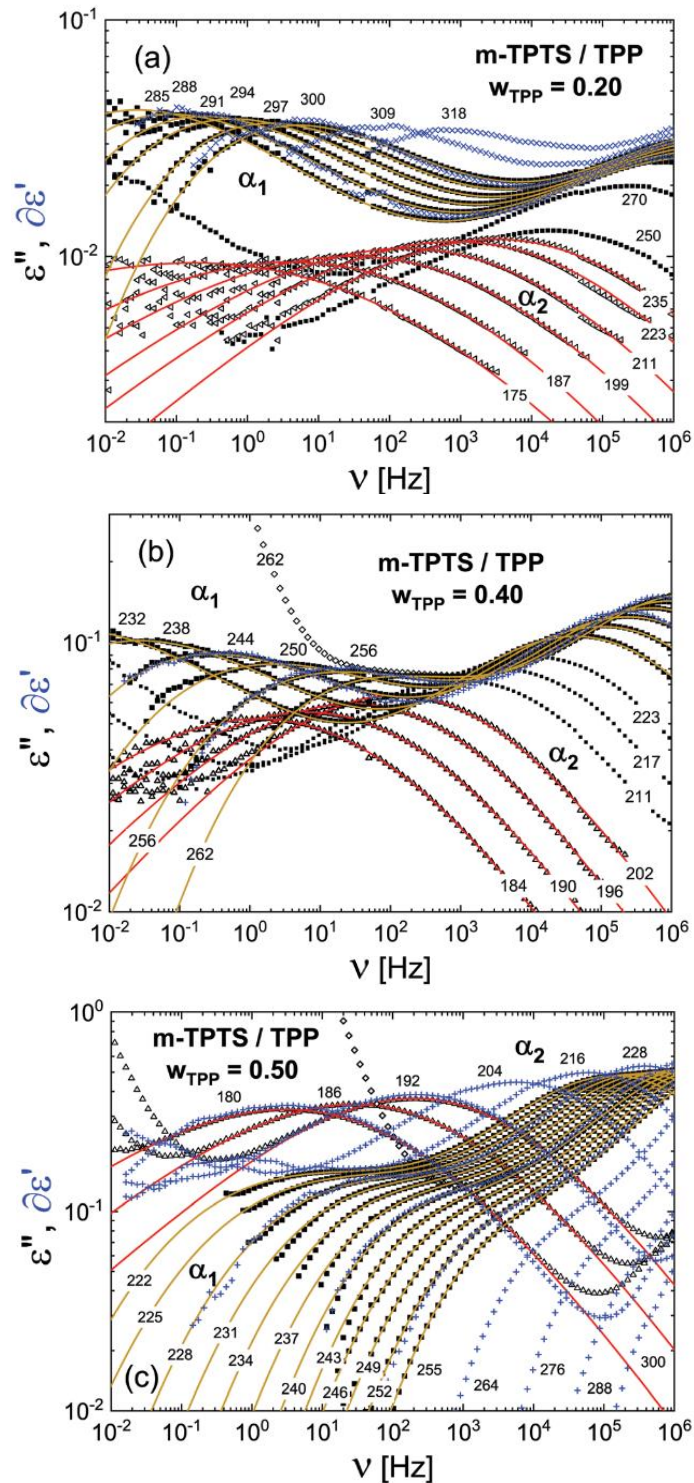


Figure 4.4.10: Dielectric spectra ϵ'' of (a) $w_{TPP} = 0.20$, (b) 0.40, and (c) 0.50 (squares). DC conductivity contribution is subtracted (if possible). Original data is shown for one temperature (open diamonds). Temperatures in K are given. Yellow lines denote composite fits, red lines are HN fits to α_2 (open triangles). Fit parameters are included in Fig. 4.4.6, Fig.4.4. 8 and Fig. 4.4.11. For selected temperatures, the derivative data $\partial\epsilon'$ is shown (blue crosses).

Additionally, derivative data $\partial\varepsilon'$ (blue crosses) are included in Fig. 4.4.10, showing perfect agreement with ε'' and providing further insight for higher temperatures, once a composite fit is no more possible due to the α_2 -relaxation leaving the measurement window. In particular, the $w_{TPP} = 0.50$ sample provides the best glimpse into the temperature dependence of the two sub-spectra in the mixture. The relatively weak α_1 -relaxation decreases in amplitude up to the highest temperature measured and becomes less and less separated from the α_2 -relaxation, which itself increases in amplitude with temperature. One could speculate that the α_1 -relaxation could even disappear at highest temperatures.³¹ But still, the ω^1 behaviour respectively the introduced cut off at the low frequencies of the slowest process (α_1) can prominently be observed in the derivative data $\partial\varepsilon'$. Another feature is important to be mentioned: Although the sample contains only 50 – 80% of the weakly polar high- T_g component, the α_1 -relaxation strength is much higher than that of the neat m-TPTS.

Next, we consider quantitatively the relaxation strength $\Delta\varepsilon$ of the two main relaxations as revealed by our analysis for all investigated concentrations, corrected for the Curie Law ($\Delta\varepsilon(w_{TPP}, T) \cdot T$), in Fig. 4.4.11(a). As the relaxation strengths become much smaller than expected from a linear concentration dependence, we plotted the data on a semi-log scale. Starting at high $w_{TPP} \geq 0.70$, the total relaxation strength $\Delta\varepsilon$ is determined purely by the relaxation strength $\Delta\varepsilon_{\alpha_2}$ (open circles) of TPP (cf. Fig. 4.4.5 and Fig. 4.4.17), showing only a slight deviation from a Curie temperature behaviour with a tendency to become stronger towards pure TPP. For $w_{TPP} < 0.70$, essentially a Curie law applies for $\Delta\varepsilon$ (squares). For intermediate concentrations $w_{TPP} = 0.20$ up to 0.50, $\Delta\varepsilon$ is composed of strongly temperature dependent relaxation strengths $\Delta\varepsilon_{\alpha_1}$ and $\Delta\varepsilon_{\alpha_2}$. Thereby $\Delta\varepsilon_{\alpha_1}(T)$ (crosses) decreases with increasing temperature. On the other hand, $\Delta\varepsilon_{\alpha_2}(T)$ (open circles) shows an opposite effect. In the case of $w_{TPP} = 0.20$ and 0.40, the two relaxations exhibit similar strengths ($\Delta\varepsilon_{\alpha_1}(T)$ crosses $\Delta\varepsilon_{\alpha_2}(T)$) although the relaxation strength of the neat components differ by a factor of 240.

Correspondingly, at lowest $w_{TPP} \leq 0.10$, the relaxation strength $\Delta\varepsilon_{\alpha_1}$, which is associated with the high- T_g component, shows an enhanced relaxation strength, with a slight negative temperature dependence, compared to neat m-TPTS. In contrast, $\Delta\varepsilon_{\alpha_2}(T)$ shows a very small absolute value for $w_{TPP} = 0.10$ (orange circles), but is growing with temperature. Assuming this temperature dependence to hold up to highest temperatures (dashed orange line), one

receives for the total relaxation strength $\Delta\varepsilon$ again a constant value (orange open squares) at temperatures, where $\Delta\varepsilon_{\alpha_1}$ was analyzed.

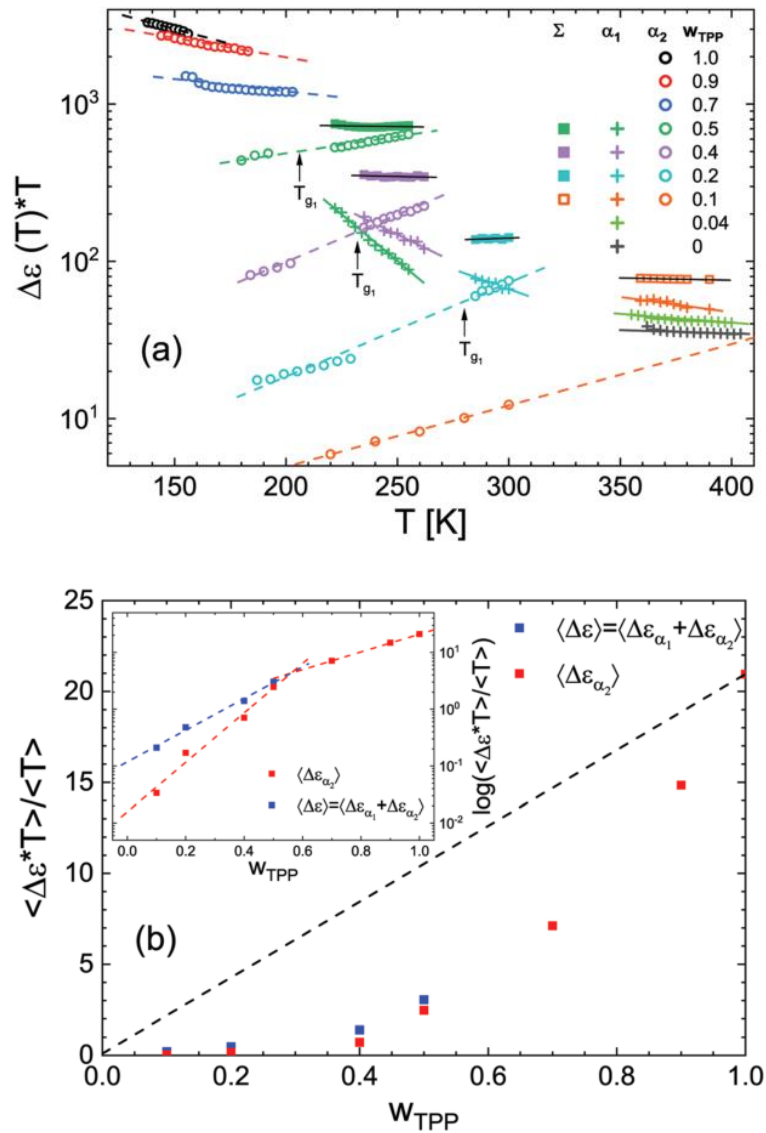


Figure 4.4.11: (a) Curie corrected relaxation strength $\Delta\varepsilon(w_{TPP}) \cdot T$ for α_1 (plusses), α_2 (circles) and the sum of both (squares) on a logarithmic scale. The gap in between of one concentration is due to the used composite fit at high T and HN fit at low T . In between, no appropriate fit was possible. Lines are guides for the eye. For $w_{TPP} = 0.10$, $\Delta\varepsilon_{\alpha_2}$ was linearly approximated (dashed orange line) and used to calculate the total $\Delta\varepsilon$ (orange open squares). (b) Temperature averaged relaxation strength $\langle \Delta\varepsilon(w_{TPP}) \cdot T \rangle / \langle T \rangle$ for the α_2 -relaxation (red squares) and the overall relaxation $\Delta\varepsilon$ (blue squares). Dashed line shows the expected behavior for ideal mixing. Inset: Logarithmic y-axis with lines as guide for the eye.

To get an overview of the concentration dependence of $\Delta\varepsilon(w_{TPP})$, the mean relaxation strength after Curie correction ($\langle \Delta\varepsilon(w_{TPP}, T) \cdot T \rangle / \langle T \rangle$) is displayed in Fig. 4.4.11(b). As the contribution of the α_1 -relaxation can be ignored at $w_{TPP} \geq 0.70$, the relaxation strength $\Delta\varepsilon_{\alpha_2}$ (red squares) represents essentially the total $\Delta\varepsilon$, as said. Only at $w_{TPP} \leq 0.50$ the total strength $\Delta\varepsilon$ (blue squares) is larger than that of $\Delta\varepsilon_{\alpha_2}$. Importantly, the concentration

dependence strongly deviates from a linear dependence expected for ideal mixing (dashed line). For example, adding only 30% of the high- T_g component reduces $\Delta\varepsilon_{\alpha_2}$ by a factor of about 4. A linear concentration dependence is actually observed for the β -relaxation (see Fig. 4.4.15). Once again, we emphasize that this strongly anomalous behaviour is not caused by filling factors lower than one as special care has been taken to assure complete filling. A similar finding was reported for a polymeric mixture before.²⁸ The inset of Fig. 4.4.11(b) shows the dependence on logarithmic scales, revealing two “branches” of exponential concentration dependence above and below $w_{TPP} > 0.50$. From the strongly non-ideal concentration dependence of $\Delta\varepsilon_{\alpha_1}(T)$ and $\Delta\varepsilon_{\alpha_2}(T)$, severe doubts appear interpreting such behaviour as changes in molecular populations – as done before (cf. also Discussion).^{22,23,31}

4.4.4.5. Time constants and T_g

Fig. 4.4.12 shows the most probable time constants as determined by “peak-picking” for the main relaxations showing a distinguishable peak from dielectric loss data $\varepsilon''(\omega)$ (τ_{α_1} : filled circles, τ_{α_2} : open diamonds) and derivative data $\partial\varepsilon'$ (τ_{α_1} : pluses, τ_{α_2} : crosses). Additionally, to settle the high temperature behaviour, NMR time constants from T_1 relaxation data are added (τ_{α_1} : stars, τ_{α_2} : open stars).⁴³

The trend as observed in the spectra is confirmed in the time constants: With low TPP concentrations, both processes are far apart and cannot be seen in a single spectrum due to the frequency window of the DS analyser. Upon mixing, both processes approach each other until they can be both detected in a single spectrum for concentrations $w_{TPP} \geq 0.20$. Specifically, at $w_{TPP} \geq 0.50$, the α_1 -relaxation times τ_{α_1} (pluses) are all determined from the derivative relaxation data $\partial\varepsilon'$, due to its strongly enhanced sensitivity – for the first time up to highest concentrations (compared to previous work^{22,24}) The corresponding time constants τ_{α_2} from this method (crosses) perfectly match them from ε'' (open diamonds). A non-Arrhenius temperature behaviour is generally observed for the α_1 -process. The corresponding $T(\tau_{\alpha_1} = 100 \text{ s}) = T_{g1}$ values are displayed in Fig. 4.4.13. A continuous decrease with increasing TPP content is observed, a behaviour well documented for many mixed systems (plasticizer effect).

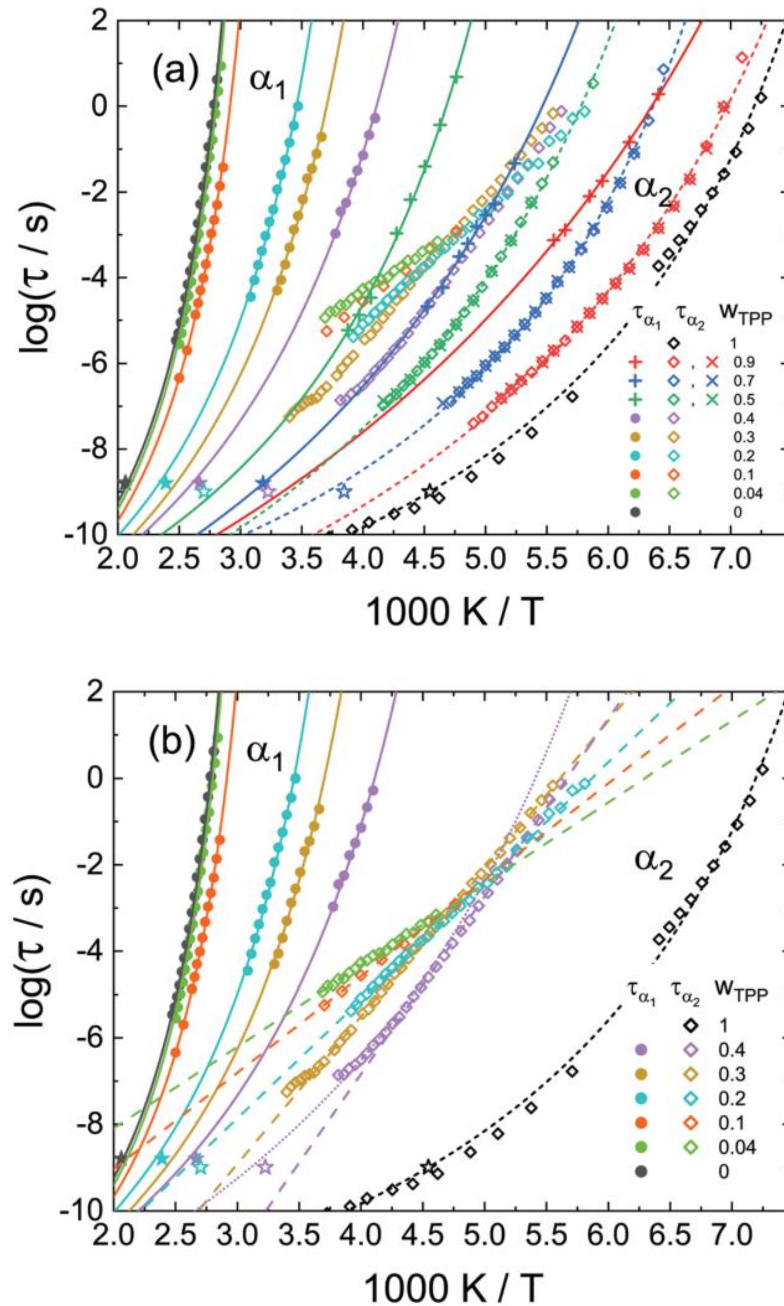


Figure 4.4.12: Time constants τ from peak picking for the α_1 - (circles, pluses, stars) and the α_2 -process (open diamonds, crosses, open stars). Concentration is colour coded. For $c_{\text{TPP}} = 0.9, 0.7$ and 0.5 , the time constants (pluses and crosses) are determined from $\partial \epsilon'$. Stars are from NMR relaxation.⁴³ (a) Non-Arrhenius temperature dependence is shown as lines (α_1) and dashed lines (α_2). (b) Selected time constants from (a) in the concentration range with Arrhenius temperature dependence of τ_{α_2} . Neat components for comparison.

For the α_2 -process, a non-Arrhenius behaviour is observed for neat TPP and binary mixtures of down to $w_{\text{TPP}} = 0.50$ (Fig. 4.4.12(a)). For lower concentrations $w_{\text{TPP}} \leq 0.40$, an Arrhenius temperature dependence is observed (Fig. 4.4.12(b)). For decreasing TPP concentrations the apparent activation energy of this process decreases. As confirmed by NMR,⁴³ the α_2 -process reflects an isotropic reorientation of the TPP molecules and thus one can define a second glass

transition temperature, T_{g_2} by extrapolating to $\tau(T_g) = 100s$. The curve $T_{g_2}(w_{TPP})$ passes through a maximum with decreasing w_{TPP} (cf. Fig. 4.4.13), a behaviour reported in dynamically asymmetric binary glasses.^{22,24} We note that even at high TPP concentrations we are able to identify two distinct T_g values from DS. The such obtained T_g values are confirmed by DSC experiments.

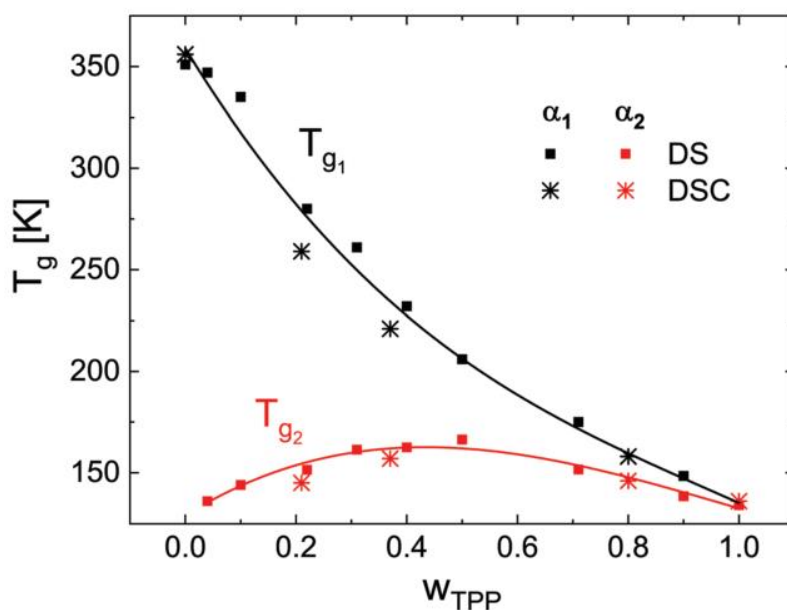


Figure 4.4.13: Glass transition temperature $T_g(w_{TPP})$ from DS (squares) and DSC (stars). T_{g_1} (α_1 -process, m-TPTS dynamics) is shown in black and T_{g_2} (α_2 -process, TPP dynamics) in red.

A subtle feature may be recognized when inspecting $\tau_{\alpha_2}(T)$ in detail for concentrations for which an Arrhenius temperature dependence is observed (cf. Fig. 4.4.12(b)). At high temperatures, $\tau_{\alpha_2}(T)$ deviates from the extrapolation of the Arrhenius behaviour and the data display a weak non-Arrhenius trace. This feature may be a reminiscence of a fragile-to-strong transition occurring close to T_{g_1} , a phenomenon observed before.^{22,31}

4.4.4.6. β -process

In contrast to neat m-TPTS, neat TPP displays a β -relaxation, which is observed in all mixtures, too. Fig. 4.4.14(a) shows exemplarily the dielectric susceptibility spectra of neat TPP and of the binary mixtures $w_{TPP} = 0.04, 0.30$ and 0.70 at temperatures between 100K and 140 K, displaying solely the β -relaxation.

As expected from a relaxation process determined by a distribution of activation energies,⁵⁴ the amplitude decreases with decreasing temperature while the spectra broaden.

Furthermore, the intensity of the β -relaxation decreases with decreasing TPP concentration. More precisely, the corresponding relaxation strength $\Delta\varepsilon_\beta(T = 100\text{ K})$ increases linearly with w_{TPP} (see Fig. 4.4.15.). The relaxation strength $\Delta\varepsilon_\beta$ was determined with an appropriate fitting function.⁵⁵ In addition, a weak but continuous shift of the relaxation maxima to higher frequencies is observed for decreasing w_{TPP} . This can directly be seen in Fig. 4.4.14(b), where the time constants τ_β extracted from the relaxation peaks ($\tau_\beta = 1/(2\pi\nu_p)$) are shown. An Arrhenius like temperature dependence is found for all concentrations. The corresponding activation energy $E_{A\beta}$ changes with concentration, which is shown as inset in Fig. 4.4.14(b). Whereas the β -relaxation of neat TPP shows an activation energy of $E_{A\beta} = 27.4\text{ kJ/mol}$, the value steadily decreases to $E_{A\beta} = 19.5\text{ kJ/mol}$ at a concentration $w_{\text{TPP}} = 0.04$. It has to be mentioned, that such a large concentration dependence was not found in our previous investigated binary mixtures, although, TPP was used as additive.^{22,29} But only for completeness, the β -relaxation is shown here. Therefore, we will not further discuss this process.

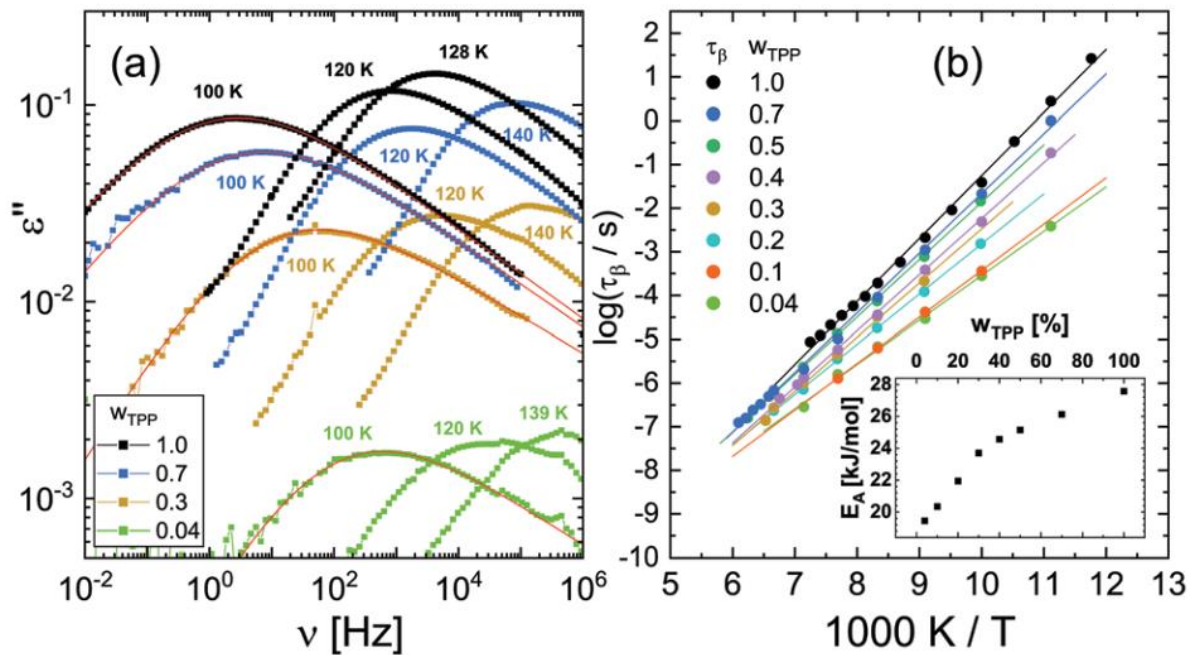


Figure 4.4.14: (a) Dielectric spectra ε'' of neat TPP and the binary mixtures $w_{\text{TPP}} = 0.04, 0.30$ and 0.70 at temperatures between 100 K and 140 K . Red lines are interpolations to determine the relaxation strength $\Delta\varepsilon_\beta$ with an appropriate fitting function.⁵⁵ Concentration is colour coded. (b) Time constants of the β -process $\tau_\beta(T)$ at different concentrations. Inset displays the concentration dependence of the activation energy.

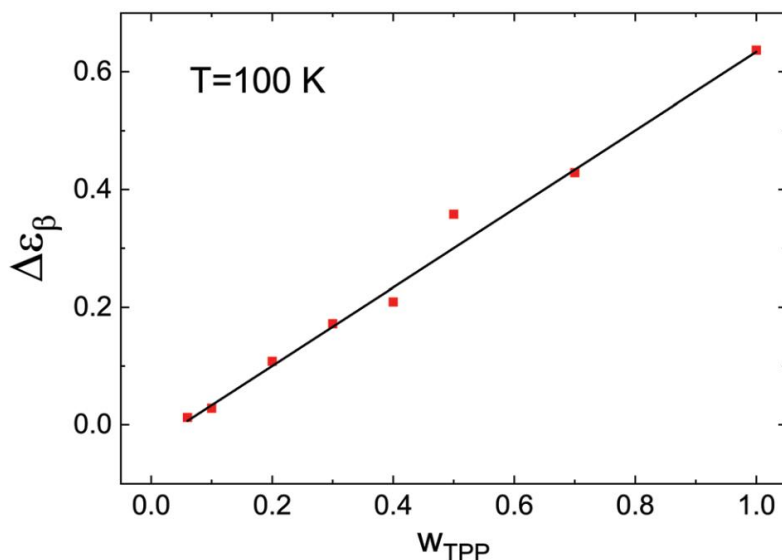


Figure 4.4.15: β -relaxation strength $\Delta\epsilon_{\beta}(w_{TPP})$ determined at $T = 100$ K with an appropriate fitting function.⁵⁵

4.4.5. Discussion and Conclusion

With the present non-polymeric asymmetric binary glass former, we are able to cover the full concentration range ($0.04 < w_{TPP} < 0.90$) by dielectric spectroscopy. As said, our previous studies were hampered by the fact that the samples tend to de-mix/crystallize. In addition to a secondary β -process, two main relaxation processes, α_1 and α_2 , are identified at all concentrations. They are characterized by well separated time scales. We attribute α_1 to the dynamics associated with the high- T_g component and α_2 with that of the additive (low- T_g component).

Compared to the relaxation spectra of neat glass formers, the evolution of the relaxation spectra shows unusual features which are again summarized in Fig. 4.4.16. Just for didactic purpose, we re-scaled the spectra in a way to document best the evolution of the component spectra with concentration. Whereas the α_1 -relaxation broadens on the high-frequency flank of the relaxation peak, the α_2 -relaxation becomes broader on the low-frequency side progressively with adding additive or high- T_g component, respectively. Basically, the broadening of the component's spectra is only confined by the time constant of the other component. As expected for the slowest relaxation in a liquid, the low-frequency flank of the α_1 -relaxation displays a $\epsilon'' \propto \omega^1$ behaviour (see Fig. 4.4.16). In both cases FTS does not apply any longer and the spectra cannot be reproduced by functions of Kohlrausch- or CD-type, for

example. At lowest additive concentration, the α_2 spectra become such broad that they tend to disappear in the noise of the instrument; no saturation of the broadening is observed at lowest TPP concentration (see inset of Fig. 4.4.16(b)) in contrast to the behaviour of the α_1 -relaxation (cf. Fig. 4.4.8(b)). For example, it is a remarkable fact that at $w_{TPP} = 0.04$ (cf. Fig. 4.4.18) still highly decoupled dynamics of TPP is observed in an essentially arrested high- T_g matrix. Thus, it is difficult to foresee the transition to the infinite-dilution limit, expecting that one added molecule probes the dynamics of the high- T_g component. All in all, the described spectral features closely resemble those in polymer-additive systems.^{22, 28}

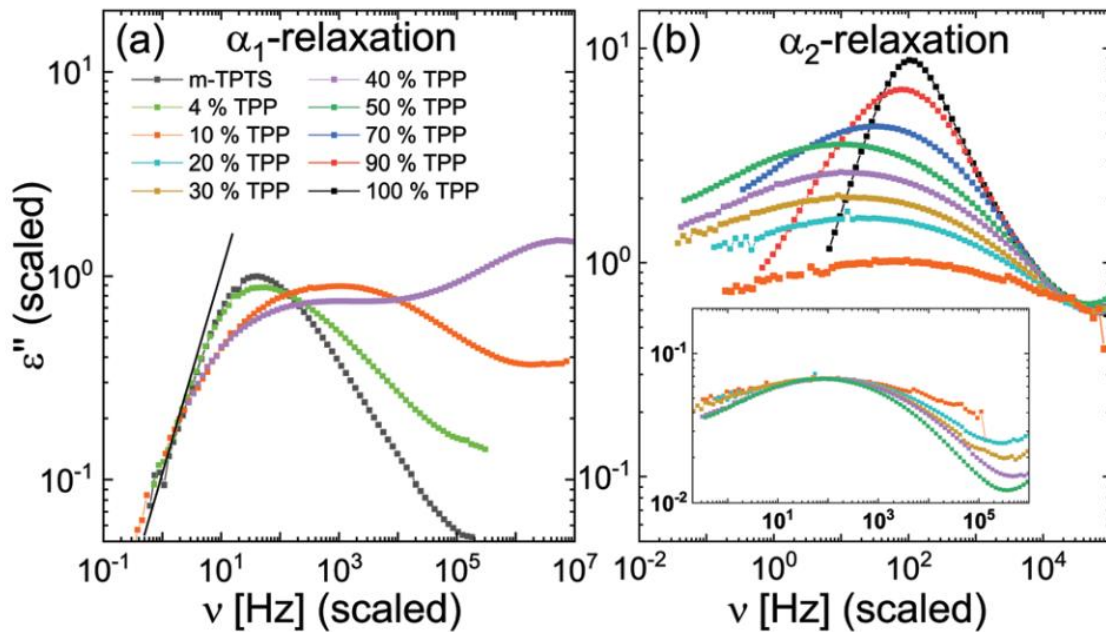


Figure 4.4.16: Overview of the dielectric spectra evolution with concentration for (a) the α_1 -relaxation and (b) the α_2 -relaxation. Comparable time constants/temperatures were used. The concentration is colour coded. The α_1 -relaxation spectra were scaled on the low frequency side and the α_2 -relaxation spectra on the high frequency side. Inset of (b): α_2 -relaxation spectra scaled onto peak position and height.

Regarding the time constants of the additive, one observes a crossover from a non-Arrhenius temperature dependence at high concentration to an Arrhenius at low concentration. There is some indication that a “fragile-to-strong” transition is also observed for a given concentration, i.e., around T_{g_1} , $\tau_{\alpha_2}(T)$ crosses over to Arrhenius behaviour upon cooling. Anticipating our results from a follow-up NMR study which are supported by our previous investigations,^{28,30} the dynamics of the TPP molecules is dynamically strongly heterogeneous: molecules undergo isotropic liquid-like reorientation on very different time scales. This allows us to define a second isodynamic point $T_{g_2} = T_{g_2}(w_{TPP})$, which passes through a maximum indicating extreme separation of the component dynamics at low additive concentration. Of

course, this temperature characterizes the slow-down of the additive dynamics in an essentially arrested high- T_g matrix, thus may involve a different type of glass transition as suggested by MD simulations as well as analyses by mode coupling theory.^{13,14,16,56} Specifically, a dynamical decoupling of large and small particle species was reported. The large particles exhibit a standard glass transition controlled by the cage effect, while the small particles still remain mobile within the arrested matrix of the large particles and undergo finally at lowest temperatures a localization transition. In contrast, and in accordance with our results, the dynamics of the high- T_g component m-TPTS is essentially homogeneous.⁴³ In this context, another MD simulation is of interest, which investigated a mixture of two water-like model molecules with different polarities such that the dynamical contrast is large whereas the mixture remains miscible.¹⁷ Again, dynamical decoupling was observed and the fast component displays quasi-logarithmic correlation decays together with a sub-diffusive regime in the mean square displacement. In contrast, the dynamics of the slow component resembles essentially that of neat glass formers. The growing concentration fluctuations upon cooling, characteristic of approaching spinodal decomposition, control the spatially heterogeneous dynamics.

This difference of the dynamics leads us to a different interpretation of the observed broadening of the spectra of the high- T_g and the low- T_g component, respectively. On the one hand, the low-frequency broadening of the additive spectra, indeed, reflects heterogeneous dynamics. The corresponding “true” time constant as given by the spectral density at zero frequency (or as integral over the correlation function) is determined by the longest time, which is actually difficult to access because the low-frequency flank is partly obscured by the spectral contribution associated with the high- T_g component. Consequently, the TPP time constants $\tau_{\alpha_2}(T)$ given in Fig. 4.4.12 represent the most probable time constant reflecting the major part of the spectrum of the TPP sub-ensemble. The difference between T_{g_1} and T_{g_2} specifies the extent of time scale separation in the mixture. We emphasize that around T_{g_2} a broad glass step is also monitored in the DSC signal (cf. Fig. 4.4.2). On the other hand, the spectra of the high- T_g component become overall broader and, importantly, display a stronger relaxation strength compared to that of the neat component. For example, adding only 4% TPP, the spectra significantly broaden (see Fig. 4.4.16). However, the corresponding high-frequency broadening of the spectra does not originate from molecules that reorient

isotropically at those frequencies. These spectral features are probably of similar quality as that of the excess wing documented in the spectra of neat glass formers. It is a kind of precursor relaxation of the main relaxation.

The most unusual result reported by our study and not covered by our previous investigations concerns the concentration dependence of the total dielectric relaxation strength $\Delta\varepsilon$. Due to the low polarity of the high- T_g component, it basically reflects the relaxation strength of the additive. While $\Delta\varepsilon(T)$ essentially follows a Curie law, its concentration dependence strongly deviates from that expected by ideal mixing. Actually, this is not observed for the case when a high- T_g component carries the high dipole moment.³⁴ Thus, care has to be taken to interpret the fraction $\Delta\varepsilon_{\alpha_i}/\Delta\varepsilon$ as reflecting the corresponding population of the respective sub-ensemble of the component.

Here, recent simulation work of the dielectric spectra of molecular binary systems may be of relevance.⁵⁷ It indicates significant difference between the collective (coherent) and the self (incoherent) reorientational dynamics. In particular, the coherent additive correlation function shows in addition to a short time decay a plateau essentially persisting up to a time scale on the order of that of the matrix - a feature not observed in the incoherent correlation function. In other words, the collective dynamics of the additive only fully decays to zero when the matrix relaxes, whereas the incoherent dynamics lead to a low-frequency broadening with a cut-off at the time scale of the high- T_g dynamics as modelled by our approach. For example, a single additive molecule could leave the matrix sites on the time scale τ_{α_2} but other molecules visit an identical site, thus keeping some correlations up to the time scale τ_{α_1} at which the matrix relaxes. Similar effects were reported when simulating mixtures of particles (lacking orientational degrees of freedom) of disparate sizes.¹³

Like Blochowicz and co-workers,^{22,23,31} we previously interpreted the higher relaxation strength of the α_1 -relaxation with respect to the that of the neat system as an indication that part of the additive molecules take part in the α_1 -relaxation of the high- T_g component and finally are released at a certain high temperature.^{24,28} Possibly, as the simulations suggest, the enhanced relaxation strength of the α_1 -relaxation may also result from a persistent correlation induced by the high- T_g matrix on the TPP molecules: In any case, the strongly enhanced relaxation strength $\Delta\varepsilon_{\alpha_1}$ must not be interpreted as reflecting an underlying distribution of

the liquid-like high- T_g component dynamics. Given that ^{31}P NMR probes single-particle (incoherent) dynamics, our follow-up NMR study will address the question up to what extent the enhanced relaxation strength $\Delta\varepsilon_{\alpha_1}$ can be attributed to a slow TPP sub-ensemble. Thus, in applying different NMR techniques, we will re-iterate the sketched issues.

Conflicts of interest

There are no conflicts to declare.

4.4.6. Acknowledgements

This research was funded by the Deutsche Forschungsgemeinschaft (DFG, German Research Foundation), Grant Numbers Schm 703/9-1, RO 907/19, and SFB 840. F.K. acknowledges support from the Elite Network of Bavaria (ENB) within the Elite Study Program Macromolecular Science. TK and ER also acknowledge the support by Prof. Dr. Jürgen Senker.

4.4.7. Appendix

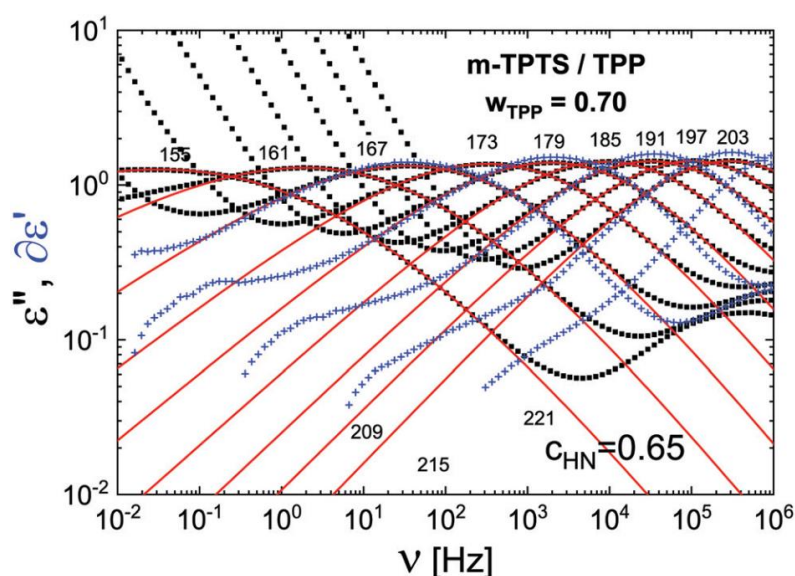


Figure 4.4.17: Dielectric spectra ε'' of the binary mixture $w_{\text{TPP}} = 0.90$ (black squares, HN fits as red lines). For selected temperatures, the derivative relaxation data $\partial\varepsilon'$ (blue crosses) are shown. An additional low intensity relaxation contribution is recognized at lowest frequencies (α_1), which cannot be resolved in ε'' . Fit parameters are included in Fig. 4.4.6 and Fig. 4.4.11.

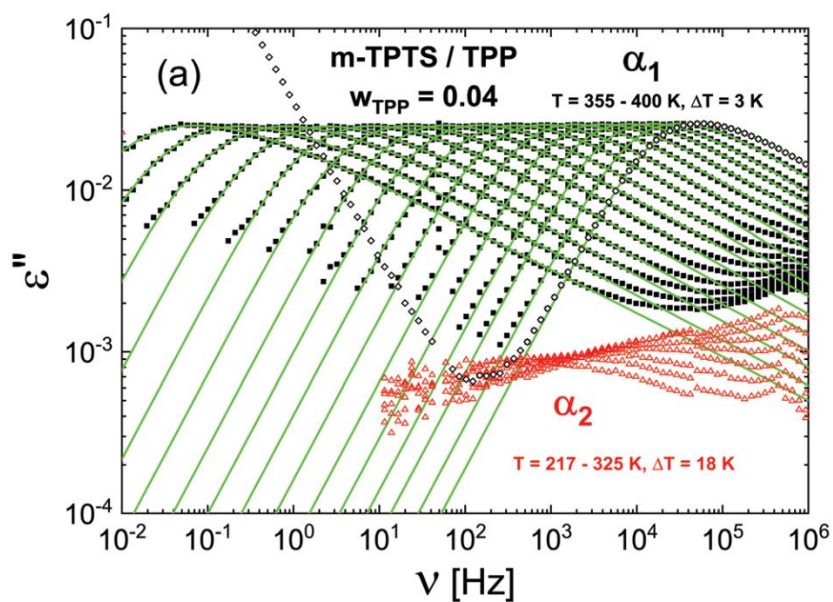


Figure 4.4.18: Dielectric spectra ε'' of $w_{TPP} = 0.04$ (squares, α_2 -spectra as open red triangles). Original data is shown for $T=400$ K (open diamonds). Green lines are GCD-fits. Fit parameters are included in Fig. 4.4.8. and Fig. 4.4.11.

4.4.8. Acknowledgements

This research was funded by the Deutsche Forschungsgemeinschaft (DFG, German Research Foundation), Grant Numbers Schm 703/9-1, RO 907/19, and SFB 840. F. K. acknowledges support from the Elite Network of Bavaria (ENB) within the Elite Study Program Macromolecular Science. T. K. and E. R. also acknowledge the support by Simon Winterstein and Jürgen Senker.

4.4.9. References

- [1] M. D. Ediger, *Spatially heterogeneous dynamics in supercooled liquids*, *Annu. Rev. Phys. Chem.*, **2000**, *51*, 99–128.
- [2] P. Lunkenheimer, U. Schneider, R. Brand and A. Loidl, *Glassy dynamics*, *Contemp. Phys.*, **2000**, *41*, 15–36.
- [3] G. Floudas, M. Paluch, A. Grzybowski and K. Ngai, *Molecular dynamics of glass-forming systems. Effects of pressure*, Springer, Berlin, Heidelberg, **2011**.
- [4] P. G. Wolynes and V. Lubchenko, *Structural glasses and supercooled liquids. Theory, experiment, and applications*, Wiley, Hoboken, New Jersey, **2012**.
- [5] N. Petzold, B. Schmidtke, R. Kahlau, D. Bock, R. Meier, B. Micko, D. Kruk and E. A. Rössler, *Evolution of the dynamic susceptibility in molecular glass formers: results from light scattering, dielectric spectroscopy, and NMR*, *J. Chem. Phys.*, **2013**, *138*, 12A510.
- [6] P. J. Hains and G. Williams, *Molecular motion in polystyrene-plasticizer systems as studied by dielectric relaxation*, *Polymer*, **1975**, *16*, 725–729.
- [7] M. Scandola, G. Ceccorulli and M. Pizzoli, *Composition dependence of the glass transition of polymer diluent mixtures: 2. Two concomitant glass transition processes as a general feature of plasticized polymers*, *Polymer*, **1987**, *28*, 2081–2084.
- [8] Y. He, T. R. Lutz, M. D. Ediger, M. Pitsikalis, N. Hadjichristidis and E. D. von Meerwall, *Miscible Polyisoprene/Polystyrene Blends: Distinct Segmental Dynamics but Homogeneous Terminal Dynamics*, *Macromolecules*, **2005**, *38*, 6216–6226.
- [9] T. R. Lutz, Y. He and M. D. Ediger, *Segmental Dynamics of Dilute Polystyrene Chains in Miscible Blends and Solutions*, *Macromolecules*, **2005**, *38*, 9826–9835.
- [10] G. Goracci, A. Arbe, A. Alegría, Y. Su, U. Gasser and J. Colmenero, *Structure and component dynamics in binary mixtures of poly(2(dimethylamino)ethyl methacrylate) with water and tetrahydrofuran: A diffraction, calorimetric, and dielectric spectroscopy study*, *J. Chem. Phys.*, **2016**, *144*, 154903.

- [11] Y. Kaneko and J. Bosse, *Dynamics of binary liquids near the glass transition: a mode-coupling theory*, J. Non-Cryst. Solids, **1996**, 205-207, 472–475.
- [12] S.-H. Chong, W. Götze and A. P. Singh, *Mode-coupling theory for the glassy dynamics of a diatomic probe molecule immersed in a simple liquid*, Phys. Rev. E, **2000**, 63, 011206.
- [13] A. J. Moreno and J. Colmenero, *Relaxation scenarios in a mixture of large and small spheres: Dependence on the size disparity*, J. Chem. Phys., **2006**, 125, 164507.
- [14] T. Voigtmann and J. Horbach, *Double transition scenario for anomalous diffusion in glass-forming mixtures*, Phys. Rev. Lett., **2009**, 103, 205901.
- [15] T. Voigtmann, *Multiple glasses in asymmetric binary hard spheres*, EPL, **2011**, 96, 36006.
- [16] T. Sentjabrskaja, E. Zaccarelli, C. D. Michele, F. Sciortino, P. Tartaglia, T. Voigtmann, S. U. Egelhaaf and M. Laurati, *Anomalous dynamics of intruders in a crowded environment of mobile obstacles*, Nat. Commun., **2016**, 7, 11133.
- [17] N. Müller and M. Vogel, J. Chem. Phys., *Relation between concentration fluctuations and dynamical heterogeneities in binary glass-forming liquids: A molecular dynamics simulation study*, **2019**, 150, 64502.
- [18] L. A. Utracki and B. D. Favis, in *Handbook of Polymer Science and Technology*, ed. N. P. Cheremisinoff, Marcel Dekker, Inc., New York, **1989**.
- [19] M. Pizzoli, M. Scandola and G. Ceccorulli, *Molecular motion in polymer-diluent systems: polystyrene tritolylphosphate*, Eur. Polym. J., **1987**, 23, 843–846.
- [20] T. Sakaguchi, N. Taniguchi, O. Urakawa and K. Adachi, *Calorimetric Study of Dynamical Heterogeneity in Blends of Polyisoprene and Poly(vinylethylene)*, Macromolecules, **2005**, 38, 422–428.
- [21] T. P. Lodge, E. R. Wood and J. C. Haley, *Two calorimetric glass transitions do not necessarily indicate immiscibility: The case of PEO/PMMA*, J. Polym. Sci. B Polym. Phys., **2006**, 44, 756–763.

- [22] R. Kahlau, D. Bock, B. Schmidtke and E. A. Rössler, *Dynamics of asymmetric binary glass formers. I. A dielectric and nuclear magnetic resonance*, J. Chem. Phys., **2014**, *140*, 44509.
- [23] T. Blochowicz, S. A. Lusceac, P. Gutfreund, S. Schramm and B. Stühn, *Two glass transitions and secondary relaxations of methyltetrahydrofuran in a binary mixture*, J. Phys. Chem. B, **2011**, *115*, 1623–1637.
- [24] B. Pötzschner, F. Mohamed, A. Lichtinger, D. Bock and E. A. Rössler, *Dynamics of asymmetric non-polymeric binary glass formers-A nuclear magnetic resonance and dielectric spectroscopy study*, J. Chem. Phys., **2015**, *143*, 154506.
- [25] S. P. Bierwirth, C. Gainaru and R. Böhmer, *Coexistence of two structural relaxation processes in monohydroxy alcohol-alkyl halogen mixtures: Dielectric and rheological studies*, The Journal of Chemical Physics, **2018**, *149*, 44509.
- [26] J. Colmenero and A. Arbe, *Segmental dynamics in miscible polymer blends: recent results and open questions*, Soft Matter, **2007**, *3*, 1474–1485.
- [27] D. Cangialosi, A. Alegría and J. Colmenero, *"Self-concentration" effects on the dynamics of a polychlorinated biphenyl diluted in 1,4-polybutadiene*, J. Chem. Phys., **2007**, *126*, 204904.
- [28] D. Bock, R. Kahlau, B. Pötzschner, T. Körber, E. Wagner and E. A. Rössler, *Dynamics of asymmetric binary glass formers. II. Results from nuclear magnetic resonance spectroscopy*, J. Chem. Phys., **2014**, *140*, 94505.
- [29] B. Pötzschner, F. Mohamed, C. Bächer, E. Wagner, A. Lichtinger, D. Bock, K. Kreger, H.-W. Schmidt and E. A. Rössler, *Non-polymeric asymmetric binary glass-formers. II. Secondary relaxation studied by dielectric, ²H NMR, and ³¹P NMR spectroscopy*, J. Chem. Phys., **2017**, *146*, 164504.
- [30] D. Bock, T. Körber, F. Mohamed, B. Pötzschner and E. A. Rössler, in *The Scaling of Relaxation Processes*, ed. F. Kremer and A. Loidl, Springer, Cham, Switzerland, **2018**, pp. 173–201.

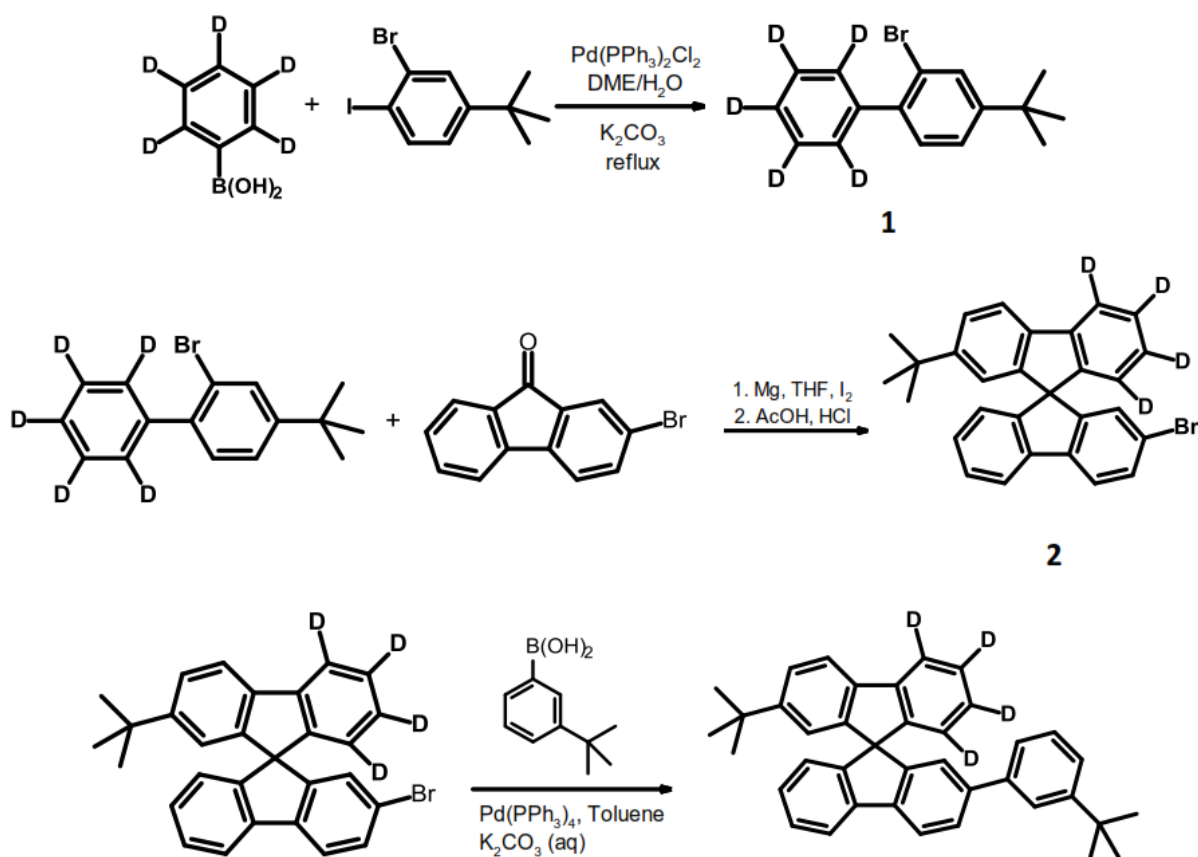
- [31] T. Blochowicz, S. Schramm, S. Lusceac, M. Vogel, B. Stühn, P. Gutfreund and B. Frick, *Signature of a type-A glass transition and intrinsic confinement effects in a binary glass-forming system*, Phys. Rev. Lett., **2012**, *109*, 35702.
- [32] B. Frick, C. Alba-Simionesco, G. Dosseh, C. Le Quellec, A. J. Moreno, J. Colmenero, A. Schönhals, R. Zorn, K. Chrissopoulou, S. H. Anastasiadis and K. Dalnoki-Veress, *Inelastic neutron scattering for investigating the dynamics of confined glass-forming liquids*, J. Non-Cryst. Solids, **2005**, *351*, 2657–2667.
- [33] D. Bock, N. Petzold, R. Kahlau, S. Gradmann, B. Schmidtke, N. Benoit and E. A. Rössler, *Dynamic heterogeneities in glass-forming systems*, J. Non-Cryst. Solids, **2015**, *407*, 88–97.
- [34] T. Körber, R. Minikejew, B. Pötzschner, D. Bock and E. A. Rössler, *Dynamically asymmetric binary glass formers studied by dielectric and NMR spectroscopy*, Eur. Phys. J. E, **2019**, *42*, 143.
- [35] B. Pötzschner, F. Mohamed, C. Bächer, E. Wagner, A. Lichtinger, R. Minikejew, K. Kreger, H.-W. Schmidt and E. A. Rössler, *Non-polymeric asymmetric binary glass-formers. I. Main relaxation studied by dielectric, ²H NMR, and ³¹P NMR spectroscopy*, J. Chem. Phys., **2017**, *146*, 164503.
- [36] F. Krohn, C. Neuber, E. A. Rössler and H.-W. Schmidt, *Organic Glasses of High Glass Transition Temperatures Due To Substitution with Nitrile Groups*, J. Phys. Chem. B, **2019**, *123*, 10286–10293.
- [37] T. Körber, F. Krohn, C. Neuber, H.-W. Schmidt and E. A. Rössler, *Main and secondary relaxations of non-polymeric high-T_g glass formers as revealed by dielectric spectroscopy*, Phys. Chem. Chem. Phys., **2020**, *22*, 9086–9097.
- [38] C. Lorthioir, A. Alegría and J. Colmenero, *Out of equilibrium dynamics of poly(vinyl methyl ether) segments in miscible poly(styrene)-poly(vinyl methyl ether) blends*, Phys. Rev. E, **2003**, *68*, 31805.
- [39] S. Valenti, S. Capaccioli and K. L. Ngai, *Contrasting two different interpretations of the dynamics in binary glass forming mixtures*, J. Chem. Phys., **2018**, *148*, 54504.

- [40] K. L. Ngai, S. Valenti and S. Capaccioli, *Molecular dynamic in binary mixtures and polymer blends with large difference in glass transition temperatures of the two components: A critical review*, J. Non-Cryst. Solids, **2019**, 119573.
- [41] S. Adishchev, D. Bock, C. Gainaru, R. Kahlau, B. Micko, N. Petzold, B. Pötzschner and E. A. Rössler, *Reorientational Dynamics of Organophosphate Glass Formers – a Joint Study by ^{31}P NMR, Dielectric Spectroscopy and Light Scattering*, Z. Phys. Chem., **2012**, 226, 1149–1168.
- [42] R. Kahlau, T. Dörfler and E. A. Rössler, *Secondary relaxations in a series of organic phosphate glasses revealed by dielectric spectroscopy*, J. Chem. Phys., **2013**, 139, 134504.
- [43] T. Körber and E. A. Rössler, to be published, **2021**.
- [44] C. J. F. Böttcher and P. Bordewijk, *Dielectrics in time-dependent fields*, Elsevier, Amsterdam, 2nd edn., **1978**.
- [45] F. Kremer and A. Schönhal, *Broadband Dielectric Spectroscopy*, Springer, Berlin, Heidelberg, **2003**.
- [46] R. Kahlau, D. Kruk, T. Blochowicz, V. N. Novikov and E. A. Rössler, *Generalization of the Cole–Davidson and Kohlrausch functions to describe the primary response of glass-forming systems*, J. Phys.: Condens. Matter, **2010**, 22, 365101.
- [47] S. Havriliak and S. Negami, *A complex plane representation of dielectric and mechanical relaxation processes in some polymers*, Polymer, **1967**, 8, 161–210.
- [48] T. Blochowicz, *Broadband dielectric spectroscopy in neat and binary molecular glass formers : Frequency and time domain spectroscopy, non-resonant spectral hole burning*, Universität Bayreuth, **2003**.
- [49] M. Wübbenhorst and J. van Turnhout, *Analysis of complex dielectric spectra. I. One-dimensional derivative techniques and three-dimensional modelling*, J. Non-Cryst. Solids, **2002**, 305, 40–49.
- [50] A. Savitzky and M. J. E. Golay, *Smoothing and Differentiation of Data by Simplified Least Squares Procedures*, Anal. Chem., **1964**, 36, 1627–1639.

- [51] P. A. Gorry, *General least-squares smoothing and differentiation by the convolution (Savitzky-Golay) method*, *Anal. Chem.*, **1990**, *62*, 570–573.
- [52] H. Wagner and R. Richert, *Equilibrium and Non-Equilibrium Type β -Relaxations: *d* - Sorbitol versus *o* -Terphenyl*, *J. Phys. Chem. B*, **1999**, *103*, 4071–4077.
- [53] D. Bock, R. Kahlau, B. Micko, B. Pötzschner, *On the cooperative nature of the β -process in neat and binary glasses: a dielectric and nuclear magnetic resonance spectroscopy study*, G. J. Schneider and E. A. Rössler, *J. Chem. Phys.*, **2013**, *139*, 64508.
- [54] A. Kudlik, S. Benkhof, T. Blochowicz, C. Tschirwitz and E. Rössler, *J. Mol. Struct.*, 1999, *479*, 201–218.
- [55] T. Blochowicz, C. Tschirwitz, S. Benkhof and E. A. Rössler, *The dielectric response of simple organic glass formers*, *J. Chem. Phys.*, **2003**, *118*, 7544–7555.
- [56] A. J. Moreno and J. Colmenero, *Anomalous dynamic arrest in a mixture of large and small particles*, *Phys. Rev. E*, **2006**, *74*, 21409.
- [57] T. Blochowicz and co-workers, to be published, 2021.

4.4.10. Supporting Information

Synthetic route towards m-TPTS-*d*₄:



Synthesis of **1**: 2.00 g (15.75 mmol) phenyl-*d*₅-boronic acid and 4.45 g (13.1 mmol) of 3-bromo-4-iodo-*tert*-butylphenyl boronic acid are dissolved in 45 mL of DME and 7.5 mL of H_2O . 2.55 g of K_2CO_3 is added, then the mixture is flushed with Argon under stirring for 30 minutes. 110 mg of $\text{PdCl}_2(\text{PPh}_3)_2$ are added, and Argon is flushed for another 30 minutes. Afterward, the mixture is heated to 80 °C for 18 h.

After cooling, DME is removed under reduced pressure, and 80 mL of H_2O and 40 mL of ether are given to the residue. The phases are separated, and the aqueous phase is washed with ether. The combined organic phases are dried over MgSO_4 , and the solvent is removed under reduced pressure. The crude product is further purified by column chromatography with hexane to yield 3.1 g (80 %) of a colorless liquid with a distinct odor.

^1H NMR (300 MHz, CDCl_3): δ = 1.36 (s, 9H, *t*-Bu-H), 7.27 (m, 1H, Ar-H), 7.38 (dd, 1H, Ar-H), 7.67 (d, 1H, Ar-H).

Synthesis of **2**: 3.1 g (12.2 mmol) of **1** is mixed with 370 mg of Mg and one spatula tip of I₂ in 30 mL of dry THF and heated under reflux. 3.1 g (12.0 mmol) 2-bromo-fluorenone are dissolved in 10 mL of dry THF. After 5 h, the Grignard reagent is transferred to the fluorenone solution with a syringe and stirred under reflux for further 17 h. Then a few drops of AcOH are given to the solution upon which it clarifies. THF is removed under reduced pressure, and the remaining material is dissolved in 30 mL AcOH and 2 mL of 32 % HCl and heated under reflux for 5 h. The product is precipitated with MeOH, filtered, washed with hexane and EtOH, and dried to yield 3.0 g (55 %) of a colorless powder.

¹H NMR (300 MHz, CDCl₃): δ = 1.18 (s, 9H, *t*-Bu-H), 6.72 (m, 2H, Ar-H), 6.85 (dd, 1H, Ar-H), 7.12 (dt, 1H, Ar-H), 7.37 (dt, 1H, Ar-H), 7.44 (dd, 1H, Ar-H), 7.48 (dd, 1H, Ar-H), 7.70 (dd, 1H, Ar-H), 7.76 (dd, 1H, Ar-H), 7.82 (m, 1H, Ar-H).

Synthesis of **m-TPTS-d₄**: 2.97 g of **2** (6.53 mmol) is dissolved in 100 mL dry THF with 1.51 g 3-*tert*-butylphenyl boronic acid (8.48 mmol). 60 mL 2M K₂CO₃-solution is added and Ar flushed for 30 minutes. 196 mg Pd(PPh₃)₄ (0.17 mmol) is added to the mixture, and Ar flushed for another 30 minutes. The mixture is then refluxed for 17 h. After cooling the phases are separated, the organic phase is washed with brine, dried over MgSO₄, and the solvent removed under reduced pressure. The crude product is further purified by column chromatography with cyclohexane / EtAc in a gradient from 100:1 to 20:1 to yield 2.84 g (80 %) of a white solid. After sublimation, a total of 1.73 g is yielded.

¹H NMR (300 MHz, CDCl₃): δ = 1.17 (s, 9H, *t*-Bu-H), 1.30 (s, 9H, *t*-Bu-H), 6.73 (m, 1H, Ar-H), 6.78 (dd, 1H, Ar-H), 6.92 (dd, 1H, Ar-H), 7.10 (td, 1H, Ar-H), 7.15 – 7.30 (m, 3H, Ar-H), 7.34 – 7.46 (m, 3H, Ar-H), 7.61 (dd, 1H, Ar-H), 7.77 (dd, 1H, Ar-H), 7.87 (m, 1H, Ar-H), 7.89 – 7.93 (dd, 1H, Ar-H).

4.5. Poly(olefin sulfone)s as new resist materials for thermal scanning probe lithography

Felix Krohn,^a Armin W. Knoll,^b Samuel Bisig,^c Francesca Ruggeri,^b Christian Neuber,^{a} and Hans-Werner Schmidt^{a*}*

^a Department of Macromolecular Chemistry and Bavarian Polymer Institute, University of Bayreuth, 95440 Bayreuth, Germany

^b IBM Research Zurich, Säumerstraße 4, 8803 Rüschlikon, Switzerland

^c Heidelberg Instruments Nano, Technoparkstraße 1, 8005 Zürich, Switzerland

The results are intended for publication.

4.5.1. Abstract

Thermal scanning probe lithography (t-SPL) is a maskless lithographic technique able to generate three-dimensional patterns and features in the order of 10 nm in size. So far, only one resist material, poly(phthal aldehyde) (PPA) meets the requirements of decomposition behavior, pattern stability, and etch-resistance that are needed for its application. In this work, we evaluate poly(olefin sulfone)s, a class of polymers that was examined as resist materials for lithography in the 1980s but has since been almost forgotten, as possible resist materials for t-SPL. The polymers are easily accessible *via* free radical polymerization and show complete decomposition below 300 °C. Their writing sensitivity is comparable to that of PPA. 3D patterning and high-resolution 2D patterning with down to 10 nm half-pitch are demonstrated. In contrast to PPA, poly(olefin sulfone)s are acid-resistant, and thus generated patterns persist in an acidic environment. Sequential Infiltration Synthesis using standard Al₂O₃-atomic layer deposition processes is used to generate an etch-resistant hard mask yielding a selectivity of 3.75 against SiO₂.

4.5.2. Introduction

On the chase of ever smaller feature size in lithography fulfilling Moore's Law, today's nanofabrication has reached a turning point. The current workhorse of large-volume semiconductor fabrication, DUV immersion lithography using a 193 nm ArF laser, has already exceeded the expectations of its possible resolution, being used for the production of the 10 nm node.¹ This resolution is, however, dependent on a quadruple patterning technique, which drastically increases the complexity and costs of the process. Further increase in resolution requires the use of 13.5 nm EUV lithography. Although a lot of progress was made, still some issues are faced using EUV, such as a trade-off between resolution, line edge roughness and sensitivity limiting the throughput in high-resolution fabrication,^{2,3} the stochastic effect of scattered electrons,⁴ or the migration of photons from photoacid generators resulting in the blur effect.^{5,6} Furthermore, the high costs of EUV lithography regarding tool and fabrication of masks urge the need for maskless technologies enabling low-volume production at reasonable costs, mask production, and prototyping of devices.⁷

Among maskless techniques, e-beam lithography (EBL) is widely used as it offers both, high throughput and sub-20 nm resolution, however, not simultaneously.⁸ But similar to EUV lithography, EBL faces issues such as a trade-off between resolution and sensitivity⁹ or the proximity effect due to scattered electrons causing errors in the written structures.¹⁰ Especially on insulating substrates, trapped charges induced by the charged electron beam might cause pattern distortion.¹¹ Furthermore, the field size in EBL is limited, which requires stitching of smaller fields. The occurring stitching error may well be in the range of the pattern size, i.e. 10 nm or above.¹²

A further example of a maskless lithographic method is scanning probe lithography (SPL). Scanning probes are capable to address and modify surface structures on the atomic scale¹³ and a wide variety of processes can be controlled using a sharp tip. Consequently, several different SPL techniques were developed in the last decades.⁷ Among those, thermal scanning probe lithography (t-SPL) stands out in terms of resolution and throughput. Using poly(phthalaldehyde) (PPA) as a resist material and a probe heated to 700 °C – 1000 °C, any programmed shape can be written into the resist, either of two-dimensional or three-dimensional nature.¹⁴ Due to the thermally triggered evaporation of the resist, no development step is needed. The sensitivity of the writing procedure relies on the self-amplified depolymerization of PPA, where the cleavage of one bond in the polymer chain yields a complete unzipping of the whole chain, reducing the amount of energy that has to be introduced into the resist.¹⁵ Recently, sub-10 nm feature size and 14 nm half-pitch pattern transfer into silicon were demonstrated using t-SPL.¹⁶ The fabrication of such small features requires the use of ultra-thin resist layers (< 10 nm) to keep the aspect ratio of the structures reasonable. This makes the pattern transfer into the substrate difficult. To address this issue, complex stacks involving several layers of organic and inorganic material as well as metal lift-off processes can be used.¹⁷ An elegant answer to this issue is the treatment of the patterned resist with Sequential Infiltration Synthesis (SIS) creating a continuous etch resistant hard mask for the transfer process.¹⁸

One of the key advantages of t-SPL is the *in-situ* metrology which, in combination with the nature of a ‘direct-development’ patterning, enables a closed-loop control that allows parameter adjustments during the writing procedure.¹⁹ Furthermore, the scanning probe also allows the non-destructive *in-situ* imaging of surface features which enables a high stitching and overlay accuracy. 3 nm precise overlay fabrication of metal contacts to nanowires was

demonstrated.²⁰ The combination of t-SPL with a laser combines the high-resolution t-SPL process with low resolution but fast optical lithography in a mix-and-match process.²¹

Commercialization and wider application of t-SPL is still in its infancy, however, a couple of applications show the potential that this technique can offer to the community. This includes "classical" lithographic applications such as the fabrication of phase masks for electron microscopy in silicon nitride or the fabrication of chemical guiding patterns for the directed self-assembly of block copolymers.²² Using other materials than PPA, the patterning of a thermochromic luminescent supramolecular polymer resulting in topographic as well as fluorescent nanostructures²³ or the use of a *bombyx mori* silk fibroin as resist material was demonstrated, utilizing the latter, however, t-SPL could not feature the direct-development method.²⁴ Further applications of t-SPL were demonstrated preparing devices used in aqueous environments, such as nanofluidic devices^{25,26} or a replication of tissue microenvironment for cell culture.²⁷ Clearly, the capabilities of t-SPL have by far not yet been fully exploited. The evaluation of further materials that may be patterned using t-SPL will be a crucial step in extending its range of applications. This applies in particular for acid resistant materials, as PPA is labile towards acids,²⁸ preventing its application in acidic media.

Poly(olefin sulfone)s are a class of polymers that are known for many decades.^{29,30} They are easily accessible *via* free-radical polymerization in liquid SO₂ acting as both co-monomer and solvent, at low temperatures. Many of the hitherto investigated poly(olefin sulfone)s undergo depolymerization under the stimulus of heat, high-energy radiation, or bases.³¹⁻³⁷ Thus, applications as deep-UV and electron beam resist were discussed, but the sensitivity to elevated temperatures prevented further industrial application and interest in the material decreased.³⁸⁻⁴⁰ In recent years, however, poly(olefin sulfone)s regained attention in fields where heat sensitivity is beneficial, such as smart materials.^{41,42} UV lithography was conducted using photo-base generators, but the structures obtained remained in the μm -range.⁴³⁻⁴⁵ Also EUV experiments were conducted, yielding features with 30 nm half-pitch.⁴⁶

Two depolymerization mechanisms were proposed for poly(olefin sulfone)s, both of which may be occurring in the same polymer. One of the proposed mechanisms is a β -elimination, probably involving a cyclic intermediate, the other one involves a C-S-main chain scission creating a radical pathway.^{33,44,47} The elimination pathway includes H⁺-abstraction and thus

may be catalyzed by bases, while the radical pathway usually occurs under higher temperatures.

In this study, we evaluate the use of poly(olefin sulfone)s as new resist materials for t-SPL, both in a neat and a chemically amplified approach. 3D and high-resolution 2D patterning are demonstrated. The resistivity of the resist towards acidic media is examined. SIS is used for the generation of a hardmask for the etch process.

4.5.3. Materials and methods

Polymerizations were carried out in a pressure glass vessel. 5 mL 2-methyl pentene (TCI) or cyclohexene (Sigma-Aldrich), respectively, were filled into the glass vessel which was then sealed and cooled to $-78\text{ }^{\circ}\text{C}$. Subsequently, about a four-time volume excess of SO_2 was condensed into the vessel. 0.5 mL t-BuOOH (5 – 6 M in decane, Sigma-Aldrich) was added to the mixture, the vessel was shaken extensively and the reaction was run for up to four hours. The mixture was then dissolved in CHCl_3 upon warming to room temperature, precipitated in methanol, and dried *in vacuo* at $50\text{ }^{\circ}\text{C}$. The yielded poly(2-methylpentene sulfone) is denoted as PMPS and the poly(cyclohexene sulfone) as PCHS. For measurements with added salts, the polymer and the salt were thoroughly ground with a pestle and mortar.

Thermogravimetric analysis (TGA) was conducted on a Mettler TGA/DSC3 with a heating rate of 10 K/min under air flow. The dynamic mechanical analysis was performed on a Mettler DMA1 with a heating rate of 2 K/min and a frequency of 2 Hz. Scanning Thermal Analysis was conducted in a Netzsch STA 449 C Jupiter with a Bruker Vertex 70 FTIR spectrometer and a Netzsch Aeolos QMS 403 C mass spectrometer attached. SEC measurements were conducted with THF containing 0.25 % tetrabutylammonium bromide (TBAB) as eluent. The chromatograph was equipped with two Varian Mixed-C columns (330 x 7.5 mm) and run at room temperature at a flow rate of 0.5 mL min^{-1} using a refractive index detector. The SEC was calibrated with PS purchased by Polymer Standard Service as external standard and 1,2-dichlorobenzene as internal standard. Spin coating was performed at 2,500 rpm with a post apply bake of 2 minutes at $120\text{ }^{\circ}\text{C}$ for all poly(olefin sulfone)s. T-SPL was carried out on in the home-built scanning probe system as previously described.^{14,16} Atomic layer deposition was performed in an Ultratech/Cambridge Savannah ALD system using subsequent trimethyl

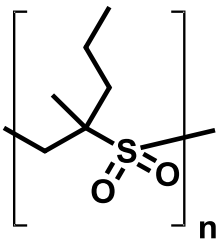
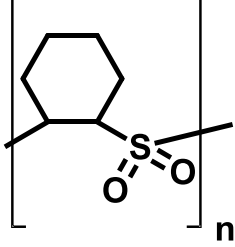
aluminium (Strem chemicals) and water (MilliQ) pulses. For any one cycle, the pulse time was 0.015 seconds with a 10-second waiting interval between every two pulses. Layer thicknesses were determined by applying a mechanical scratch that was inspected using atomic force microscopy. Cyclohexene (Sigma Aldrich), 1-methyl-2-pentene (TCI), SO₂ (Rießner Gase), crosslinked Polystyrene and all solvents (p.a., VWR) were used as received. Test grade 4'' silicon wafers from Siegert with 300 nm thermal SiO₂ were used.

4.5.4. Results and Discussion

4.5.4.1. Polymer characterization

For the evaluation of poly(olefin sulfone)s as resist materials for t-SPL, two polymers - poly(2-methylpentene sulfone) (PMPS) and poly(cyclohexene sulfone) (PCHS), both exhibiting rather low ceiling temperatures⁴⁸ - have been synthesized and characterized, as shown in Table 4.5.1. Due to the high molecular weight of the polymers (the SEC curve runs out of our PS calibration at 2,000 kg/mol) only corresponding peak molecular weights are given rather than M_n or M_w. The curves show a typical broad molecular weight distribution as expected from a free-radical polymerization (*see Supporting Information*).

Table 4.5.1: Structures, T_g, T_{ceiling}, and M_{peak} of here investigated poly(olefin sulfone)s.

| Poly(2-methylpentene sulfone) PMPS | Poly(cyclohexene sulfone) PCHS |
|---|--|
|  |  |
| T _g ^a : 78 °C | T _g ^a : 118 °C |
| T _{ceiling} : -31 °C ⁴⁸ | T _{ceiling} : 26 °C ⁴⁸ |
| M _{peak} : 530 kg/mol | M _{peak} : 246 kg/mol |

^{a)} Measured by DMA at 2 Hz and 2K/min analyzing the peak of the tan delta.

Figure 4.5.1 shows the measured TGA curves for PMPS, PCHS, and the reference material PPA and Table 4.5.2 corresponding temperatures of 50 % weight loss. All polymers show a complete decomposition below 350 °C. While PMPS shows a very similar decomposition behavior as compared to PPA, the decomposition of PCHS occurs at higher temperatures, with an approximately 60 °C higher $T_{-50 \text{ wt}\%}$. Both poly(olefin sulfone)s show a pronounced two-step degradation in the TGA curve, for PMPS the first step is finished at about 170 °C and for PCHS at about 220 °C.

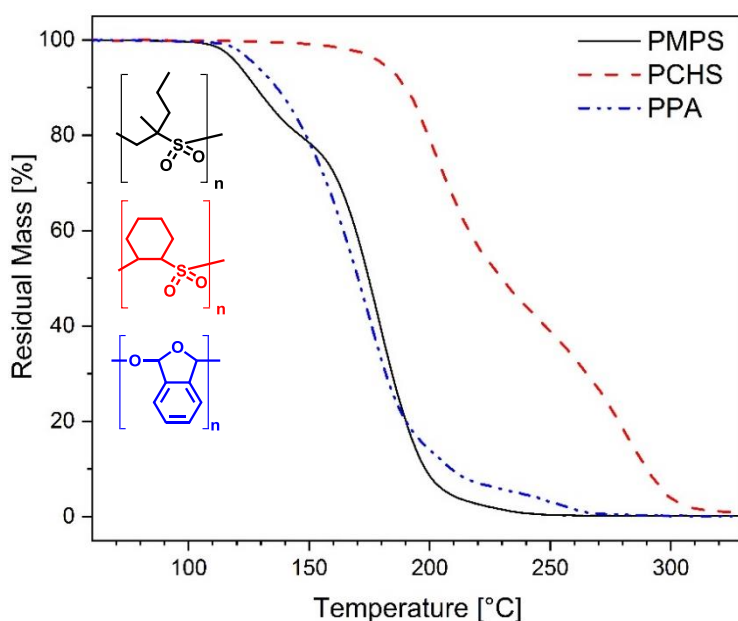


Table 4.5.2: $T_{-50 \text{ wt}\%}$ values for investigated polymers.

| Polymer | $T_{-50 \text{ wt}\%}$ ^{b)} |
|--------------------|--------------------------------------|
| PMPS | 175 °C |
| PCHS | 230 °C |
| PPA (reference) | 170 °C |

^{b)} measured by TGA with 10 K/min under air atmosphere.

Figure 4.5.1: TGA curves of investigated poly(olefin sulfone)s (PMPS and PCHS) and PPA as reference material.

4.5.4.2. Chemically amplified decomposition

The poly(olefin sulfone) decomposition is known to be catalyzed by bases. UV-lithography has been reported using poly(olefin sulfone)s along with photo base generators.⁴³⁻⁴⁵ In t-SPL, however, the stimulus leading to the reaction in the resist material is thermal energy rather than UV-exposure. Therefore, a thermal rather than a photo base generator is needed to boost the decomposition of the polymer. Quaternary ammonium salts are known to undergo decomposition at elevated temperatures to yield a basic tertiary amine. A variety of quaternary ammonium salts with different alkyl chains and counter ions is readily available on the market. To reveal the influence of alkyl chains and counter ions tetraalkylammonium halides with alkyl chains from C₁ to C₆ and chloride, bromide, and iodide counter ions are

investigated herein. Results of mixtures with further salts can be seen in the Supporting Information.

Figure 4.5.2 exemplarily shows the TGA curves for neat poly(cyclohexene sulfone) (PCHS), for neat tetrabutylammonium chloride (TBAC), for a mixture of 6.2 wt% TBAC in PCHS as well as the heat flow during the TGA measurement (SDTA) of pure TBAC to show the melting and decomposition behavior of this salt. It is observable that the addition of the salt has a strong effect on the decomposition behavior of the polymer. The TGA curve of the mixture shows a one-step decomposition occurring at much lower temperatures as compared to neat PCHS. The pure TBAC salt shows a melting point at 75 °C and a beginning decomposition at about 180 °C with most of the weight loss occurring around 200 – 220 °C. Pure PCHS starts to decompose in a similar temperature range, at about 180 – 200 °C, with most of the weight loss occurring in a broad range between 200 and 300 °C. The addition of TBAC to PCHS shifts the beginning of the decomposition to less than 150 °C, with most of the weight loss occurring between 150 and 210 °C. Most of the decomposition of the mixture is already finished when the neat salt component has not yet been decomposed to the base. We assume that some of the thermally generated base molecules are already set free at temperatures of about 150 °C and are being consumed by a reaction with the polymer. The continuous uptake of the reaction product leads to a shift in the equilibrium onto the product side, hence the salt is decomposing in the polymer at lower temperatures as compared to the neat material.

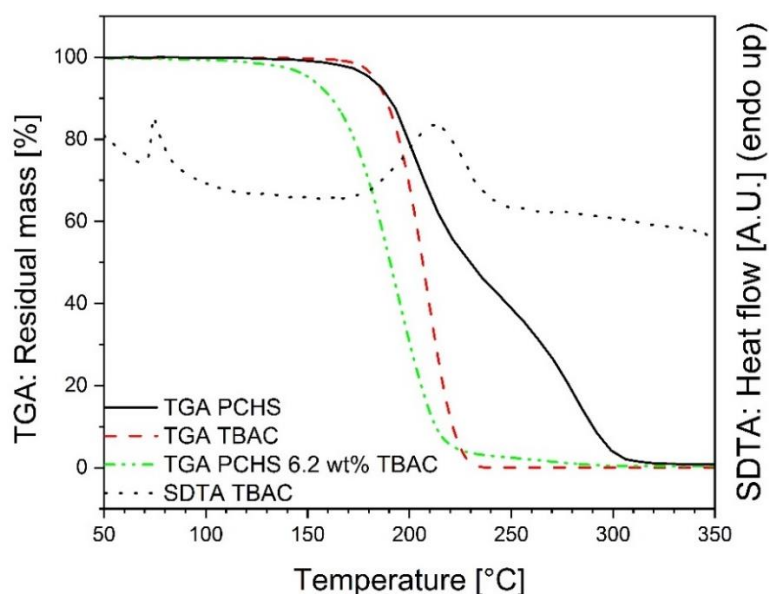


Figure 4.5.2: TGA curves (left Y-axis) of neat PCHS (black line), neat TBAC (red line), a mixture of PCHS with 6.2 wt% TBAC (green line), and the SDTA of TBAC (right Y-axis, dotted line).

Figure 4.5.3 shows the TGA curves of PCHS with added tetraalkylammonium halide salts. In Figure 4.5.3A, tetraalkylammonium chlorides with alkyl chains from C₁ to C₆ are shown. Figure 4.5.3B shows tetrabutylammonium halide salts with chloride, bromide, and iodide counter ions. All salt concentrations were calculated to yield the same molar concentration of the salt, which was selected to be equal to the concentration in a mixture with 5 wt% tetrapropylammonium chloride.

From Figure 4.5.3A it is observable that the decomposition temperature is strongly affected by the length of the alkyl chain, with a decreasing decomposition temperature for increasing chain lengths. This difference is rather strong for C₁ to C₄, while mixtures with salts of C₄, C₅, and C₆ have a very similar decomposition behavior. In Figure 4.5.3B the influence of the halide counter ion on the decomposition is shown. While mixtures with bromide and iodide salts have a very similar decomposition behavior, mixtures with chloride salts show a significantly lower decomposition temperature.

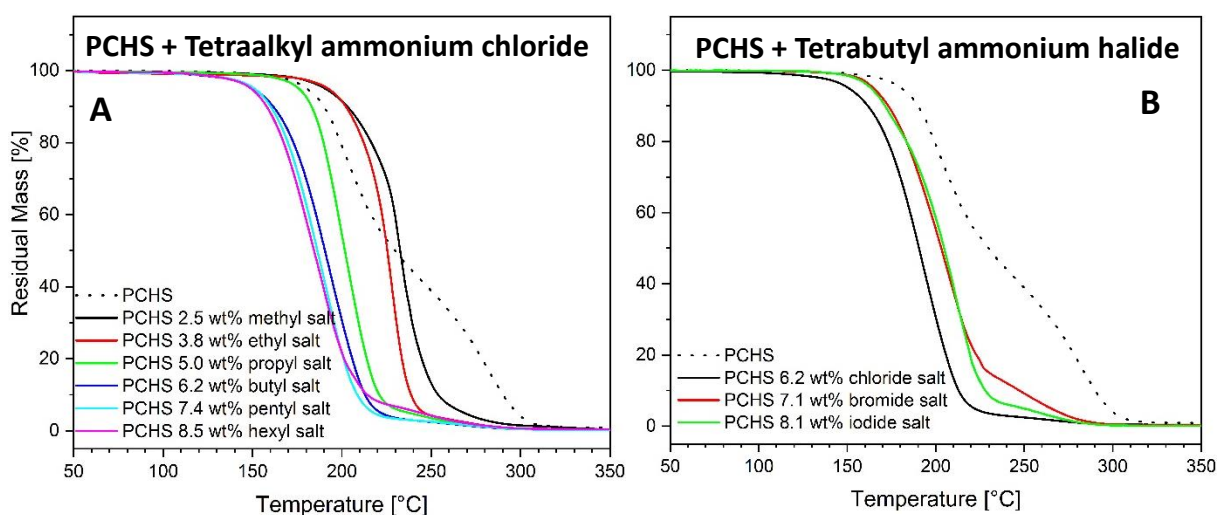


Figure 4.5.3: A: TGA curves for PCHS with added tetraalkylammonium chlorides (solid lines) and neat PCHS (dotted line). B: TGA curves for PCHS with added tetrabutylammonium halide (solid lines) and neat PCHS (dotted line). All salts have the same molar concentration of 3.35 mol% according to the polymer repeating unit.

Figure 4.5.4A gives an overview of the T_{-50 wt%} values measured for all tetraalkylammonium halides with alkyl chains from C₁ to C₆ and chloride, bromide, and iodide counter ions. The trends extracted from Figure 4.5.3 are generally confirmed for mixtures with all investigated salts. The best performances are given for mixtures with tetraalkylammonium chloride with the alkyl chain being either butyl, pentyl, or hexyl. Their T_{-50 wt%} values are 190 °C, 186 °C, and 184 °C, respectively, which is close to the T_{-50 wt%} values as observed for PMPS or PPA (compare

with Table 4.5.2). Mixtures with other tetraalkylammonium salts such as ones with oxidizing side groups (nitrate, perchlorate) have also been measured, however, the results were not as promising. These results can be seen in the Supporting Information.

Figure 4.5.4B shows the dependence of the decomposition behavior on the concentration of the salt, exemplarily shown for tetrabutylammonium chloride (TBAC). A decreasing decomposition temperature is observed with increasing salt content from about 2 % to 9 % of TBAC. The latter is the lowest decomposition temperature observed in this series, while for a higher concentration, the decomposition temperature slightly increases again. For lower concentrations of about 2 – 4 wt%, the TGA curve shows a pronounced decrease of the slope at about 20 % residual mass, thus complete decomposition occurs only at above 250 °C, whereas for higher concentration, full decomposition is already achieved at 220 °C.

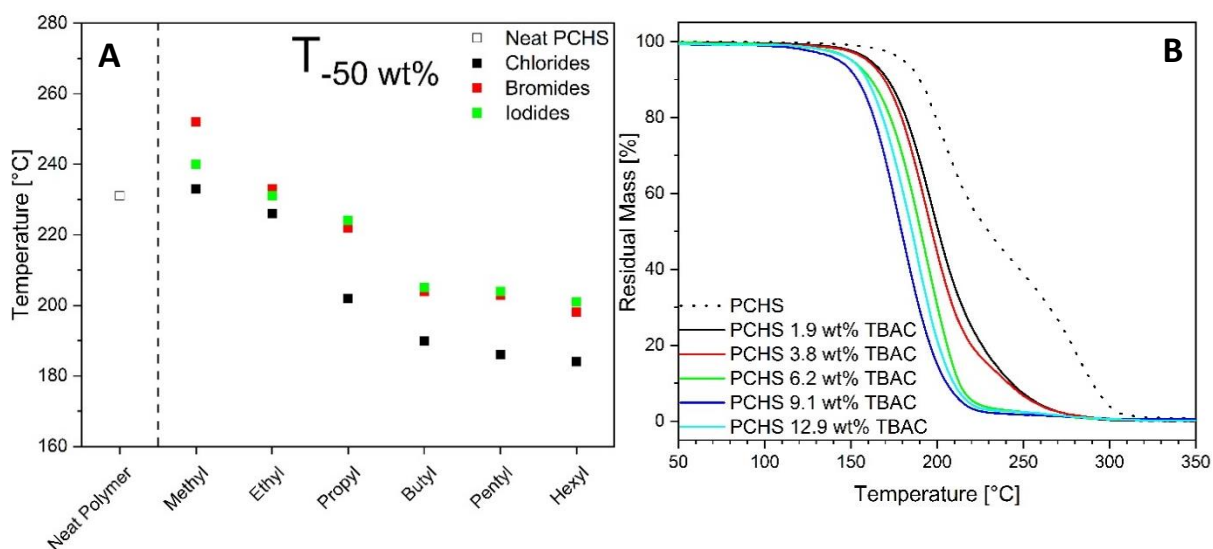


Figure 4.5.4: A: $T_{-50 \text{ wt}\%}$ for neat PCHS and PCHS with 3.35 mol% (according to the number of repeating units) added tetraalkylammonium halide. B: TGA curves for PCHS with added tetrabutyl ammonium chloride of different concentrations (solid lines) and neat PCHS (dotted line).

Figure 4.5.5 shows the TGA curves for PMPS with two concentrations of added TBAC. In contrast to PCHS, a less strong influence of the salt on the decomposition of PMPS is observed. While the decomposition temperature is only slightly affected by the salt, a steeper curve progression is achieved for the PMPS / TBAC mixtures. Generally, a huge impact of any investigated salt on the PMPS decomposition was nowhere observed. This may probably be because most of the polymer is already decomposed when the effect of the salt kicks in.

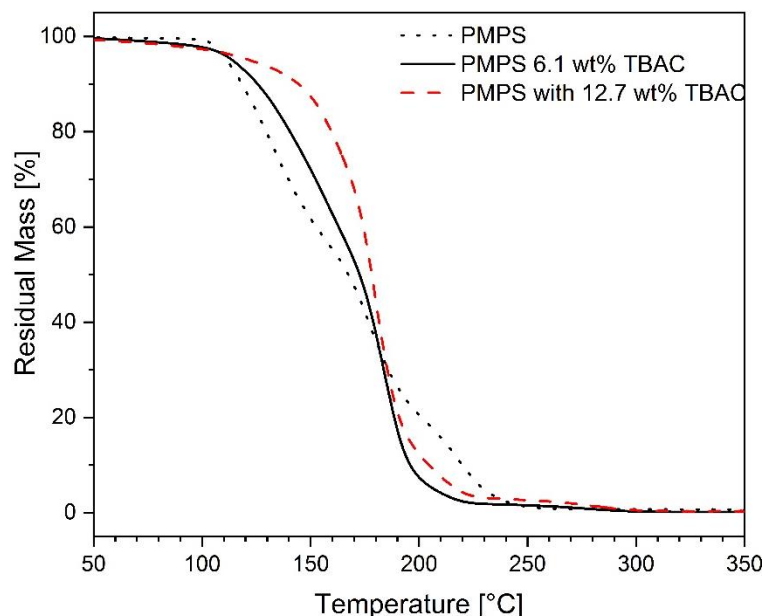


Figure 4.5.5: TGA curves for PMPS with 6.1 wt% and 12.7 wt% of added tetrabutylammonium chloride (solid lines) and neat PMPS (dotted line).

To analyze the mechanism of the decomposition with and without added salt, we performed Scanning Thermal Analysis measurements which are shown and discussed in the Supporting Information.

4.5.4.3. Patterning

In Figure 4.5.6 an image of the Bayreuth Festspielhaus written into PMPS, PCHS, and PCHS + 10 % TAAC, respectively, with a tip temperature of 1000 °C is shown. All images nicely show the details of the building. To evaluate the writing capability of the polymers, these images were patterned with temperatures between 900 °C (800 °C for PMPS) and 1200 °C. The standard deviation of the height sensor for the area of the image where the feedback loop was adjusted was calculated for all different temperatures. These results are shown in Table 4.5.3. With a tip temperature of 1000 °C the lowest standard deviation is observed for all systems. At 1000 °C and above, the writing behavior of all polymers is very similar. The lowest standard deviation is observed for PMPS, followed by PCHS, while for the system PCHS / TAAC the highest standard deviation is observed. At 900 °C, all images show “hiccups”, i.e. defects usually associated with the loss of collected material at the tip. These “hiccups” indicate incomplete resist evaporation. This effect is higher for both PCHS containing systems.

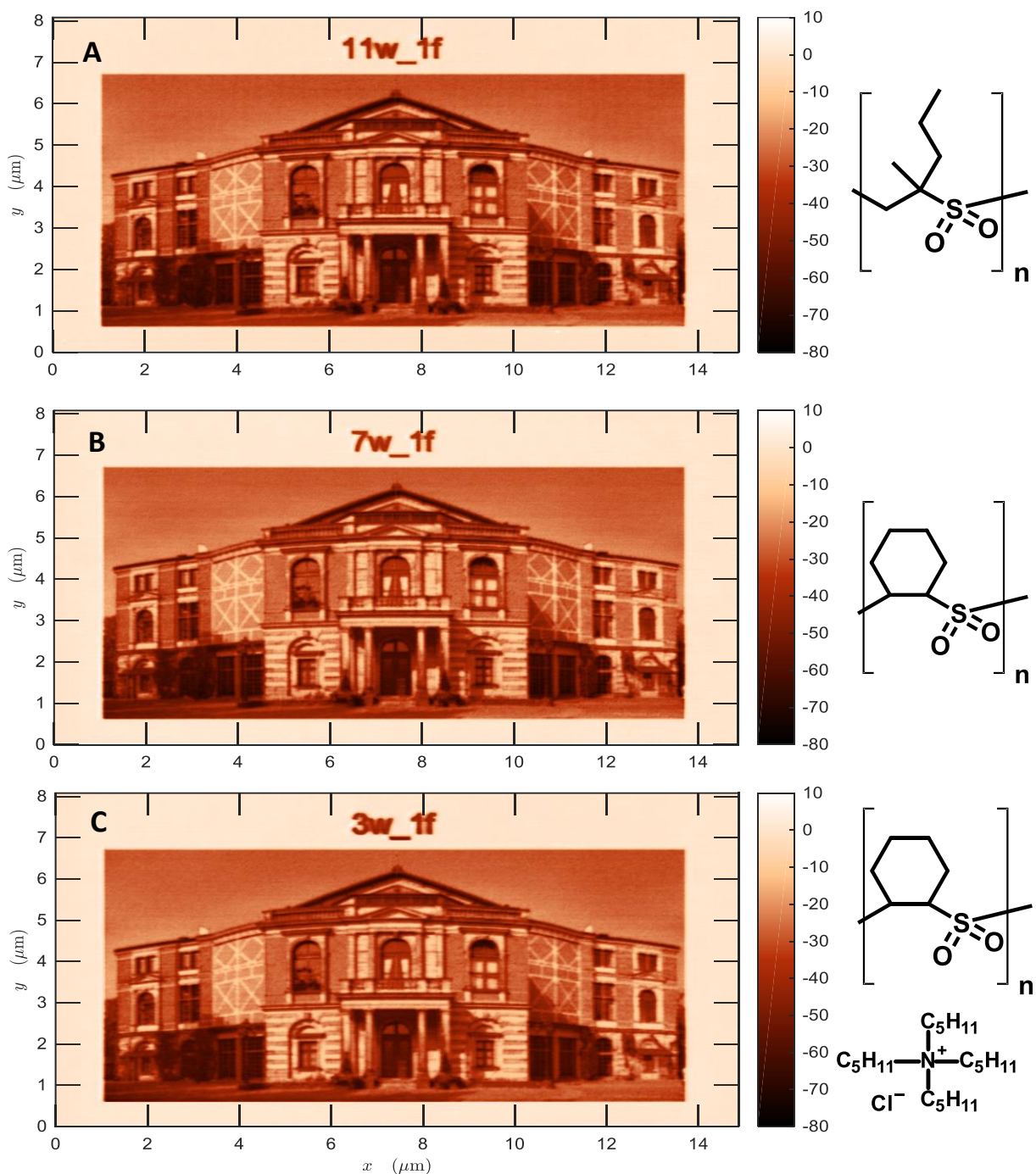


Figure 4.5.6: 3D image of the Bayreuth Festspielhaus written with 1000 °C tip temperature into A: PMPS; B: PCHS; and C: PCHS + TAAC. Original Photo © Guido Radig under CC BY-SA 3.0.

In contrast to the similar pattern quality of all polymers, the endurance behavior is different. While with PMPS many images can be patterned in series, for the PCHS / TAAC mixture a decrease in pattern quality is observed after few images. This decrease is permanent and cannot be fixed by several tip cleaning events. The assumed tip contamination was confirmed by an SEM image of the tip which is shown in Figure 4.5.7. Clearly, a build-up of material at the radius of the tip can be seen. Neither a change from the pentyl salt TAAC to the butyl salt

TBAC nor higher tip temperatures could prevent tip contamination. As both, the polymer and the salt, are decomposed completely in the TGA below 350 °C we assume a reaction of the salt decomposition products with the tip as the most reasonable explanation for tip contamination. Neat PCHS behaves much better in terms of endurance as compared to the mixture with TAAC, however, “hiccups” and pattern defects are observed regularly indicating a steady build-up of material at the tip. In conclusion, PMPS was identified to be the most promising candidate for high-resolution patterning in terms of endurance and pattern quality.

Table 4.5.3: Height sensor standard deviations of the Festspielhaus images taken at different temperatures. Only the area where the feedback-loop was regulated is considered.

| | PMPS | PCHS | PCHS + 10 % TAAC |
|---------|------|------|---------------------|
| 1200 °C | 5.36 | 5.42 | 5.80 |
| 1100 °C | 4.85 | 5.05 | 5.39 |
| 1000 °C | 4.78 | 5.04 | 5.28 |
| 900 °C | 5.77 | 6.89 | 6.49 |
| 800 °C | 5.44 | | |

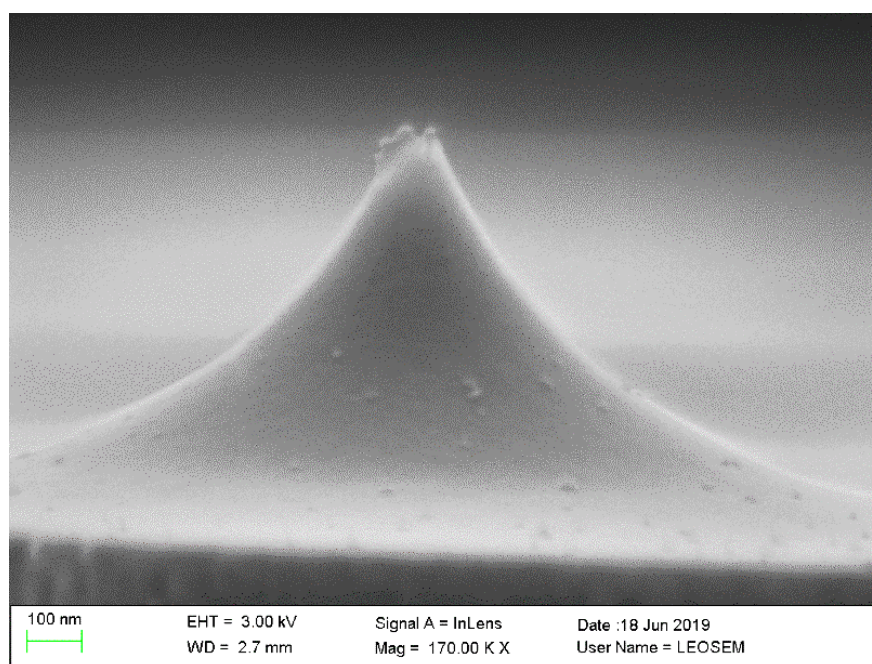


Figure 4.5.7: SEM image of the after the patterning of a PCHS / TBAC mixture.

Contrary to PPA, poly(olefin sulfone)s are not labile in an acidic environment. Stability towards acidic conditions could offer new applications for generated patterns or structures. Figure 4.5.8 shows an image of the Bayreuth Festspielhaus written into PMPS before and after 1 h immersion in a 0.1 M HCl bath. The immersion in the bath does not change the image, all features are still present. A 24 h immersion was conducted as well, however, the acid solution floated the polymer film from the substrate. The patterns were still observable in an optical microscope, but no AFM images could be obtained. For further studies, optimizations have to be done concerning the adhesion of the polymer film to the substrate. As a reference, a PPA film was immersed into 0.1 M HCl solution upon which it disappeared instantaneously.

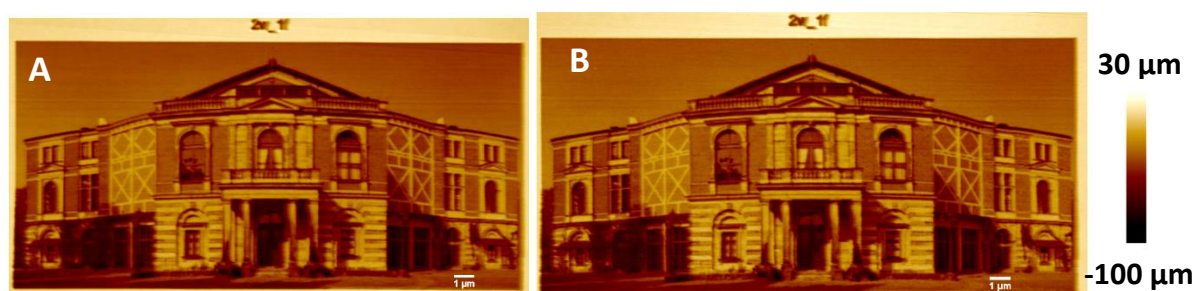


Figure 4.5.8: A: Image of the Bayreuth Festspielhaus written into PMPS. B: The same image after 1 h immersion in 0.1 M HCl ($\text{pH} = 1$). Original Photo © Guido Radig under CC BY-SA 3.0.

As PMPS showed the most promising writing behavior of the investigated polymers and very good endurance, high resolution patterning has been attempted. Between the substrate and the resist, a 5 nm layer of crosslinked polystyrene (x-PS) was deposited. The polystyrene acts as a heat buffer layer, as the silicon would withdraw too much thermal energy from the tip during writing, as well as a mechanical buffer layer by preventing the tip from scratching on the hard silicon surface causing tip wear. Furthermore, x-PS as a material is selected as it will not be infiltrated by the later applied Sequential Infiltration Synthesis.

In Figure 4.5.9, a line-and-space pattern written into a PMPS film of 7 nm thickness can be seen as well as the cross-section of the line-and-space pattern of the highest resolution. 10 nm half-pitch could be written 3 nm deep into the polymer, whereas complete removal of the resist, i.e. 7 nm writing depth, was achieved with a resolution of 27 nm half-pitch.

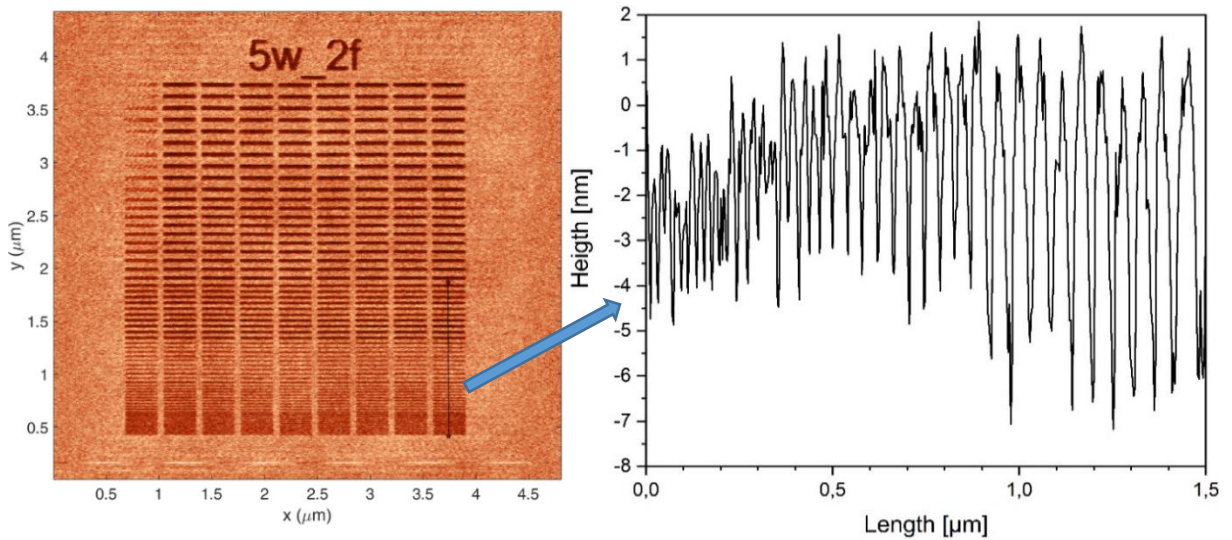


Figure 4.5.9: Line-and-space pattern written into 7 nm PMPS with 1000 °C tip temperature and cross section of the line and space patterns with 10 to 27 nm half pitch.

4.5.4.4. Sequential Infiltration Synthesis

To increase the etch resistance of the aliphatic PMPS, the polymer can be treated with Sequential Infiltration Synthesis (SIS) using standard ALD processes. This process was first documented for PMMA in 2011 by Tseng *et al.*⁴⁹ Certain polymers containing free electron pairs can absorb lewis-acidic precursors such as trimethylaluminum. Subsequent reaction with water yields organo-aluminum species dispersed in the polymer rather than building an Al₂O₃-layer on top of the material, as schematically shown in Figure 4.5.10. By doing so the infiltrated polymer forms a continuous hard mask for the etch process, enabling better pattern transfer into the underlying substrate.

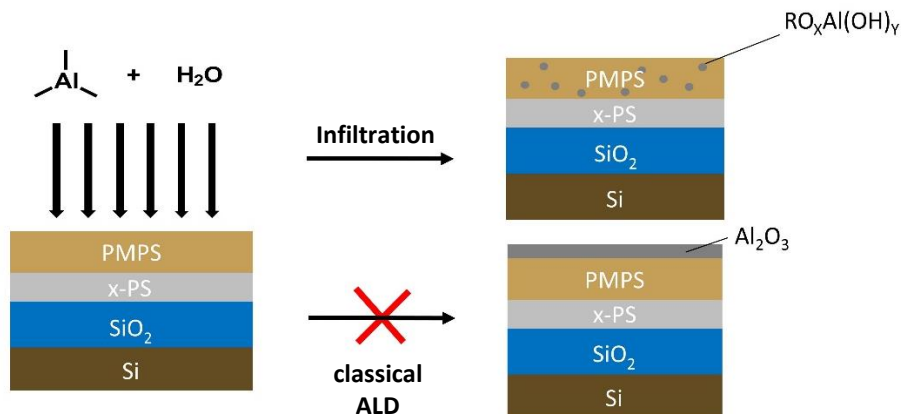


Figure 4.5.10: Scheme of Sequential Infiltration Synthesis using standard ALD processes.

We investigated the influence of SIS on the film thickness at 40 °C (well below T_g of PMPS) and at 80 °C (ca. at T_g of PMPS). This is shown in Figure 4.5.11. Completely different behaviors are observed for both temperatures. For infiltration at 80 °C with few cycles of SIS, the polymer layer thickness increases by a much higher extent than what would be expected for standard ALD. The expected layer thickness increase would be at 0.8 Å/cycle. However, up to 15 cycles, the average increase is 4.1 Å/cycle. With more than 15 cycles, the increase in the layer thickness is reduced to 1 Å/cycle, which is close to the theoretical 0.8 Å/cycle. For SIS at 40 °C, the layer thickness is increased less than for 80 °C, 2.7 Å/cycle up to 25 cycles. With more than 25 cycles, the increase is at a tremendous 10 Å/cycle.

For both temperatures, with 30 or more cycles of SIS, the film gets partly destroyed by forming holes during the often-repeated infiltration. Therefore we assume a softening and foaming behavior of the film during the often-repeated infiltrations at 40 °C which would explain the drastic increase of the layer thickness. At 80 °C, close to T_g , the film rather collapses and hence the increase in layer thickness is reduced. Therefore, 25 cycles of ALD were selected as the most promising number of cycles to achieve maximum etch resistance without the destruction of the film. Etch investigations demonstrate that the etch resistance of the infiltrated film is drastically increased. While without SIS, the polymer film vanishes within few seconds under plasma treatment disabling all pattern transfer, the selectivity against SiO₂ is increased to 3.75 after 25 cycles SIS at 80 °C.

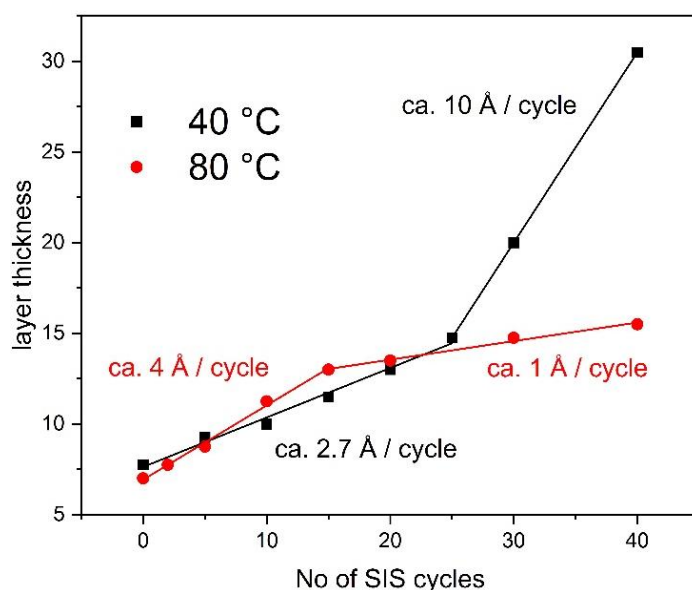


Figure 4.5.11: Layer thicknesses increase of a 7 nm PMPS film after different numbers of SIS cycles at 40 °C and 80 °C.

The pattern stability of the applied polymer material during the SIS process is a crucial requirement for a successful pattern transfer. As SIS is an exothermic process and thin layers usually show higher molecular mobility as compared to bulk material, pattern quality may suffer during SIS. The influence of 25 cycles of SIS at 40 °C on a line and space pattern in a 7 nm thin PMPS film is depicted in Figure 4.5.12. The infiltrated patterns still show all structural features that are also present in the neat patterns before SIS cycling. However, line-and-space patterns show an increased depth of 9 – 10 nm due to the higher thickness of the polymer film after infiltration.

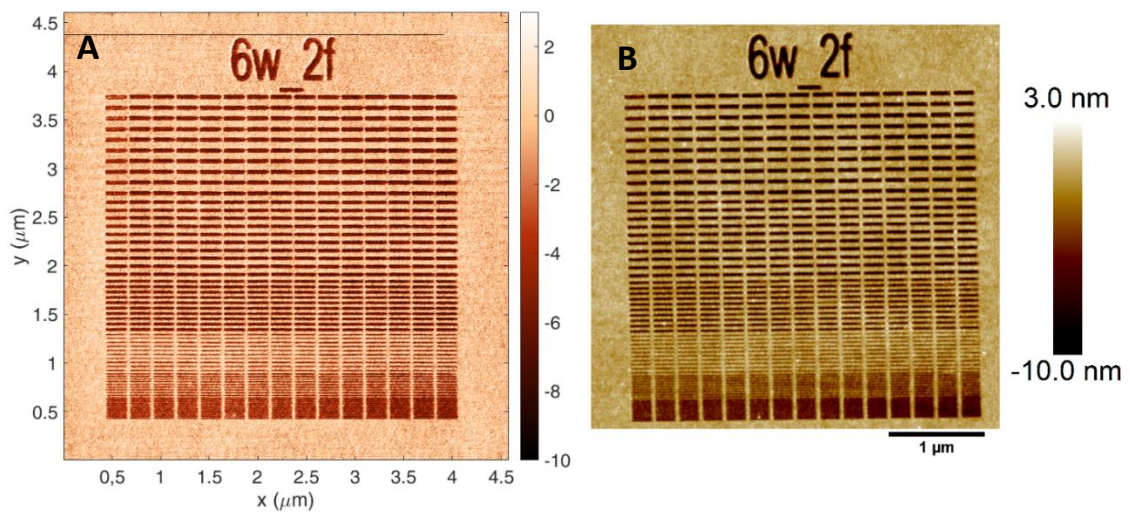


Figure 4.5.12: A: Line and space pattern written into 7 nm PMPS. Measured with t-SPL tool during patterning. B: The same pattern, but after 25 cycles of Al_2O_3 -SIS, measured with AFM.

4.5.5. Conclusion and outlook

Two different poly(olefin sulfone)s, poly(2-methyl-1-pentene sulfone) and poly(cyclohexene sulfone), were synthesized, characterized, and their nano-patterning capabilities for t-SPL investigated. Both polymers exhibit a writing sensitivity comparable to that of PPA, the standard resist material used in t-SPL. Tetraalkylammonium chlorides can be used as thermal base generators thereby decreasing the decomposition temperature of poly(cyclohexene sulfone). However, this does not result in a higher writing sensitivity but generates tip contaminations.

3D-patterning and high-resolution 2D-patterning have been demonstrated, the latter with 10 nm half-pitch lines written 3 nm into PMPS, and 27 nm half-pitch lines were written down

to the ground of the resist material. Acid resistivity of the polymer has been demonstrated by immersion of a patterned thin film in 0.1 M HCl solution, after which the pattern remained unspoiled.

Using SIS, an etch-resistant hard mask was prepared that shows a selectivity of 3.75 against SiO₂. In the next future, reactive-ion etching of the obtained structures has to be carried out to demonstrate the transfer behavior of high-resolution patterns into the substrate.

4.5.6. Acknowledgement

STA measurements were carried out by Ingrid Otto at the chair of Electrochemical Process Engineering at the University of Bayreuth. F.K. acknowledges support from the Elite Network of Bavaria (ENB) within the Elite Study Program Macromolecular Science.

4.5.7. References

- [1] M. Neisser and S. Wurm, *ITRS lithography roadmap: 2015 challenges*, *Av. Opt. Technol.*, **2015**, 4, 9425.
- [2] K. Matsuzawa, T. Fujii, S. Matsumara, T. Yamada, Y. Komuro, D. Kawana and K. Ohmori, *Challenges to Overcome Trade-Off between High Resolution and High Sensitivity in EUV lithography*, *J. Photopoly. Sci. Technol.*, **2016**, 29, 489–493.
- [3] H. Yamamoto, Y. Vesters, J. Jiang, D. de Simone, G. Vandenberghe and T. Kozawa, *Role of Metal Sensitizers for Sensitivity Improvement in EUV Chemically Amplified Resist*, *J. Photopoly. Sci. Technol.*, **2018**, 31, 747–751.
- [4] P. de Bisschop, *Stochastic effects in EUV lithography: random, local CD variability, and printing failures*, *J. Micro/Nanolith. MEMS MOEMS*, **2017**, 16, 1.
- [5] D. de Simone, A.-M. Goethals, F. van Roey, T. Zheng, P. Foubert, E. Hendrickx, G. Vandenberghe and K. Ronse, *Progresses and Challenges of EUV Lithography Materials*, *J. Photopoly. Sci. Technol.*, **2014**, 27, 601–610.
- [6] N. Fu, Y. Liu, X. Ma and Z. Chen, *EUV Lithography: State-of-the-Art Review*, *J. Microelectron. Eng*, **2019**, 2, 1–6.
- [7] R. Garcia, A. W. Knoll and E. Riedo, *Advanced scanning probe lithography*, *Nat. Nanotechnol.*, **2014**, 9, 577–587.
- [8] T. R. Groves, D. Pickard, B. Rafferty, N. Crosland, D. Adam and G. Schubert, *Maskless electron beam lithography: prospects, progress, and challenges*, *Microelectron. Eng.*, **2002**, 61-62, 285–293.
- [9] T. Kozawa and T. Tamura, *Theoretical study on trade-off relationships between resolution, line edge roughness, and sensitivity in photomask production by electron beam lithography*, *Jpn. J. Appl. Phys.*, **2019**, 58, 76501.
- [10] W. Mi and P. Nillius, *Efficient proximity effect correction method based on multivariate adaptive regression splines for grayscale e-beam lithography*, *J. Vac. Sci. Technol. B*, **2014**, 32, 31602.

- [11] K. M. Satyalakshmi, A. Olkhovets, M. G. Metzler, C. K. Harnett, D. M. Tanenbaum and H. G. Craighead, *Charge induced pattern distortion in low energy electron beam lithography*, J. Vac. Sci. Technol. B, **2000**, *18*, 3122.
- [12] R. K. Dey and B. Cui, *Stitching error reduction in electron beam lithography with in-situ feedback using self-developing resist*, J. Vac. Sci. Technol. B, **2013**, *31*, 06F409.
- [13] D. M. Eigler and E. K. Schweizer, *Positioning single atoms with a scanning tunnelling microscope*, Nature, **1990**, *344*, 524–526.
- [14] A. W. Knoll, D. Pires, O. Coulembier, P. Dubois, J. L. Hedrick, J. Frommer and U. Duerig, *Probe-based 3-D nanolithography using self-amplified depolymerization polymers*, Adv. Mat., **2010**, *22*, 3361–3365.
- [15] O. Coulembier, A. Knoll, D. Pires, B. Gotsmann, U. Duerig, J. Frommer, R. D. Miller, P. Dubois and J. L. Hedrick, *Probe-Based Nanolithography: Self-Amplified Depolymerization Media for Dry Lithography*, Macromolecules, **2010**, *43*, 572–574.
- [16] Y. K. Ryu Cho, C. D. Rawlings, H. Wolf, M. Spieser, S. Bisig, S. Reidt, M. Sousa, S. R. Khanal, T. D. B. Jacobs and A. W. Knoll, *Sub-10 Nanometer Feature Size in Silicon Using Thermal Scanning Probe Lithography*, ACS Nano, **2017**, *11*, 11890–11897.
- [17] H. Wolf, C. Rawlings, P. Mensch, J. L. Hedrick, D. J. Coady, U. Duerig and A. W. Knoll, *Sub 20 nm Silicon Patterning and Metal Lift-Off Using Thermal Scanning Probe Lithography*, J. Vac. Sci. Technol. B, **2015**, *33*.
- [18] J.-F. d. Marneffe, B. T. Chan, M. Spieser, G. Vereecke, S. Naumov, D. Vanhaeren, H. Wolf and A. W. Knoll, *Conversion of a Patterned Organic Resist into a High Performance Inorganic Hard Mask for High Resolution Pattern Transfer*, ACS nano, **2018**, *12*, 11152–11160.
- [19] P. C. Paul, A. W. Knoll, F. Holzner, M. Despont and U. Duerig, *Rapid turnaround scanning probe nanolithography*, Nanotechnology, **2011**, *22*, 275306.
- [20] C. Rawlings, H. Wolf, J. L. Hedrick, D. J. Coady, U. Duerig and A. W. Knoll, *Accurate Location and Manipulation of Nanoscaled Objects Buried under Spin-Coated Films*, ACS Nano, **2015**, *9*, 6188–6195.

- [21] C. Rawlings, Y. K. Ryu, M. Rüegg, N. Lassaline, C. Schwemmer, U. Duerig, A. W. Knoll, Z. Durrani, C. Wang, D. Liu and M. E. Jones, *Fast turnaround fabrication of silicon point-contact quantum-dot transistors using combined thermal scanning probe lithography and laser writing*, *Nanotechnology*, **2018**, *29*, 505302.
- [22] S. Gottlieb, M. Lorenzoni, L. Evangelio, M. Fernández-Regúlez, Y. K. Ryu, C. Rawlings, M. Spieser, A. Knoll and F. Perez-Murano, *Corrigendum: Thermal scanning probe lithography for the directed self-assembly of block copolymers*, *Nanotechnology*, **2017**, *28*, 289501.
- [23] S. T. Zimmermann, D. W. R. Balkenende, A. Lavrenova, C. Weder and J. Brugger, *Nanopatterning of a Stimuli-Responsive Fluorescent Supramolecular Polymer by Thermal Scanning Probe Lithography*, *ACS Appl. Mater. Interfaces*, **2017**, *9*, 41454–41461.
- [24] S. T. Zimmermann, *Nanoscale Lithography and Thermometry with Thermal Scanning Probes*, Lausanne, **2018**.
- [25] C. Schwemmer, S. Fringes, U. Duerig, Y. K. Ryu and A. W. Knoll, *Experimental Observation of Current Reversal in a Rocking Brownian Motor*, *Phys. Rev. Lett.*, **2018**, *121*, 104102.
- [26] M. J. Skaug, C. Schwemmer, S. Fringes, C. D. Rawlings and A. W. Knoll, *Nanofluidic rocking Brownian motors*, *Science*, **2018**, *359*, 1505–1508.
- [27] S. W. Tang, M. H. Uddin, W. Y. Tong, P. Pasic, W. Yuen, H. Thissen, Y. W. Lam and N. H. Voelcker, *Replication of a Tissue Microenvironment by Thermal Scanning Probe Lithography*, *ACS Appl. Mater. Interfaces*, **2019**, *11*, 18988–18994.
- [28] J. M. Schwartz, O. Phillips, A. Engler, A. Sutlief, J. Lee and P. A. Kohl, Stable, *High-Molecular-Weight Poly(phthalaldehyde)*, *J. Polym. Sci. Part A: Polym. Chem.*, **2017**, *55*, 1166–1172.
- [29] W. G. Barb, *The Copolymerization of Styrene and Sulphur Dioxide. I. Properties and Composition of the Copolymer, and Evidence for the Existence of a Styrene/Sulphur Dioxide Complex*, *Proc. Roy. Soc. A: Math. Phys.*, **1952**, *212*, 66–80.

- [30] E. H. Hill and J. R. Caldwell, *Polysulfones of norbornene and derivatives*, J. Polym. Sci. A Gen. Pap., **1964**, 2, 1251–1255.
- [31] J. Herz, D. Hummel and C. Schneider, *Die strahlenchemische Darstellung von Polystyrolsulfonen bei verschiedenen Temperaturen. II. Teil: Die Reaktion bei tiefen Temperaturen*, Macromol. Chem. Phys., **1963**, 64, 95–109.
- [32] J. Herz, D. Hummel and C. Schneider, *Die strahlenchemische Darstellung von Polystyrolsulfonen bei verschiedenen Temperaturen. I. Teil: Die Reaktion bei Zimmertemperatur (30°C)*, Macromol. Chem. Phys., **1963**, 63, 12–29.
- [33] R. E. Yardley, A. R. Kenaree and E. R. Gillies, *Triggering Depolymerization: Progress and Opportunities for Self-Immolative Polymers*, Macromolecules, **2019**, 52, 6342–6360.
- [34] M. J. Bowden and L. F. Thompson, *Electron irradiation of poly(olefin sulfones). Application to electron beam resists*, J. Appl. Polym. Sci., **1973**, 17, 3211–3221.
- [35] D. O. Hummel and H.-D. R. Schüddemage, *Thermischer Abbau von Polysulfonen*, Koll. Z. Z. Polym., **1966**, 210, 97–102.
- [36] M. A. Naylor and A. W. Anderson, *Thermal Stability of Various Olefin-SO₂ Polymers*, J. Am. Chem. Soc., **1954**, 76, 3962–3965.
- [37] J. R. Brown and J. H. O'Donnell, *Radiolysis of Poly(butene-1 sulfone) and Poly(hexane-1 sulfone)*, Macromolecules, **1972**, 5, 109–114.
- [38] M. J. Bowden and L. F. Thompson, *Polystyrene(Styrene Sulfone) - A sensitive Ion-Millable Positive Electron Beam Resist*, J. Electrochem. Soc., **1974**, 121, 1620–1623.
- [39] M. J. Bowden and L. F. Thompson, *Effect of olefin structure on the vapor-development of poly(olefin sulfones) under electron irradiation*, Polym. Eng. Sci., **1977**, 17, 269–273.
- [40] H. Hiraoka and L. W. Welsh in *Polymers in Electronics*, ed. T. Davidson, American Chemical Society, Washington, D.C., **1984**, 55–64.
- [41] J. M. Lobez and T. M. Swager, *Disassembly of Elastomers: Poly(olefin sulfone)-Silicones with Switchable Mechanical Properties*, Macromolecules, **2010**, 43, 10422–10426.

- [42] J. M. Lobez and T. M. Swager, *Radiation detection: resistivity responses in functional poly(olefin sulfone)/carbon nanotube composites*, *Angew. Chem. Int. Ed.*, **2010**, *49*, 95–98.
- [43] T. Sasaki, T. Kondo, M. Noro, K. Saida, H. Yaguchi and Y. Naka, *Photoinduced depolymerization in poly(olefin sulfone) films comprised of volatile monomers doped with a photobase generator*, *J. Polym. Sci. A Polym. Chem.*, **2012**, *50*, 1462–1468.
- [44] T. Sasaki and H. Yaguchi, *Photoinduced unzipping depolymerization of poly(olefin sulfone)s possessing photobase generator and base amplifier*, *J. Polym. Sci. A Polym. Chem.*, **2009**, *47*, 602–613.
- [45] H. Yaguchi and T. Sasaki, *Photoinduced Depolymerization of Poly(olefin sulfone)s Possessing Photobase Generating Groups in the Side Chain*, *Macromolecules*, **2007**, *40*, 9332–9338.
- [46] K. J. Lawrie, I. Blakey, J. P. Blinco, H. H. Cheng, R. Gronheid, K. S. Jack, I. Pollentier, M. J. Leeson, T. R. Younkin and A. K. Whittaker, *Chain scission resists for extreme ultraviolet lithography based on high performance polysulfone-containing polymers*, *J. Mater. Chem.*, **2011**, *21*, 5629.
- [47] M. J. Bowden, L. F. Thompson and W. Robinson, *Thermal degradation of poly(1-butene sulfone)*, *Macromolecules*, **1982**, *15*, 1417–1422.
- [48] S. R. Sandler and W. Karo, *Polymer Syntheses*, Academic Press, New York, **1980**.
- [49] Y.-C. Tseng, Q. Peng, L. E. Ocola, D. A. Czaplewski, J. W. Elam and S. B. Darling, *Enhanced polymeric lithography resists via sequential infiltration synthesis*, *J. Mater. Chem.*, **2011**, *21*,

4.5.8. Supporting Information

4.5.8.1. Size-exclusion chromatography

Figure 4.5.13 shows the SEC chromatogram of PMPS and PCHS. Both polymers show a similarly broad molecular weight distribution. Peak molecular weight of PCHS is 246 kg/mol and of PMPS 530 kg/mol. The calibration of the column ends at 2,000 kg/mol.

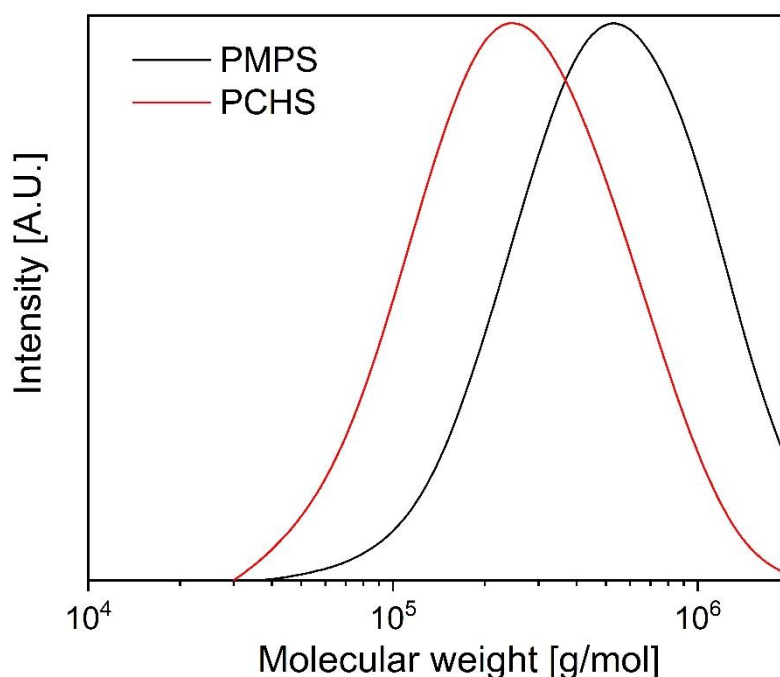


Figure 4.5.13: Size-exclusion chromatogram of PMPS and PCHS.

4.5.8.2. Scanning thermal analysis

In order to understand the influence of the TBAC concerning the decomposition of the PCHS, scanning thermal analysis (STA) measurements have been conducted, where the decomposition products are analyzed by mass spectrometry and FTIR spectroscopy. Figure 4.5.14 shows the mass traces of the STA measurements for neat PCHS (Figure 4.5.14A, left) and for a mixture of PCHS and 6.19 % TBAC (Figure 4.5.14B, right).

For the STA of neat PCHS, all mass traces with significant peaks are shown. A strong increase in the intensity of most signals at the beginning decomposition can be observed above 120 °C. The peak of these signals is at about 200 °C, after which a slow decrease in the signal intensity takes place. Above 300 °C, where a complete material decomposition is observed in TGA, the STA signal intensity decreases quickly. The m/z numbers of those signals can be explained as

fragments or the M^+ -signal of the two monomers. (Note: The molar mass of cyclohexene is 82 g/mol, the molar mass of SO_2 is 64 g/mol). However, the intensity of a couple of signals ($m/z = 58, 78, 84, 94, 110$) increases above 250 °C. This is the same temperature range where the step in the TGA curve of neat PCHS is observed. It can be noted that the fragments with $m/z = 84, 94,$ and 110 are heavier than any of the two monomers of the polymer. Therefore we suggest that other reactions besides a defined decomposition into monomers takes place.

In Figure 4.5.14B, all mass traces that are already shown in Figure 4.5.14A are depicted. Except for an earlier increase of the intensity, up to 200 °C the curves look very similar to the ones for neat PCHS. However, there is already a strong decrease in intensity above 200 °C. Additionally, the signals that only appeared at above 250 °C in the neat PCHS measurement do not have a higher intensity than typical background scattering.

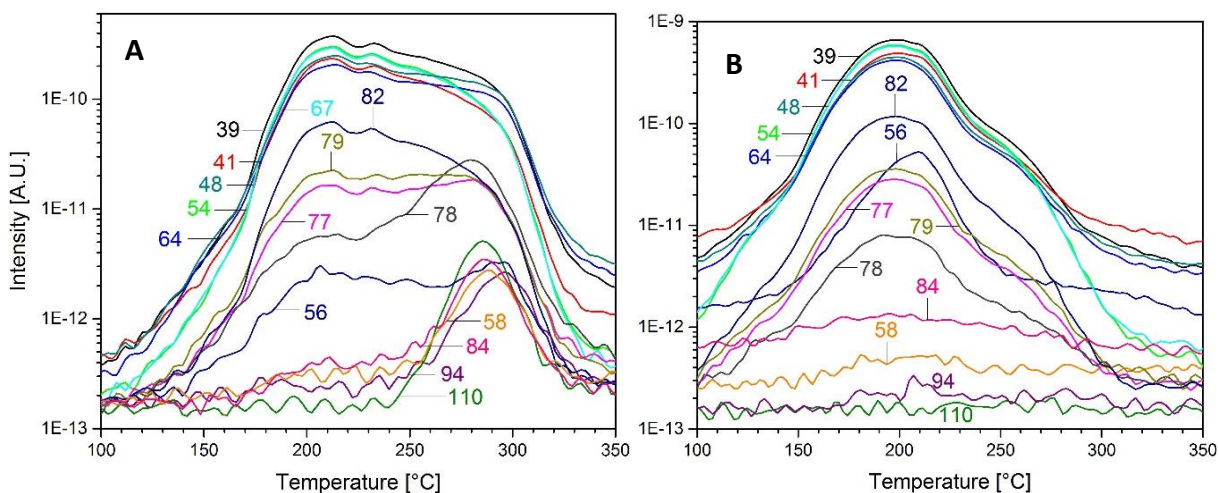


Figure 4.5.14: A: STA mass traces for neat PCHS. B: STA mass traces for PCHS containing 6.2 % TBAC.

A further hint to the nature of the formed decomposition products can be given by the FTIR spectra of the decomposition products. Figure 4.5.15A shows the FTIR spectra that have been recorded during the decomposition of neat PCHS at 203 °C and 302 °C, respectively. In the spectrum recorded at 203 °C, all of the peaks can be either assigned to cyclohexene (the peaks below 1100 cm^{-1} , at 1440 cm^{-1} , and between 2800 cm^{-1} and 3100 cm^{-1}) or to SO_2 (at 1170 cm^{-1} and 1380 cm^{-1}). The spectrum recorded at 302 °C also shows all the peaks observed at 203 °C and additionally a pronounced peak at 1710 cm^{-1} . In Figure 4.5.15B, the normalized intensity of the FTIR signal at 1710 cm^{-1} is compared to the mass trace of $m/z = 58$ from the neat PCHS and the PCHS + TBAC measurement. Whereas no peak can be observed in the FTIR signal for

the PCHS + TBAC measurement, the FTIR peak and the mass trace peak from the neat PCHS measurement match each other very well. An FTIR signal of 1710 cm^{-1} is in the region that usually can be assigned to C=O double bonds. A further look into the m/z numbers appearing at above $250\text{ }^{\circ}\text{C}$ in the neat PCHS measurements shows that some of them can be observed as adducts of 16 from other appearing peaks, such as 78, 94, and 110. Therefore, we conclude that the step in TGA during the decomposition of neat PCHS is due to a transition from the elimination pathway to the radical pathway of the depolymerization. The formed radicals may then react with oxygen yielding fragments of higher m/z than the pure monomers. The addition of the base catalyzes the elimination pathway, as described above. This results in a more defined and faster depolymerization which would be beneficial for the writing procedure in t-SPL.

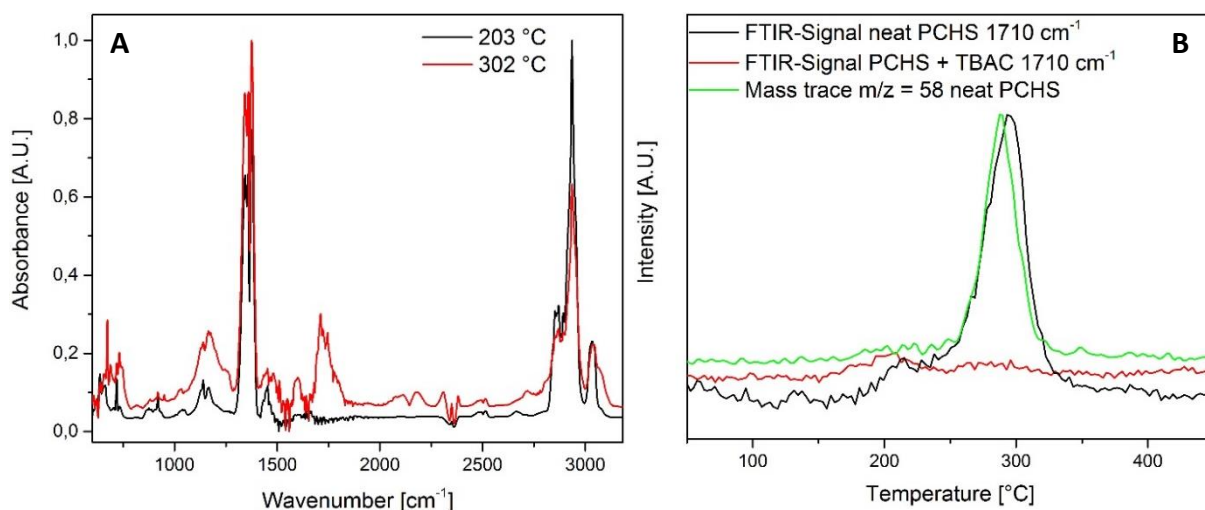


Figure 4.5.15: A: FTIR spectra recorded at $203\text{ }^{\circ}\text{C}$ (black line) and $302\text{ }^{\circ}\text{C}$ (red line). B: Overlay of the relative intensity of the bands at 1710 cm^{-1} of neat PCHS (black line), PCHS + TBAC (red line) and the product of the mass trace of $m/z = 58$ of neat PCHS (green line). The curves of neat PCHS have been normalized to the peak maximum.

4.5.8.3. Further PCHS / salt mixtures

Figure 4.5.16 shows the TGA curves of PCHS with Benzyltriethylammonium chloride (BTEAC), tetrabutylammonium nitrate (TBAN), and tetrabutylammonium perchlorate (TBAPC). Although two highly oxidizing anions were used, none of the compounds improved the decomposition behavior of PCHS compared with the best performing tetraalkylammonium halide. While the mixture with TBAN shows an early onset of its decomposition, it decomposes in several steps. Complete decomposition is reached not before $300\text{ }^{\circ}\text{C}$ for all salts, which is not earlier compared to neat PCHS.

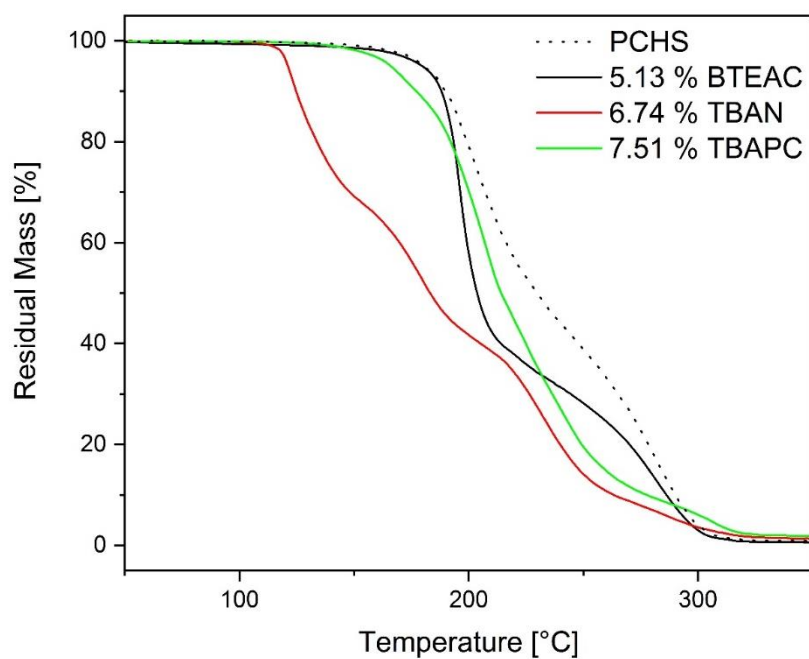


Figure 4.5.16: TGA curves of neat PCHS, PCHS with benzyltriethylammonium chloride (BTEAC), tetrabutylammonium nitrate (TBAN), and tetrabutylammonium perchlorate (TBAPC).

5. Danksagung

Eine solche Doktorarbeit kann natürlich niemals ohne die Hilfe und Mitarbeit anderer Personen fertiggestellt werden. An dieser Stelle möchte ich deshalb denjenigen danken, die – direkt oder indirekt – zum Gelingen dieser Arbeit beigetragen haben.

An erster Stelle gilt mein besonderer Dank meinem Doktorvater Prof. Hans-Werner Schmidt für die hochinteressante, interdisziplinäre Themenstellung, die vielen gewinnbringenden Diskussion sowie das außerordentliche Vertrauensverhältnis. Ich habe in den vergangenen Jahren die Freiheit bei der Ausgestaltung des Themas, die Möglichkeiten der Präsentation meiner Ergebnisse sowie die erstklassige Ausstattung am Arbeitsplatz sehr zu schätzen gewusst!

Auch Dr. Christian Neuber, der mir zu jeder Zeit mit Rat und Tat zur Seite stand, gebührt ein riesiges Dankeschön! Ohne seine Beteiligung an Diskussionen zu wissenschaftlichen Fragestellungen, seiner Hilfe bei technischen und administrativen Problemen und seine fortwährenden Unterstützung und seinen Input wäre diese Arbeit um ein vielfaches schwieriger geworden.

Ein weiteres großes Dankeschön gebührt Prof. Dr. Ernst Rößler, der mir während unserer Kooperation geduldig Relaxationsphänomene und dielektrische Spektroskopie näher gebracht hat. Die produktiven Diskussionen und Besprechungen haben unser Thema stets voran gebracht.

Auf Seiten der AG Rößler gilt mein besonderer Dank meinem Kooperationspartner Thomas Körber. Während unserer Zusammenarbeit konnten wir jeweils viel vom anderen lernen und so das gemeinschaftliche Projekt mit einem tollen Ergebnis beenden. Insbesondere danke ich Thomas für seine geduldigen Erklärungen von physikalischen Phänomenen. Weiterhin haben Rafael Minikejew und Dr. Fathia Mohammed viel zu den Messungen und der Auswertung der dielektrischen Spektren beigetragen. Ohne die beiden hätte ich die ganze Messapparatur wohl nur halb so gut verstanden. Danke auch an Dr. Björn Pötzschner und Max Flämig aus der AG Rößler, die mich gut aufgenommen und unterstützt haben.

Auf Seiten von IBM geht mein besonderer Dank an Dr. Armin Knoll, der unsere Kooperation vorangetrieben hat und meine Besuche in der Schweiz, für die ich sehr dankbar bin,

ermöglichte. Ein weiterer Dank geht an Samuel Bisig von Heidelberg Instruments für die Unterstützung während des Projekts sowie seine t-SPL-Patterns. Danke an Dr. Francesca Ruggeri (IBM) für den Patterntansfer mit RIE sowie Dr. Heiko Wolf (IBM) für die Hilfe im Chemielabor in Rüschlikon. Und selbstverständlich Danke an alle für die freundliche Aufnahme und Unterstützung während der zwei Wochen in der Schweiz.

Mein Auslandsaufenthalt an der Cornell University wäre nicht ohne die Unterstützung von Prof. Christopher K. Ober möglich gewesen. Vielen Dank, dass ich zwei Monate in Ithaca verbringen durfte! Danke auch an Dr. Florian Käfer, der mir sehr geholfen hat, mich dort zurecht zu finden, sowie dem Staff des CNF, die immer hilfsbereit waren und mir bei meiner Arbeit dort stets behilflich waren. Und vielen Dank an alle, die ich in Ithaca kennen lernen durfte.

Ein besonderer Dank geht an Petra Weiß und Christina Wunderlich für Ihre herausragende Unterstützung bei organisatorischen Angelegenheiten jedweder Art.

Danke an unseren IT-Support Alex und Jonas für schnelle Problemlösungen.

Danke an Ingrid Otto vom Lehrstuhl für Werkstoffverfahrenstechnik für die STA-Messungen sowie Markus Hund vom Lehrstuhl für Physikalische Chemie II für die Hilfe bei den AFM-Messungen.

Vielen Dank an das Elitenetzwerk Bayern für die Unterstützung bei meinem Auslandsaufenthalt sowie für die Möglichkeit, spannende Seminare zu besuchen und über den Tellerrand der Chemie hinauszublicken. Ein besonderer Dank für die Organisation geht an Christina Wunderlich, Dr. Daniel Wagner und Dr. Klaus Kreger.

Ohne Geldgeber kann eine wissenschaftliche Arbeit nicht durchgeführt werden. Daher vielen Dank an das 7th Framework Programme der Europäischen Union sowie die DFG für die finanzielle Förderung dieser Arbeit.

Einen großen Dank an die gesamte Mannschaft der Makromolekularen Chemie I für das wirklich hervorragende, kooperative Arbeitsklima! Das hat einen wichtigen Teil zum Spaß an der ganzen Arbeit geleistet.

Vielen Dank an alle Leute vom Kickertisch für die schönste (Neben-)Beschäftigung des Tages: Basti, Hannes, Cheating, Welzebub, Christoph, Philip, Markus, Jessy, Dr. John, Patrick, Jonas, Johannes, Francesco und wen ich noch vergessen haben sollte...*“nochma nüber?”*

8 Jahre Studium und Promotion an der Universität Bayreuth neigen sich nun dem Ende zu, und viele Menschen hatten Anteil an einer großartigen Zeit hier! Ich werde höchst wahrscheinlich den einen oder anderen vergessen, aber, ich versuche mein Bestes: Bernhard, Patrick, Miri, Anna, Danilo, Matthias, Andy, Hubi & Lena, Christoph, Jannik, Alex, Heike, alle aus der alten PCI, meine Badmintonmannschaft, meine Band, die Uni-Rennradgruppe, meine vielen Mitbewohner...

Ganz am Ende gilt ein großer Dank meiner Familie für ihre fortwährende Unterstützung! Danke vor allem an Mama & Papa, dass ihr immer für mich da seid! Ihr seid die Besten!

(Eidesstattliche) Versicherungen und Erklärungen

(§ 9 Satz 2 Nr. 3 PromO BayNAT)

Hiermit versichere ich eidesstattlich, dass ich die Arbeit selbstständig verfasst und keine anderen als die von mir angegebenen Quellen und Hilfsmittel benutzt habe (vgl. Art. 64 Abs. 1 Satz 6 BayHSchG).

(§ 9 Satz 2 Nr. 3 PromO BayNAT)

Hiermit erkläre ich, dass ich die Dissertation nicht bereits zur Erlangung eines akademischen Grades eingereicht habe und dass ich nicht bereits diese oder eine gleichartige Doktorprüfung endgültig nicht bestanden habe.

(§ 9 Satz 2 Nr. 4 PromO BayNAT)

Hiermit erkläre ich, dass ich Hilfe von gewerblichen Promotionsberatern bzw. –vermittlern oder ähnlichen Dienstleistern weder bisher in Anspruch genommen habe noch künftig in Anspruch nehmen werde.

(§ 9 Satz 2 Nr. 7 PromO BayNAT)

Hiermit erkläre ich mein Einverständnis, dass die elektronische Fassung meiner Dissertation unter Wahrung meiner Urheberrechte und des Datenschutzes einer gesonderten Überprüfung unterzogen werden kann.

(§ 9 Satz 2 Nr. 8 PromO BayNAT)

Hiermit erkläre ich mein Einverständnis, dass bei Verdacht wissenschaftlichen Fehlverhaltens Ermittlungen durch universitätsinterne Organe der wissenschaftlichen Selbstkontrolle stattfinden können.

Bayreuth, den

Felix Krohn